University of Bath

PHD

Development of new flavin-catalysed reactions

Molloy, Chris

Award date:
2018

Awarding institution:
University of Bath

Link to publication

Alternative formats
If you require this document in an alternative format, please contact:
openaccess@bath.ac.uk

Copyright of this thesis rests with the author. Access is subject to the above licence, if given. If no licence is specified above, original content in this thesis is licensed under the terms of the Creative Commons Attribution-NonCommercial 4.0 International (CC BY-NC-ND 4.0) Licence (https://creativecommons.org/licenses/by-nc-nd/4.0/). Any third-party copyright material present remains the property of its respective owner(s) and is licensed under its existing terms.

Take down policy
If you consider content within Bath's Research Portal to be in breach of UK law, please contact: openaccess@bath.ac.uk with the details. Your claim will be investigated and, where appropriate, the item will be removed from public view as soon as possible.

Download date: 05. May. 2023

University of Bath

PHD

Development of new flavin-catalysed reactions

Molloy, Chris

Award date:
2018

Awarding institution:
University of Bath

Link to publication

General rights
Copyright and moral rights for the publications made accessible in the public portal are retained by the authors and/or other copyright owners and it is a condition of accessing publications that users recognise and abide by the legal requirements associated with these rights.

- Users may download and print one copy of any publication from the public portal for the purpose of private study or research.
- You may not further distribute the material or use it for any profit-making activity or commercial gain
- You may freely distribute the URL identifying the publication in the public portal ?

Take down policy
If you believe that this document breaches copyright please contact us providing details, and we will remove access to the work immediately and investigate your claim.

Download date: 31. May. 2019

DEVELOPMENT OF NEW FLAVIN–CATALYSED REACTIONS

Christopher Derek Molloy

A thesis submitted for the degree of Doctor of Philosophy

University of Bath

Department of Chemistry

June 2018

COPYRIGHT
Attention is drawn to the fact that copyright of this thesis rests with its author. A copy of this thesis has been supplied on condition that anyone who consults it is understood to recognise that its copyright rests with the author and they must not copy or use it or use material from it except as permitted by law or with the consent of the author.

This thesis may be made available for consultation within the University Library and may be photocopied or lent to other libraries for the purpose of consultation.

[Signature] [Date]

This thesis may be made available for consultation within the University Library and may be photocopied or lent to other libraries for the purposes of consultation with effect from……

Signed on behalf of the School of Chemistry .....

Abstract

Synthetic riboflavin mimics have been utilised for the development of a range of environmentally friendly sulfide oxidation reactions. The mechanics of these reactions, and their context in the wider body of science, is discussed. Reagents for the formation of sulfoxides and sulfoximines with flavins are presented. Hydrazine is shown to be a flavin reductant, and this reduced flavin is able to use atmospheric oxygen as a terminal oxidant to yield a range of sulfoxides from sulfides at low catalyst loading, in good to excellent yields. Hydroxylamine is used to generate sulfoxides from the corresponding sulfide. The kinetics of this reaction are investigated, with continuous flow NMR spectroscopy and this evidence is used to propose a mechanism. The interaction of sodium azide with flavin is investigated in an attempt to understand and prevent the flavin degradation, in an effort to develop an environmentally benign procedure for sulfur-nitrogen bond formation. Additionally, it was also found that ammonium carbamate can be used for the one-step formation of sulfoximines from their corresponding sulfides. This reaction similarly suffers from the flavin decomposition observed between sodium azide and flavin (which leads to catalyst deactivation), and methods to halt this degradation are investigated.

Acknowledgements

Firstly, thanks must go to Dr Dave Carbery for his support, enthusiasm and encouragement in chasing down interesting science throughout the course of my PhD. I am confident that the freedom I was given to investigate a new spot or colour change has allowed me to develop skills that will serve me for the entirety of my professional career to come.

Secondly, I must thank Dr K. Tobias Butler, my secondary supervisor. Without his willingness to take on a student with no qualifications in computational chemistry other than enthusiasm, I would have remained ignorant of this increasingly important branch of chemistry.

To my industrial supervisor, Dr Steve Raw at AstraZeneca. My three months at AZ we're hugely valuable, both in terms of the equipment, and the expertise that I had access to. His encouragement to meet with a variety of current employees resulted in interesting and eye-opening conversations which led me to view the wider field of chemistry from a vantage point of which I had not previously been aware. I am also grateful for his company on lunch time runs through the stunning Macclesfield countryside.

I am indebted to Carbery group for making my arrival in Bath so painless. Fab, Cristina and Christina made my time in Bath a joy to work with from the very beginning. Alex's return to the group, after his placement at GSK, and the subsequent arrival of Matt, all contributed in creating an atmosphere in which it was possible to truly enjoy working hard.

Cristina was a great friend and mentor during my early times in Bath. Without her guidance and friendship, I would be a much less well-developed chemist and person than I am now. Working in the fume hood next to Fab has been an absolute pleasure and my time in the lab would have been immeasurably worse without her calm and collected oversight.

Thank you too to Dr John Lowe and Dr Catherine Lyall, for tolerating me regularly popping my head into your office to "just ask a quick question" about NMR, whether it be theoretical or technical. To Dr Anneke Lubben for her guidance in mass spectrometry, to Kate Wittering, for her crystallography work and to Andrew Hall for his assistance with continuous flow NMR.

I am also grateful to several other researchers who made the hard times more bearable. Jen, Steve and Rob, if I ever needed reminding that I wasn't the only person struggling, I needed to only pop into your office.

Credit must go to Alex and Chris, who showed me part of the joy of research was found in the continuing of scientific discussion well into the evening.
And finally, to Eilidh, who has been endless source encouragement and support.

Contents

List of Figures, Schemes and Tables

Figures

Schemes

Tables

Abbreviations

Ac	acetyl
Ar	aryl
A.U.	arbitrary units
Bn	benzyl
br.	broad
cat.	catalyst
δ	chemical shift relative to Me_4Si in parts per million
d	doublet
DCM	dichloromethane
DFT	density functional theory
DMA	dimethylacetamide
DMF	dimethylformamide
DMSO	dimethyl sulfoxide
DMS	dimethyl sulfide
e^-	electron
ee	enantiomeric excess
EPR	electron paramagnetic resonance
eq	molar equivalents
ES	electrospray
Et	ethyl
FAD	flavin adenine dinucleotide
FMN	flavin mononucleotide
GC	gas chromatography
h	hours
HPLC	high performance liquid chromatography
IPA	isopropanol
^{i}Pr	isopropyl
IR	infrared
k_{obs}	observed rate constant
LED	light emitting diode
m-	meta
M	mol L^{-1}
MAO	monoamine oxidase
mCPBA	meta-chloroperbenzoic acid
Me	methyl
MeSal	3-methylsalicylate
min.	minutes
MS	mass spectrometry
MW	microwave
NAD	nicotinamide adenine dinucleotide
NHC	N-heterocyclic carbine
^{n}Hep	n-heptyl
NMR	nuclear magnetic resonance
^{n}Pr	n-propyl
o-	ortho
Oxone®	potassium peroxymonosulfate

p-	para
Petrol	40:60 petroleum ether
Ph	phenyl
phen	1,10-phenanthroline
q	quartet
r.t.	room temperature
s	singlet
SET	single electron transfer
sex.	sextet
SPS	solvent purification system
t	triplet
^{t}Bu	tert-butyl
TEMPO	(2,2,6,6)-Tetramethylpiperidin-1-yl-oxyl
TFA	trifluoroacetic acid
TFE	2,2,2,-trifluoroethanol
THF	tetrahydrofuran
TLC	thin layer chromatography
TMS	trimethylsilyl
UV	ultraviolet

1. Introduction to flavin catalysis

1.1. Riboflavin

Riboflavin is formed from the nitrogen rich heterocyclic pteridine ring **1** fused to an additional benzene ring on one side, forming an isoalloxazine **2,** which is fully oxidised to the corresponding imide on the other. Additionally, there is a ribityl group on a single nitrogen in the centre ring **3** (Figure 1).[1]

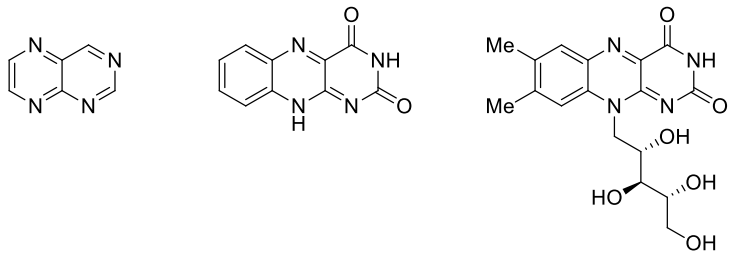

Figure 1 Riboflavin building blocks

1.1.1. History of Flavins

Riboflavin (Vitamin B2) **3,** is a prevalent enzyme cofactor found throughout nature, with almost 3% of genes of all genes in prokaryotic and eukaryotic genomes predicted to encode for flavin adenine dinucleotide.[2] Flavins were first reported as a component of cow's milk in the late 1870's.[3] Blyth isolated a bright yellow substance that he termed lactochrome, which was later demonstrated to be riboflavin. After Blyth's initial discovery, the report went unnoticed until the late 1920's when riboflavin began to be isolated from a wide variety of sources. It was recognised as a constituent part of the B vitamin complex and it's structure proven by synthesis in 1934 by Karrer *et al.*[4] Once the structure had been confirmed, the name riboflavin was formally adopted to replace the variety of nomenclature that had been used previously. That nomenclature usually described the source from which the compound had been isolated (ovoflavine, lactoflavine, uroflavine, etc).

1.1.2. The role of flavin in nature

As flavoproteins were isolated from a wide range of natural sources, their biological importance began to be grasped. Otto Warburg discovered a yellow residue in yeast, while conducting his pioneering work into the mechanism of biological respiration.[5] The protein was shown to catalyse the oxidation of another vitamin cofactor, nicotinamide adenine

dinucleotide phosphate (NADPH). Upon further investigation of this yellow residue, the Swedish biochemist, Hugo Theorell, found that the enzyme could be precipitated at acidic pH, into a colourless apoprotein, leaving the yellow flavin-containing supernatant. Neither the apoprotein nor the remaining flavin could catalyse NADPH on its own, however, activity was resumed upon reconstitution.[6] This yellow pigment was seemingly identical to the riboflavin isolated from other sources, however, the riboflavin would not reconstitute enzyme activity when combined with the apoprotein. Theorell discovered that the difference in enzyme activity could be attributed to the yeast isolated flavin containing an ester linked terminal phosphate residue. This form of flavin became known as flavin mononucleotide **4** (Figure 2).

In the mid 1930's, Hans Krebs recognised the importance of a further flavo-protein, *D*-amino acid oxidase (DAAO), in various mammalian livers and kidneys.[7] Warburg and Christian, in a similar vein to Theorell's previous experiment, demonstrated that this new flavo-protein suffered a loss of activity when separated into the apoprotein and flavin cofactor, while regaining activity upon recombination.[8] However, activity did not return up mixing with either riboflavin **3** or flavin mononucleotide (FMN) **4**. The cofactor was determined to be the condensation product of FMN and adenosine monophosphate (AMP), flavin adenine dinucleotide (FAD) **5** (Figure 2).

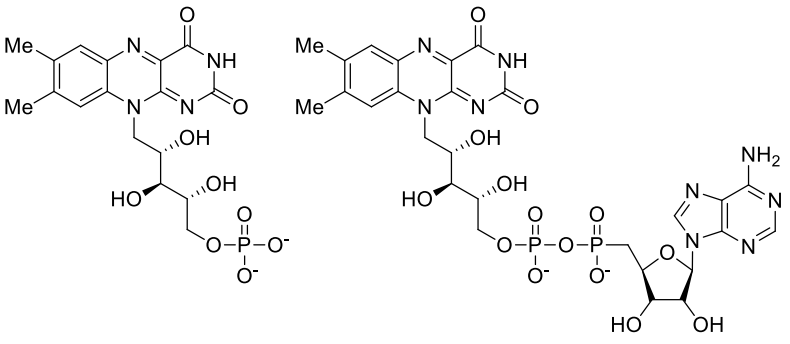

4
Flavin mononucleotide (FMN)

5
Flavin adenine dinucleotide (FAD)

Figure 2 Flavins found in nature

Flavins can exist in three redox forms, the most stable oxidised form **6**, an intermediate radical semiquinone form **7** and a fully reduced form **8**. This chemical versatility results in the involvement of flavins in a wide range of biological reactions. Their ability to catalyse two electron dehydrogenations of numerous substrates has given them a central role in biological aerobic metabolism (Figure 2). Furthermore, their ability to take part in one

electron transfer to various metal centres allows flavins to form part of multi-redox-centre enzymes (Scheme 1).

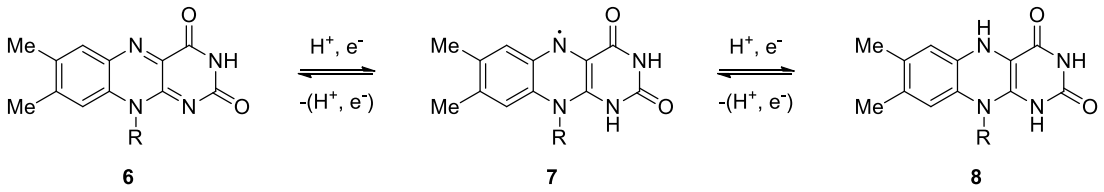

Scheme 1 The oxidised, semiquinone and reduced flavin flavin forms

Furthermore, their ability to take part in one electron transfer to various metal centres allow flavins to contribute to multi-redox-centre enzymes, such as NADPH **9** reduction. Flavins are crucial for the reduction of NADPH, which relies on transfer of electrons to give the reduced form, NADP+ **10**, a critical step in cytochrome P450 enzymatic chain reactions (Scheme 2).[9,10] Further examples of multi-redox centre enzymes include succinate dehydrogenase[11] and xanthine oxidoreductase.[12]

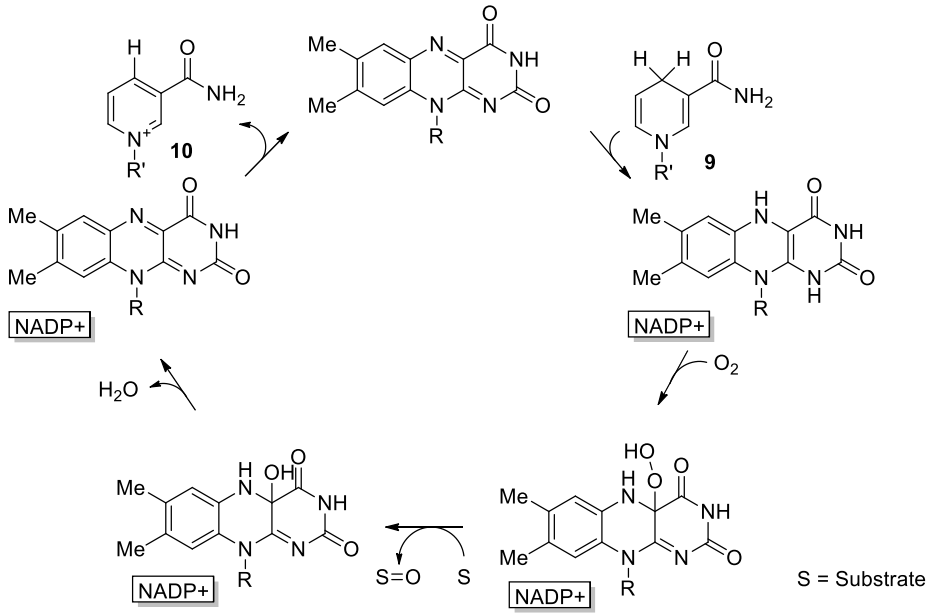

Scheme 2 Catalytic cycle of NADPH and its reduction by flavin mononucleotide.

Riboflavin binding proteins are also involved in the development of chicken and mammalian foetuses[13,14] and are suspected of playing a role in programmed cell death.[15] Flavoproteins are also critical in detoxification of aromatic pollutants in soil.[16] Furthermore, as a photoactive species, it is involved with several light-dependent processes, such as photosynthesis[17] and the photoreduction of DNA dimers.[18]

1.1.3. Biosynthesis

When found in nature, riboflavin is synthesised from guanosine triphosphate (GTP) **11**, in a complex reaction involving six enzyme activities. GTP is converted to the pyrimidinone 5'-phosphate **12**, priming the compound for the addition of the ribityl side chain, which is achieved *via* ring deamination **13**, side chain reduction **14** and finally dephosphorylation **15**. This intermediate undergoes condensation with 3-hydroxy-2-butanone 4-phosphate **17** to yield 6,7-dimethyl-8-ribityllumazine **18**. The enzyme, ribC, then forms the final riboflavin motif **3** (Scheme 3).[19]

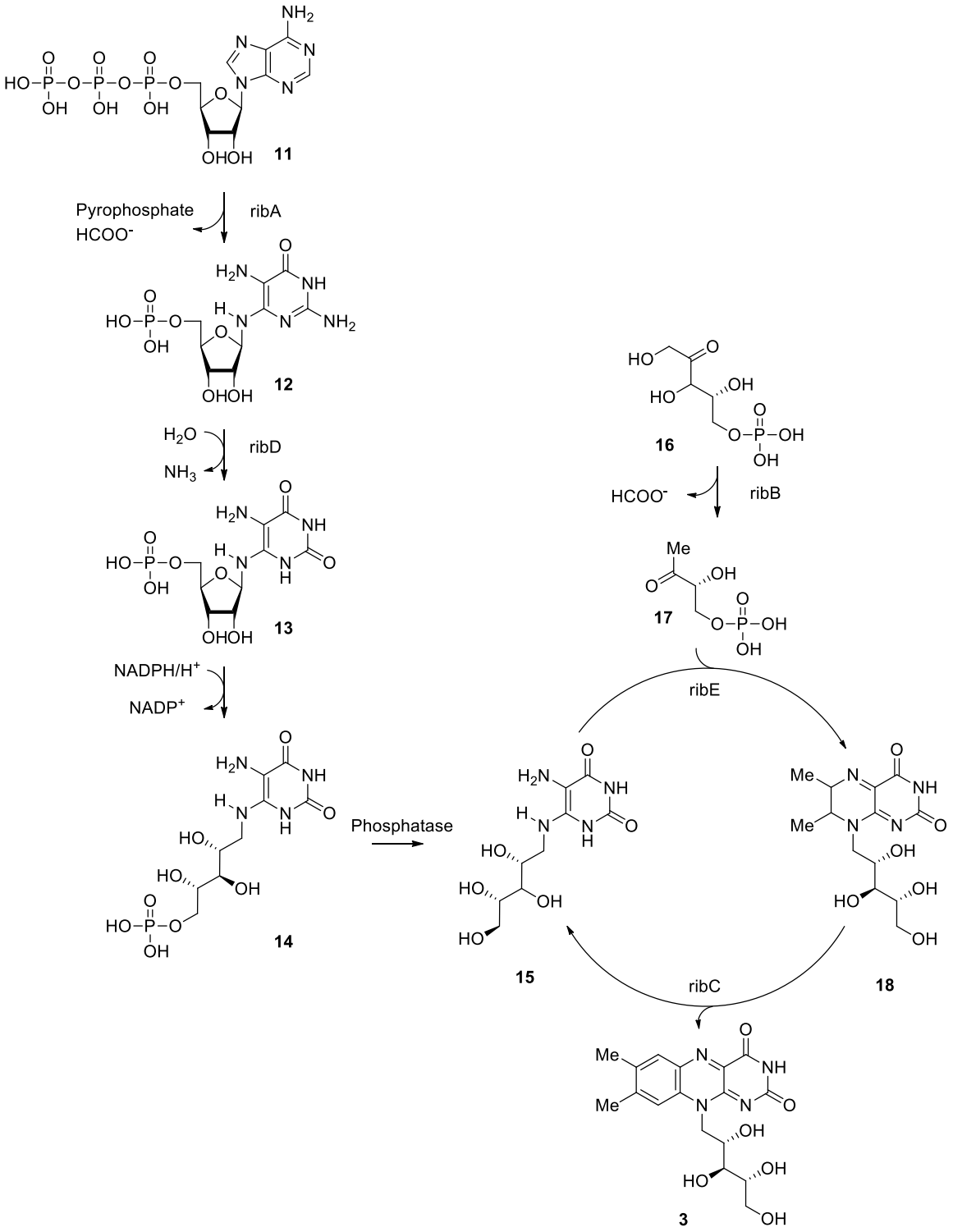

Scheme 3 Riboflavin synthesis in nature

1.2. Properties of flavins

When not enzyme-bound (for example free in solution), a mixture of reduced and oxidised flavin sit in equilibrium with each other.[20] At pH 7 approximately 5% radical semiquinone is observed in an equimolar mixture of oxidised and reduced flavin, although protein binding can have a significant effect on this equilibrium. The semiquinone exists in a neutral or anionic form and upon binding to a specific protein can have a significant effect on the original pKa of ~ 8.5 (Scheme 4).

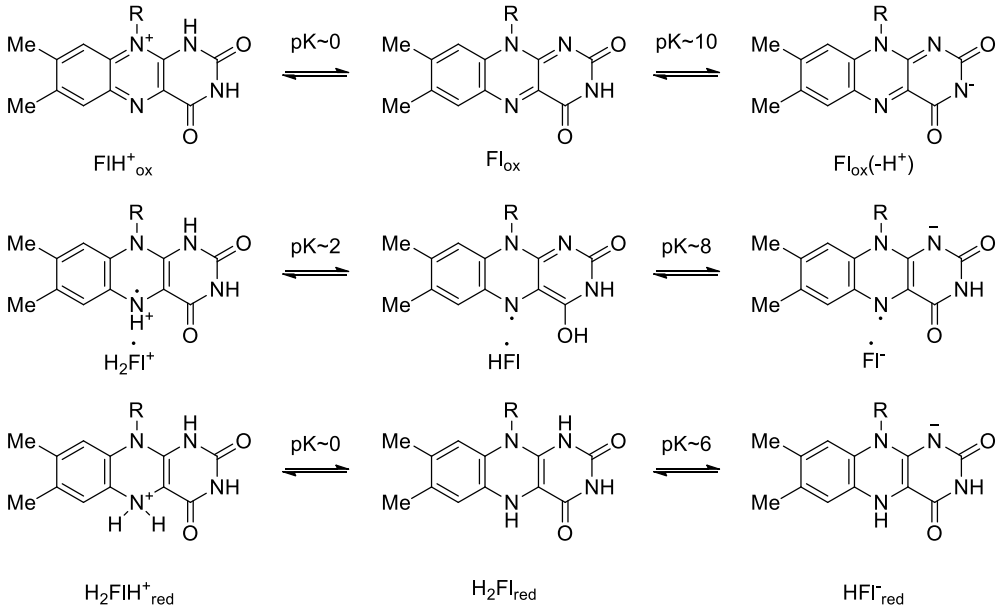

Scheme 4 Acid-base equilibria of ozidised and reduced flavin

The key step in a large proportion of flavoprotein-reducing dehydrations is a two-electron reduction of the substrate. The subsequent reduced flavin (H_2Fl_{red}) is reoxidized in either a two-electron process or in single one-electron steps.

Reduced flavins are highly reactive towards molecular O_2, which can be harnessed for a range of oxidation techniques, including electron transfer, dehydrogenation and oxygen transfer (Scheme 5). The active flavin species in these reactions**,** originates from the addition of molecular oxygen into the reduced flavin **20**, forming a highly reactive hydroperoxide **21**. The pendant oxygen can then be useful for a number of synthetic transformations such as Baeyer-Villiger expansions[21] or aromatic hydroxylations.[22]

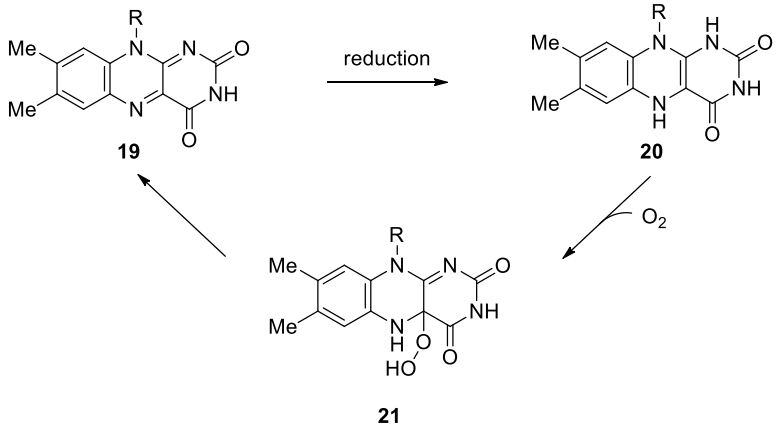

Scheme 5 General scheme for the formation of hydroperoxyflavin

1.3. Flavoproteins

Many of the reaction properties of flavoproteins also occur *in vivo*, as is the case with liver flavoenzymes, such as FAD-containing monooxygenase, which catalyse a range of small molecule transformations. These transformations are particularly favourable with soft nucleophiles, including the oxidation of amines,[23] sulphides,[24] aldehydes[25] and aromatic rings.[26] When considered *in vivo*, the flavin must be reduced by an external cofactor. UDP-*N*-acetylenolpyruvylglucosamine reductase (MurB) is an example of an enzyme monomer containing one FAD molecule. MurB catalyses the NADPH-dependent reduction of enolpyruvyl-UDP-*N*-acetylglucosamine, **22,** to the corresponding D-lactyl product, UDP-*N*-acetylmuramic acid **23**. The FAD co-factor is reduced by NADPH, and once $NADP^+$ has dissociated substrate **22** can bind, allowing it to be reduced (Scheme 6).[27]

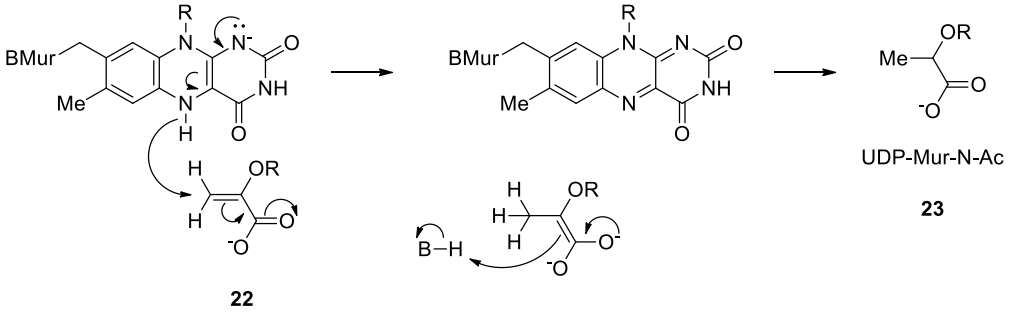

Scheme 6 Flavin catalysed UDP-N-acetylmuramic acid formation

FMO's contain an FAD prosthetic group (a coenzyme that is tightly or covalently bound) and a binding factor.[28] They tend to have two-electron redox character, with the semiquinone state playing an insignificant role in transitions. One exception is the one-electron reduction of O_2 by the reduced flavin, resulting in a caged radical pair **24**. This radical pair now has a

number of possible routes, it can dissociate into its component parts; of a neutral flavin radical and a superoxide **25**. Alternatively, it can collapse to the previously discussed nucleophilic flavin peroxide **26** (which becomes more electrophilic upon protonation to the hydroperoxide **27**). This peroxide species can then eliminate to hydrogen peroxide or undergo a further single electron transfer, both routes yielding the oxidised flavin **6** (Scheme 7).[29]

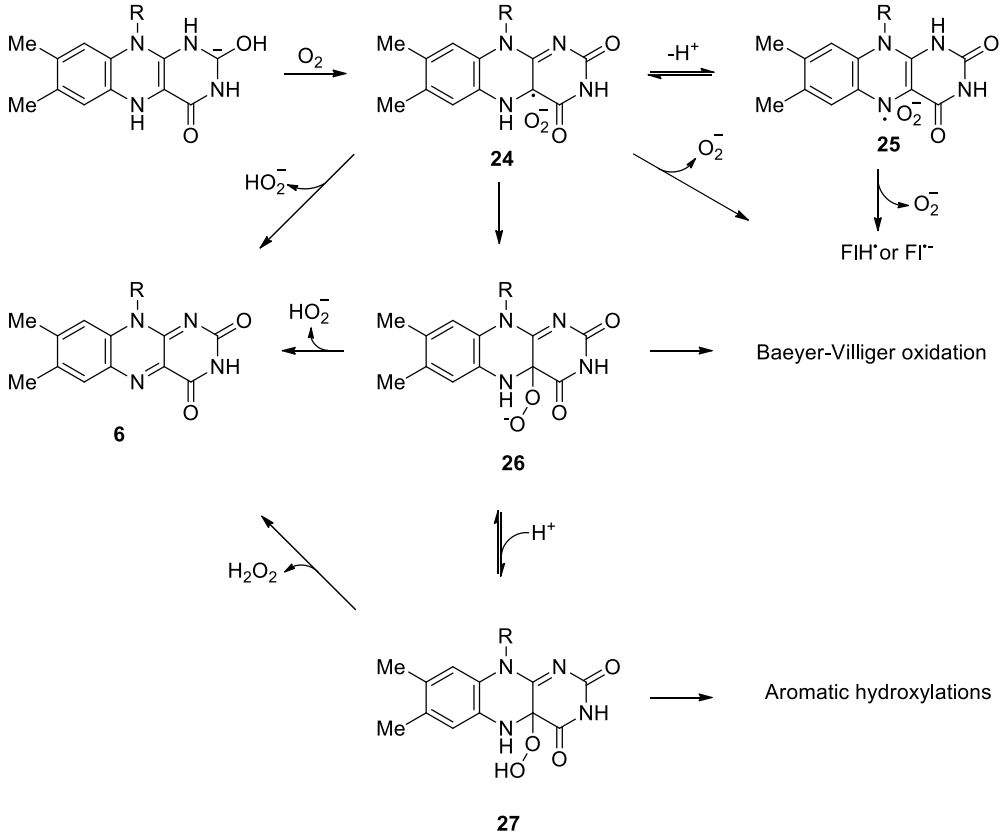

Scheme 7 Chemical reactions that mediated by reduced flavin and oxygen

1.3.1. Flavoprotein bioluminescence

Flavins are involved in the production of light in bioluminescent bacteria, which alludes to their capability for photocatalysis, and there have been reports on their bioluminescence for 150 years.[30] The voyage of the HMS Challenger describes, unbeknownst to the authors, the bioluminescence of the luciferase upon reaction with reduced flavin and oxygen.[31] This example can be reproduced in a controlled environment through the flavin catalysed oxidation of aliphatic-aldehydes. The authors postulate that nucleophilic attack of the at the carbonyl comes from a formal peroxy flavin **26**, forming the flavin-carboxylic acid intermediate **29**. The light emission is attributed to the rearomatization of the excited hydrated flavin **28**, upon release of water, regenerating the original FMN **6**.[32] This example

demonstrates nucleophilic attack of the flavin hydroperoxide **27** electrophilic carbonyl (Scheme 8).

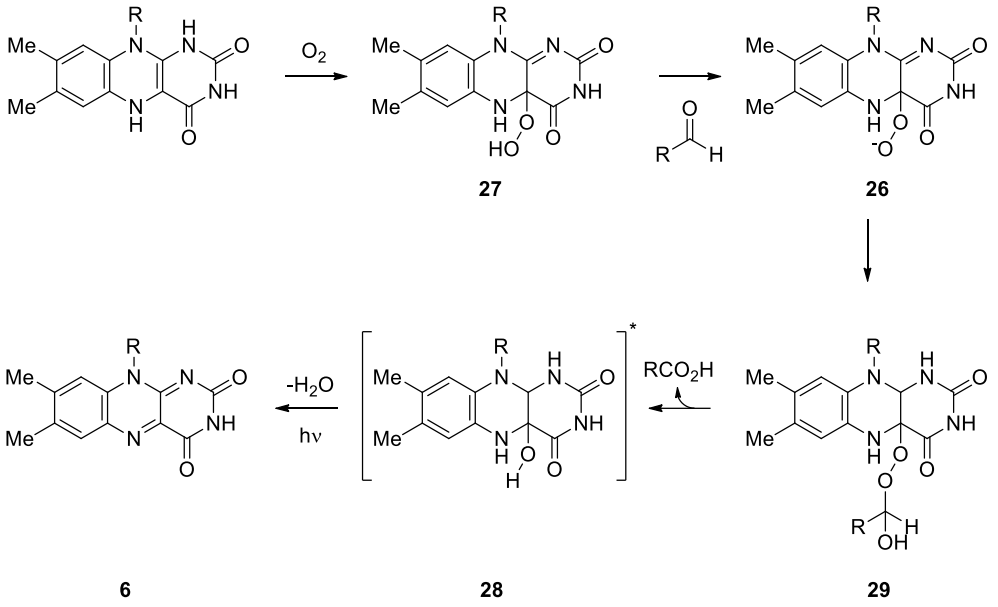

Scheme 8 Hydroperoxyflavin catalysed carbonyl oxidation

1.3.2. Flavoprotein Monooxygenases (FMO's)

A common property of flavoprotein monooxygenases is the mechanistic use of either NADH or NADPH to reduce the FAD flavin form, followed by reaction of the reduced form with molecular oxygen, which generates the reactive oxygen species responsible for oxidation of the substrate. The flavin peroxide can act as a potent nucleophile, and can be utilised by a sub group of aromatic hydroxylases to introduce an additional oxygen into a ring system adjacent to the ketone group already in place, in a Baeyer-Villiger type oxidation (Scheme 9).[33] This peroxy adduct falls into an alternative sub class of monooxygenases; oxygen-insertion reactions.

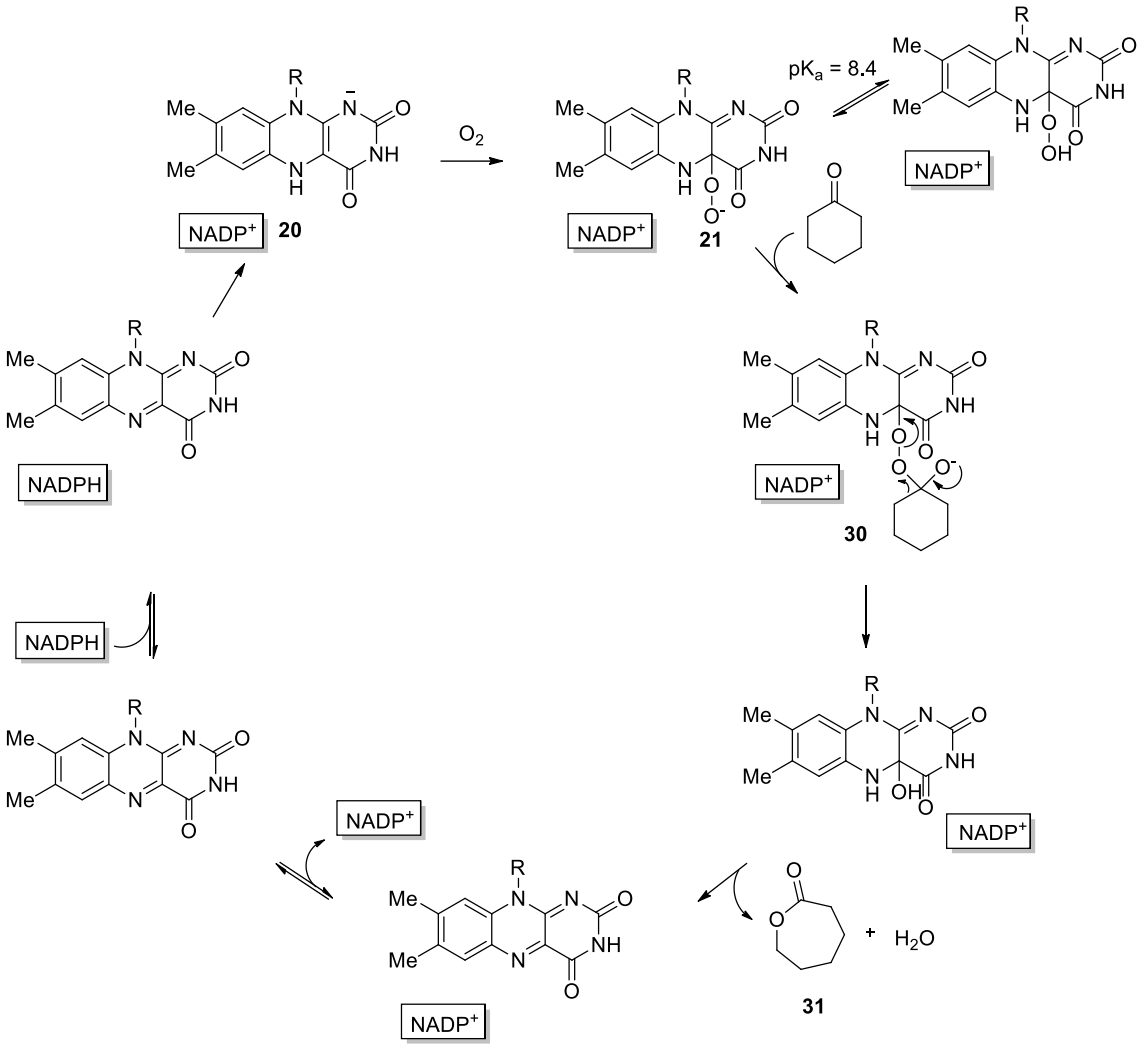

Scheme 9 Cyclohexanone monooxygenase action

The reduced flavin is formed upon reaction with NADPH **20**, which then reacts with O_2 to form the hydroperoxyflavin as seen previously **21**. The hydroperoxy flavin then performs nucleophilic attack on the cyclohexanone, forming a cyclohexanone flavin adduct **30**. The carbon-carbon bond is then broken upon collapse of the oxygen lone pair and cleavage of the flavin, forming **31** and liberating water. The remainder of the catalytic cycle is responsible for the regeneration of the neutral flavin **19** through the loss of $NADP^+$.

Alternatively, the hydroperoxy flavin enzymes can act as potent electrophiles, which can be used for the insertion of hydroxy groups in the *meta* position of 4-hydroxy-benzoic acid **33**. One such enzyme that performs this transformation is 4-hydroxybenzoate 3-monooxygenase (PHBH) (Scheme 10).[34]

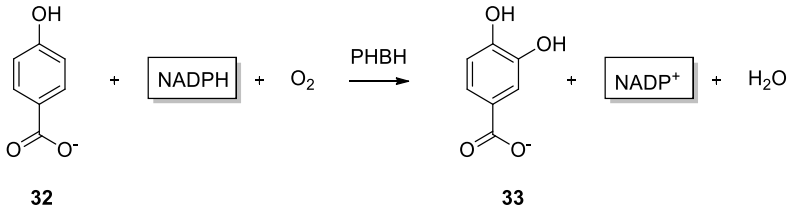

Scheme 10 Hydroxylation of *p*-4-hydroxy-benzoic acid with PHBH

The hydroxylation of 4-hydroxy-benzoic acid **32** results in the formation of 3,4-dihydroxybenzoic acid **33**.

In the aromatic hydroxylases sub group, there is a control mechanism to prevent NAD(P)H being consumed, when the substrate to be hydroxylated is not present. For reduction of the flavin by NAD(P)H to occur, a complex of oxidised enzyme and aromatic substrate is required. The presence of this complex leads to as much as a 100,000-fold increase in rate (k_2) in comparison to no substrate (k_1) (Scheme 11

Scheme 11).[35]

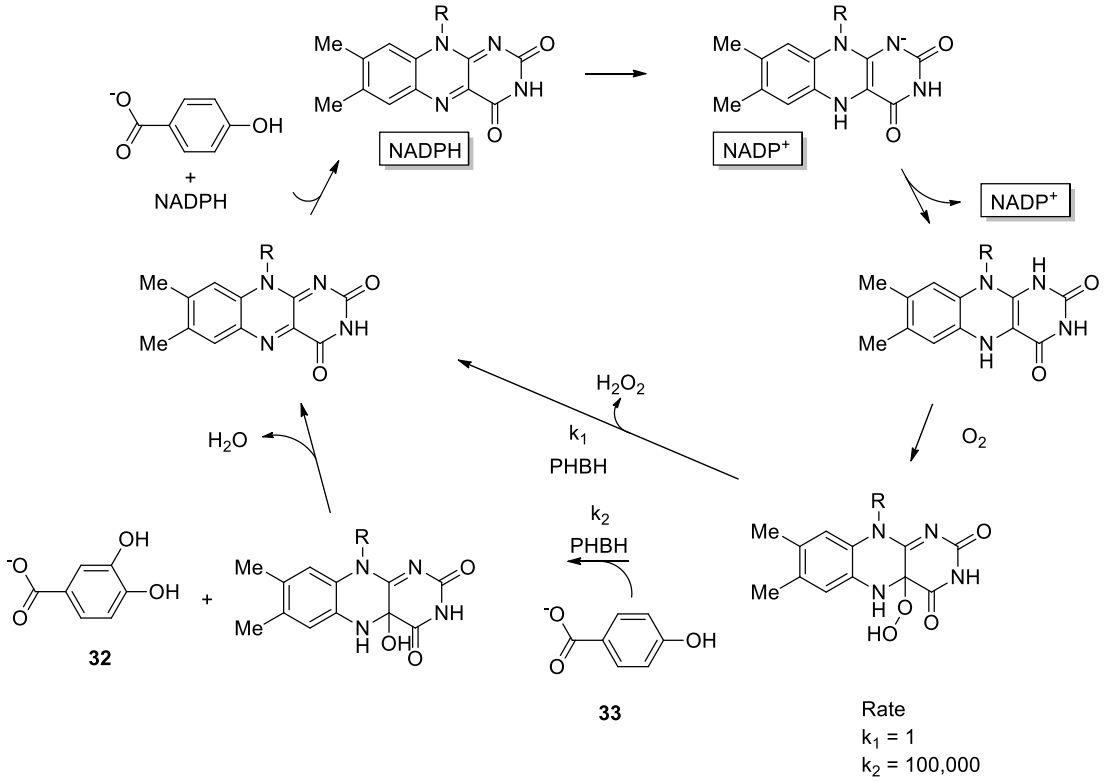

Scheme 11 Rate comparison of PHBH with and without **33**

This electrophilic mechanism for control is highly unstable in the absence of the substrate **33**. Nucleophillic monooxygenases display an alternative control mechanism, whereby the peroxide complex is stabilised by the protein such that it is only reactive in the presence of substrate. It is stabilised to such a degree that it can be isolated by low-temperature chromatography.[36]

1.4. Reductase, Dehydrogenases and Electron Transferases

1.4.1. Acetyl-CoA Dehydrogenases

This class of widely occurring enzymes take part in the oxidation of fatty acids. In acetyl-CoA dehydrogenases, the reduced flavin component is reduced by successive one-electron transfers to a secondary flavoprotein, the electron-transfer flavoprotein (ETF). In mammals, this is then reoxidized by a final flavoprotein, ETF-ubiquinone. Significant research efforts have been made to investigate the reaction mechanisms of these dehydrogenase enzymes, which determined the initial step to be removal of the α-proton from **34** by an aspartate residue in the active-site, followed by a concerted hydride transfer from the β-position yielding the reduced flavin (Scheme 12). This reaction leads to the formation of the α,β-unsaturated carbonyl motif **35**.[37]

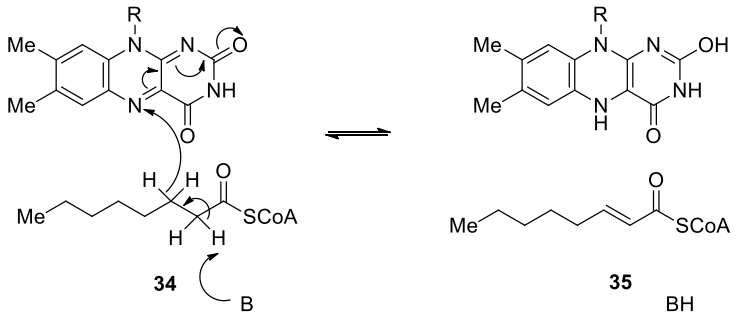

Scheme 12 Dehydrogenation of a normal substrate by acyl-CoA dehydrogenases

1.4.2. Flavin monooxygenase biomimicry

Naturally occurring flavins such as FMN and FAD have been extensively investigated to understand their applicability towards synthetic reactions in organic synthesis. It is possible to remove the protein environment and, using a charged flavinium **36**, form a hydroperoxyl flavin species **37** with molecular oxygen as a terminal oxidant (Scheme 13).

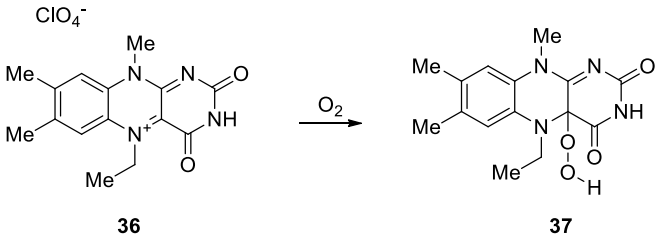

Scheme 13 Scheme of oxidation from aldehydes to carboxylic acids with perchlorate ion flavin

This initial discovery found the flavin form to be highly unstable, undergoing the reverse reaction, eliminating H_2O_2, resulting in the neutral flavin.[38] The first stable hydroperoxyflavin to be synthesised independent of an enzyme was reported by Bruice and Kemal in 1976. They stabilised the enzyme independent flavin with the use of a perchlorate counterion **37**, and were then able to achieve the oxidation of aldehydes to the corresponding carboxylic acids, with the hydroperoxyflavin formed (Scheme 14).

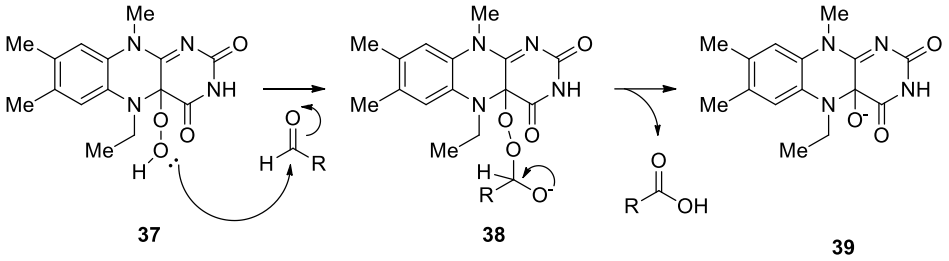

Scheme 14 Bruice and Kemal aldehyde oxidation[38]

The hydroperoxyflavin **37** demonstrated luminescence upon mixing with aldehydes, making it the first synthetic mimic of bacterial luciferase. However, conversion to carboxylic acids from the corresponding aldehydes was low.[38]

The oxidative capacity of the hydroperoxyl flavin **37** was investigated and compared to other common oxidizing agents. **37** was observed to have a signifincantly higher oxidative capacity than *t*ert-butyl hydroperoxide (*t*BuOOH) **40**, by a factor of ~ 10^3 – 10^6, whereas it has an oxidative capacity ~ 10^3 lower than *meta*-chloroperoxybenzoic acid (*m*CPBA) **41** (Figure 3).

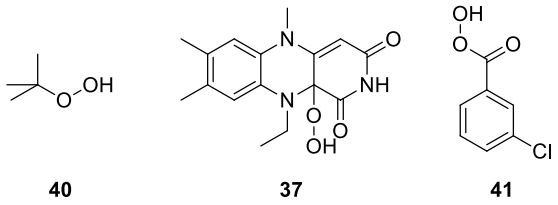

Figure 3 Relative oxidative capacities of common oxidants

The three rate constants each represent a different oxidation; K_I – the oxidation of I^-, k_s – the oxidation of thioxane and k_n – the oxidation of *N*,*N*-dimethylbenzylamine (Scheme 15).

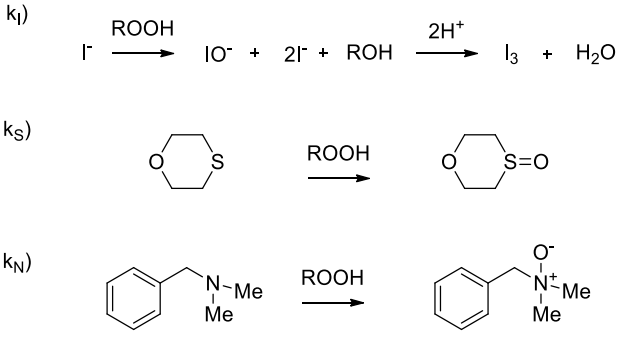

Scheme 15 Reactions to determine relative rate constats for various peracids

These electrophilic reactions were subsequently summarised by Brucie *et al.* in 1983, and can be found below (Table 1).[39]

Table 1 Rate relative to entry 2 to for a range of peroxyacid oxidations

Entry	Structure	k_I	k_S	k_N
1	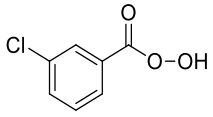	7.6×10^2	7.4×10^2	(2.14×10^3)
2	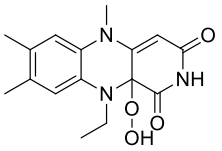	1.0 ($6.0\ M^{-1}\ s^{-1}$)	1.0 ($0.12\ M^{-1}\ s^{-1}$)	1.0 ($0.12\ M^{-1}\ s^{-1}$)
3	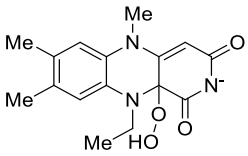	3.0×10^{-1}	5.7×10^{-2}	8.6×10^{-2}
4	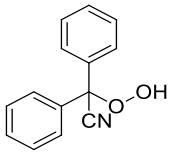	5.6×10^{-2}	8.7×10^{-1}	3.3×10^{-1}
5	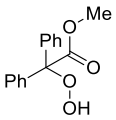	5.5×10^{-2}	3.2×10^{-2}	1.1×10^{-2}
6	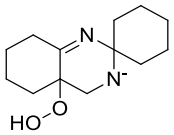	9.0×10^{-3}	9.2×10^{-4}	1.2×10^{-4}
7	H_2O_2	1.0×10^{-3}	1.4×10^{-4}	2.8×10^{-5}
8	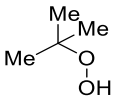	1.0×10^{-3}	5.8×10^{-5}	$>1.0 \times 10^{-6}$

Table 1 shows that the peroxy flavin (entry 2) is an excellent oxidant, with only *m*CPBA (entry 1) having a superior rate across the range of peracids investigated. The replacement of a nitrogen site with a carbon (entry 3) has a significant effect on rate, with this compound being two orders of magnitude slower for the oxidations of thioxane and *N*,*N*-

dimethylbenzylamine. H_2O_2 (entry 7) is a significantly slower oxidant, witih the oxidation of *N*,*N*-dimethylbenzylamine being fivefold slower.

The authors also investigated the propensity for **37** to catalyse epoxide formation upon reaction with alkenes. Initially the reaction was conducted in *t*-butanol and DMF, and these reactions yielded no formation of epoxide, just a gradual decay of the peroxyflavin **37** to the neutral flavin **42** (Scheme 16).

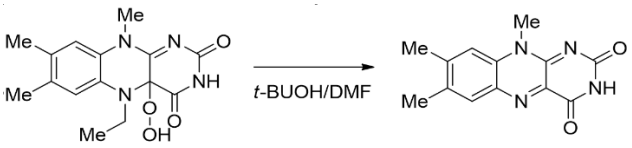

37 **42**

Scheme 16 Degradation of hydroperoxyflavin

When the solvent was changed to chloroform ($CHCl_3$), the stability of **37** was significantly decreased, and a more diverse range of decomposition products were observed. There was no epoxide formation observed with **37**. The authors ultimately observed formation of epoxide in 31 % yield.

Oae *et al.* showed that flavin hydroperoxide was not as selective towards amines as its natural counterpart, demonstrating oxidation of all types of amine (not merely secondary and tertiary as is the case with natural flavin monooxygenases), generating benzaldehyde oxime, hydroxylamines, nitrones and amine *N*-oxides from their corresponding amines.[40] The hydroperoxy flavin was generated from hydrogen peroxide (H_2O_2) and a flavinium salt in the oxidised redox form, rather than from a reduced flavin and atmospheric O_2, as observed in nature. This allows for the possibility of an oxidative and a reductive catalytic cycle, one relying on H_2O_2 as a terminal oxidant and the other relying on O_2 as a reductant to recycle the active catalyst (Scheme 17).

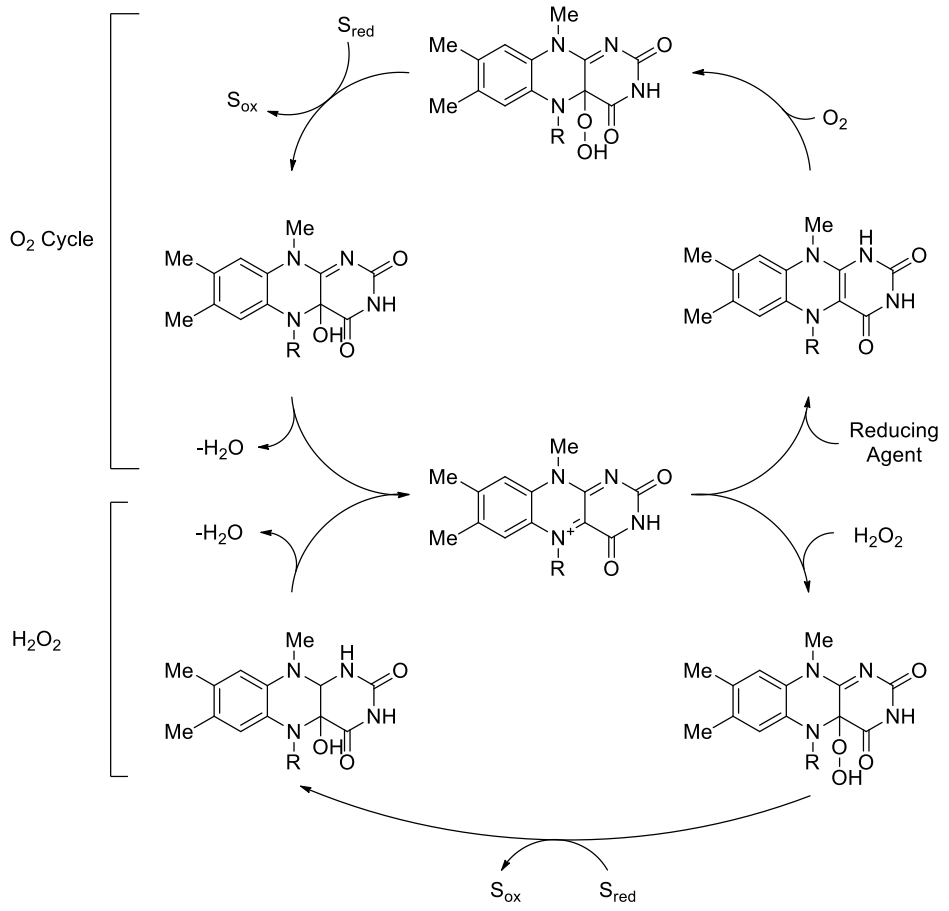

Scheme 17 Two flavin catalytic cycles for generating hydroperoxy flavins

The potential of flavins as catalysts for organic synthesis was first realised by Murahashi *et al.* when they demonstrated the oxidation of sulfides and secondary amines utilising a perchlorate counterion to the flavinium, with H_2O_2 as the oxidant. Both the sulfide and imine were competent substrates for electrophilic oxidation, with both sulfoxide and nitrone being obtained in good yields (Scheme 18).[41]

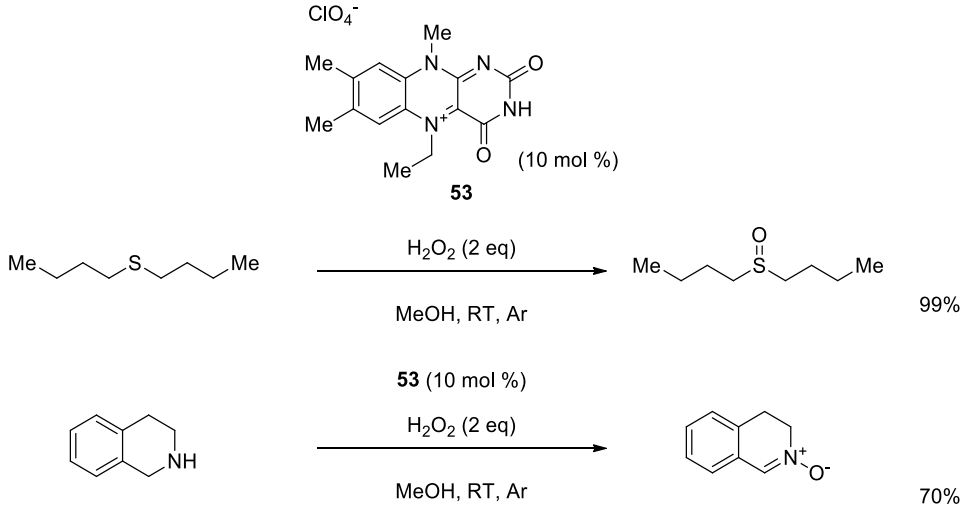

Scheme 18 Catalytic perchlorate flavinium oxidation of sulfides and amines

This group later ammended this reaction by using atmospheric oxygen as the terminal oxidant with hydrazine monohydrate (N_2H_4•H_2O) added to facilitate the reduction of the flavin, and the reaction solvent changed to trifluoroethanol.[42] This allowed for a significant reduction in catalyst loading which could be attributed to the increased solubility of dioxygen gas in the solvent.[43] N_2H_4•H_2O is used stoichometrically to generate the reduced dihydroflavin, which reacts with O_2 to form the hydroperoxyflavin (Scheme 19).

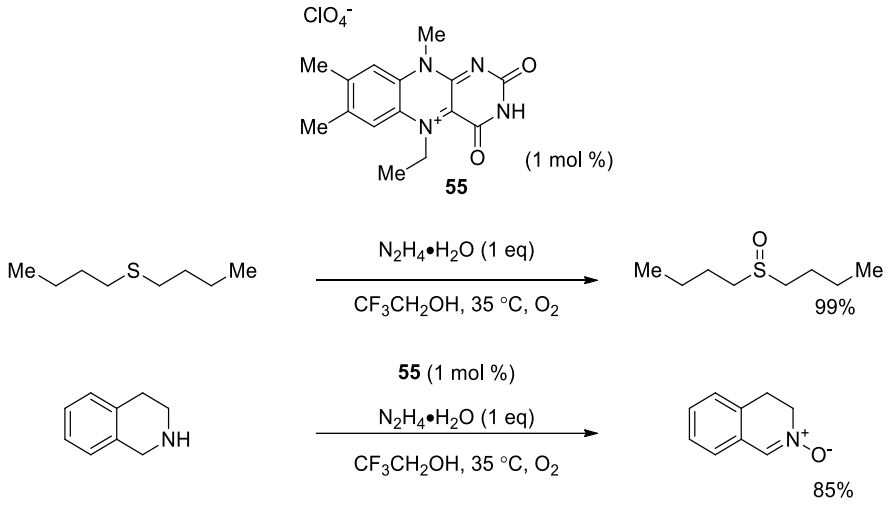

Scheme 19 Examples of hydrazine as a reductant

The Carbery group have used a modified bridged flavinium catalyst in order to achieve oxidation of sulfides utilising hydrogen peroxide as a terminal oxidant.[44] The group were able to develop a system with extremely low catalyst loading (1.8 mol %) and investigated the electronic effects of the substrates (Scheme 20).

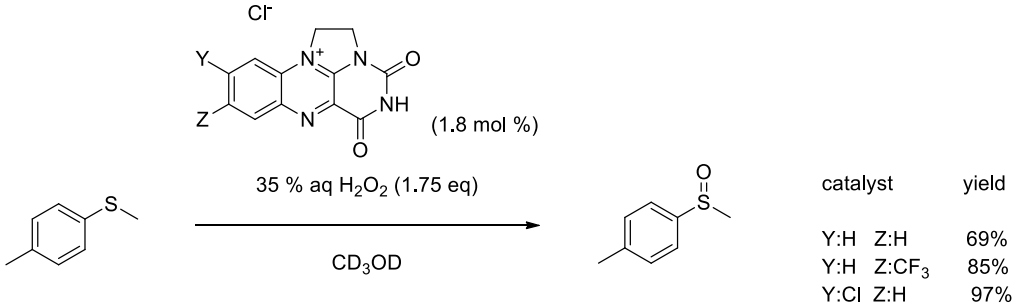

Scheme 20 Carbery Marsh Reaction Scheme

They noted that when the reaction was performed with sulfides containing electron donating substituents (methoxy, amino), sulfoxide formation was achieved in under 1 hour at room temperature. Whereas reaction with sulfides containing electron withdrawing substituents (cyano), the reaction has a significantly increased reaction time of 12 hours to reach completion. This observation is consistent with the previously proposed electrophilic

reaction mechanism for oxygen transfer. The efficiency of 3 distinct organocatalysts were investigated, with all 3 being found to be effective towards sulfoxidation, with the 8-Cl derivative being the most effective. Methanol was chosen as the reaction solvent as it offered the best yields, which was suggested to be due to the increased solubility of the catalyst, over other solvents investigated (dimethylfomamide and chloroform).

Cibulka *et al.* further expanded upon the scope of bridged flavinium catalysts when they used valinol to prepare chiral organocatalysts **55** for the enantioselective synthesis of sulfoxides. The introduction of the isopropyl group creates a new stereogenic centre on the flavin, which leads to the formation of two hydroperoxyflavin diastereomers **56** and **57**. The respective hydroperoxy diastereomers were formed in a 3:1 ratio (Scheme 21), although, its use a chiral catalyst was poor, with a maximum *e.e.* generated of a < 5%, *i.e.*, the mixture was racemic.[45]

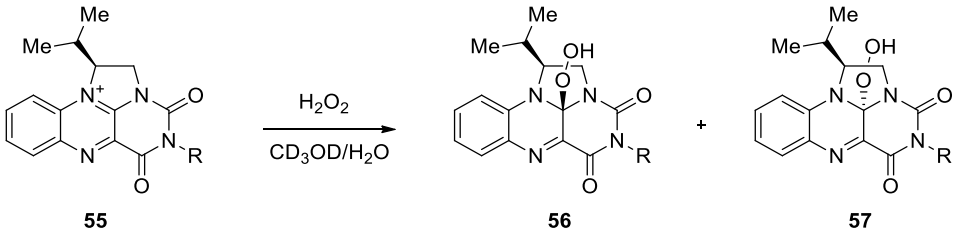

Scheme 21 Valinol hydroperoxyflavin diastereomers

The group also attempted the oxidation of amines but were limited by the degradation of the catalyst under the reaction conditions, obtaining the *N*-oxide product in 18% (Scheme 22).

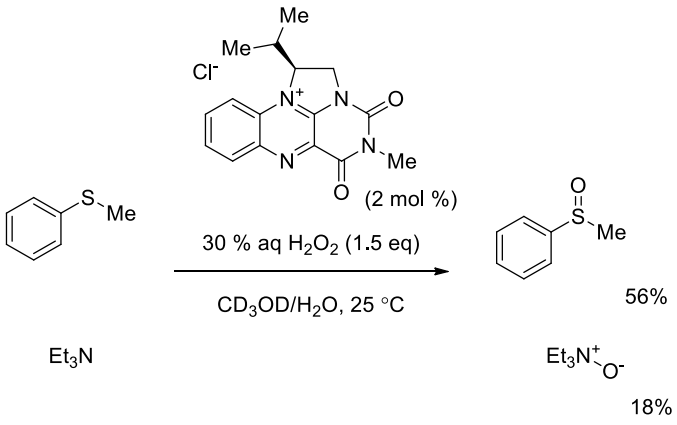

Scheme 22 Sulfur oxidation with valinol flavinium

More recently, in 2013, Imada *et al.* developed an aqueous method for the oxidation of sulfides relying on ascorbic acid as a reductant for the flavinium perchlorate salt (Scheme 23).[46] Aqueous conditions are highly favourable as their "green" nature makes them ideally scalable for industry, however, perchlorate salts must be avoided due to their potentially explosive nature, hampering the use of this transformation in industry.[47]

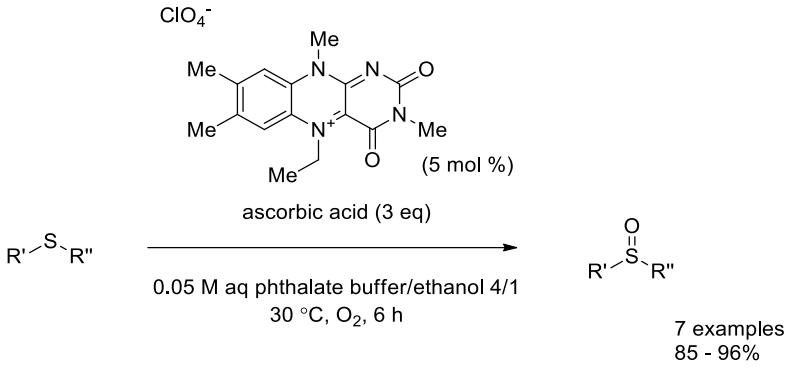

Scheme 23 Flavin perchlorate sulfoxide transformation

Murahashi *et al.* reported the aerobic oxidation of sulfides and thiols (to disulfide) using a formic acid and triethylamine system to reduce the flavin, using molecular oxygen as the terminal oxidant (Scheme 24). The group investigated a range of flavin catalysts and maintained excellent yields while changing the counterion (triflate to perchlorate) and by inserting hydroxymethyl or hydroxyethyl groups and even the protected riboflavin form.[48]

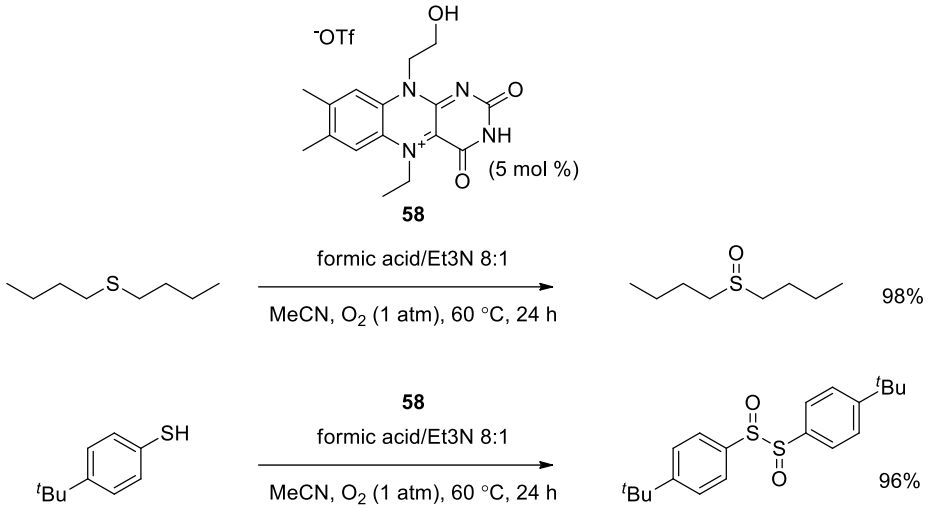

Scheme 24 Triethylamine/formic acid flavin reduction

The Cibulka group succeeded in harnessing flavinium catalysis for the oxidative hydroxylation of substituted arylboronic acids, with a selection of reductants using O_2 as the terminal oxidant to give a diverse range of phenols in high yields.[49] The use of aqueous media as a reaction solvent was favourable due to the poor solubility of many boronic acids, however, the protocol made use of the potentially explosive perchlorate anion (Scheme 25).[50]

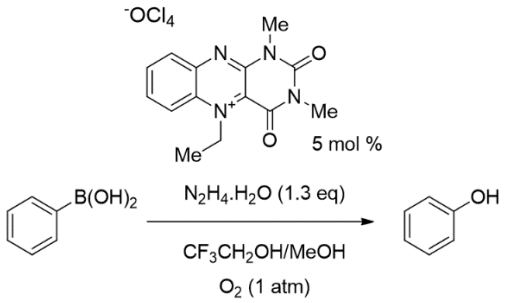

Scheme 25 Arylboronic acids with O_2

1.5. Nucleophilic reactions of flavin hydroperoxides

1.5.1. Baeyer-Villiger Reaction

The majority of the reactions that have been investigated so far have been where the flavin hydroperoxide is behaving as an electrophile. However, there have been several transformations reported where the transformation relies upon nucleophilic attack from the hydroperoxide moiety. The most well-known of these transformations is the Baeyer-Villiger oxidation (BV), which is frequently performed using a peracid such as *m*CPBA to oxidise ketones and aldehydes (Scheme 26).[51]

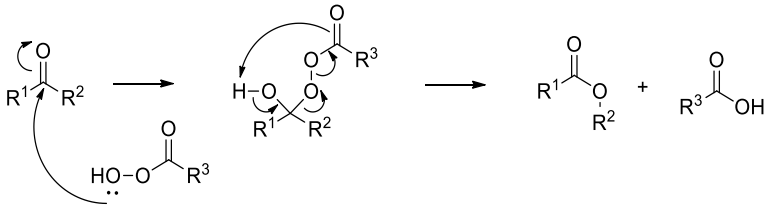

Scheme 26 General Baeyer-Villiger oxidation with peracid

Furstoss *et al.* used a perchlorate flavinium to catalyse the Baeyer-Villiger oxidation of cyclobutanones to λ-lactones.[52] The use of hydrogen peroxide as terminal oxidant allowed them to generate the product in good yields with short reaction times (Scheme 27).

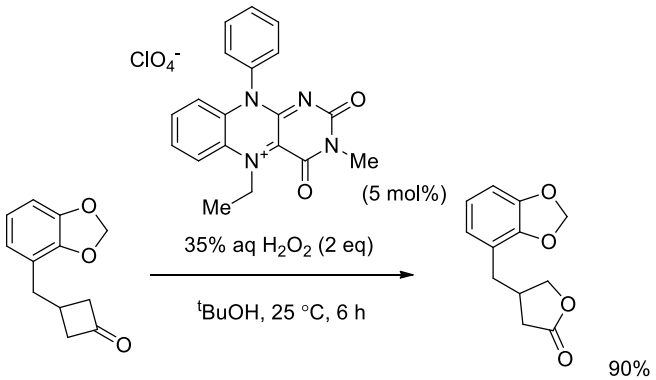

Scheme 27 Furstoss' cycloobutanone ring expansion with H_2O_2

The group were also able to achieve ring expansion of the significantly less strained 2-methoxycyclohexanone, albeit a longer reaction time of 24 h was required to obtain a 45 % yield.

This Furstoss preparation is similar to the Baeyer-Villiger oxidation of cyclobutanone to lactone achieved by the Cibulka group using the valinol-derived flavinium catalyst (Scheme 28). This is assisted by the ring strain from the 4-membered system making ring expansion favourable.[45] Cibulka *et al.* did not report any *e.e.* in the lactone product, and only starting material was recovered from the non-catalysed experiment.

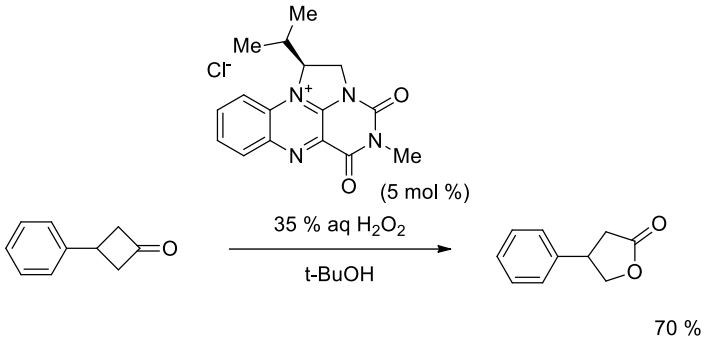

Scheme 28 Bayer-Villiger reported by Cibulka *et al.*[45]

The proposed reaction mechanism is initiated by the attack from the nucleophilic hydroperoxyflavin to the carbon of the carbonyl of the starting material **59**. This creates a transition state where the substrate is bound to the flavin catalyst, through the hydroperoxide unit **60**, in contrast to the electrophilic reaction mechanism the breaking of the oxygen-oxygen bond is normally concerted (Scheme 29).

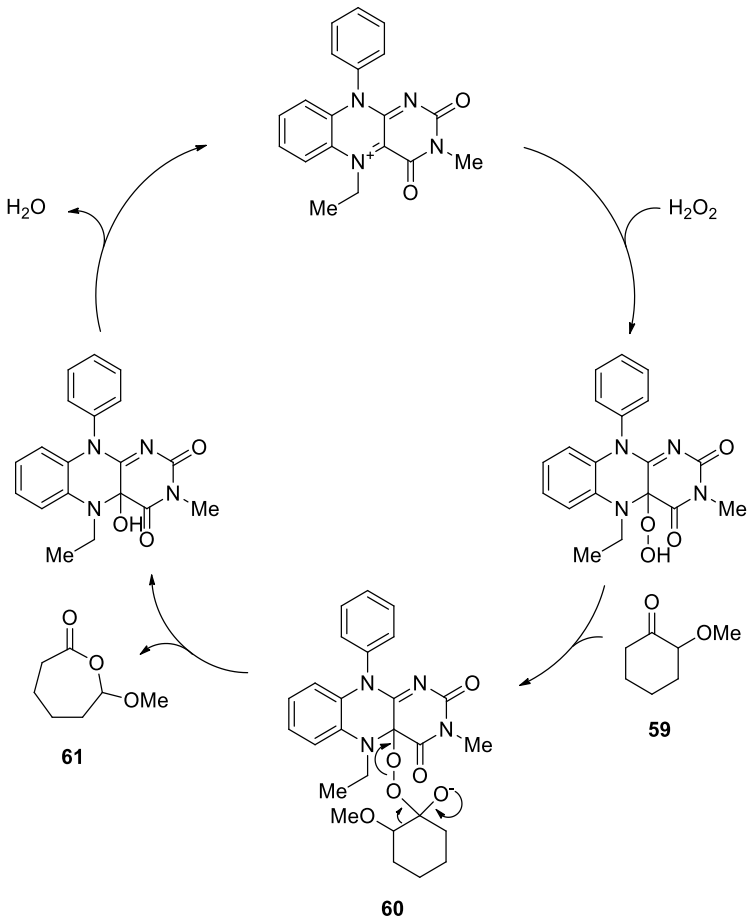

Scheme 29 General nucleophilic BV reaction

The lone pair of the oxygen then reforms then oxygen-carbon double bond, which breaks the carbon-carbon bond, and subsequently breaks the oxygen-oxygen bond, liberating the product **61**. Water is then released from the flavin, and the active catalyst is reformed upon rearomatisation.

The Baeyer-Villiger oxidation was also investigated by Murahashi *et al*. who prepared a synthetic flavin **62** in just 4 steps from natural (-)-riboflavin for the preparation of lactone with molecular oxygen acting as the oxidant and zinc dust as the reductant (Scheme 30).

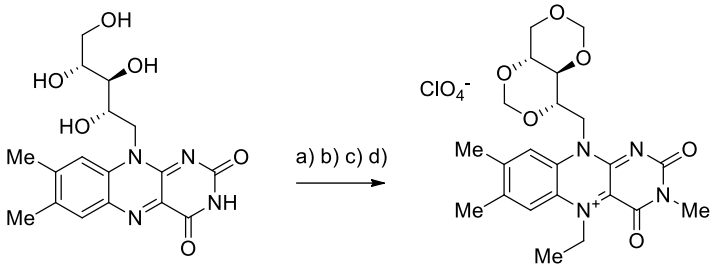

62

a) HCHO, HCl, 60 °C, 3 days; b) CH_3I, K_2CO_3, DMF, RT, overnight;
c) CH_3CHO, $NaBH_3CN$, $Na_2S_2O_4$, DMF, 60 °C, 2 h; d) $NaNO_2$, $HClO_4$, $NaClO_4$, 0 °C.

Scheme 30 Catalyst preparation from riboflavin in 4 steps

They found that their developed catalyst was able to form the ring expanded product in good yields in the presence of zinc and molecular oxygen (Scheme 31). Although the authors make no comment, it is possible that the mechanism for increased reaction rate is due to sulfide complexation with Zn.

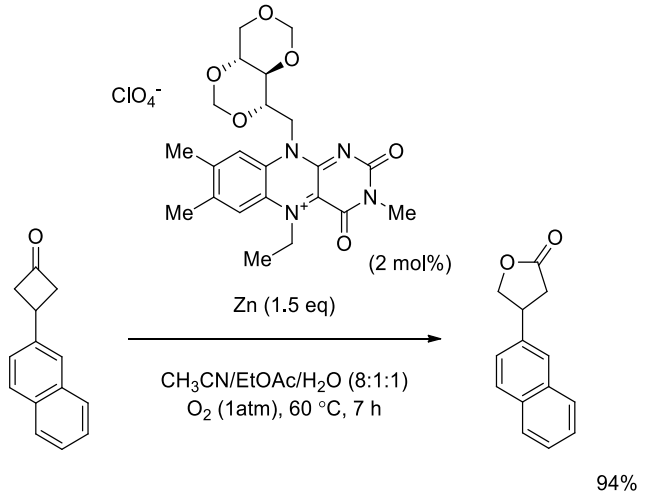

Scheme 31 Lactone preparation with zinc and O_2

The group examined the preference for the nucleophilic and electrophilic mechanisms by performing a competing reaction with naphthalene substituted cyclobutanone and methyl(*p*-tolyl)sulfide. They found that the protocol heavily favoured the formation of the lactone product over the sulfoxide (Scheme 32).

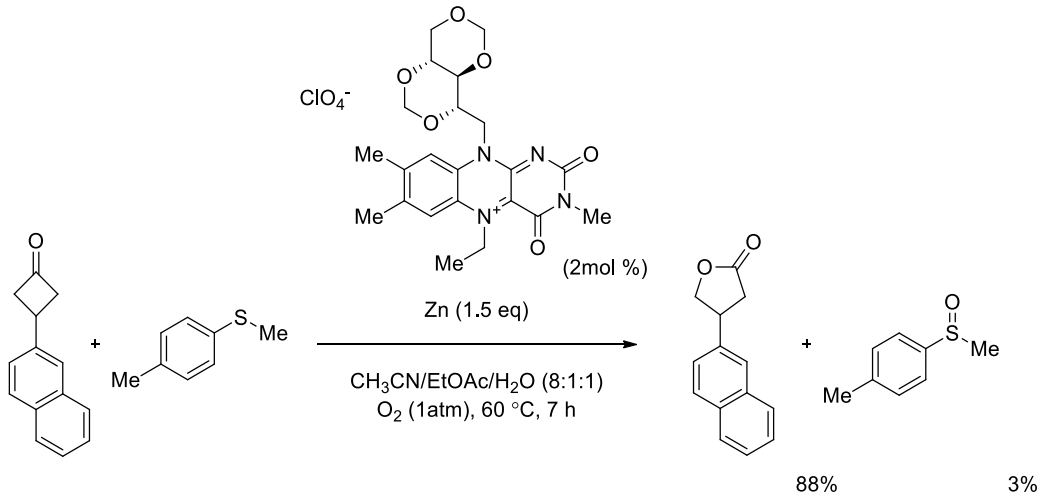

Scheme 32 Demonstrating Zn flavin reduction results in an electrophilic reaction mechanism

Upon formation of the hydroperoxy flavin with hydrogen peroxide (instead of Zn/O_2) or when the non-nucleophilic solvent trifluoroethanol is used, the preference for nucleophilic oxidation is reversed, with sulfoxide formation taking precedence (

Scheme 33). The authors used conditions previously reported by Mazzini *et al.* with their own catalyst to measure selectivity.[52]

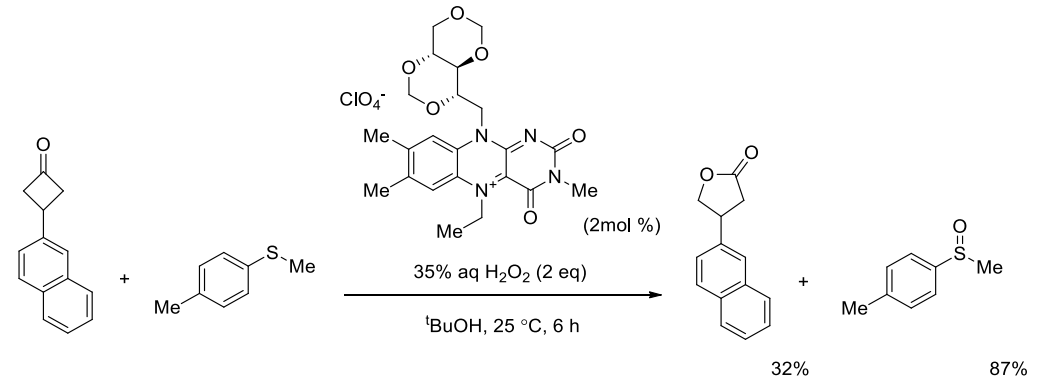

Scheme 33 Demonstrating hydroperoxyflavin formed with H_2O_2 results in an electrophilic reaction mechanism

Through extensive stopped flow studies the authors rationalised this observation through the formation of the hydroperoxyflavin (FlEtOOH) undergoing oxidation of the sulfide, resulting in the hydroxyflavin (FlEtOH) (Scheme 34).[42]

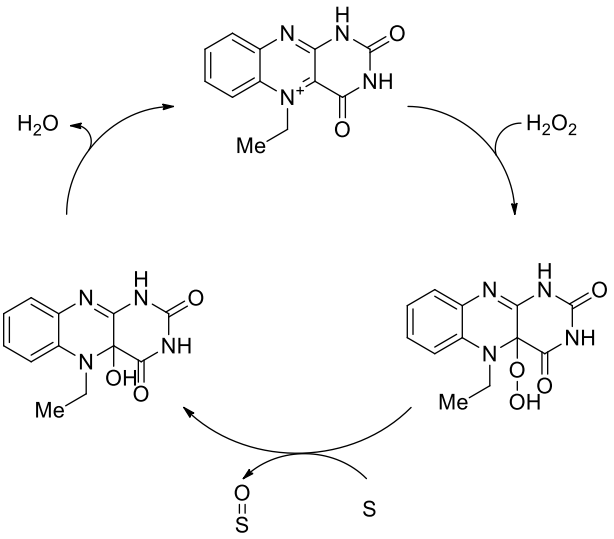

Scheme 34 Flavin and hydrogen peroxide catalytic cycle

The flavinium ion undergoes attack by the nucleophilic hydrogen peroxide, forming the hydroperoxyflavin, which is then prone to nucleophilic attack by the sulfide. The active catalyst is then regenerated through dehydration.

This is in contrast to the nucleophilic reaction where the authors postulate that the zinc facilitates a two-electron reduction the flavin cation ($FlEt^+$), giving the reduced flavin ($FlEt^-$). Reaction with O_2 yields the peroxyflavin anion $FlEtOO^-$ which shows preference for the oxidation of ketones to give the resulting lactones. The flavin catalyst then undergoes dehydrogenation, generating $FlEt^+$ and completing the catalytic cycle.[53]

1.5.2. Dakin Oxidation

At the University of Texas, the Foss group developed a Dakin oxidation, notably using a neutral hydroperoxy flavin as a catalyst. The protocol relied on stoichiometric amounts of a Hantzsch ester to achieve catalyst turnover with molecular oxygen as an oxidant. This method allowed for the preparation of phenols in good yields, and the group found that the oxidation was proceeded by a nucleophilic reaction mechanism when acetonitrile was used as a solvent.[54]

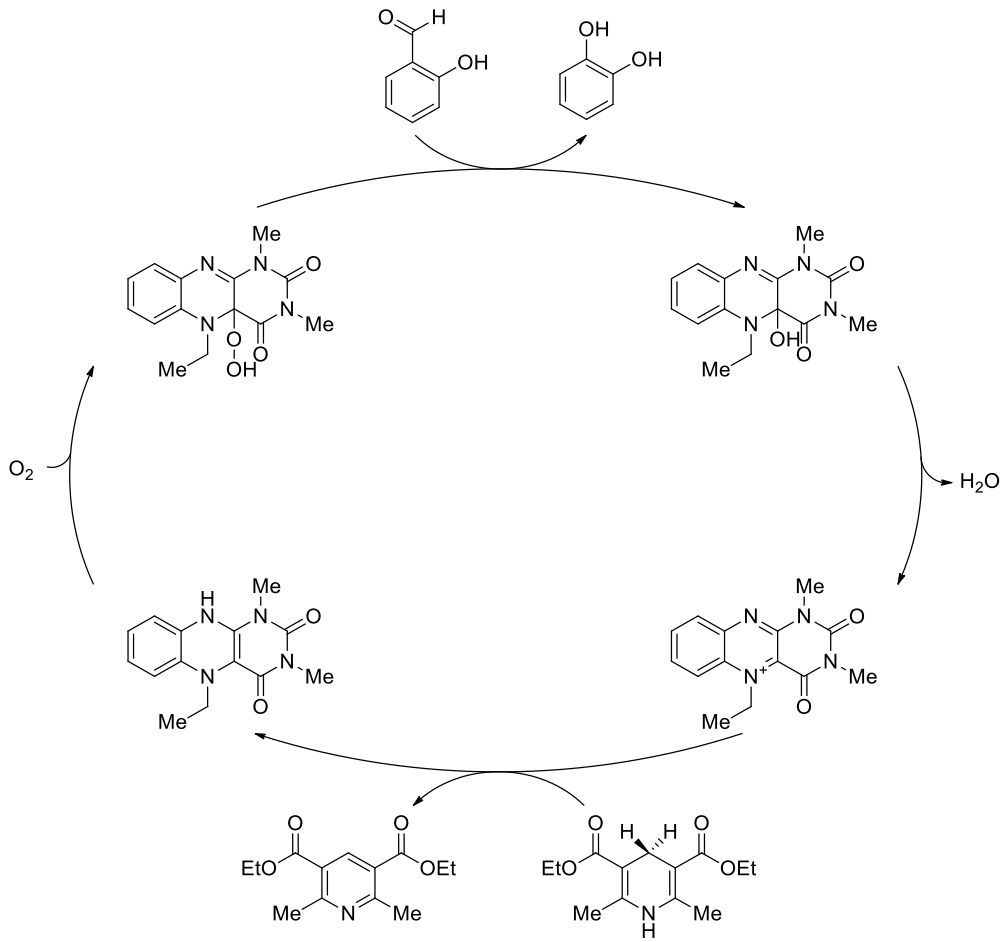

Scheme 35 Hantzsch Ester and Neutral Peropxy Flavin

However, the Foss group also noted that when TFE was used as a solvent, the selectivity could be switched to electrophilic addition. The authors attribute this switch in selectivity to the hydrogen bonding ability of the solvent acting to stabilize the *O-O* bond of the hydroperoxyl flavin during cleavage.

1.6. Photoactive flavin catalysed oxidation

The photolytic properties of flavins have investigated since shortly after the initial discovery of the flavins. Two potential environments exist whereby photochemistry can take place: photoreduction (reaction in the presence of external electron donors) and photobleaching (reaction in the absence of an electron donor).[55] Photobleaching is an irreversible process, making it unsuitable as a mechanism for catalysis, meaning that external electron donors must be used.[56]

The absorption spectra of riboflavin shows significant absorption between 300 and 500 nm, with the $\pi \rightarrow \pi^*$ transition at 440 nm, making visible light the optimum source for excitation of the flavin (Figure 4).[57] The excited flavin species has greater oxidising character than the flavin in the ground state allowing it to more readily oxidise a substrate. After oxidation the reduced flavin is then reoxidized by O_2 in air, generating H_2O_2.

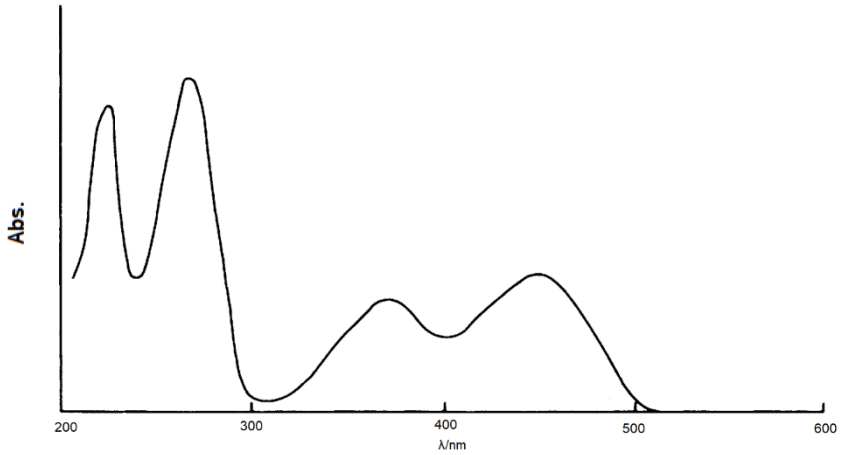

Figure 4 The absorption spectra of riboflavin in an aqueous solution[57]

In 2010, Lechner and König demonstrated the oxidation of amines to aldehydes and ketones by flavins excited at 440 nm by LED sources. The use of visible light allowed them to demonstrate a mild procedure for the acceleration of amine oxidations without any evidence of overoxidation to the corresponding acid (Scheme 36).[58] Reaction temperature was not reported, which is important to ensure the absence of thermal effects upon the reaction.

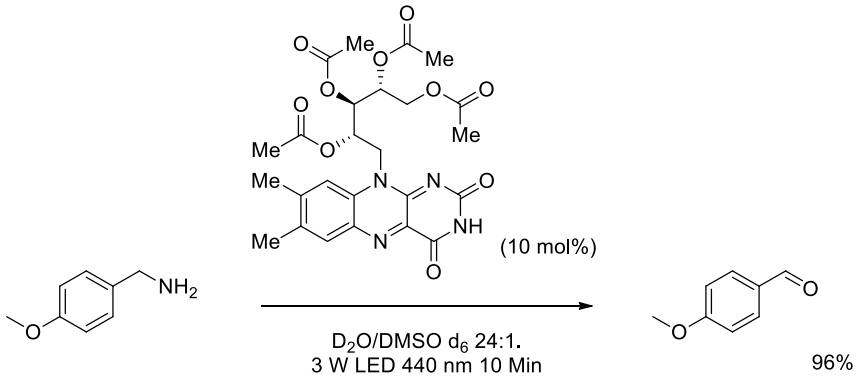

Scheme 36 Lechner and Konig amine oxidation

The group also succeeded in the photocatalytic deprotection of *p*-methoxybenzyl (PMB), with tolerance for alkenes, benzyl-protected esters and alcohols. Both protocols necessitate the presence of benzylic amines with an electron rich aromatic group to facilitate the transformation (Scheme 36).

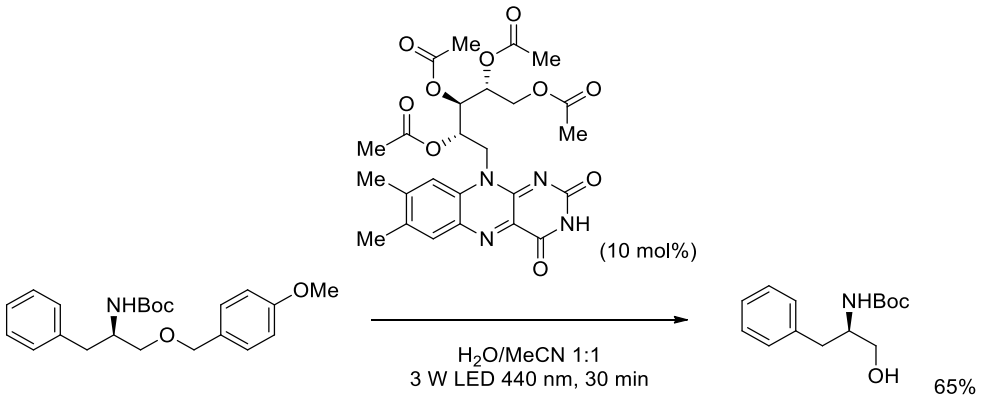

Scheme 37 PMB deprotection

The deprotection protocol was limited to primary amines as the oxidation of secondary amines by the riboflavin tetraacetate could not be controlled.

The König group also developed a procedure for the photooxidation of alcohols, again using O_2 as a terminal oxidant. The group investigated the effect of both covalently bound thiourea and the use of thiourea as an additive and found significant improvement in turnover numbers. Using thiourea as an additive led to an increase in turnover number of 95, however when substituting thiourea functionality onto the flavin, turnover numbers of up to 580 were seen. The authors attributed to the ability of the thiourea to act as an electron-transfer mediator for the photooxidation of the initial alcohol (Scheme 38).[59]

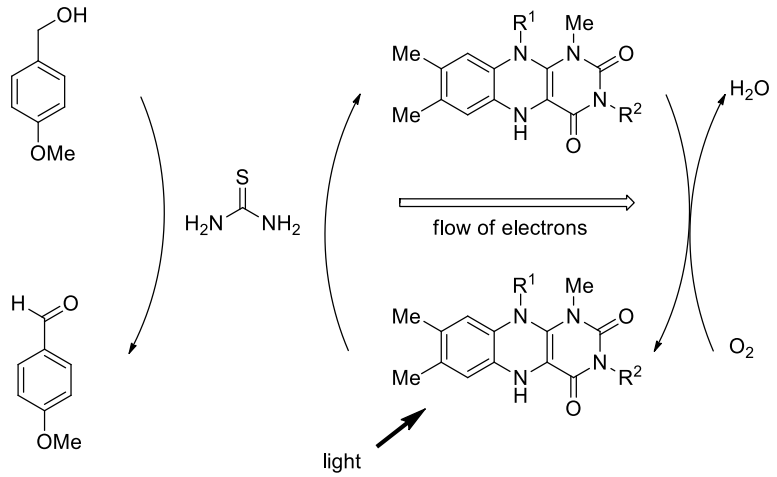

Scheme 38 Thiourea-mediated photooxidation of 4-methoxybenzyl alcohol

They then expanded the scope of the oxidation of alcohols by succeeding in immobilising the flavin on a silica gel solid support (Table 2). The solid support had an impact on turnover numbers when the thiourea substituted flavin was used (from 580 to 10).

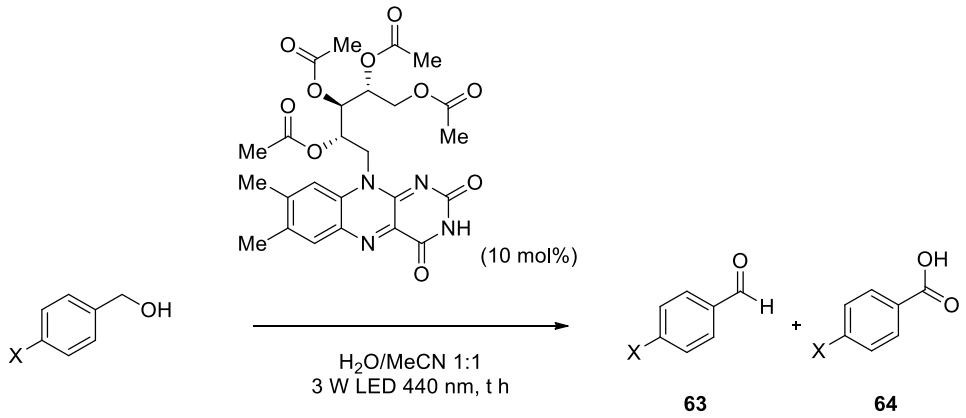

Table 2 Expanded scope of the oxidation of alcohols

Entry	X	t (h)	63	64
1	OMe	2	71	19
2	OMe	1	83	17
3	OMe	0.25	65	3
4	Me	2	41	9
5	H	2	44	0
6	COOMe	2	36	0
7	COOH	2	24	0

The authors were able to achieve acceptable turnover numbers (280) with a riboflavin derived catalyst and good stability which could be used for 3 reaction cycles without drop off in catalytic activity. Immobilisation also resulted in the overoxidation of aldehyde to the corresponding carboxylic acid, however, the authors were able to minimise this through shortened reaction times. [60]

1.7. Asymmetric flavin catalysis

The first example of an asymmetric oxygen transfer reaction by a synthetic flavin was reported by Toda *et al*. who developed a new cyclic flavin with axial chirality. The group successfully demonstrated the oxidation of sulfides to the corresponding sulfoxide. The cyclophane bridge of the flavin inhibits the formation of the hydroperoxy flavin on that face, causing oxygen transfer to occur from a single flavin face. The authors postulated that the reaction proceeds *via* an electrophilic reaction mechanism, due to the poor yield when the aromatic ring is substituted with the strongly electron withdrawing cyano substituent. An

enantiomeric excess of 65% was achieved with the substrate 4-(methylthio)toluene (Scheme 39).[61]

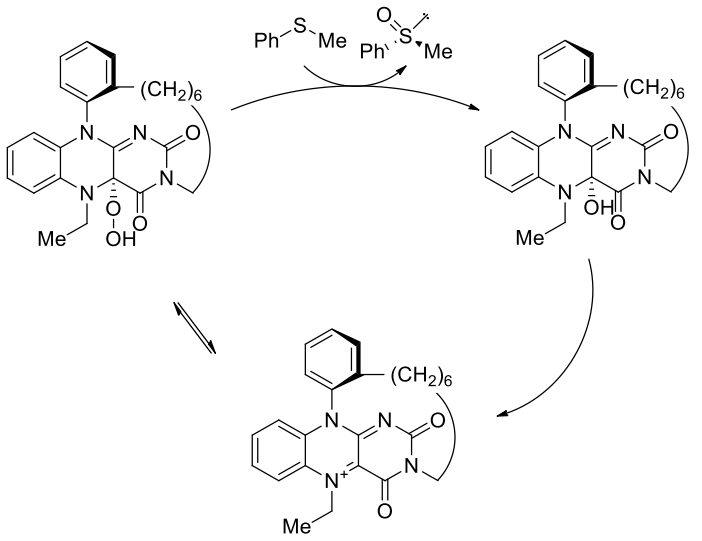

Scheme 39 First example of asymmetric flavin catalysis

Murahashi *et al*. developed a similar strategy for chiral flavin catalysis again utilising a cyclophane bridge for the transformation of naphthyl sulfide to give the corresponding chiral sulfoxide in excellent yield in 72% *e.e.* (Scheme 40).[62] The conditions were not reported in the review and are labelled as unpublished in the reference.

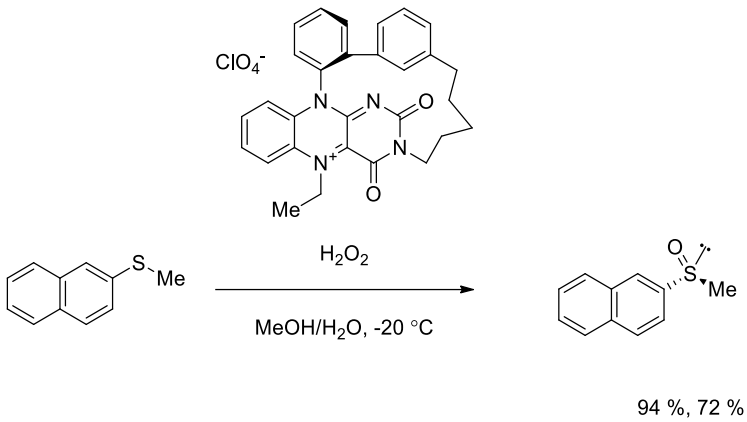

94 %, 72 % *e.e.*

Scheme 40 Murahashi protocol for the oxidation enantiopure oxidation of sulfides

Cibulka and co-workers then expanded the scope of chiral flavinium catalysis by using a perchlorate salt to affect the enantioselective formation of sulfoxides.[63] The oxidation of alkyl aryl sulfides with hydrogen peroxide as oxidant was demonstrated. It was found that the enantiomeric ratio was affected by the chosen solvent system, and unaffected by temperature. The formation of sulfoxides with *e.e.* values ranging from 4 – 54% were demonstrated (Scheme 41).

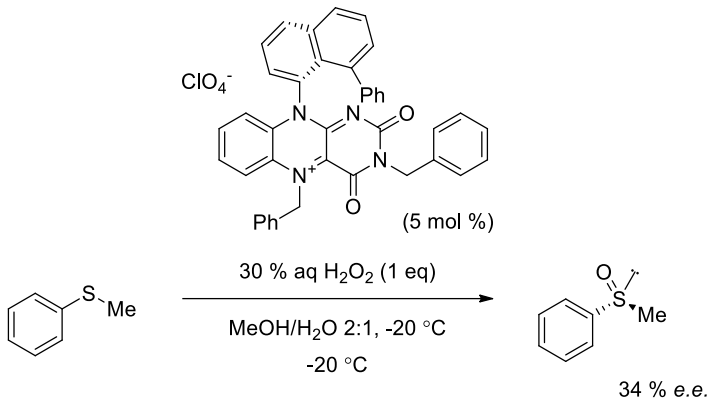

Scheme 41 Cibulka's asymmetric sulfide oxidation

A further successful iteration for asymmetric flavin catalysis was developed for the nucleophilic mechanism with a Baeyer-Villiger reaction. Murahashi and co-workers demonstrated the ring expansion of cyclobutanones with a novel chiral bisflavinium perchlorate catalyst. The developed procedure used hydrogen peroxide, forming the optically active lactones in up to 74% *e.e.* The authors suggested that the C_2-symmetric bisflavin achieves enantioselectiveity by blocking the plane of the other flavin moiety in the system. Enantioselectivity was highly dependent on the solvent system, with protic solvents resulting in high *e.e.* values, although sometimes serving to increase the rate of background or side reactions, which led to the final TFE/MeOH/H_2O solvent system (Scheme 42).[64]

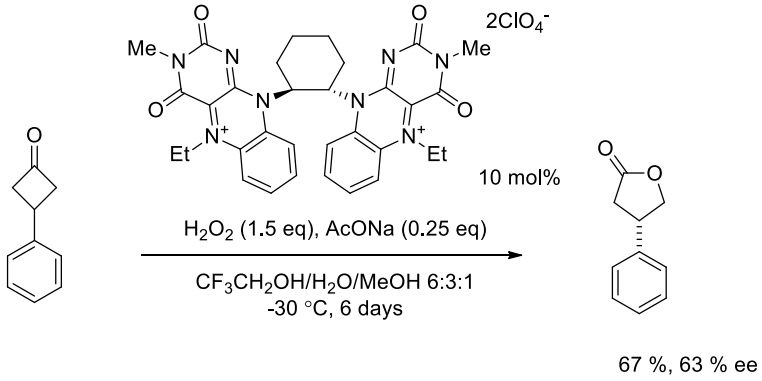

Scheme 42 Murahashi bis flavin

In 2016, Yamamoto *et. al.* developed a range of flavinium catalysts with various bulky substitutions on the bridge (Figure 5), which were then tested for their use in asymmetric Baeyer-Villiger oxidation.[21]

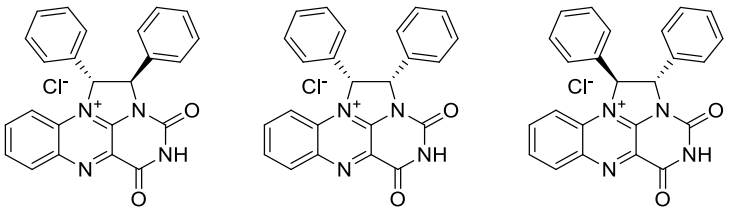

Figure 5 Phenyl groups inserted on the bridge by Yamamoto *et. al.*[21]

The authors found that the introduction of a cinchona derived co-catalyst was essential for enhancing both the catalytic and stereoselectivity, with range of cinchona alkaloids tested (Figure 6).

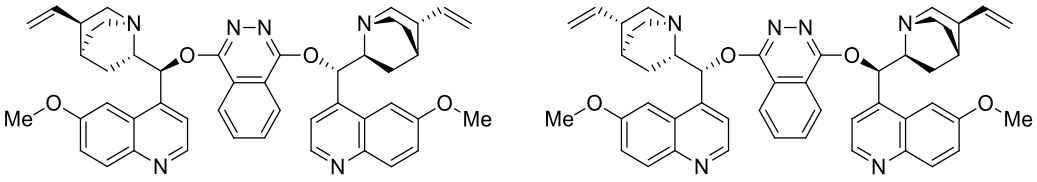

Figure 6 Cinchona alkaloids and their derivatives investigated my Yamamoto *et. al.*

The alkaloids investigated were $(DHQ)_2PHAL$ **68** and $(DHQD)_2PHAL$ **68** and both generated reasonable levels of *e.e.* in preliminary reactions. H_2O_2 was used to generate the active catalytic flavin species and the cinchona species formed an ion pair which was highly successful in generating enantiopure cyclobutanones, with *e.e.*'s of up to 96%, albeit in poor yield (Scheme 43).[21]

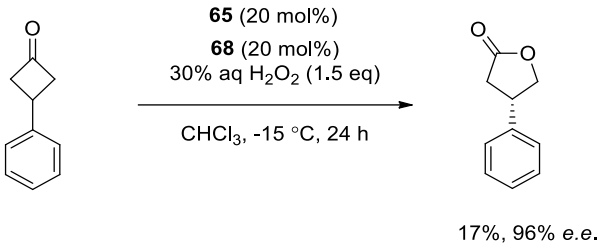

Scheme 43 Flavin ion pair catalysis

By using the antipode of both the flavin catalyst and the cinchona derivative co-catalyst, the group were able to preferentially form the opposite enantiomer in 80% *e.e.* and with a significantly improved yield (Scheme 44).

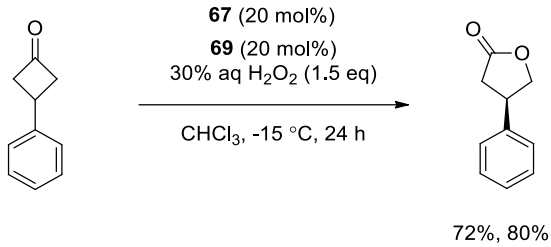

Scheme 44 Using the antipode catalysts to generate the opposite enantiomer

1.8. An Introduction to Sulfoximines

In 1992, Trost recognised the potential power of the sulfoximine moiety, labelling them ''chemical chameleons'' for asymmetric synthesis.[65] This statement was due in part to the quaternary stereogenic centre at the sulfur, and in part to their ability to act as either an electrophile or a nucleophile depending on the conditions (Figure 7).

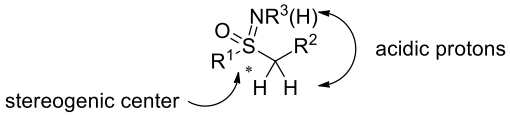

Figure 7 The chemical versatility of sulfoximines

The stereogenic centre on the sulfur makes a compound asymmetric when $R^1 \neq R^2$. The nitrogen of the sulfoximine is both nucleophilic and basic which can allow for further functionalisation and by appending desirable R groups at the C and N atoms to provide additional coordination sites, they can act as chiral ligands, making them useful for metal catalysed transformations. Finally the acidity of the immine hydrogen and H^1 can be tuned by altering the R groups, when R^1 = Ph, R^2 = H, R^3 = H the immine hydrogen is acidic (pK_a ~ 24) and when R^1 = Ph, R^2 = H, R^3 = Me, the pK_a ~ 32.[66,67]

1.8.1. Discovery

Sulfoximines were first discovered when dogs fed with wheat bleached with nitrogen trichloride became ill and died.[68] Investigation into the cause of death led to the isolation of methionine sulfoximine **70** in 1946, and it was subsequently synthesised for the first time in 1952. Canine death made it obvious that this compound was toxic and it was subsequently discovered that buthionine sulfoximine **71** was also toxic (Figure 8).[69] It reduces levels of glutathione, an important antioxidant required in the neutralisation of free radicals in the body and thus causes an increase in oxidative stress.

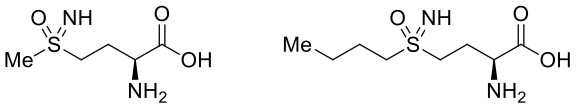

70 **71**

Figure 8 Biologically active sulfoximines

Sulfoximines have been deemed as a neglected opportunity in medicinal chemistry,[70] and exploration of that chemical space is dependent upon the ability to synthesise a range of compounds. Drugs containing the sulfoximine moiety are beginning to make it to clinical trials. Proline-rich tyrosine kinase 2 inhibitors were investigated to target osteoporosis by Pfizer and **72** was found to have high stability in human liver microsomes (HLMs).[71] Researchers at Bayer Pharma AG investigated the pharmacopore in a cyclin-dependent kinase (CDK) inhibitor project, and in phase 1, found **73** to have very potent antiproliferative activity but shows no off-target inhibition (Figure 9).[72]

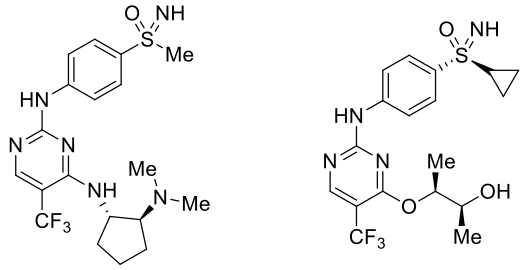

72 **73**

Figure 9 Pharmaceutically relevant compounds with a sulfoximine core

1.8.2. Early Preparation

The first synthesis of a sulfoximine came shortly after the initial isolation of methionine sulfoximine in 1952. The desired diethylsulfoximine **74** was prepared by treatment of diethylsulfoxide with sodium azide and sulfuric acid. The authors postulated hydrazoic acid was formed *in situ* which underwent nucleophilic attack by the sulfide to form the sulfoximine (Scheme 45).[78]

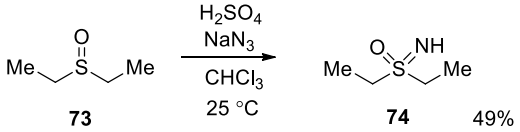

73 **74** 49%

Scheme 45 Sulfoximine synthesis with sodium azide

A significant drawback of this original synthetic method is that the use of sodium azide leads to the (desired) generation of hydrazoic acid, which is a primary explosive as well as a toxic

gas that binds to cytochrome c oxidase, which prevents the binding of oxygen at the active site, causing cell death.[73] Furthermore, this route can lead to partial racemisation in the case of enantiopure sulfoxides.[74]

Several improvements have been made to the original synthesis and Johnson *et al.* succeeding in performing the reaction on a 70 g scale for the formation of racemic methyl phenyl sulfoximine **76** from methyl phenyl sulfoxide **75** (Scheme 46).[75]

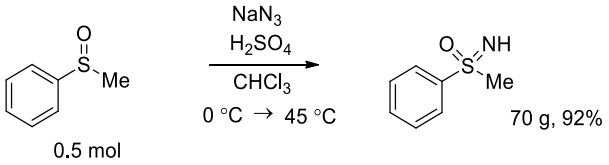

Scheme 46 Large-scale synthesis of methyl phenyl sulfoximine

1.8.3. Current Approaches to Sulfoximines

Sulfoximine synthesis can be divided into two classes (Scheme 47). The first class is preparation *via* sulfur (IV) precursors (sulfoxides and sulfilimines).

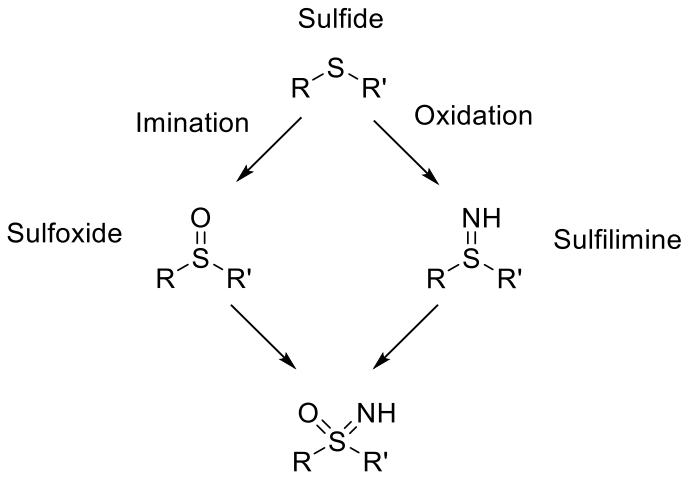

Scheme 47 General routes to sulfoximines via sulfur (IV) precursors

When starting from sulfides, both oxygen transfer and nitrogen transfer must be achieved to form the sulfoximine. Oxygen transfer from sulfides to sulfoxides is far more prevalent in the literature than nitrogen transfer to form sulfilimines, although both routes have been used to prepare sulfoximines.

The second class is preparation from sulfur (VI) compounds (sulfonimidoyl halogenides and sulfonimidates. Access to sulfoximines *via* sulfur (VI) precursors allows access to chiral sulfoximines from cyclic starting sulfinamides (*Scheme* 48).

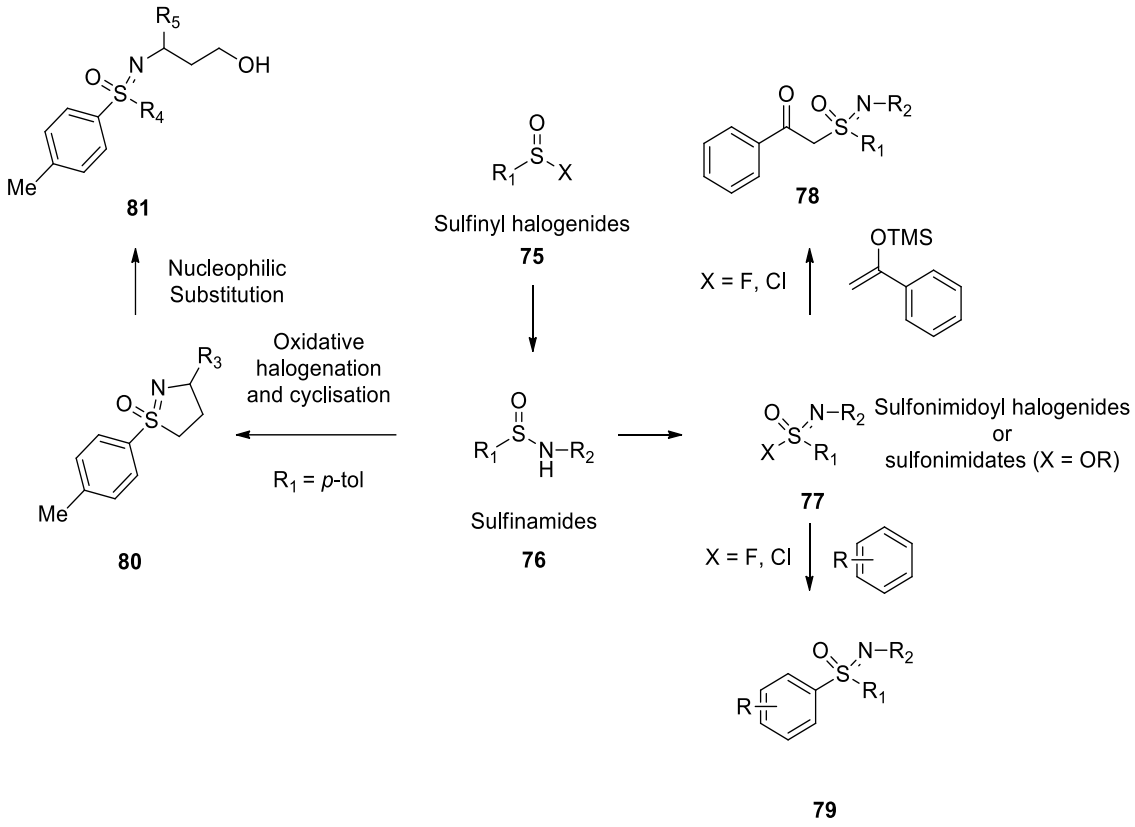

Scheme 48 Routes to sulfoximines via sulfur (VI) precursors

1.9. Sulfoximines from Sulfoxides and Sulfilimines

1.9.1. Access to Tosyl bound *N*-sulfoximines

One method to form sulfoximines is *via* the sulfoxide. The most reliable method to access optically pure sulfoximines from sulfoxides has been found to be through the use of a nitrene reagent which generally proceed with retention of the stereochemistry at the sulfur. Notable examples include iminations involving TsN_3 with copper powder to form optically pure sulfoximines from chiral sulfoxides (

Scheme 49).[76]

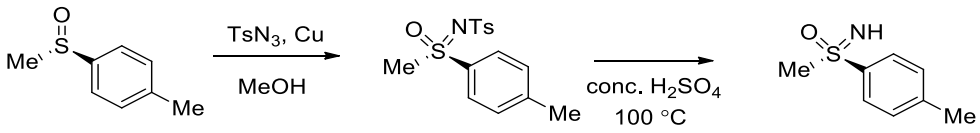

Scheme 49 Using nitrenes to access to sulfoximines

Müller *et al.* developed a highly efficient methodology for the synthesis of enantiopure sulfoximines under mild conditions. The group used CuOTf and a hypervalent iodine species

to give both high yields (79-93%) and very good retention of stereochemistry (98% ee) (Scheme 50).[77]

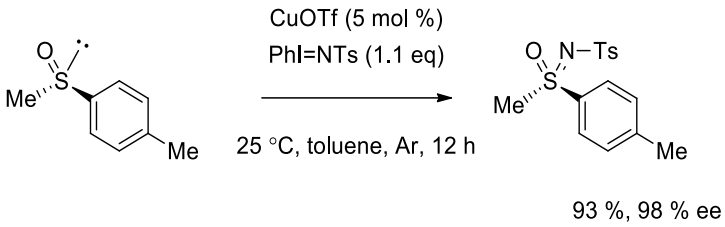

Scheme 50 Müller *et al*.'s demonstration of retention of stereochemistry

However, the authors found it difficult to subsequently remove the *N*-bound tosyl group highlighting a key problem with sulfoximine synthesis in general. It is often necessary to use an *N*- substituent in order to achieve sulfoximine formation, however it is not always facile to subsequently remove the group.

An early tosyl group removal was published in 1989 by Johnson *et al.*,[78] who used sodium anthracenide to give good yields of the aryl N-H sulfoximine **82 - 85** (Scheme 51).

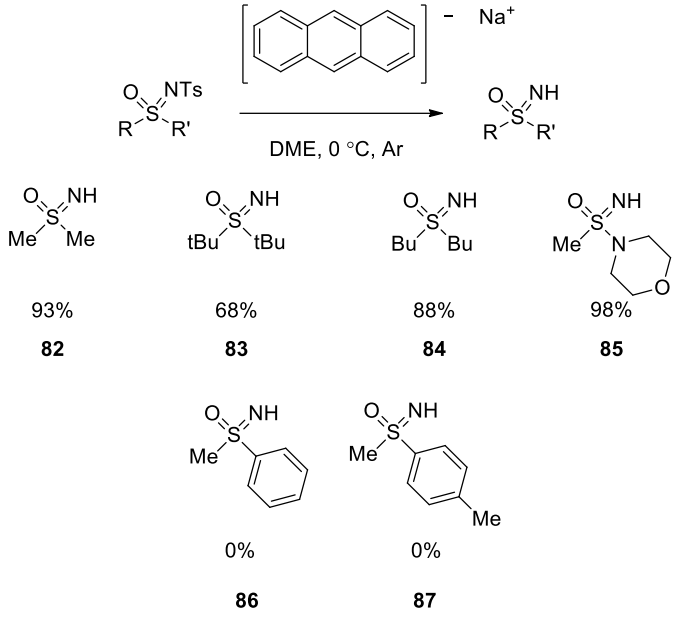

Scheme 51 Efficient removal of N-bound tosyl groups

However, this method proved to only be successful towards dialkyl substituted sulfoximines, with no effect towards aromatic substituted sulfoximines **86, 87**.

It would be preferable to develop methods to synthesise sulfoximines with an N-H group, as this would both increase step economy and allow greater scope, making the new method ideal for the synthesis of compounds for industry, especially pharmaceuticals. Synthetic methods for the removal of other substituents have been developed with some success,

notably the removal of a Boc protecting group with trifluoroacetic acid proceeds in high yields under mild conditions.[79]

1.9.2. Access to cyano bound *N*-sulfoximines

A further synthetic route to sulfoximines from sulfides, is *via* sulfilimines. Mancheno *et al.* used NBS and cyanamide to access the desired *N*-cyano sulfilimine (Table 3).[80] They also observed sulfoxide formation as a side-product, but found this could be prevented by careful control of the reaction conditions.

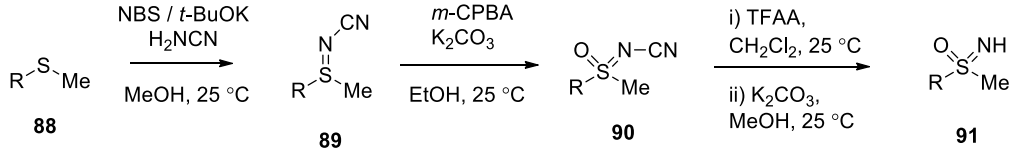

Table 3 Access to free sulfoximines via cyano N-bound sulfilimine

Entry	R	Yield (%)
1	C_6H_5	66
2	4-OMe-C_6H_4	94
3	*4*-NO_2-C_6H_4	39
4	2- C_5NH_4	51
5	2-Naphyl	83

This reaction led to very good yields for the formation of the sulfilimine. The high number of steps needed to access the N-H sulfoximine sometimes led to poor overall yield (entry 3). However, this synthetic route was later used to prepare sulfoximines on the multi gram scale.[81]

1.9.3. Direct access to N-H sulfoximines

Significant efforts have been made to synthesise enantiomerically pure sulfoximines. A versatile methodology was developed by Tamura *et al*. who treated sulfoxides **91** the iminating agent, *o*-mesitylenesulfonyl-hydroxylamine (MSH) **92** to form sulfoximine salts **93**, which were then converted in high yields to the desired sulfoximine **94**, by treatment with sodium methoxide (Table 4).[82]

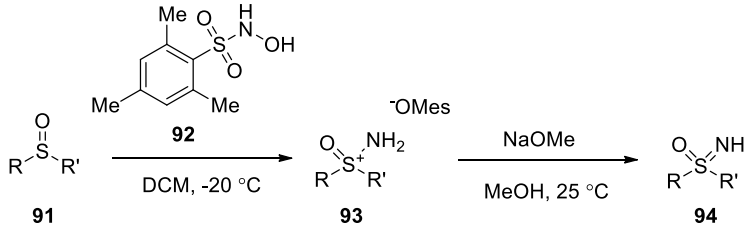

Table 4 Access to free NH-Sulfoximine

Entry	R	R'	Yield (%)
1	CH_3	CH_3	66
2	$N\equiv C\text{-}C_2H_4$	$N\equiv C\text{-}C_2H_4$	76
3	$HO\text{-}C_2H_4$	$HO\text{-}C_2H_4$	83
4	C_6H_5	$Cl\text{-}C_3H_6$	82
5	C_6H_5	$HC\equiv C-CH_2$	73

This synthesis gave easy access to a range of sulfoximines under mild conditions. However, despite MSH having the same disadvantages as hydrazoic acid, namely its unstable nature,[83] it should not be overlooked as a reagent.[84]

1.9.4. Access to Sulfoximines *via* imination of sulfoxides

Sulfilimines are most commonly accessed by oxidative imination from sulfides, but can be accessed by imination of sulfoxides, and the stereochemistry can be controlled through inversion (Scheme 52a) or retention (Scheme 52b).[85]

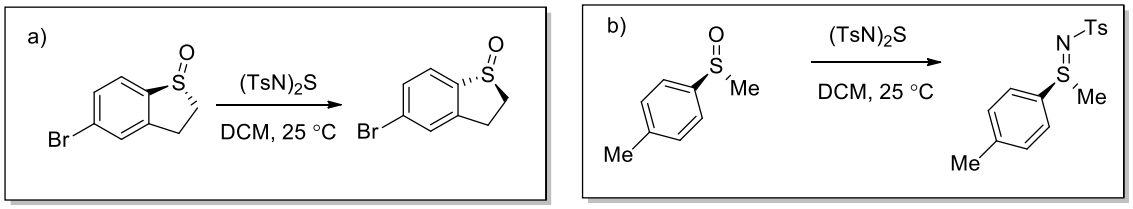

Scheme 52 Obtaining sulfilimines from sulfoxides

This route can provide the opportunity to obtain enantiopure sulfilimines from optically active sulfoxides.[86] The sulfilimine can then be oxidised with $KMnO_4$ with retention of stereochemistry to give enantiopure sulfoximines (Scheme 53). This oxidation is also possible with *m*-CPBA[87] or H_2O_2.[88]

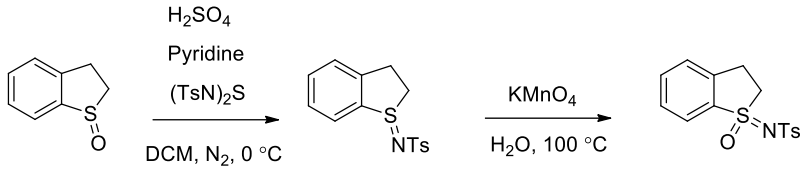

Scheme 53 Preparation of sulfilimines from sulfoxides

Sabol *et al.* showed that imination of sulfoxides does proceed with the inversion of stereochemistry from the sulfoxides to the sulfilimine, when *p*-toluenesulfonamide was used as an iminating agent in the presence of phosphorous pentoxide and triethylamine (Scheme 54).[89] This transformation ultimately allows retention of stereochemistry of the initial sulfoxide as the inversion step is substitution, not addition.

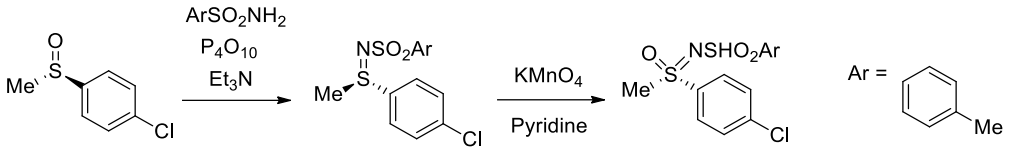

Scheme 54 Sulfoxide to sulfoximine transformation via sulfilimine with retention of stereochemistry wrt sulfoxide

Christensen found that *N,N'*-bis(toluene-*p*-sulfonyl)sulfur diimide **95** could act as an iminating agent for optically active sulfoxides to yield inversion of stereochemistry in the corresponding sulfilimine (Table 5). However he also demonstrated that stereochemistry could be controlled by the solvent system, to retain the stereochemistry of the sulfoxide (entries 2 and 4).[90]

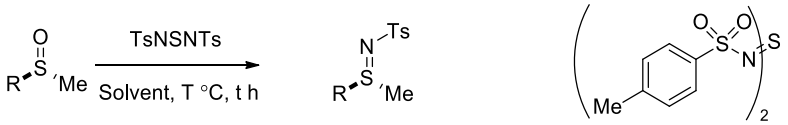

95

Table 5 Facile access to sulfoximines from sulfonimidoyl halogenides

Entry	R	Solvent	t (h)	T (°C)	Yield (%)	Stereochemistry
1	4-Me-C_6H_4	pyridine	18	22	93	Inversion 95:3
2	4-Me-C_6H_4	benzene	18	22	95	Retention 95:3
3	C_4H_9	pyridine	1	-15	88	Inversion >94
4	C_4H_9	benzene	0.7	23	97	Retention 88-94

This result is significant as it can be used to generate enantiopure sulfoximines from the non-racemic sulfoxide precursor with control of stereochemistry. The mechanisms for inversion

or retention have been previously discussed,[91] however, the authors do not elaborate on the effect that the solvent has upon this transformation.

1.9.5. Access to Sulfoximines from sulfonimidoyl halogenides and sulfonimidates

Generation of sulfoximines from sulfur (IV) precursors (sulfoxides and sulfilimines) is a method that fundamentally relies on generation of enantiopure sulfoxides. This is possible by a variety of approaches, including metal catalysed,[92] non-metal catalysed reactions,[93] and kinetic resolutions.[94] If the need for enantiopure sulfoxides is to be avoided then sulfoximine synthesis must instead be approached from sulfur (VI) precursors such as sulfonimidoyl halogenides and sulfonimidates.

Methodology already in place for the preparation of sulfoximines from sulfur (IV) precursors, meant that synthetic routes from sulfur (VI) precursors must be facile, or allow access to a range of sulfoximines that are otherwise inaccessible. Sulfinamides can be prepared from sulfinyl chlorides[95] which can be oxidised by various sources of electrophilic chlorine to form sulfonimidoyl chlorides.[96] The sulfonimidoyl fluoride can then function as the electrophile in a Friedel-Crafts reaction to yield sulfoximines (Table 6).[97]

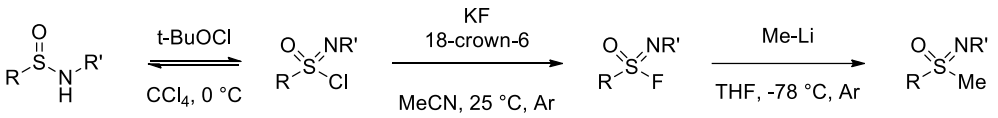

Table 6 Facile access to sulfoximines from sulfonimidoyl halogenides

Entry	R	R'	Yield (%)
1	C_6H_5	4-Cl-C_6H_4	79
2	C_6H_5	4-MeO-C_6H_4	84
3	C_6H_5	2-pyridyl	84
4	C_6H_5	C_6H_5	95
5	1-naphthyl	Me	95

This route, discussed by Johnson *et al.* crucially allows the synthesis of a range of N bound substituents (entries 1-5). However, the NH-sulfoximine was not directly accessible.

In general, sulfonimidoyl chlorides are highly susceptible to reduction and consequently cannot be used with main group organometallics such as organolithium or Grignard reagents.

Harmata, however, developed an organoaluminium mediated technique for the transfer of ethyl groups with good to excellent yields of a range of functional groups (Table 7).[98]

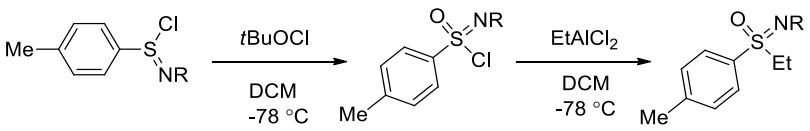

Table 7 Demonstrating resistance to organometallic mediated reduction.

Entry	R	Yield (%)
1	C_6H_5	94
2	2-CH_3-C_6H_4	75
3	2-Br-C_6H_4	83
4	2-NO_2-C_6H_4	76
5	CH_2-C_6H_4	63

Notably, as the yield is often poor for organometallic reduction, the *para*-nitro yield is also very good (entry 4)

1.9.6. Kinetic resolution to give optically active sulfoximines

A key step towards the synthesis of chiral sulfoximines is the preparation of enantiopure starting material. Preparation of the corresponding precursor on large scales can be difficult and consequently a method to form optically active sulfoximines has been demonstrated *via* the synthesis of a racemic starting material, *N*-methyl-*N*-phenylsulfoximine. This racemate can then be resolved with camphorsulfonic acid **97** giving the enantiopure sulfoximine (Scheme 55).[99,100]

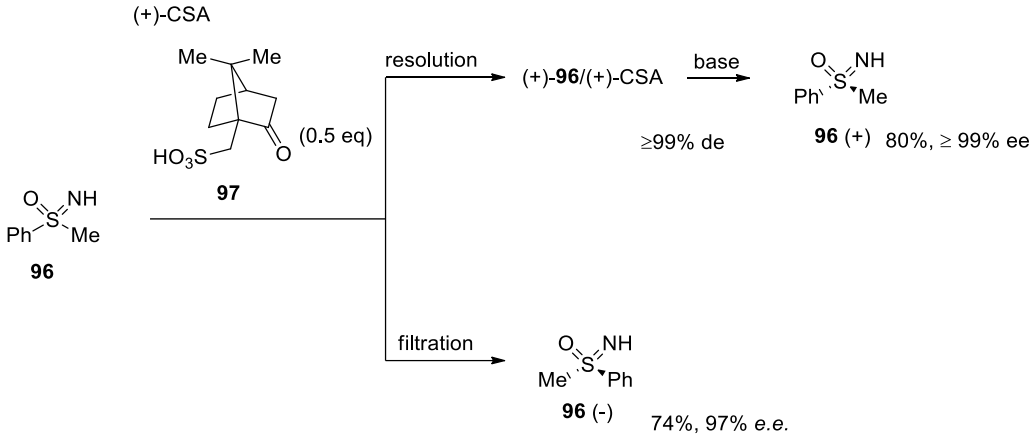

Scheme 55 Resolution with camphorsulfonic acid

The *e.e.* values are excellent for both enantiomers, however, as with any kinetic resolution, maximum yield is limited to 50 % in each case.

This method has seen multiple improvements and is now used for mole scale kinetic resolution. However, it is yet to be efficiently applied to the separation of any chiral sulfoximines other than methyl phenyl sulfoximine.[101]

1.10. Metal catalysed imination using iminoiodinanes

Sulfoximine synthesis has improved significantly since their initial discovery and isolation in the early 1950s. The methods explored thus far in this introduction have been largely metal-free. Historically, the primary difficulty with metal-mediated synthesis is that they often result in *N*-substituted sulfoximines. As previously mentioned, in many cases this *N*-bound substituent is difficult to remove in order to give the synthetically useful sulfoximine.

In 1998 Bach *et. al.* were able to form Boc protected sulfoximines **98** with $FeCl_2$ catalysed iminations (Table 8).[102] While the Boc group proved easy to remove, the catalytic system was limited by poor catalytic efficiency, and the use of toxic and unstable Boc azide.

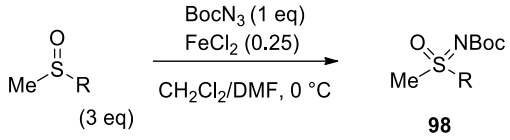

Table 8 Facile access to sulfoximines from sulfonimidoyl halogenides

Entry	R	Yield (%)
1	Bn	70
2	Ph	45
3	Me	64
4	4-OMe-C_6H_4	52

In 2006 the use of $Fe(acac)_3$ (Table 9) was found to be significantly more efficient than previous Fe(II) catalysed reactions, when 4-Nitrobenzenesulfonamide **99** was used as a nitrogen source.[103] This synthetic method didn't suffer from either the high catalyst loadings or high equivalents of the nucleophilic sulfoxide previously reported with Fe(II) catalysis.

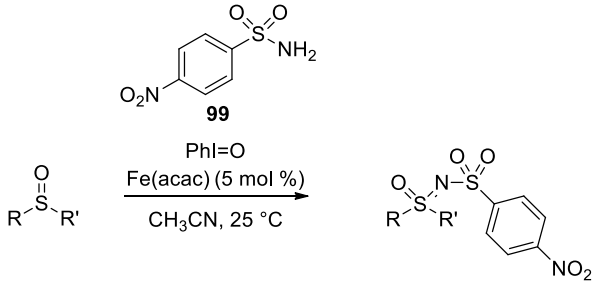

Table 9 $Fe(acac)_3$ catalysed sulfoximine formation

Entry	R	R'	T (h)	Yield (%)
1	Ph	Me	1	96
2	*t*-Bu	Me	2	80
3	Ph	Ph	6	80
4	Ph	Vinyl	8	72

This reaction tolerated aromatic and aliphatic groups well (entries 2 and 3). However, imination of heteroaromatic sulfoxides bearing bulky substituents was unsatisfactory using this method. The group did manage to access optically pure sulfoximines in good yields and with conservation of enantiomeric purity (Scheme 56).

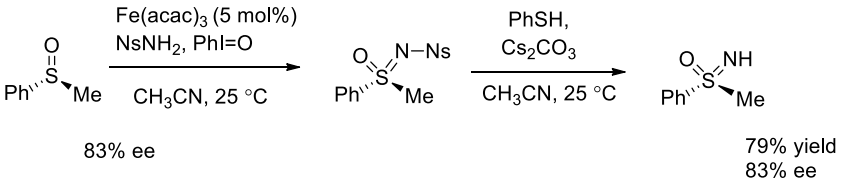

Scheme 56 Fe(III) catalysed synthesis of enantiopure sulfoximines

The same group managed to access substrates bearing bulky substituents or heteroaromatic substrates by using $Fe(OTf)_2$ and PhI=NNs **100**.[104] The catalyst was easily prepared from iron powder and trifluoromethanesulfonic acid, and could be used with low catalyst loading of 2.5 % (Table 10). The Ns group was not removable and the synthetically useful NH-sulfoximine was not accessible *via* this method.

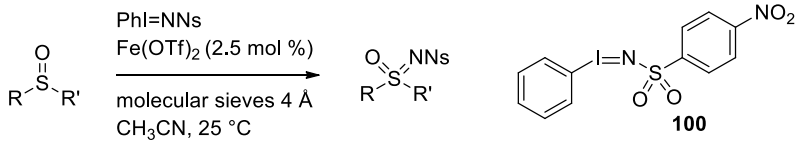

Table 10 Fe(II) catalysed access to bulky substituents and heteroaromatic substrates

Entry	R	R'	Product	Yield (%)
1	Bn	C_6H_5	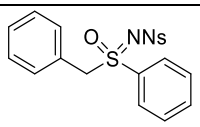	96
2	2-OMe-C_6H_4	C_6H_5	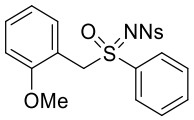	96
3	*i*-Pr	*i*-Pr	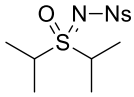	60
4	*t*-Bu	C_6H_5	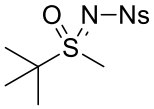	86

In 2002 several reports were published employing the catalyst CuOTf as a copper catalyst. Cu(I) systems were shown to work well for the synthesis of *N*-tosyl sulfoximines, however CuOTf was expensive and needed to be handled in a glovebox as it is hygroscopic.[105]

The first publication using the more stable, cheaper Cu(II) catalyst came from Malacria *et al.*in 2002. Using copper(II) triflate and N-tosyliminophenyl-iodinane (PhI=NTs), this group were able to demonstrate a wide substrate scope to give N-Ts sulfoximines in good yields (Scheme 57).

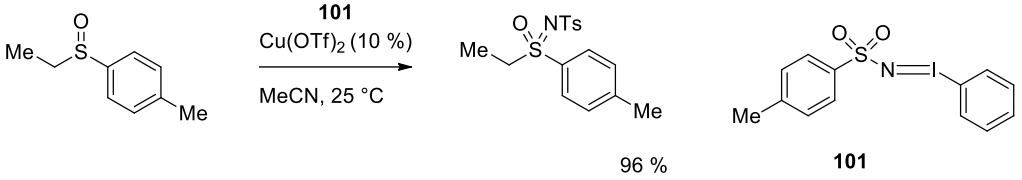

Scheme 57 Cu(II) catalysed sulfoximine synthesis

Having demonstrated that iodinanes could be employed as an iminating reagent under mild conditions, their use was soon expanded to form sulfoximines with a range of metal catalysis. Bolm *et al.* discovered a mild oxidative rhodium catalysed imination, crucially demonstrating removal of the *N-t*rifluoroacetyl group to give the NH-sulfoximine (Table 11).[106]

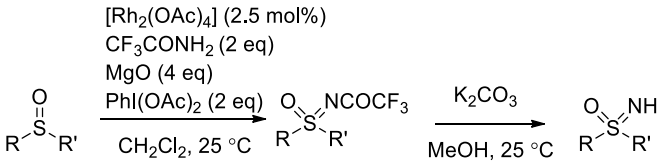

Table 11 Rh(II) catalysed access to sulfoximines

Entry	R	R'	Free Sulfoximine Yield (%)
1	C_6H_5	Me	71
2	C_6H_5	C_6H_5	68
3	-[CH_2CH_2]$_2$-		88
4	4-Me-C_6H_4	Me	76

Recently, the first metal catalysed direct synthesis of NH-sulfoximines has been achieved using Rh(II) and O-(2,4-dinitrophenyl)hydroxylamine (Table 12).[107]

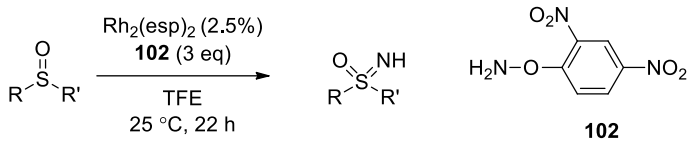

Table 12 Direct Rh(II) Synthesis of free sulfoximines

Entry	R	R’	Yield
1	C_6H_5	Me	78
2	4-C_6H_4	Me	84
3	4-Cl-C_6H_4	Me	90
4	4-$COCH_3$-C_6H_4	Me	58
5	Naphthyl	Me	38

The group were able to synthesise a range of NH-sulfoximines in mostly good yields. The ability to synthesise the free sulfoximine directly is a significant step forward in the synthesis of sulfoximines, however metal catalysis can be prohibitively expensive for large scale; for example the cost of $Rh_2(esp)_2$, is over £300 g^{-1}.

An alternate iodinane approach was discovered by Cho *et al*. They used silver nitrate in combination with 4,4′,4″-tri-*tert*-butyl-2,2′:6′,2″-terpyridine (*t*Bu_3tpy) to replace rhodium, a far cheaper alternative (Table 13).[108]

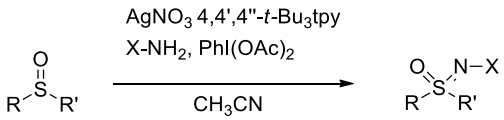

Table 13 Ag(I) catalysed access to protected sulfoximines

Entry	R	R’	X	Yield (%)
1	C_6H_5	C_6H_5	Ns	98
2	-[CH_2CH_2]$_2$-		Ns	84
3	C_6H_5	-CH=CH_2	Ns	92
4	C_6H_5	Me	Ts	79
5	C_6H_5	Me	SES	83
6	C_6H_5	Me	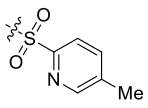	73

With *t*Bu$_3$tpy acting as a ligand the formation of the sulfoximine was more efficient than with the optimised rhodium system. The Ns group was not removable and the synthetically useful NH sulfoximine was not accessible *via* this method.

A common method of sulfur nitrogen bond formation is through the use of stoichiometric hypervalent iodine species acting in the presence of some metal catalyst to form an electrophilic source of nitrogen. Recently conditions were published by Bull *et al.* for the metal free preparation on NH-sulfoximine from sulfoxiude using phenyliodine diacetate and ammonium carbamate (Scheme 58).[109]

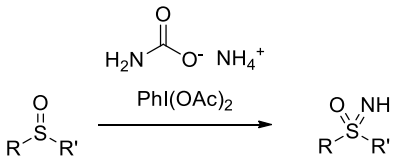

Scheme 58 Bull *et al.* sulfoximine preperation

Reboul *et al.* investigated the reaction in order to shed mechanistic insight on the formation of sulfoximines.[110] The group proposed that in the presence of sulfide, the reaction would proceed *via* the indonitrene to form the corresponding indonium sulfilimine. It was anticipated the displacement of iodobenzene would yield the formation of a thiazine, containing a SN triple bond, which could undergo hydrolysis resulting in the desired sulfoximine. The presence of a thiazine transition state had previously been hypothesised by Yoshimura in the hydrolysis of diarylhalosulfilimines,[111] and Bolm for the synthesis of sulfondiimines by oxidative imination of sulfiliminium salts.[112]

It was observed that performing performing the reaction with phenyl benzyl sulfide resulted in a 1:1 mixture of the corresponding N-H sulfoximine and the *N*-acylated sulfoximine. The authors considered a Ritter type mechanism to explain this result,[113] suggesting that the acyl group was supplied by the solvent (Scheme 59). However, this hypothesis was easily ruled out by replacing acetonitrile with propionitrile, which did not affect the outcome of the reaction, confirming the acetyl group originated from the hypervalent iodine species.

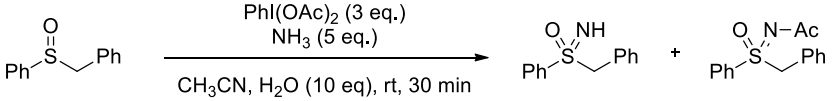

Scheme 59 Formation of N-H and *N*-acylated sulfoximine

In their reaction optimisation, it was found that water was required for the formation of the *N*-acylated sulfoximine as without the aqueous media, the free N-H sulfoximine was formed exclusively, and in excellent yield (Scheme 60).

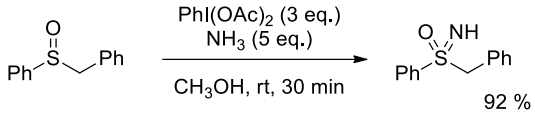

Scheme 60 Free N-H sulfoximine formation

With these results in hand, it was hypothesised that formation of the N-H sulfoximine was *via* attack by methanol on the methoxy-λ^6-sulfaneitrile with the concurrent formation of dimethylether. In the formation of the 1:1 mixture of *N*-acylated sulfoximine and N-H sulfoximine, the *N*-acylated sulfoximine is formed *via* the N-H sulfoximine (Scheme 61).

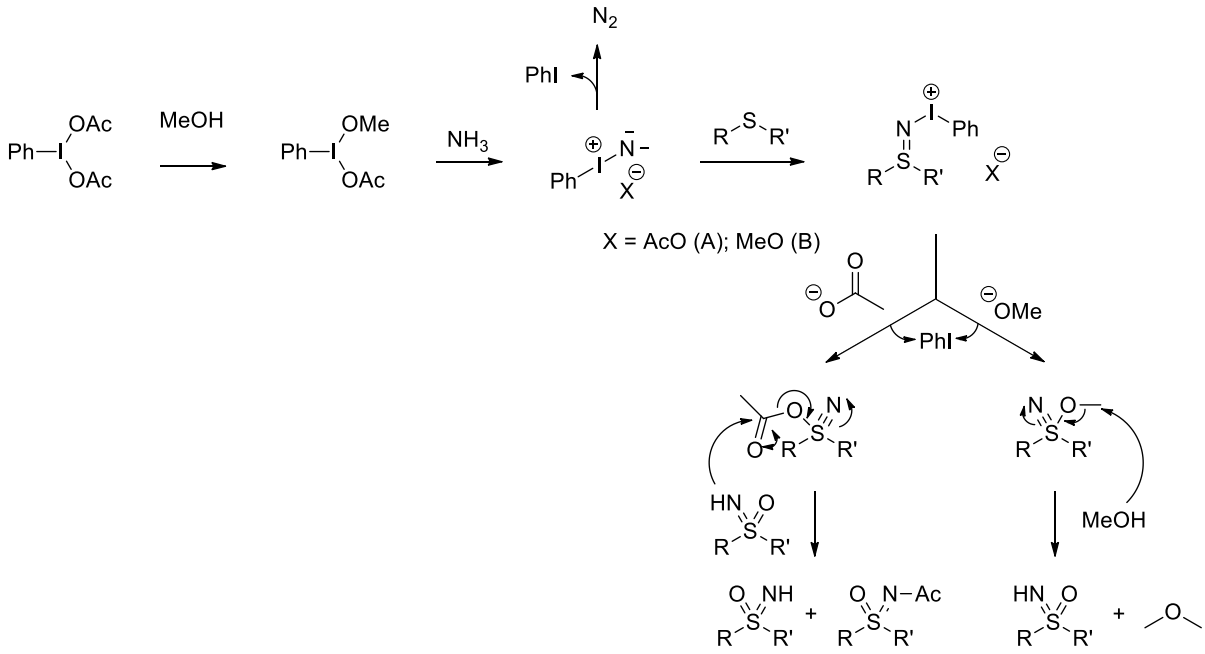

Scheme 61 Proposed reaction mechanism for sulfoximine formation

A key step in the reaction is the formation of the *O*-acyl and *O*-methyl thiazines, which is contingent upon methanol ligand exchange with (diacetoxyiodo)benzene. The group used HRMS experiments to confirm the existence of the thiazine intermediates, finding that the results supported their mechanistic hypothesis.

2. Flavin Catalysed Sulfide Oxidation

2.1. Sulfur Oxidation

Sulfoxides are compounds that contain a sulfinyl (SO) group along with two alkyl or aryl groups, with an oxidation state of +4. Sulfoxides are most commonly formed through the oxidation of sulfides. Their trigonal pyramidal shape comes from two sulfur-carbon bonds, a sulfur-oxygen bond and a lone pair of electrons on the sulfur atom, creating tetrahedral electron pair geometry.[114] When the two carbon groups are inequivalent, a chiral centre is generated at sulfur, with chiral sulfoxides having significant use in agricultural (Endosulfan, **103**) and pharmaceutical applications (Esomeprazole, **104** and Armodafinil, **105**) (Figure 10). The sulfur-oxygen bond has characteristics of both a dative bond (whereby one species acts as a donor and the other as an acceptor) and a polarised double bond (such as a carbonyl group) in terms of bond strength. The electrostatic component of the bond creates a significant sulfur-oxygen dipole, with the negative charge concentrated on the oxygen.

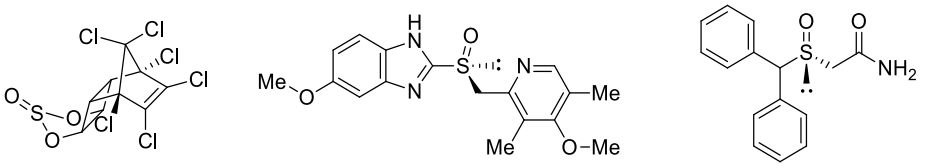

Endosulfan **103** | Esomeprazole **104** | Armodafinil **105**

Figure 10 Examples of sulfoxides used in pharmaceutical and agricultural industries

With prochiral sulfides offering a relatively simple route to potentially useful chiral sulfoxides, research into their synthesis is well established, with a variety of well understood metal and non-metal catalysed protocols available. Sodium periodates and perborates have proved themselves to be suitable oxidants for formation of sulfoxides and sulfones, although overoxidation was sometimes unavoidable (Scheme 62).[115–117]

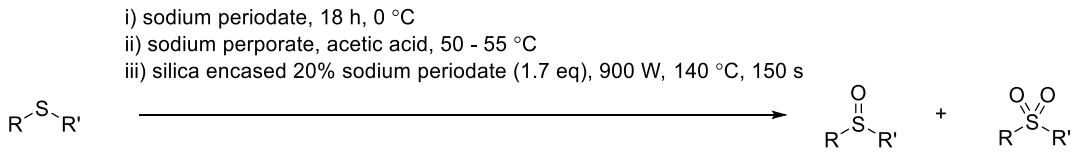

Scheme 62 Sodium periodates and perborates routes to sulfoxides i)[116] ii)[117] iii)[115]

Potassium persulfate and peroxymonosulfate (Oxone®) **106** are popular commercially available potassium salts that have been used for sulfide oxidation to the corresponding sulfone (Scheme 63).[118–120] However, halting the oxidation at the sulfoxide has only recently been successfully reported, with Yu *et al.*controlling the stoichiometry of Oxone® to prevent overoxidation (Scheme 63).[7]

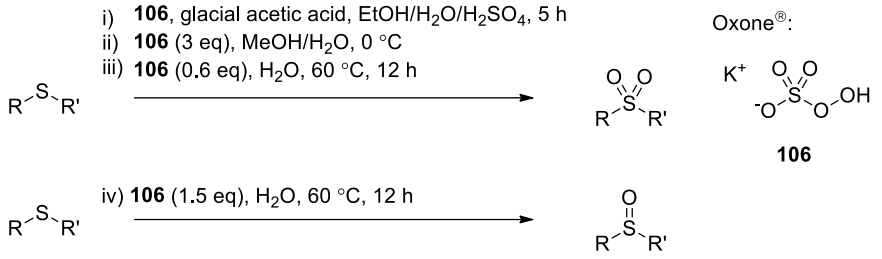

Scheme 63 Sulfide oxidation techniques using Oxone i)[118] ii)[119] iii)[120] iv)[120]

Nitric acid was used to prepare sulfones without the need for additional metals or catalysts. Additionally, the authors reported they were able to recover and re-use the nitric acid. However, this route was only demonstrated for the oxidation of alkyl sulfides, which could be due to poor functional group tolerance. (Scheme 64).[121]

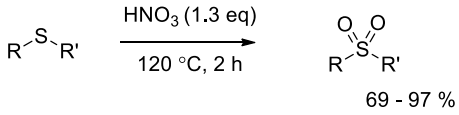

Scheme 64 Nitric acid routes to sulfones

Recent years have seen further developments in the sulfide oxidation, with milder and greener protocols. Iron catalysis was shown to utilise O_2 a terminal oxidant with the readily available $Fe(acac)_2$ **107**, when PEG 1000 was used as a solvent. The authors hypothesised that a key component of the reaction was the electron-rich PEG 1000 which served to stabilise the active Fe(IV) oxo-species that is formed *in situ*, (Scheme 65). [122]

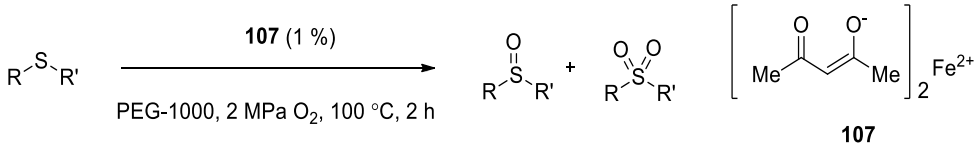

Scheme 65 $Fe(acac)_2$ catalysed routes for sulfone formation

A range of PEG molecular weights from 200 to 20 000 g.mol^{-1} were investigated, with yields of ≤ 5% observed with both low (200 g mol^{-1}) and high (20 000) molecular weights. There was some overoxidation to the sulfone, but the major product was the sulfoxide.

A range of synthetic routes have relied on hydrogen peroxide as a terminal oxidant, catalysed by various metal salts. The use of hydrogen peroxide provides good atom economy and in combination with select metals, can yield the desired oxidised sulfur compound with good

efficiency. The first example of zinc catalysis for the oxidation of sulfides to sulfones was reported in 2014 and used hydrogen peroxide as a green oxidant and 1,8-Diazabicyclo[5.4.0]undec-7-ene (DBU) **108** as a ligand (Scheme 66).[123]

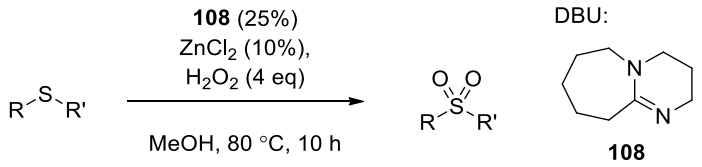

Scheme 66 Zinc as a hydrogen peroxide reaction partner

Zinc salts are inexpensive, abundant and environmentally benign, satisfying increasing demand for greener reagents.

Further transition metal that have been applied to the synthesis of sulfoxides and sulfones include Niobium[124] Vanadium [125] Tellurium[126] Mangenese [127] Scandium[128] Osmium[129] Titanium[130] Rhenium[131] Ruthenium[132] Chromium[133] Tungsten.[134]

In January 1984, Henri Kagan and Philippe Pitchen reported the first example of oxidation of simple sulfides into optically active sulfoxides, using a modification of the Sharpless epoxidation conditions.[135,136] This preparation was not the first example of synthesis of chiral sulfoxides, however, it improved upon previous publications as it did not require prochiral sulfides to form asymmetric sulfoxides, allowing the scope of the reaction to be significantly wider reaching (Scheme 67).

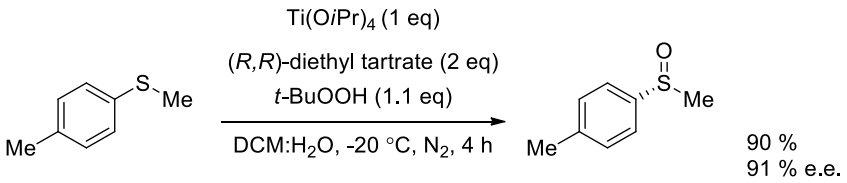

Scheme 67 Kagan *et al.* asymmetric oxidation of sulfides to sulfoxides

Kagan *et al.* succeeded in preparing (*R*)-(+)-methyl *p*-tolyl sulfoxide in 90 % yield with excellent enantiomeric excess of 91% with a short reaction time. Notably, the reaction could withstand significantly longer reaction times, with up to 12 h being tolerated without loss of selectivity, suggesting any background reaction was suitably halted at –20 °C. However, an increase in temperature led to an unacceptable loss in selectivity even after halting the reaction after a short time period (Scheme 68).

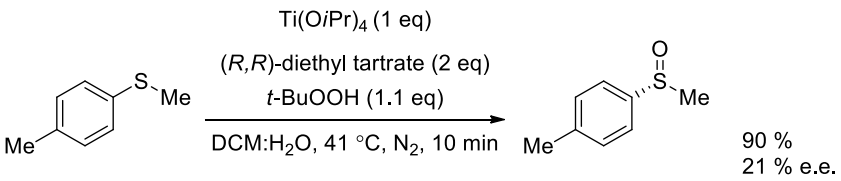

Scheme 68 Demonstrating the impact of increased temperature upon selectivity

This report was followed by a further publication by Kagan *et al.* about expansion of the substrate scope and investigation of the effects of water and temperature on the reaction. This, along with competition reactions and a Hammett correlation plot allowed the authors to propose a reaction mechanism.[137] The rate of reaction was accelerated by electron withdrawing groups (such as NO_2), indicating electrophilic attack on the sulfur. *e.e*. did not appear to be affected by aryl substitution, remaining between 75% and 90% and without any apparent correlation between electron withdrawing and donating groups. Modena and co-workers independently reported the synthesis of chiral sulfoxides by modification of the Sharpless epoxidation conditions in 1984.[138] These seminal publications marked a considerable increase in the ease of accessibility of asymmetric sulfoxides and spawned significant growth in this research area.

The use of stoichiometric titanium was a significant drawback in this reaction that was addressed by Kagan *et* al. in 1996.[139] The group found that isopropyl alcohol could act as a replacement for the water in their system of asymmetric oxidation by cumyl hydroperoxide. The addition of molecular sieves allowed for the reaction to be performed catalytically with respect to the titanium complex (Scheme 69).

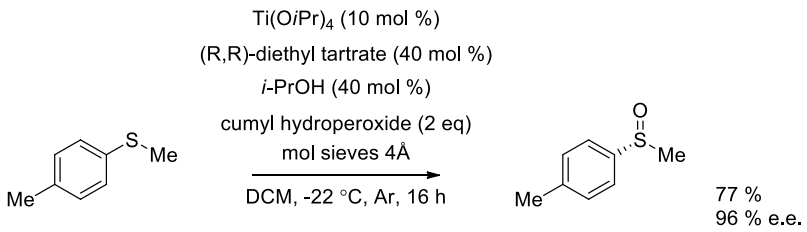

Scheme 69 Catalytic asymmetric oxidation of p-tolyl, methyl sulfide

The yield observed is slightly decreased in the catalytic preparation of asymmetric sulfoxides in comparison to the stochiometric preparation (77% compared to 90 %), however, enantiomeric excess remains excellent.

In 1998, Saha-Möller *et* al. published a titanium catalysed route to chiral sulfoxides using optically active hydroperoxides. They proposed sulfoxide coordination at the Tic enter generated a template in which the oxygen atom undergoes intramolecular atom transfer from

the bound and activated optically active hydroperoxide to the ligated sulfoxide in a stereocontrolled manner (Figure 11).[140]

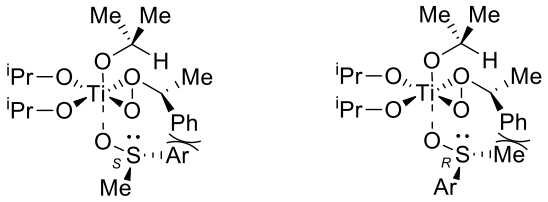

Figure 11 Proposed sulfoxide formation transition state

This observation by Saha-Möller *et* al. could support the mechanistic rationale originally postulated by Kagan *et* al. who suggested that asymmetric induction could occur at the coordination stage. This hypothesis states steric interaction between the peroxide and the sulfide would preferentially form (*R*)-(+)-methyl *p*-tolyl sulfoxide over (*S*)-(-)-methyl *p*-tolyl sulfoxide, which is consistent with the experimental results. In contrast to the work produced by Kagan *et* al., Saha-Möller *et* al. found significant over-oxidation to the sulfone which was attributed to the increased oxidising ability of their titanium catalyst.

Further asymmetric oxidations of sulfides were achieved by Palucki *et* al. who used salen ligands for their metal catalysed sulfoxide formation. They utilised manganese-based catalysis with the aforementioned chiral ligand to achieve modest selectivity and good yields of asymmetric sulfoxides (Scheme 70).[141]

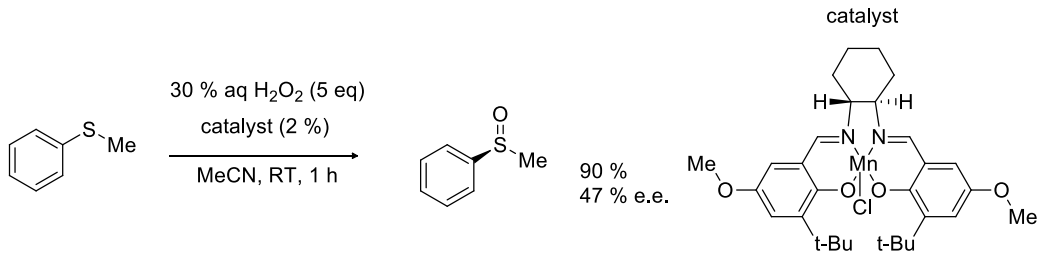

Scheme 70 Asymmetric oxidation of sulfide with H_2O_2 catalysed by (salen) Mn(III) complexes

The performance of this reaction in air, along with the use of the green oxidant hydrogen peroxide (albeit in large quantities) were advantages over Kagan *et* al.'s formation of sulfoxides. However, initially it did not provide the optical purity of the Ti metal synthetic route. Katsuki *et* al. were able to afford increased asymmetric induction (with 96 % e.e.) using PhIO as an oxidant and a slightly modified salen ligand, while maintaining high yields (96 %).[142]

Other transitions metals have been used to good effect for asymmetric sulfide oxidation. Notably vanadium catalysis was first reported in 1986 by Fujita *et* al.[143] The group achieved enantiomeric excesses of up to 40 %, which was not an improvement upon Kagan *et* al.'s modification of the Sharpless conditions, however, the reaction was catalytic, using 10 mol % vanadium.

In 1995, Bolm and Bienewald proposed an improvement to the vanadium catalysed approach to asymmetric sulfide oxidation, addressing shortcomings in previous preparations. They focused their efforts on practicability of the reaction and catalytic efficiency/longevity (turnover numbers) and not on enantioselectivity. Despite this, good enantiomeric excesses were still achieved with a range of ligands forming the chiral catalyst *in situ* from $VO(acac)_2$ (Scheme 71).[144]

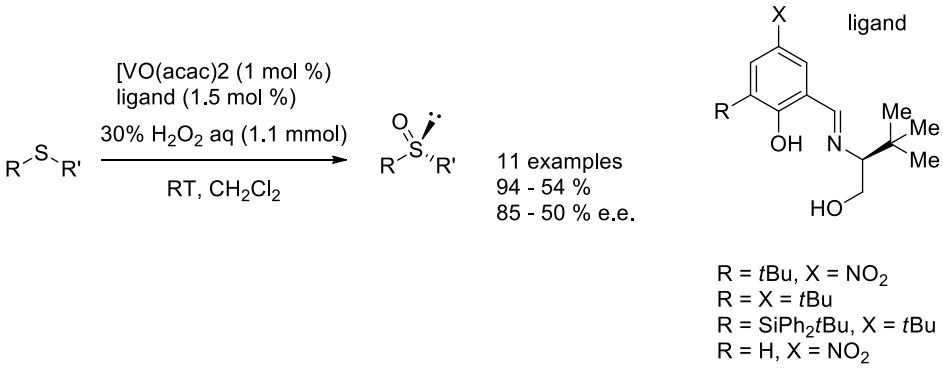

Scheme 71 Asymmetric sulfide oxidation with vanadium catalysis and H_2O_2

The authors note the simple reaction conditions needed are applicable to large scale synthesis as the reaction is not inhibited by the presence of water and can be performed under atmospheric conditions. However, although the catalytic system is highly efficient, addition of the hydroperoxide oxidant must be slow to avoid overoxidation to the sulfone.

In 2008, the pharmaceutically relevant, esomeprazole, has been synthesised on large scale in order to treat peptic ulcer disease and gastroesophageal reflux disease. The (*S*)-enantiomer was obtained *via* oxidation of a prochiral sulfide by titanium-mediated reaction with cumene hydroperoxide in the presence of (*S,S*)-diethyl tartrate (Scheme 72).

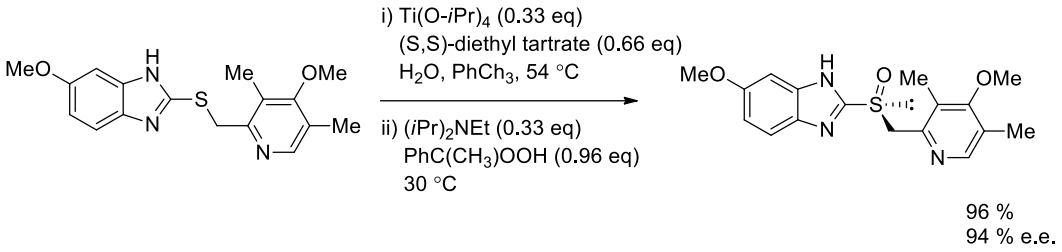

Scheme 72 Asymmetric sulfide oxidation with titanium catalysis

This modification of the initial Kagan oxidation was used to produce esomeprazole on the multi kilogram scale, demonstrating the power of titanium catalysis towards the asymmetric oxidation of sulfides.[145]

2.2. Flavin Synthesis

Flavinium chlorides were selected for their simple synthesis and stability, which had been originally developed by Sayre *et al*[146] The Carbery group managed to successfully telescope a synthetic step, further simplifying the catalysts production (Scheme 73).[147]

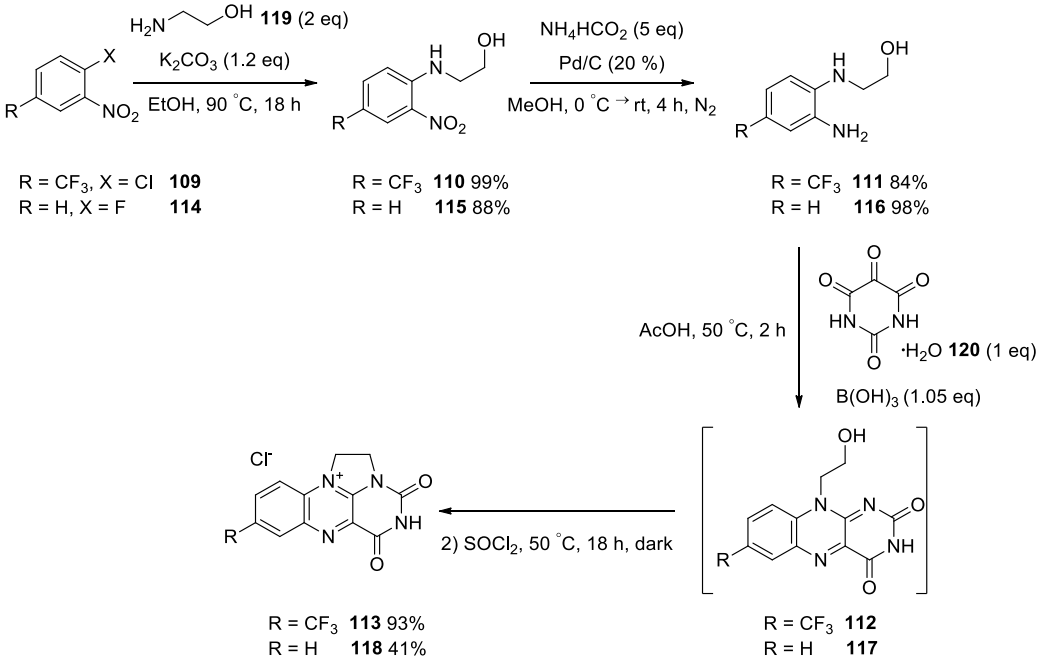

Scheme 73 Synthetic pathway to flavinium catalysts

The synthesis starts with the nucleophilic aromatic substitution of electron poor, substituted nitro-aryl halides **109 and 114**, inserting the eventual bridge of the flavinium catalyst, with ethanolamine **119**. The nitro group then undergoes transfer hydrogenation with ammonium formate and Pd(0), generating the corresponding dianiline. Condensation with alloxan monohydrate **120** yielded the flavin isoalloxazine tricycle, which was then telescoped through to the thinyl chloride mediated flavinium salt formation.

In the synthesis of chloro-substituted flavin catalyst, the reduction step is adapted due to the sensitivity of the halide under ammonium formate/palladium on carbon reduction. A reduction protocol of mossy tin in HCl was preferred to prevent dechlorination (Scheme 74).

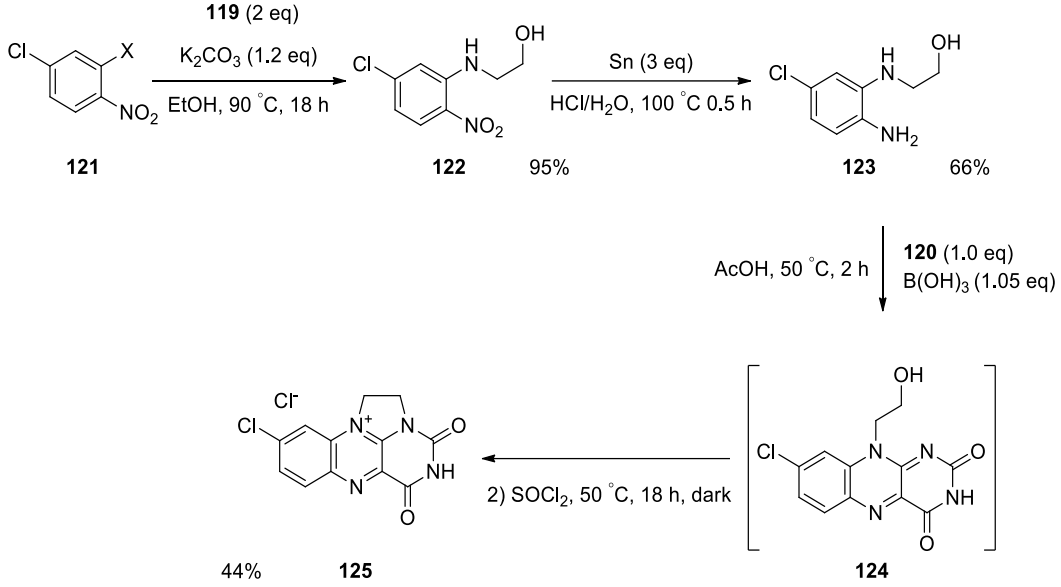

Scheme 74 Modified flavinium choloride synthesis

Hydrogen peroxide has proved to be a suitable reaction partner for flavin due to the facile formation of the hydroperoxyflavin, which acts as an oxygen transfer reagent for amine and sulfide oxidations.[42,50,148] Extensive work has gone into understanding these transformations, and consequently, the reaction mechanism is well understood.[149]

2.3. Hydrazine mediated sulfoxide formation with flavin catalysts

We were interested in the investigation of novel flavin reaction partners to achieve the oxidation of sulfides and initially focussed on the use of hydrazine as a heteroatom transfer reagent. Hydrazine is a nitrogen containing inorganic compound that is unstable in isolation that is most often used as an aqueous solution. Hydrazine had been previously used by Imada *et al.* for the perchlorate flavinium salt catalysed oxidation of sulfides to sulfoxides at slightly elevated temperatures under an oxygen atmosphere (Scheme 75).[42]

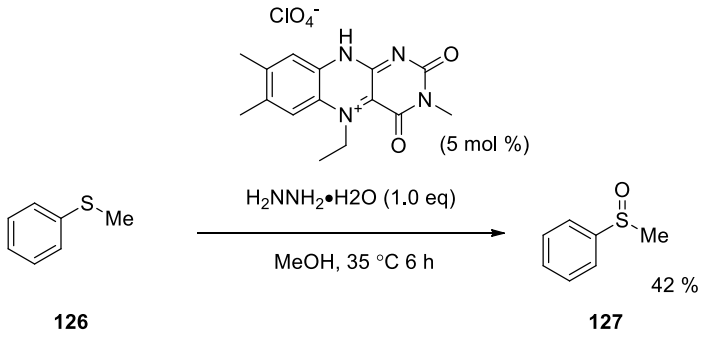

Scheme 75 Imada *et al.*'s hydrazine mediated sulfoxide formation

A modified version of the hydrogen peroxide protocol for sulfide oxidation was adopted for the transformation of sulfides (Scheme 76).

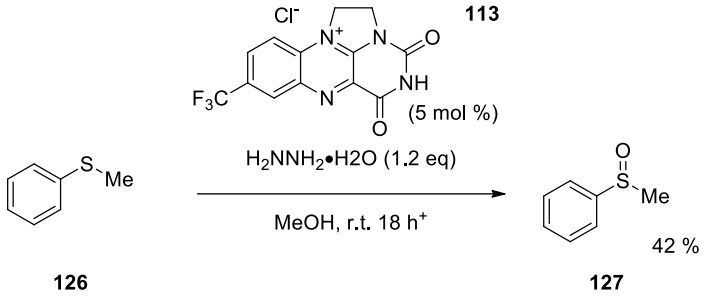

Scheme 76 Flavin catalysed methyl phenyl sulfide oxidation with hydrazine

Methyl phenyl sulfide was oxidised cleanly to methyl phenyl sulfoxide, with no overoxidation to the sulfone observed. The optimisation of the reaction system is shown below (Table 14).

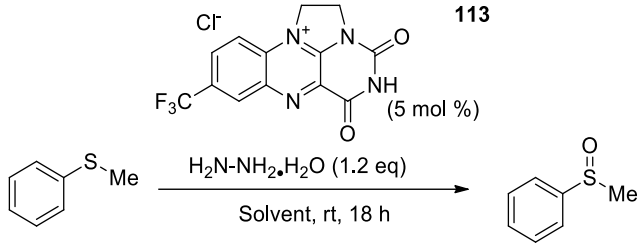

Table 14 Solvent optimisation of hydrazine sulfide oxidation

Entry	Solvent	Conversion (%)
1	Methanol	42
2	Ethanol	13
3	Dichloromethane	9
4	Chloroform	7
5	Tetrahydrofuran	26
6	Acetonitrile	19
7	Ethyl acetate	0
8	Water	0

The initial solvent screen was conducted using a variety of common laboratory solvents, with methanol (entry 1) remaining the best choice for the conversion to the sulfoxide, for which there was literature precedence.[146] Ethanol (entry 2) was also investigated and this alcohol produced the sulfoxide, albeit in a lower yield. **113** is only sparingly soluble in chlorinated solvents (entries 3 and 4) and decreased sulfoxide conversion could be attributed to this reduced solubility. Conversion with THF and acetonitrile (entries 5 and 6) as the reaction solvent are slightly lower than methanol, despite **113** having adequate flavin solubility. There was no conversion observed with ethyl acetate (entry 7), which was unexpected. Although the solubility of the catalyst is excellent in an aqueous system (entry 8), methyl phenyl sulfide is not water soluble, explaining the lack of conversion and recovery of starting material.

Following the solvent screen, optimisation of catalyst and hydrazine loading were investigated, along with further controllable variables including temperature, time and atmosphere (Table 15).

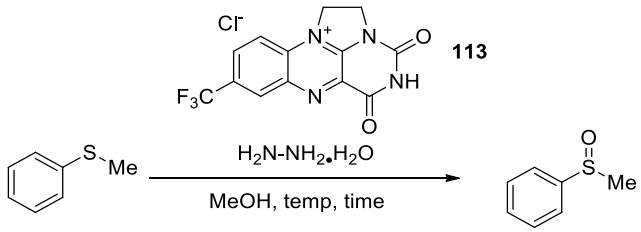

Table 15 Further hydrazine mediated sulfide optimization

Entry	Catalyst (mol %)	H_2N-NH_2 (eq)	T (° C)	t (h)	Atmosphere	Conversion (%)
1	0	1	rt	18	air	0
2	5	0	rt	18	air	0
3	5	1	rt	18	air	21
4	10	1	rt	18	air	45
5	20	1	rt	18	air	71
6	5	2	rt	18	air	17
7	10	2	rt	18	air	53
8	20	2	rt	18	air	37
9	5	4	rt	18	air	2
10	10	4	rt	18	air	33
11	20	4	rt	18	air	47
12	5	1.2	rt	24	air	42
13	5	1.2	50	24	air	44
14	5	1.2	rt	24	N_2	0
15	20	1	rt	24	air	76
16	20	1	rt	28	air	68

As you can see from the control reactions performed (entries 1 and 2), both the hydrazine and **113** are integral to sulfoxide formation. An increase in catalyst loading led to an increased sulfoxide conversion, as can be seen repeatedly (entries 3-5, 6-8, 9-11). A loading of 20 mol% resulted in excellent conversion after 28 hours, and further catalyst loading was not explored as higher catalyst loading was undesirable, as the high molecular weight of the flavin made the reaction challenging to handle. Interestingly, an increase in hydrazine, did not correlate with an increase in sulfoxide production. The greatest conversion was achieved with high catalyst loading (20%) and stoichiometric loadings of hydrazine (entry 5). In other entries of equal catalyst loading but increased hydrazine (entries 8 and 11), you can see a decrease in conversion from 71% to 37% and 47% respectively. This trend is also observed

for catalyst loadings of 5% (entries 3, 6 and 9) and 10 % (entries 4, 7 and 10). This could be attributed to the hydrazine being a 35% aqueous solution. The presence of small, but measurable amounts of water could be inhibiting the activity of the flavin catalyst, which is preferentially soluble in water over methanol, potentially creating a phase boundary between the flavin and the sulfide and causing this decrease in conversion. No meaningful increase in conversion was seen when the temperature was increased (entries 12 and 13) from room temperature (42%) to 50 °C (44%), and in an inert atmosphere, complete recovery of the starting material was achieved. Finally, an increase in time, showed reaction progression slowed after 18 hours (entries 15 and 16).

The electronics of the flavin were varied in order to investigate the effect on the yield (Scheme 77).

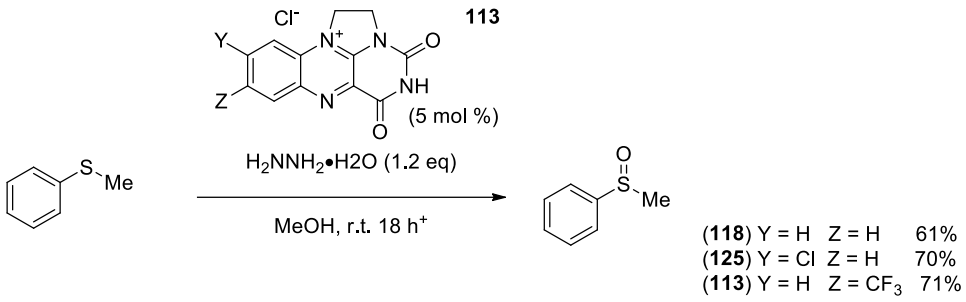

Scheme 77 Investigation into flavin electronic configuration

There was no significant difference between the trifluoroflavinium salt **113** (71%) and the chloroflavinium **125** (70%), however, there was a slight drop in sulfoxide formation with **118** (61%). As the triflouroflavinium showed the best conversion, it was taken forward for future reactions.

The optimisation showed a lack of conversion in an oxygen free environment. This result indicates that the terminal oxidant in this reaction scheme is atmospheric O_2, leading to the hypothesis of a reaction mechanism whereby the hydrazine acts to reduce the catalyst, before the formation of the hydroperoxy flavin. These results are supported by Imada *et al*, who have investigated flavin catalysed oxidation of sulfides with a similar flavin catalyst, although their system requires an oxygen atmosphere to proceed (Scheme 78).[50]

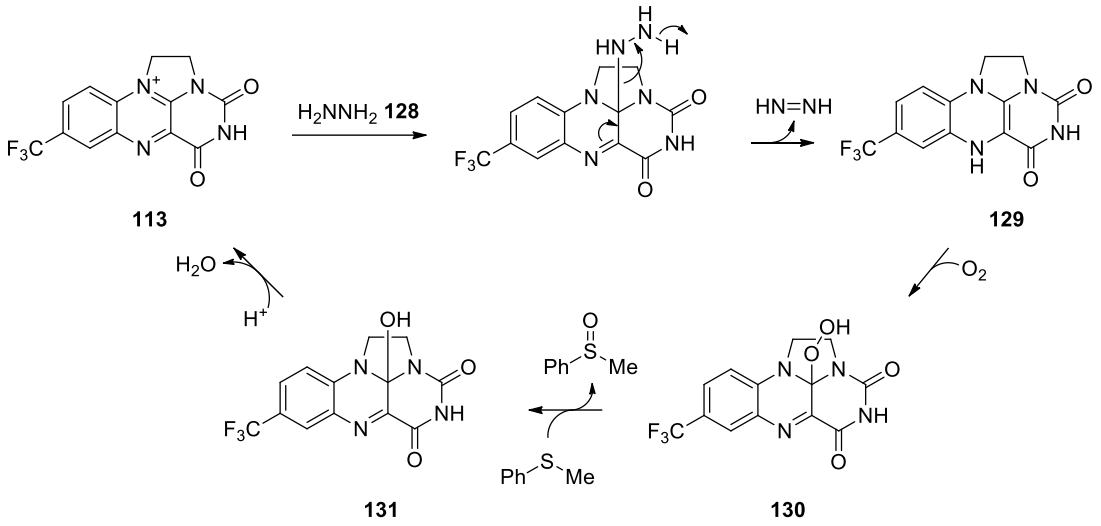

Scheme 78 Proposed mechanism for the reduction of flavin by hydrazine

Our proposed reaction mechanism is the addition of hydrazine **128** into the flavinium salt **113**, followed by elimination of diimide (HN=NH), generating the reduced flavin **129**. The hydroperoxyflavin **130** is formed from the introduction of atmospheric oxygen, and the electrophilic oxygen is prone to nucleophilic attack from the sulfide, which yields the product via mono-oxidation, leaving the hydroxyflavin **131**. Upon rearomatisation, the catalyst is then regenerated to give the active catalyst and water (Scheme 78).

As previously discussed, the mechanism of interaction between flavin and atmospheric O_2 differs from the mechanism of interaction with hydrogen peroxide. In the case of atmospheric oxygen acting as a terminal oxidant, a reductant is required to generate the dihydroflavin which is responsible for the activation of dioxygen (Scheme 79).[46]

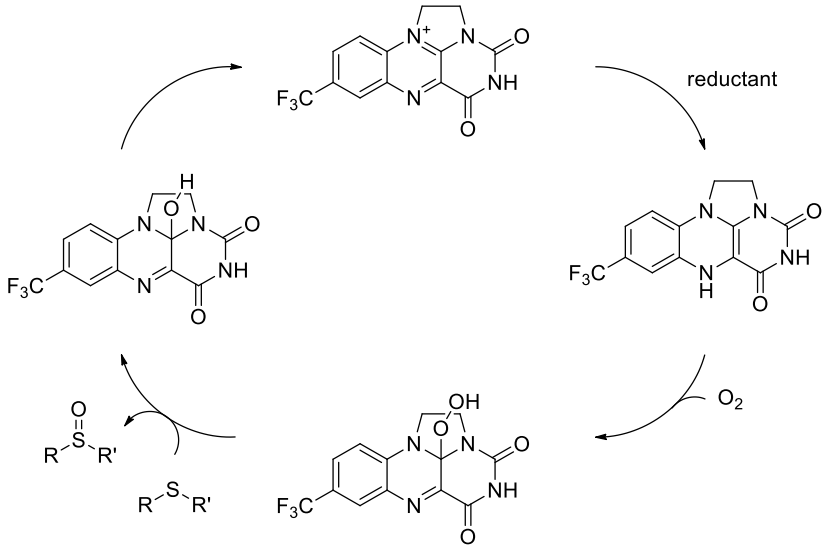

Scheme 79 General flavin oxidation scheme

The initial step is the reduction of the flavinium ion, which is achieved in this case through the use of hydrazine as a reductant, which generates diimide as a by-product (Scheme 80).

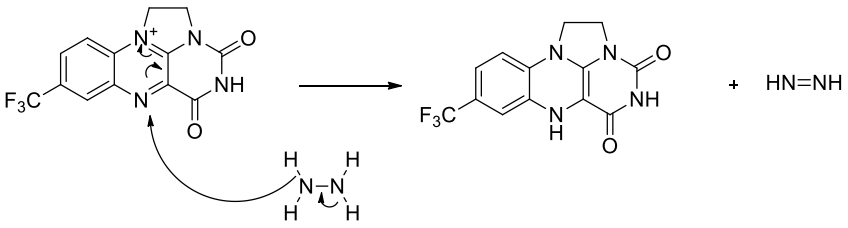

Scheme 80 Reduction of flavin and formation of diimide

The production of diimide in similar systems has been confirmed through hydrogenation of alkenes to the corresponding alkane.[150]

The following process of the introduction of oxygen to the flavin species has two key steps, initially, the generation of the anionic reduced flavin, and secondly, the generation of singlet oxygen (Scheme 81).

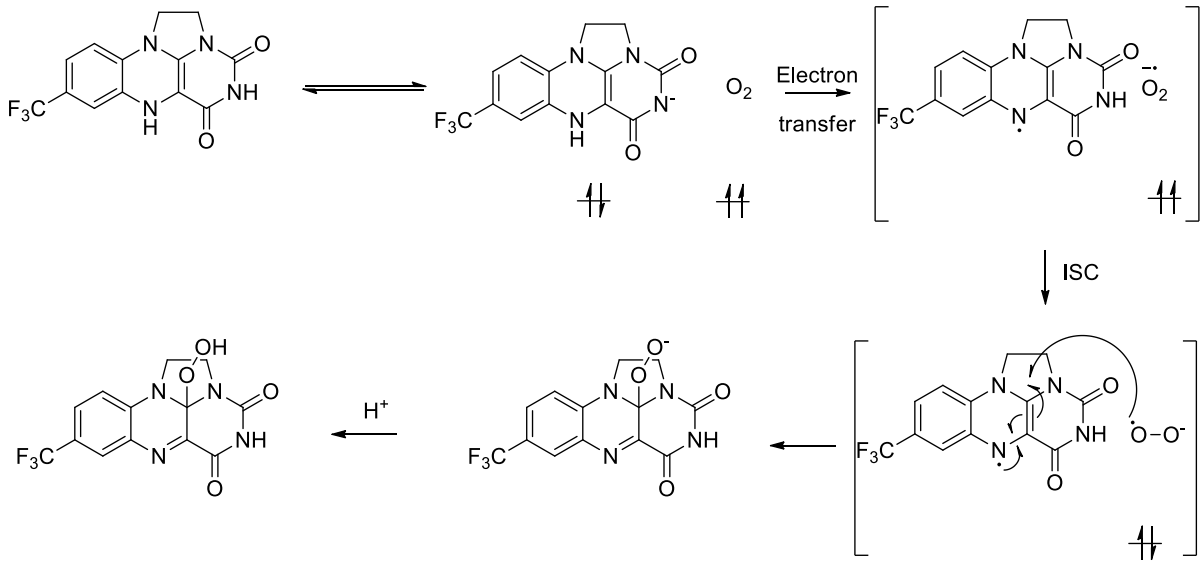

Scheme 81 Mechanism of flavin oxidation

The anionic reduced flavin is in equilibrium with the reduced flavin, upon reduction with hydrazine. The anionic species can then undergo electron transfer with O_2, and possibly proton migration, generating a radical pair. The oxygen undergoes intersystem crossing, generating singlet oxygen. This singlet oxygen can then react with the anionic reduced flavin, via a radical mechanism. Finally, the charged species is neutralised through reaction with a hydrogen ion.[151]

Following the generation of the hydroperoxyl flavin, the electrophilic pendant oxygen is then prone to nucleophilic attack from the corresponding sulfide (Scheme 82).

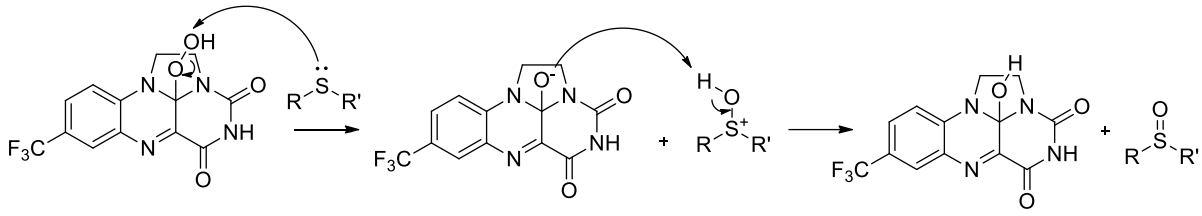

Scheme 82 Nucleophilic attack from sulfide to peroxyflavin

The initial nucleophilic attack by the sulfide leads to the generation of charged sulfur and flavinium ions, which are then neutralised upon proton transfer, which generate the desired sulfoxide (Scheme 83).[152,153]

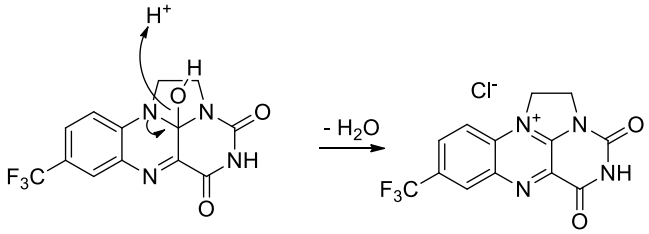

Scheme 83 Regeneration of flavinium ion

The flavinium catalyst is the regenerated as the remaining hydroxy component is lost as water.

By contrast, upon reaction with an oxidant such as hydrogen peroxide, the active hydroperoxyl species is generated in a single step, nucleophilic attack of H_2O_2 on the electrophilic flavinium carbon (Scheme 84).

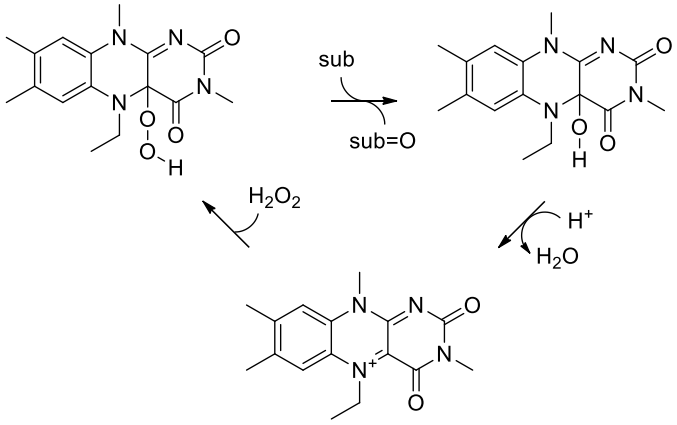

Scheme 84 Oxidation of flavin by hydrogen peroxide

A driving force behind this reaction, is the neutralisation of the flavinium ion through nucleophilic attack from the hydrogen peroxide at the highly electrophilic site of the flavin (Scheme 85).[154] Additionally, the lone pairs of electrons on adjacent oxygen atoms of H_2O_2 increase its nucleophilicity due to the alpha effect.

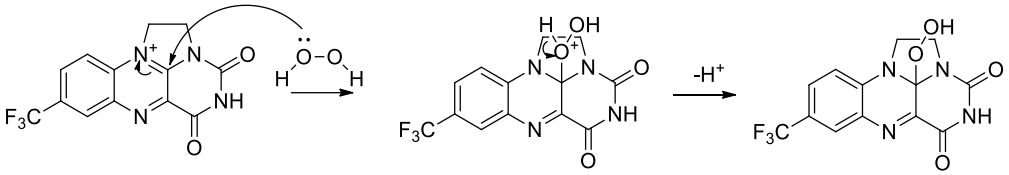

Scheme 85 Mechanism of hydroperoxide addition

A hydrogen ion is then lost to generate the active hydroperoxy catalyst, which then proceeds in an identical manner to the previous system, until the regeneration of the charged species occurs again by elimination of water.

The kinetics of this reaction were not extensively probed, however, an increase in the rate for sulfides containing electron donating groups would provide validation to our proposed reaction mechanism. An increase in electron density would increase the nucleophilic character of the sulfide, speeding up the nucleophilic attack for the formation of the sulfoxide. Conversely, we would expect to see a reduction in rate in cases of sulfides containing electron withdrawing groups. The hypothesis could be probed by an extensive substrate scope. Electron donating groups would increase the nucleophilicity of the sulfur, increasing the speed of the rate determining step.

2.3.1. Flavin + Hydrazine Substrate Scope

With optimised conditions in hand, the scope of the reaction was investigated towards a range of sulfides (Table 16).

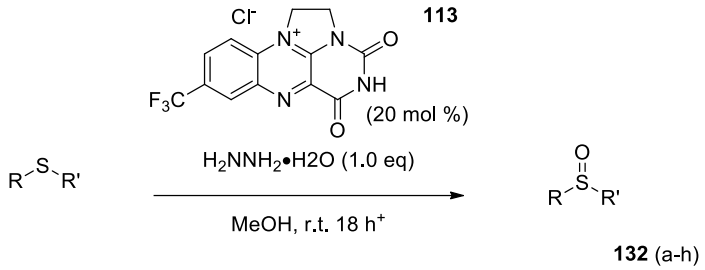

Table 16 Oxidation of sulfides with hydrazine

Entry	R	R'	Product	Isolated Yield (%)
1	C_6H_5	Me	**132a**	71
2	4-OMe-C_6H_4	Me	**132b**	87
3	C_6H_5	C_6H_5	**132c**	75
4	4-Br-C_6H_4	Me	**132d**	62
5	4-CH_3-C_6H_4	Me	**132e**	64
6	CH_2=$CHCH_2$	CH_2=$CHCH_2$	**132f**	75
7	$CH_3(CH_2)_3$	$CH_3(CH_2)_3$	**132g**	95
8	$(CH_2)_3OH$	Me	**132h**	91

All sulfides were oxidised to the corresponding sulfoxide cleanly, with no overoxidation to the sulfone, and in good to excellent yields. The reaction tolerated substitution on the phenyl well, with very good yields for methoxy and bromo and methyl substituents (entries 2, 4 and 5). Diphenyl sulfoxide was produced in good yield (entry 3), as were alkyl sulfides (entries 6 and 7). Polar oxidisable groups such as alcohols were unaffected, and the sulfoxides were formed in excellent yields (entry 8).

2.4. Alloxan and Hydrazine

While exploring additional strategies towards nitrogen transfer to sulfides, it was decided to investigate alloxan **120**, which had previously been used for heteroatom transfer within the Carbery group.[155] Alloxan is a cheap, commercially available reagent which is under explored in organic synthesis. Its primary use is to give rats type 1 diabetes for medical studies.[156] It has been observed that alloxan does not cause diabetes in humans.[157]

Alloxan was investigated as a nitrogen-transfer reagent in conjunction with hydrazine. The electrophilic carbonyl was hypothesised to be prone to attack from the hydrazine in order to create an electrophilic nitrogen with a leaving group. The result of the reaction was sulfoxide

formation which was due to reduction of alloxan by hydrazine. This resulted in oxygen transfer instead of the production of an electrophilic nitrogen centre (Scheme 86).

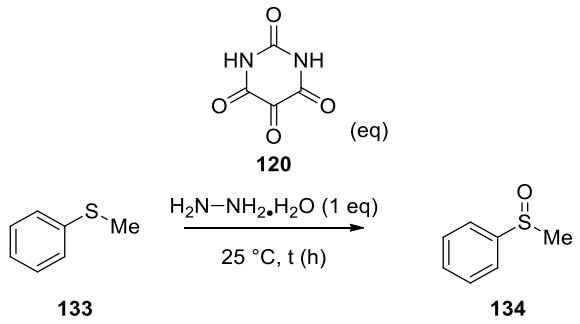

Scheme 86 Demonstration of oxygen transfer with alloxan.

A number of experiments have been carried out with alloxan in an effort to investigate whether the reaction is catalytic with respect to alloxan, and to understand where the oxygen incorporated into the product is coming from (Table 17).

Table 17 Investigating alloxan as an oxygen transfer reagent.

Entry	**Alloxan (eq)**	**Atmosphere**	**Solvent**	**t (h)**	**Conversion (%)**
1	1	N_2	MeCN	16	2
2	1	Air	MeOH	1	33
3	0.05	Air	MeOH	16	0
4	1	Air	MeOH	16	90

The oxygen in the sulfoxide was attributed to atmospheric oxygen, as there was limited conversion in an inert atmosphere (entry 1). This slight reactivity could be from some oxygen in the system, despite the anaerobic conditions. It was observed that alloxan oxidation does not operate catalytically, as there was no conversion at 5% loading (entry 3). This indicates that the alloxan species is being consumed during the reaction, and there have been reports of alloxan undergoing formation of murexide like dyes upon reactivity with amines.[158] Additionally it has been reported by Srogl and Voltrova that ascorbic acid can undergo condensation **135** upon reaction with amino acids, which could remove reacted alloxan from the system (Scheme 87).[159]

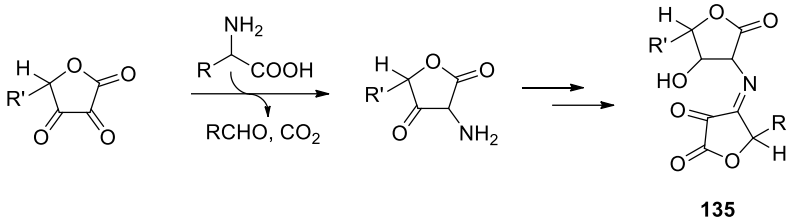

Scheme 87 Naturally occurring aerobic reaction of ascorbic acid and amino acids

Novel sulfoxide formation from commercially available starting materials has been accomplished under mild conditions and with moderate reaction times and the substrate scope of this reaction will be explored and optimised.

2.5. Aminomorpholine salts for nitrogen transfer

We then turned our attention to aminomorpholine salts as they are known in the literature for the synthesis of aziridines (Scheme 88).[160]

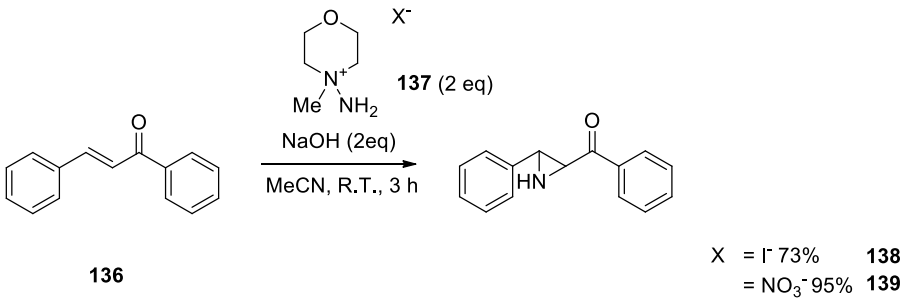

Scheme 88 Aminomorpholine salts for aziridines synthesis.

N-amino-*N*-methylmorpholinium salts **137** satisfied the desirable requirements stated for sulfilimine formation. They contain an electrophilic nitrogen, are simple to prepare and thermally stable.

The hydrazinium iodide salt **138** was initially prepared (Scheme 89). It is reported as a more facile synthesis than that of the salt possessing the nitrate counter ion, allowing **138** to be prepared on a gram scale. However, it was immediately found that the reagent was largely insoluble in a range of solvents (Scheme 89).

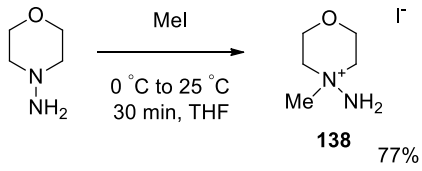

Scheme 89 Hydrazinium iodide formation.

Solubility was generally poor in, dichloromethane, ethanol, chloroform, petroleum ether, ethyl acetate and diethyl ether. Acetonitrile and methanol resulted in partial solubility however water and dimethyl sulfoxide both resulted in fully homogenous solutions. The

reaction was then attempted in water, unfortunately the sulfide was found to be insoluble in this solvent, and subsequent reactions were performed in DMSO. The reactivity of the methylaminomorpholine salts towards sulfides was investigated. Imination was then studied and 4-methoxythioanisole **140** was chosen because of the electron donating group on the aromatic ring. It was reasoned that this would make the sulfur more nucleophilic, increasing the likelihood that it would attack the electrophilic nitrogen. Imination of sulfide was subjected to the same reaction conditions as previously reported for the formation of aziridine and led to recovery of starting material (Scheme 90).

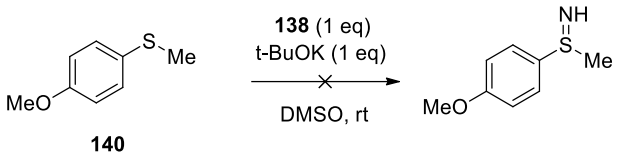

Scheme 90 Attempted sulfilimine formation.

An alternative base, as also reported for the formation of aziridine, was studied (Scheme 91). In this instance, the reaction solvent was changed in order to allow for sodium hydroxide to be adequately soluble. This too was observed to be unsuccessful by TLC and ^{1}H NMR and resulted in recovery of starting material.

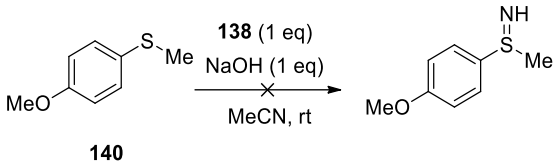

Scheme 91 Alternate method for sulfilimine formation

We considered whether the lack of reactivity of the hydrazinium salt was due to insufficient electrophilicity of the amine. If this was the case then the presence of the flavin organocatalyst would increase its electrophilicity, making it more prone to attack from the nucleophilic sulfide (Figure 12). The lone pair on the amine would bind to the flavin, generating an electrophilic nitrogen attached to a leaving group **141**.

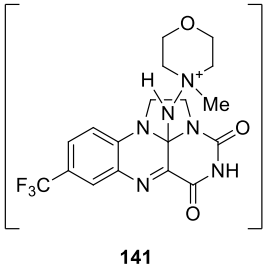

Figure 12 Postulated aminomorpholine and flavin transition state.

Upon the addition of the organocatalyst to the solution there was an immediate colour change from yellow to dark blue/black. This colour change was attributed to ion exchange with the chlorine counter ion of the flavin. The colour change of the reaction could be replicated by reaction of flavin and potassium iodide. This salt metathesis was not expected to affect the nucleophilic attack from the sulfur at the electrophilic nitrogen; however, the *N*-amino-*N*-methylmorpholinium nitrate salt **139** was synthesised to prevent unnecessary complication of the reaction (Scheme 92).

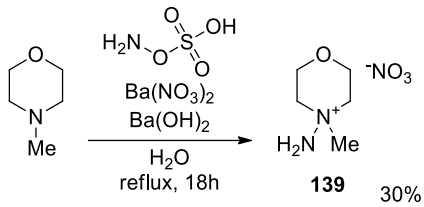

Scheme 92 Aminomorpholine nitrate synthesis.

The nitrate salt did not undergo the same colour change as the iodide salt had gone with the flavin organocatalyst, confirming our original hypothesis with regard to ion exchange. No other reaction was observed and starting material was recovered (Scheme 93).

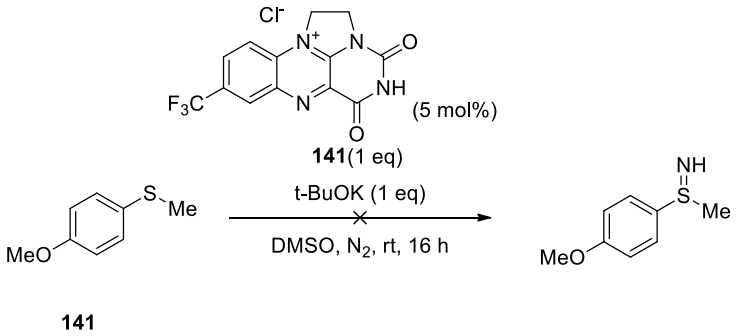

Scheme 93 Flavin catalysed sulfilimine formation.

A more nucleophilic source of sulfide could promote the formation of the desired product and the two aromatic groups of diphenyl sulfide **142** satisfied this criterion (Scheme 94).

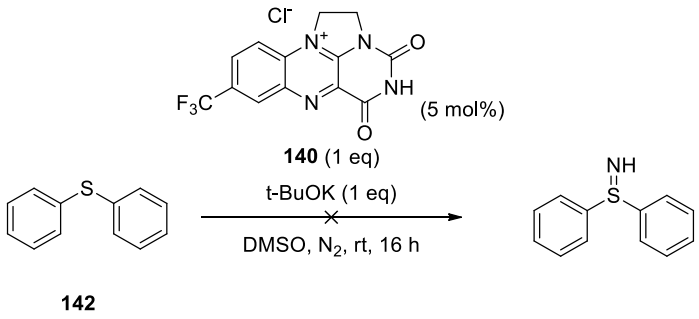

Scheme 94 Substrate modification to afford diphenyl sulfilimine.

Formation of the sulfilimine was not observed and starting material was recovered, despite the change of substrate. Diphenyl sulfide **142** was nevertheless used subsequent reactions.

It was hypothesised that the presence of base could be detrimental, and that the reaction could proceed without the presence of base (Scheme 95). This proved to be an inaccurate hypothesis and formation of the desired sulfilimine was not observed and starting material was recovered.

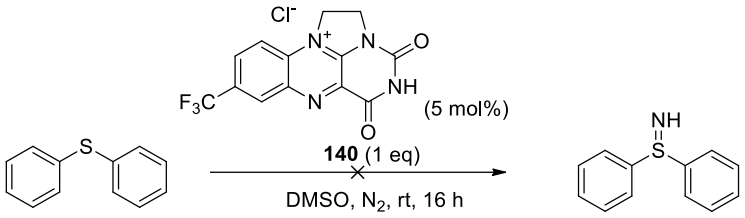

Scheme 95 Exclusion of base to afford diphenyl sulfilimine

Following the unsuccessful results of activating the nucleophilic sulfur, we hypothesised that the electrophilicity of the nitrogen could be improved (Scheme 96). The introduction of a benzoyl group on the amine, would pull electron density into the group benzene ring, making the nitrogen more electron deficient and therefore more prone to attack by the sulfur.

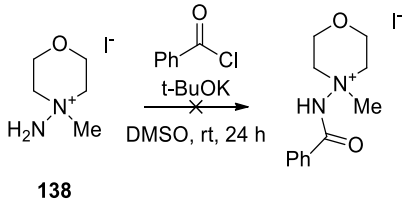

Scheme 96 Attempted hydrazinium iodide modification

No evidence was observed of formation of the desired product by TLC or by ^{1}H NMR and the **138** was recovered. It was decided not to investigate the reaction further.

The aminomorpholine salt was chosen as an electrophilic source of nitrogen, just as *m*CPBA can be used for the epoxidation of alkenes. When the source of electrophilic oxygen is a peroxyacid such as *m*CPBA, it is prone to attack from the nucleophilic π bond. This transformation is driven by the breaking of the O-O bond and is assisted by proton transfer to the ketone of the peroxyacid, which is in a favourable location in the 5-membered transition state (Scheme 97).

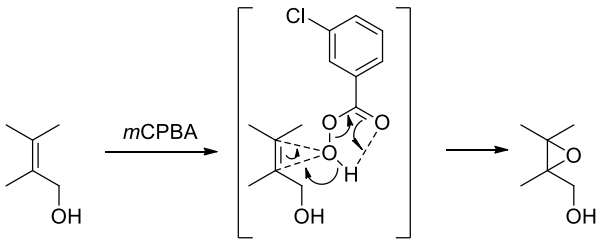

Scheme 97 Epoxide formation with *m*CPBA

Aminomorpholine salts have been used for the formation of aziridines with alkenes by Armstrong *et* al. They were found to be a highly effective aziridination reagent for the rapid conversion of chalcomes to *N*-unfunctionalised aziridines (Scheme 98).

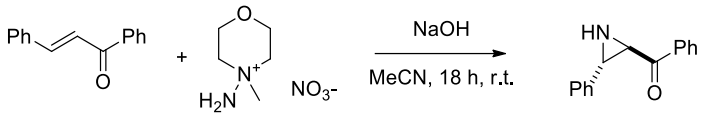

Scheme 98 Aziridine formation with aminomorpholine salts

As an aziridine is the nitrogen-containing analogue of an epoxide, it was initially assumed that the mechanism for their formation was similar with aminomorpholines, which was the reason behind their selection as a target. However, upon consideration of the mechanism it appears that it is more likely that the aziridine formation proceeds *via* nucleophilic attack from the pendant nitrogen. The authors observed a preference for electron withdrawing substituents on the under the reported reactions conditions, which in the presence of base, could indicate that the reaction is initiated by nucleophilic attack from the amine. Additionally, as the chalcone is electron deficient due to the ketone creating a Michael acceptor, it is a more potent electrophile (Scheme 99).

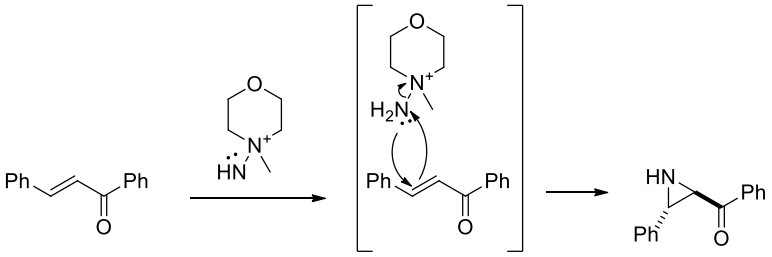

Scheme 99 Examining mechanism of aziridine formation

With this in mind, it should not be expected that the sulfilimine would be formed (Scheme 100).

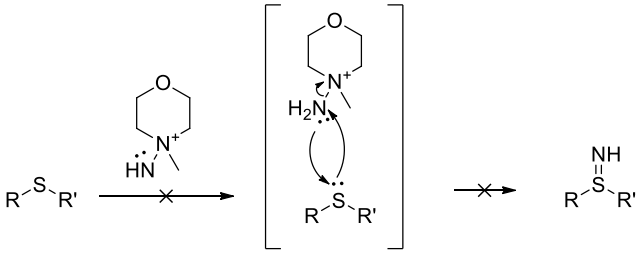

Scheme 100 Justification for lack of sulfilimine formation

3. Flavin-Catalysed Sulfide Oxidation with Hydroxylamine

Oxidation of sulfur-containing compounds is an extensive area of research with a wide range of natural processes discovered (e.g. Beggiatoa bacteria[161]). A range of metal catalysed synthetic routes have been developed that use vanadium,[162] zinc,[163] and copper,[164] to name a few. Non-meal catalysed routes have also been explored, with sodium perborate[117] and ammonium salts capable of affecting the desired transformation.[165] One such area of investigation is to use hydrogen peroxide as a green oxidant for the activation of flavins, generating the synthetically useful hydroperoxyflavin for sulfide oxidation. This procedure is well understood and often generates the corresponding sulfoxide without overoxidation to the sulfone, while the low weight hydrogen peroxide provides good atom economy.[41,44]
Despite extensive investigation into the use of the hydrogen peroxide/flavin system, there remains some inherent drawbacks with the use of this preparation. Primarily, hydrogen peroxide is often used as an aqueous solution, preventing its use in any applications that necessitate dry conditions. Furthermore, it is unsuitable for use in the oxidation of aldehyde containing sulfides due to the likely prevalence of a Dakin oxidation reaction generating the corresponding alcohol (Scheme 101).[166,167]

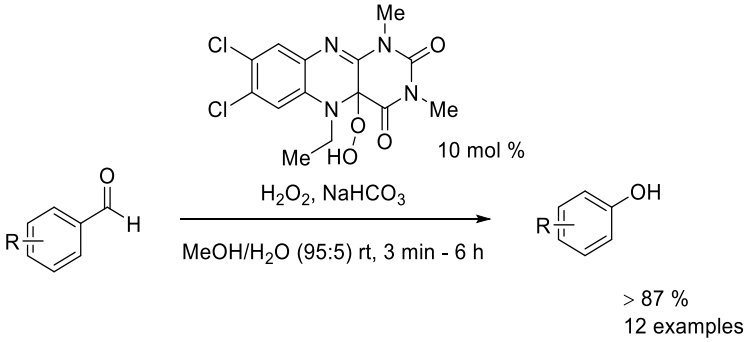

Scheme 101 Dakin oxidation and formation of alcohol in presence of flavin

3.1. *N*-hydroxybenzenesulfonamide and flavin

We are interested in expanding the scope of activation partners for the oxidation of sulfides with flavins, with the aim of addressing some of the flaws with the hydrogen peroxide/flavin partnership. After successful reactions with hydrazine it was decided to investigate further reaction partners for flavinium ions, in order to investigate reactivity towards sulfides. In the

search for a nitrogen transfer reagent, it was hypothesized that modified hydroxylamines could act as suitable synthons for sulfilimine formation. They ability to change the pendant functional group should lead to the adjustment in the reactivity of the nitrogen-oxygen bond in order to facilitate cleavage of the desired group. *N*-hydroxybenzenesulfonamide (Piloty's acid) **144** was investigated for its activity towards sulfur containing compounds. The electron withdrawing sulphonamide group should promote nucleophilic attack by the oxygen to the flavin, leaving an electrophilic nitrogen prone to subsequent nucleophilic attack from a sulfide. This would allow for the formation of a protected sulfilimine **145**, which could then be oxidised to form the sulfoximine, and finally, the sulfonamide group removed to yield the pharmaceutically desirable free NH- sulfoximine (Scheme 102).

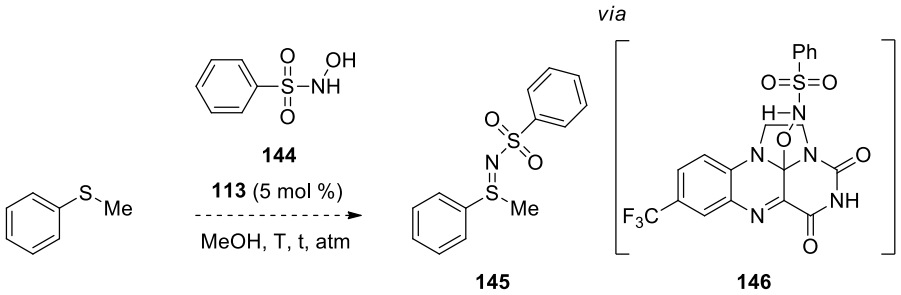

Scheme 102 Hypothesized pathway to sulfoximines with *N*-hydroxybenzenesulfonamide as a flavin reaction partner

Initially a protocol was modified from Carbery *et al*. that has been shown to achieve desirable results for the oxidation of sulfides with H_2O_2 and flavin with their simple, mild and robust preparation (Scheme 103).

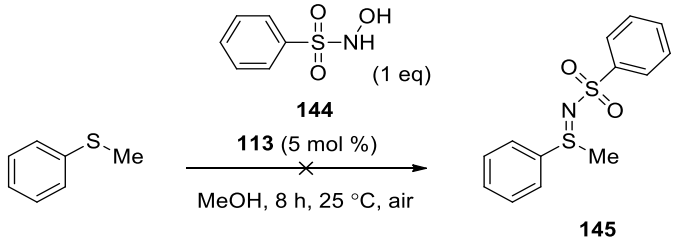

Scheme 103 Preliminary investigation into *N*-hydroxybenzenesulfonamide as a flavin reaction partner

Under the initial reaction conditions there was 100 % recovery of methyl phenyl sulfide. This was accompanied by a side reaction, as observed by TLC. One such reason for the selection of *N*-hydroxybenzenesulfonamide was its stability, as it has a relatively high melting point of 120 °C. With this in mind, initial investigations focussed on increasing the reaction temperature and varying the sulfonamide and flavin loading in order to yield

reaction at the sulfide. The reaction was also conducted in an inert atmosphere in an effort to suppress the side reaction (Table 18).

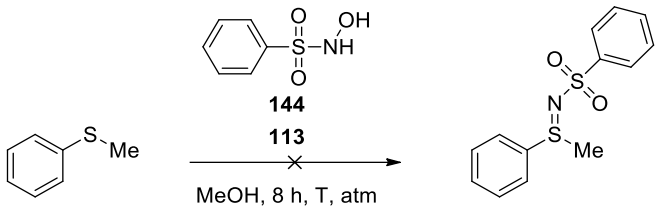

Table 18 Optimisation for sulfide reaction with *N*-hydroxybenzenesulfonamide

Entry	T °C	Atmosphere	N-hydroxybenzene sulfonamide (eq)	113 (mol %)	Sulfide Recovery (%)
1	25	Air	1.2	5	100
2	25	Air	2.0	5	100
3	25	Air	1.2	10	100
4	25	Air	1.2	100	100
5	25	Air	2.0	100	100
6	25	Air	2.0	10	100
7	25	N_2	1.2	5	100
8	25	N_2	2.0	5	100
9	25	N_2	1.2	10	100
10	25	N_2	2.0	10	100
11	65	Air	1.2	5	100
12	65	N_2	1.2	5	100

Table 18 clearly shows that N-hydroxybenzenesulfonamide is not a suitable reaction partner for flavin with regard to any reaction with sulfides, based on the reaction conditions investigated. The reagents were exposed to catalytic and stoichiometric catalyst loading, with complete recovery of starting material in all instances (entries 1-5). Increased loading of N-hydroxybenzenesulfonamide had no observable effect upon any sulfide reaction (entries 1 and 2), nor did performing the reaction in either inert or oxygenated atmospheres (entries 1 and 7). Finally, increased temperature had no impact upon the formation of any oxidised sulfur based product (entries 11 and 12).

The side reaction that was briefly mentioned was investigated and found to be a decomposition of the sulfonamide starting material, for which there was literature precedent (Scheme 104).[168]

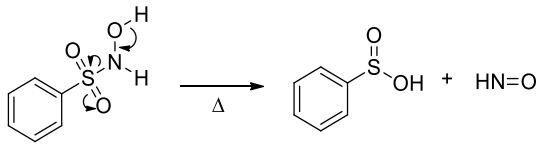

144 **145**

Scheme 104 Piloty's acid decomposition and release of nitroxyl

A nitroxyl group was released upon the breakdown of Piloty's acid, leaving benzenesulfinic acid as the detected side product. This sulfinic acid does not interact with the flavin and this breakdown could not be prevented.

3.2. Sulfur oxidation with flavin and hydroxylamine hydrochloride

We investigated the use of hydroxylamine hydrochloride as a reaction partner for flavinium salts using a modification of a procedure previously developed in the Carbery group.[44] Initially conditions led to the recovery of starting material (Scheme 105). Upon introduction of base, we were able to generate the corresponding sulfoxide.

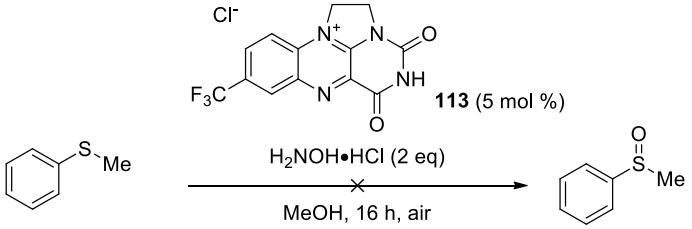

Scheme 105 Unsuccessful hydroxylamine hydrochloride mediated route

3.2.1. Optimisation of flavin catalysed sulfide oxidation

Upon investigation of appropriate base with which to take the reaction forward (Table 19).

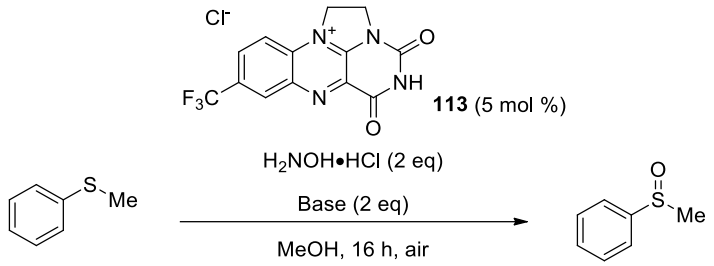

Table 19 Optimisation of base for sulfur oxidation

Entry	Base	Conversion (%)
1	-	0
2	KOH	0
3	$^{i}Pr_2NH$	78
4	Et_3N	58

Methyl phenyl sulfide was recovered in the absence of base (entry 1) and in the presence of the inorganic base potassium hydroxide (entry 2). The lack of conversion was attributed to the lack of solubility of potassium hydroxide in methanol. Methyl phenyl sulfoxide was formed cleanly and in good yields with diisopropylamine and triethylamine (entries 3 and 4).

Following the successful use of base to neutralise the hydrochloric acid salt, we had developed a novel procedure for the oxidation of sulfides with hydroxylamine hydrochloride, addressing a weakness of the aqueous hydrogen peroxide/flavin system (Scheme 106).

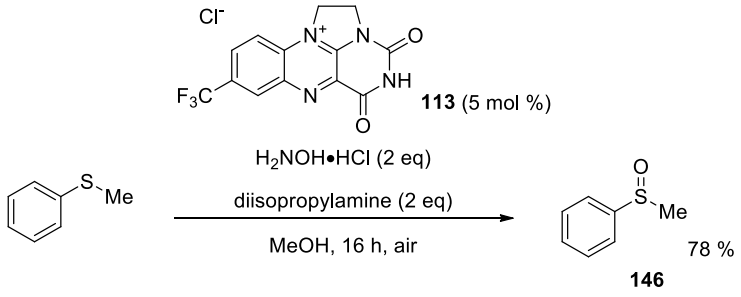

Scheme 106 Hydroxylamine hydrochloride mediated sulfide oxidation

3.3. Sulfide oxidation with flavin and aqueous hydroxylamine

It was decided to continue the investigation with an aqueous hydroxylamine solution for ease of operation (Scheme 107).

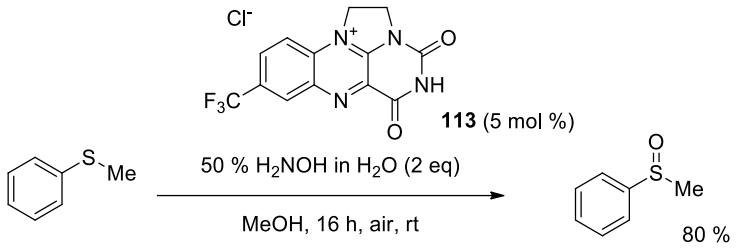

Scheme 107 Partially optimised sulfur oxidation conditions

The reaction was initially performed with methanol as a solvent due to the high solubility of the flavin catalyst. This was investigated with a solvent screen to determine whether the sulfur oxidation could be improved upon. The reaction time was decreased to 6 h for the solvent optimisation (Table 20).

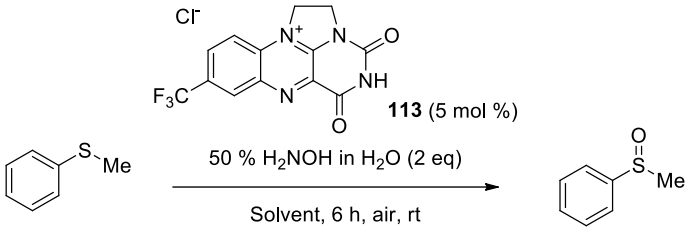

Table 20 Solvent optimisation for hydroxylamine formation of sulfoxide

Entry	Solvent	Conversion (%)
1	Chloroform	60
2	Dichloromethane	55
3	Acetonitrile	80
4	Acetone	45
5	Methanol	82
6	Ethanol	77
7	Trifluoroethanol	14
8	Water	7

Chlorinated solvents afforded modest conversions of 55 % and 60 % (entries 1 and 2). While acetonitrile afforded conversion equivalent to methanol (entry 3). Acetone resulted in a conversion of 45 % (entry 4) and ethanol was comparable to methanol with 77 % to 82 % (entries 5 and 6). Trifluoroethanol was low conversion, despite literature precedent for the solvent being successful in flavin catalysed sulfur oxidation.[42] The very low water conversion (entry 8) was attributed to the low solubility of the methyl phenyl sulfide in aqueous media. One water soluble sulfide is 2,2′-Thiodiethanol **147**, which could be used to probe the lack of conversion in this instance. However, due to the ease of which it can be

converted to the cytotoxic and vesicating mustard gas **148**, this hypothesis was not tested (Scheme 108).[169] Methanol was taken forward for all future reactions.

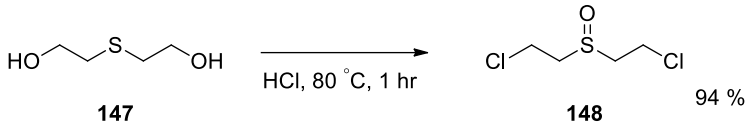

Scheme 108 1-Chloro-2-[(2-chloroethyl)sulfanyl]ethane formation from water soluble sulfide

Further optimisations were performed to investigate the ideal temperature and atmosphere, which provided an insight to the potential mechanism of action for the oxidation. A range of blanks were also obtained to confirm the necessity of individual reagents (Table 21).

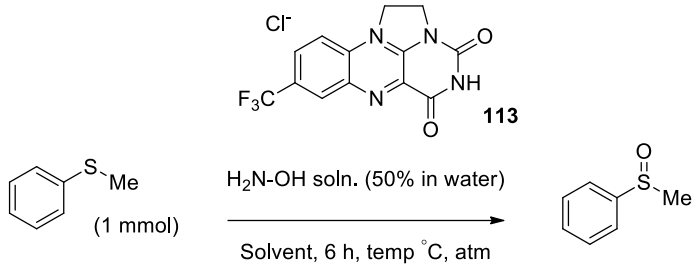

Table 21 Further optimisation

Entry	Temp °C	Atmosphere	Catalyst (mmol)	H_2NOH (mmol)	Atmosphere	Conversion %
1	25	Ar	0.05	2	Ar	0
2	50	Ar	0.05	2	Ar	0
3	65	Ar	0.05	2	Ar	0
4	25	air	0.05	2	air	42
5	50	air	0.05	2	air	44
6	65	air	0.05	2	air	40
7	25	air	0	2	air	0
8	25	air	0.05	0	air	0

In the absence of oxygen, there was no generation of sulfoxide and complete recovery of starting material (entries 1 – 3). This lack of reaction under inert conditions is a strong indicator that atmospheric oxygen is the terminal oxidant. There was no particular increase

in conversion with elevated temperatures (entries 4 – 6), which could be attributed to a decrease in levels of dissolved oxygen as the temperature increases.[170] The blank reactions confirmed that both hydroxylamine and the catalyst were integral to the sulfoxide formation (entries 7 and 8).

3.3.1. Hydroxylamine mediated sulfoxide formation mechanism

Analysis of the reaction optimisation led to the hypothesis of a reaction mechanism. Thus far, we have observed two modes of action for the oxidation of a flavin catalyst with respect to sulfide oxidation; generation of hydroperoxyflavin by some oxidant (e.g. hydrogen peroxide) or flavin reduction by some reductant (e.g. hydrazine) followed by hydroperoxyflavin formation with O_2. In both cases, the initial step is nucleophilic addition to the flavin at the most electrophilic point (Figure 13).

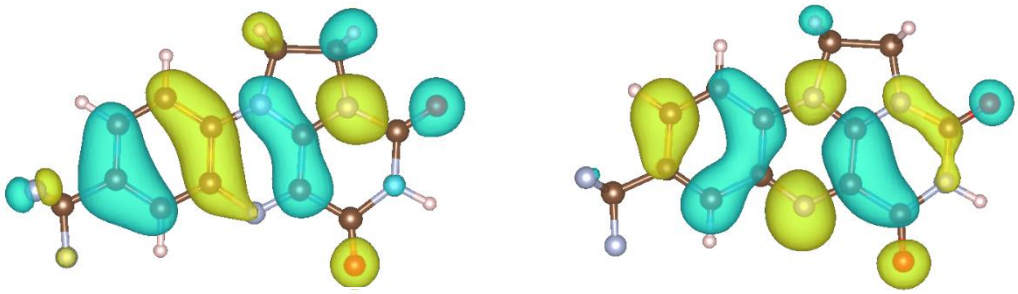

Flavin HOMO Flavin LUMO

Figure 13 Flavin HOMO and LUMO visualisations

From the visualisations of the flavin's highest occupied molecular orbital (HOMO) and lowest unoccupied molecular orbital (LUMO), we are able to use frontier molecular orbital (FMO) theory to identify electron localisation on the molecule. The frontier electron density is at its highest in the HOMO at the carbon of the isoalloxazine bound to the CF_3, which is unsurprising given the electron withdrawing nature of the trifluoro group. The LUMO shows some localisation at the expected carbon (under the bridge), which indicates it could be an appropriate electrophilic site, however, the aromatic nature of the flavin means that reactivity is not solely controlled by FMO theory, as resonance stabilisation effects are strong. In this instance there is a wealth of academic literature to indicate that the flavin reaction partner will undergo a nucleophilic addition under the bridge, in this case forming a flavin-hydroxylamine adduct.

Hydroxylamine has a pK_a of 5.95, making it a weak acid, and consequently suitable for reaction with the flavin catalyst. Hydroxylamine is unique of the flavin reaction partners we

have looked at thus far in that it is not a symmetrical molecule. This means it can form a hydroxylamine-flavin bond through either the nitrogen or oxygen atoms. If nucleophilic attack comes from the oxygen, then the resultant complex will be a distal nitrogen **149**. Alternatively, if nucleophilic attack comes from the nitrogen, the oxygen will be prone to nucleophilic attack from the nucleophilic sulfide **150** (Figure 14).

Figure 14 Proximal and distal binding sites of hydroxylamine with flavin

Only binding to the flavin through the nitrogen of the hydroxylamine allows for the nucleophilic attack of sulfide to form the sulfoxide, if the reaction is proceeding via an oxidative mechanism (Scheme 109a). Alternatively, if the first step hydroxylamine reduction of the flavin, the interaction of hydroxylamine and flavin is not dependent upon the hydroxylamine binding mode (Scheme 109b).

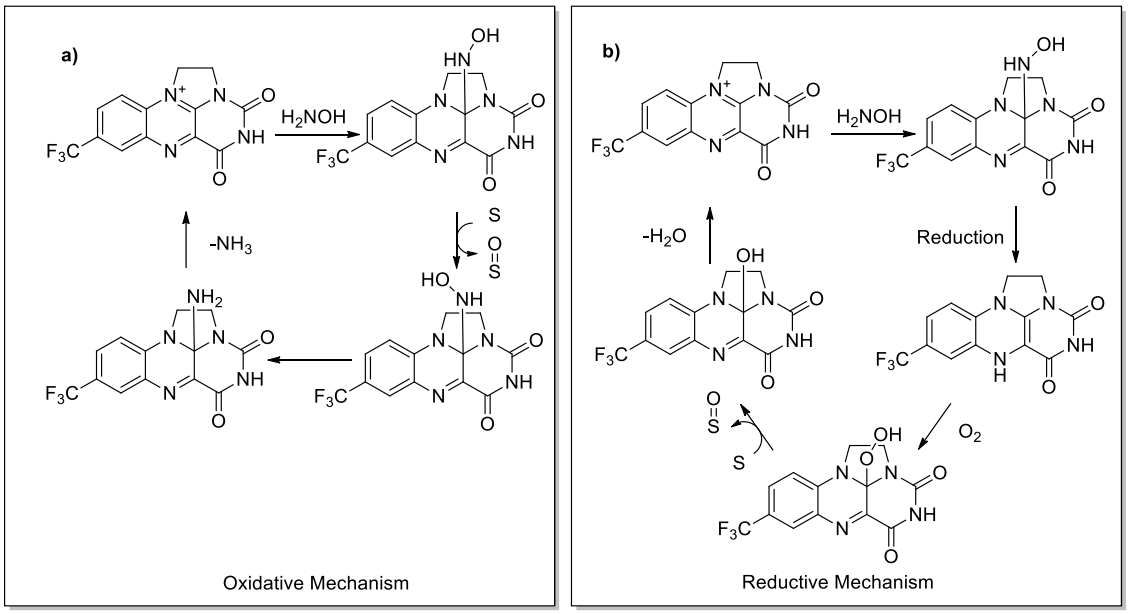

Scheme 109 Possible oxidative and reductive reaction mechanisms

Following the formation of the hydroperoxyflavin, the sulfide reacts through nucleophilic attack at the distal, electrophilic hydroperoxyl unit, to form the sulfoxide.[171] The addition of a reductant leads to the production of the reduced flavin and the hydroperoxyflavin is formed through addition of O_2 which is then prone to nucleophilic attack and sulfoxide formation.[50] This is the first example of hydroxylamine being used in the oxidation of sulfides, and it is situationally both an oxidant and a reductant.[172,173] Consequently, it's mode of action as a

reaction partner for flavin is unknown and there is little literature precedent to suggest whether the transformation will proceed *via* an initial oxidation or reduction of the flavin. Fortunately, both reaction mechanisms are well understood in their own right. A key step in the oxidation reaction would be the breaking of the nitrogen-oxygen bond, which must be broken upon nucleophilic attack by the sulfide at the electrophilic oxygen.

However, from the optimisation experiments, it was clear that the reaction didn't proceed in an inert atmosphere. This indicates that the N-O bond of hydroxylamine is not the terminal oxidant in this case and points to a hydroxylamine-mediated flavin reduction mechanism with air as a terminal oxidant. When H_2O_2 is used as a flavin reaction partner in an inert atmosphere, the yield is equivalent to when the reaction was performed in air (Scheme 110).

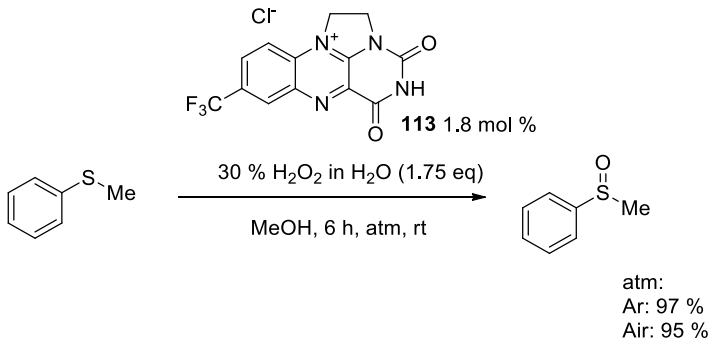

Scheme 110 Flavin catalysed sulfur oxidation with hydrogen peroxide in inert/oxygen containing atmospheres

This could be probed further by through oxygen labelling reactions, either by positive confirmation through reaction in an ^{18}O atmosphere, or by negative confirmation through reaction with labelled $H^{18}O\text{-}NH_2$. With these observations in mind, we propose a catalytic cycle consistent with Imada's proposed mechanism for the oxidation of sulfides, catalysed by flavin and a reducing reaction partner, with oxygen from air acting as a terminal oxidant (Scheme 111).[50]

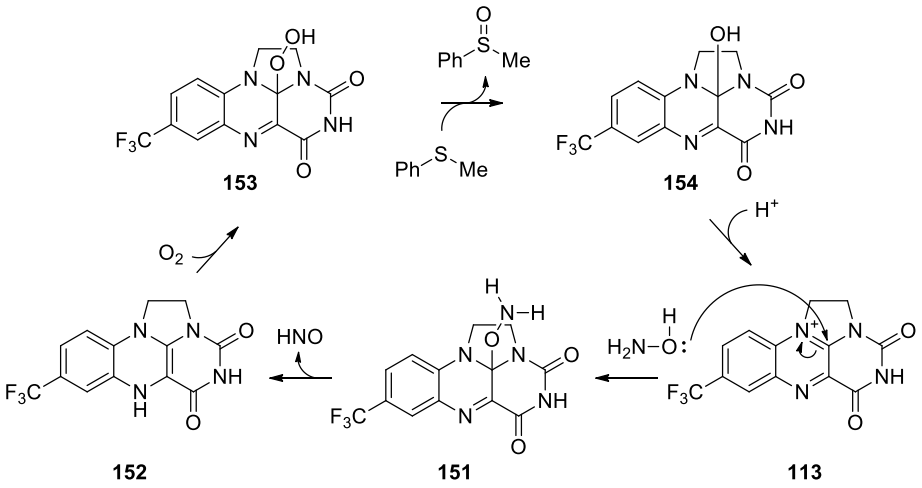

Scheme 111 Proposed reaction mechanism of flavin catalysed sulfur oxidation with hydroxylamine

3.4. Using flow NMR to probe reaction kinetics

Continuous flow is a technique that allows continuous reaction monitoring by means of constantly flowing a reaction down into the NMR probe. Back to back NMR experiments can be run sequentially for as long as is required with virtually no drawbacks. Continuous Flow NMR spectroscopy was performed on the oxidation of methyl phenyl sulfide in order to ascertain the kinetic profiles of this transformation. As the reaction is constantly monitored by NMR, a deuterated solvent was used (CD_3OD), as it was deemed preferential to artificial solvent suppression due to the closeness of the MeOH peak and the methyl peaks of interest. Methyl phenyl sulfide and methyl phenyl sulfoxide are ideal candidates for the use of flow NMR as the methyl peak is easily identifiable (**^{1}H NMR** (250 MHz, $CDCl_3$) Sulfide δ_H 2.42 (s, 3H); Sulfoxide 2.73 (s, 3H) (Scheme 112).

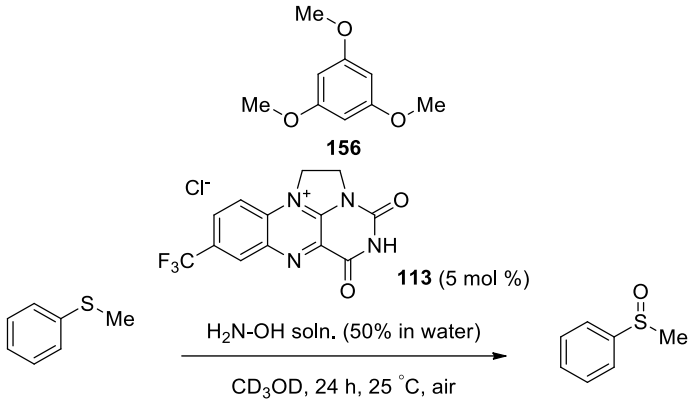

Scheme 112 Sulfur oxidation conditions for continuous flow NMR

The reaction was performed in deuterated methanol in order to prevent the spectra being dominated by solvent. Additionally, 1,3,5-trimethoxy benzene was added as an internal standard in order to calculate yield from the ^{1}H spectra.[174] The NMR spectrum showed that there is a linear relationship between consumption of methyl phenyl sulfide and production of sulfoxide. This can be clearly seen when observing the respective methyl peaks (Figure 15).

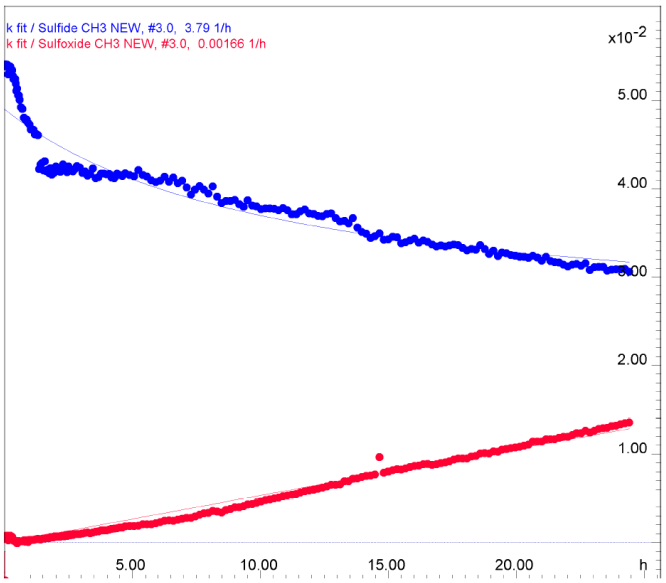

Figure 15 Relationship between methyl peaks of methyl phenyl sulfide and methyl phenyl sulfoxide

The concentration of methyl phenyl sulfide is consumed at a rate equivalent to the production of sulfoxide (Figure 15 – red) after the start of the experiment. Initially there is a significant apparent drop in sulfide concentration. This is due to an artificially high sulfide concentration in the flow **NMR** equipment as the reaction begins. It is normalised once the homogenised reaction has flowed the length of the flow apparatus. When observing the 3D plot of the full reaction the growth and consumption of the starting materials can be clearly observed (Figure 16).

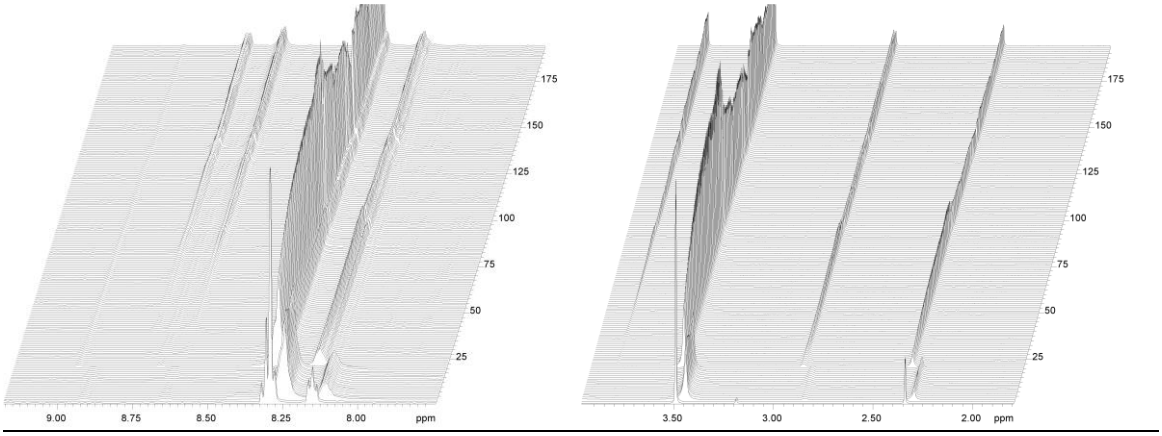

Figure 16 3d plot of flow NMR spectra

The 3d plot shows ideal separation of the peaks to use this technique for reaction monitoring (methyl phenyl sulfide ^{1}H NMR 2.40 (s, 3H), methyl phenyl sulfoxide ^{1}H NMR 2.73 (s, 3H)). It should be noted that although the spectra is suitable for this procedure, the oxidation did not reach the expected yields, as had been previously observed for this reaction. It is

possible that the use of the flow NMR kit did not allow for sufficient oxygen dissolution into the reaction, causing the lower than expected yield. The lack of paramagnetic disturbance in the continuous flow reaction monitoring could indicate that there is no radical activity in our system.

3.5. Reproducibility issues

It was hypothesised that a possible reason for the low conversion observed in the flow NMR experiment could be low levels of dissolved oxygen in the NMR system.
In order to investigate this hypothesis, the reaction was performed under the same reaction conditions in an NMR tube, without stirring (Scheme 113).

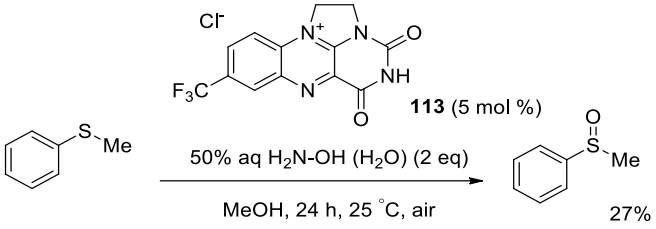

Scheme 113 Reaction undertaken in an NMR tube

It was observed that undertaking the reaction in an NMR tube had a significant impact on yield, resulting in the formation of 27 % methyl phenyl sulfoxide formed. This is consistent with the reaction being dependent on dissolved oxygen, as the NMR tube has a very limited surface area and no stirring.
In order to avoid this variable, the reaction was followed by taking aliquots from a reaction mixture at regular intervals followed by solvent removal *in vacuo*. After an aliquot had been removed, the solvent was immediately removed *in vacuo* to avoid any further reaction and a ^{1}H NMR obtained. This was repeated hourly over 6 h at which point full conversion should have been achieved. This process was repeated in triplicate (reactions 1-3) with identical reaction conditions (Figure 17).

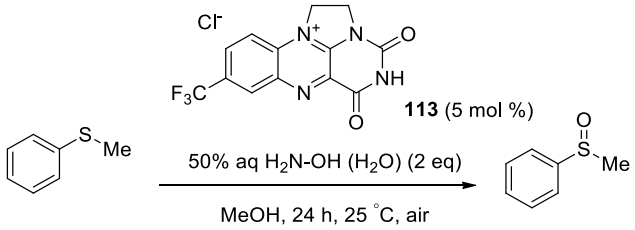

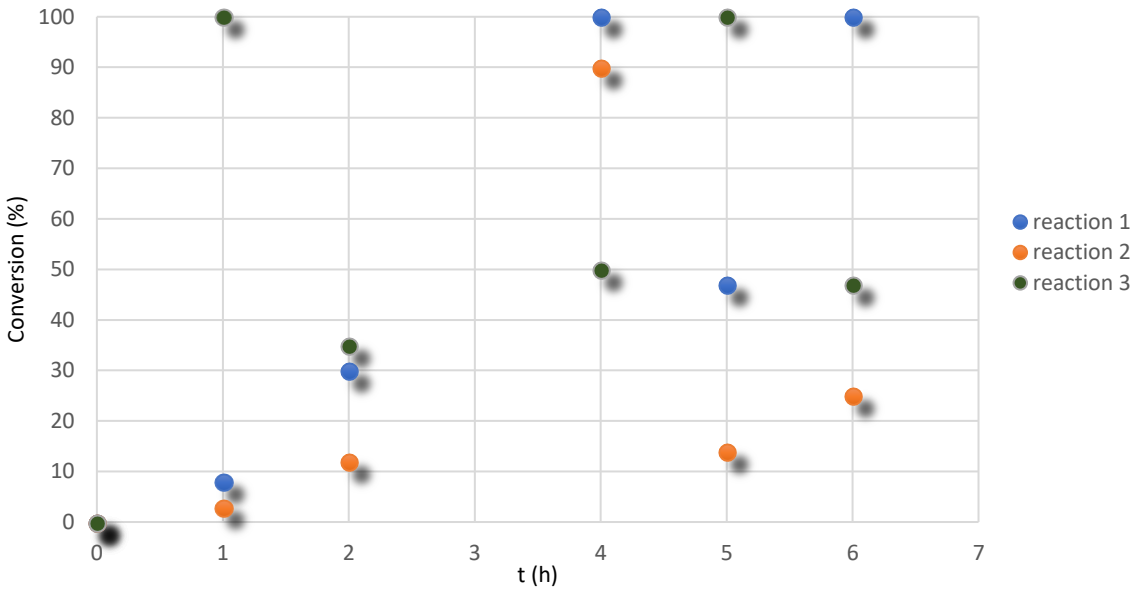

Figure 17 Variability of aliquot extracts

The experiment was repeated in triplicate, and vastly different conversions were monitored at each time point, and for each reaction. It indicates that conversion is not linear, however, no such trend was observed when the reaction was monitored by flow NMR. It was hypothesised that the observed results were not representative of the bulk reaction as no decrease in conversion was observed when the reaction was performed in an NMR tube. We initially proposed this lack of reproducibility to be due to volatility of thioanisole under vacuum (bp 188 °C). However, after exposure to low pressure conditions for 1 h, no mass loss was observed.

A second hypothesis was that a reduction in volume of solvent under reduced pressure was leading to an increased rate of reaction in the rotary evaporator. In order to investigate this hypothesis, a series of reactions were performed with varying amounts of solvent (Table 22).

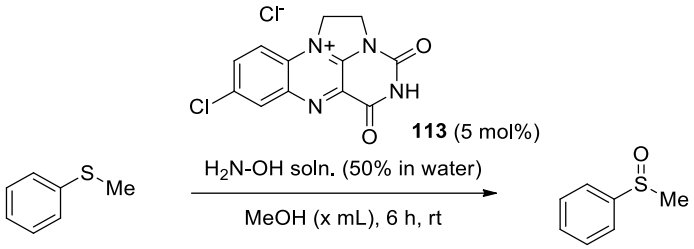

Table 22 Varying solvent volume

Entry	[sulfide] M	x (mL)	Conversion (%)
1	-	0.0	5
2	0.250	0.2	22
3	0.125	0.4	52
4	0.083	0.6	47
5	0.063	0.8	58
6	0.042	1.0	56

In order to remove the unknown variable of removing solvent in *vacuo*, the reaction was subjected to an aqueous work-up to remove the catalyst and quench the reaction. There was a significantly reduced conversion in a solvent-free reaction (entry 1), and reduced conversion with 0.2 mL solvent (entry 2). Further increase in solvent amount led to no increase in conversion (entries 3-6). Therefore, the reduction of solvent volume under reduced pressure was the significant cause of irreproducible results.

The cause of this irreproducibility remains unknown. In an effort to avoid this unwanted variable, and track the true progress of the bulk reaction, alternative methods were used to investigate the kinetics of the reaction.

3.6. Electron paramagnetic resonance (EPR) spectroscopy

EPR, or electron spin resonance (ESR) spectroscopy, is a technique used for studying unpaired electrons (radicals) in a system. The procedure is comparable to NMR resonance, but measures the excitement of electron spins, as opposed to monitor the spins of atomic nuclei. EPR relies on magnetisation to monitor radicals, and as such, requires a spin quantum number of $S \geq ½$. The magnetic moment of an electron can be split into 2 parts, spin angular momentum, and orbital angular momentum. These equations can be combined to give the total magnetic dipole moment of an electron.

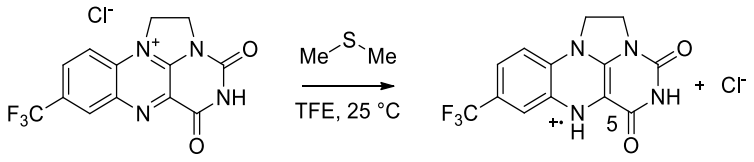

113 155

Scheme 114 Flavin radical generation with dimethyl sulfide with appropriate atom numbers

At room temperature in a liquid solution, molecular movement of the radicals is unrestricted, which results in any anisotropy in either the hyperfine splitting or the global *g* factor is observed as an average.

Isotropic coupling is observed to nearly 3 equivalent ^{14}N nuclei, giving rise to a hyperfine structure. This coupling accounts for ~ 22 MHz, resulting in a spin density of 20 % in the *2p* orbital of the ^{14}N atom. The majority of the protons lie in the same plane as the π orbital that is taken up by the unpaired electron of the semiquinone flavin ring. A significant amount of coupling was also observed at N(5) Numerical simulations were then run for these ^{14}N and semiquinone environments until there was strong agreement between the simulated and observed spectra, resulting in the proposed radical cation.[175]

This system reported in the literatures shares significant characteristics with the oxidation of sulfides by hydroxylamine, particularly in the case of the dimethyl sulfide. Murray *et al.* did not investigate any other sulfides, so the effect of different sulfides on the generation of the flavin radical is unknown. Unfortunately, it was not possible to undertake EPR experiments in the course of this project.

3.7. Following kinetics by HPLC

High-performance liquid chromatography was deemed a suitable method with which to follow the progress of the reaction. This method did not have the drawbacks encountered when following the reaction by ^{1}H NMR (no need for solvent removal), which should have allowed the true progress of the reaction to be followed. Initially, it was decided to measure the formation of the sulfoxide peak as the reaction progressed. Various reaction solvent systems were investigated however the sulfoxide peak could not be resolved sufficiently to generate reliable data.

In order to bypass the poorly resolved sulfoxide peak, the consumption of thioanisole was measured instead. A sharp peak was obtained with a short retention time as the non-polar sulfide had minimal interaction with the stationary phase of the columns investigated.

Naphthalene was introduced as an internal standard to calculate the true concentration of the starting material. Unfortunately, naphthalene also has a very short retention time and resulted in inadequate resolution between the starting material and the internal standard. Gas chromatography represents a potential alternative analytical technique for this investigation.

3.8. Sulfide Oxidation

With a reproducible procedure in hand for the clean oxidation of sulfides, without overoxidation to the sulfone or degradation of catalyst, we were able to obtain the corresponding pure sulfoxide in 16 h after separation into an organic phase, solvent removal and column chromatography. We then went on to oxidise a range of sulfides to the corresponding sulfoxides (Table 23).

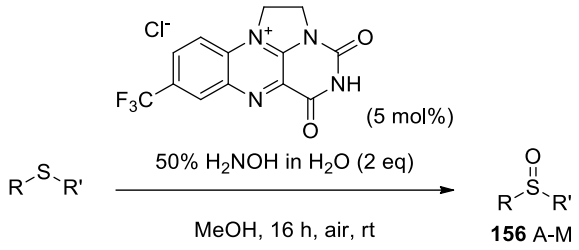

Table 23 Substrate scope for flavin catalysed sulfide oxidation with hydroxylamine

Entry	R	R'	Product	Yield/%
1	C_6H_5	Me	A	98
2	C_6H_5	C_6H_5	B	82
3	C_6H_5	$CH_2CH_2{=}CH_2$	C	48
4	4-Me-C_6H_4	Me	D	68
5	4-OMe-C_6H_4	Me	E	62
6	4-CHNOH- C_6H_4	Me	F	45
7	4-Br-C_6H_4	Me	G	22
8	Me	Me	H	52
9	Me	$(CH_2)_{11}Me$	I	51
10	Me	$(CH_2)_3OH$	J	42
11	Me	$CH_2CH_2CO_2Me$	K	35
12	$(CH_2)_3Me$	$(CH_2)_3Me$	M	38
13	$CH_2CH_2{=}CH_2$	$CH_2CH_2{=}CH_2$	N	0

The reaction was more efficient for aryl sulfides (entries 1 – 7) with excellent yields obtained in the cases of methyl phenyl sulfoxide and diphenyl sulfoxide (entries 1 and 2). Electron

donating groups such as methyl and methoxy (entries 4 and 5 respectively) resulted in good yields. The reaction tolerated functional groups well with generation of the corresponding sulfoxide without formation of side products for oxime- (entry 6) and bromo- containing substituents, although yield was low in the case of the electron withdrawing bromo group (entry 7). In general, oxidation of alkyl substituents was significantly poorer in comparison to sulfides containing an aryl substituent. Dimethyl sulfide oxidised reasonably, as did dodecyl methyl sulfide with yields of 52 % and 51 % respectively (entries 8 and 9). However, functional groups were not tolerated in the case of alkyl sulfides, with poor yields for 3-(methylthio)-1-propanol and methyl 3-(methylthio) propionate (entries 10 and 11). Recovery of starting material was observed in the case of allyl sulfide (entry 13).

3.9. Design of experiment (DoE)

3.9.1. One variable at a time optimisation

The traditional approach to experiment optimization is a “one variable at a time” (OVAT) approach, where by one input is changed while the remaining controllable variables are held constant. This input is then subsequently changed again and again until an optimum output, has been reached. This process is then repeated for all individual variables until the conditions for a wholly optimised reaction system are obtained.

Consider a 2 component reaction where reaction temperature and concentration are the two variables of interest, the key response of interest is yield (Figure 18).

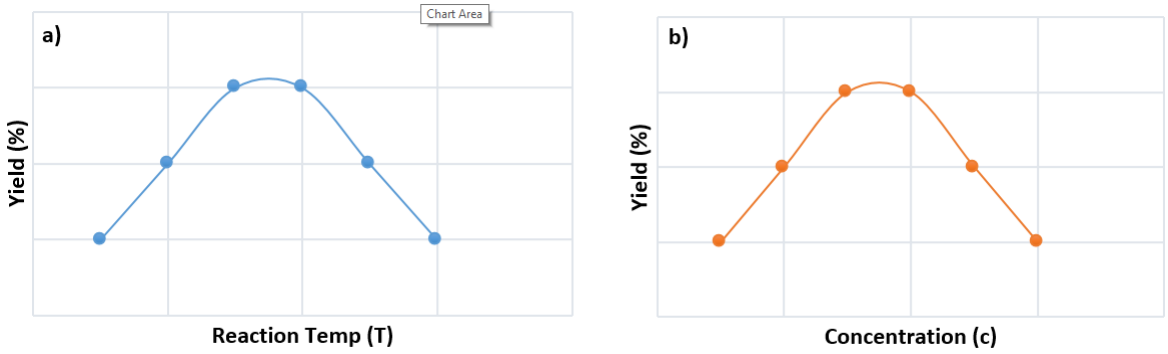

Figure 18 An OVAT approach to reaction optimisation

Temperature (Figure 18) is initially optimised, at which point that temperature value is taken forward for the optimisation of concentration (Figure 18). The OVAT approach can be continued for any number of parameters, however there are several disadvantages to consider. By changing one parameter at a time, there is no guarantee that the global optimum

has been found, and instead there is a danger that you have reached a local optimum point (Figure 19). This limited coverage of reaction design space can lead to inefficient use of time, or valuable chemical. Finally, there is no allowance for the interpretation of interactions of the variables upon one another.

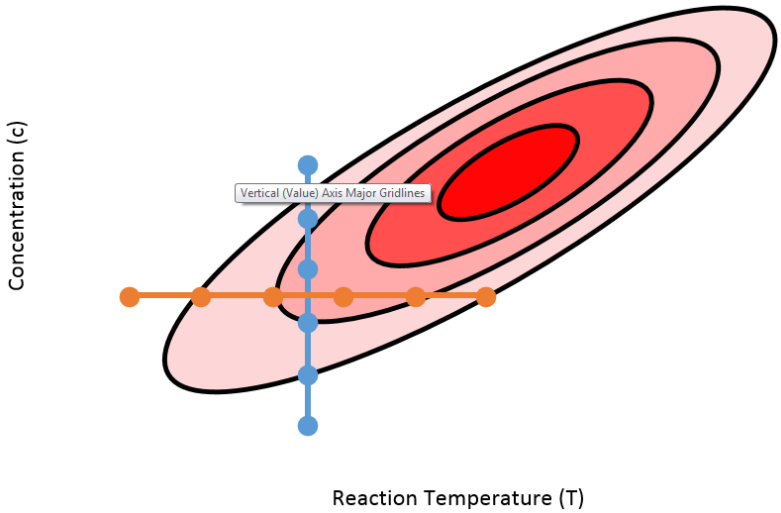

Figure 19 Demonstrating optimising to local minima

Figure 19 is a representation of how a reaction can be optimised to a local minima while neglecting the global minima for a 2 factor system. The approach scales linearly with respect to the number of variables that are to be investigated, i.e. one more variable increases the total number of reactions required as each previous variable. Furthermore, as the optimisation of each individual variable, the global optimisation is effectively a series of sequential steps, with each previous variable needing to be feely optimised before a work can begin on a subsequent variable. This drawback can result in long overall optimisation times, with the increased use of potentially expensive or toxic reagents. An alternative method to OVAT is to use a screening design approach.

3.9.2. Factorial experiment design (FED)

Just as reaction variables are defined in advance in an OVAT optimisation, the same is true of a FED. In the same 2 factor system, where reaction variables are temperature and concentration, clearly defined experimental ranges are required for the optimisation, and the minimum number of experiments is calculated from the number of variables being investigated. Unlike traditional optimisation, DoE techniques become more efficient with increased number of variables, and when conducting FED, each variable is evaluated at the extreme ends of the predefined experimental ranges. In a two-variable system, the minimum

number of experiments is 8, and the introduction of a 3rd variable (e.g. catalyst loading) leads to 12 experiments.

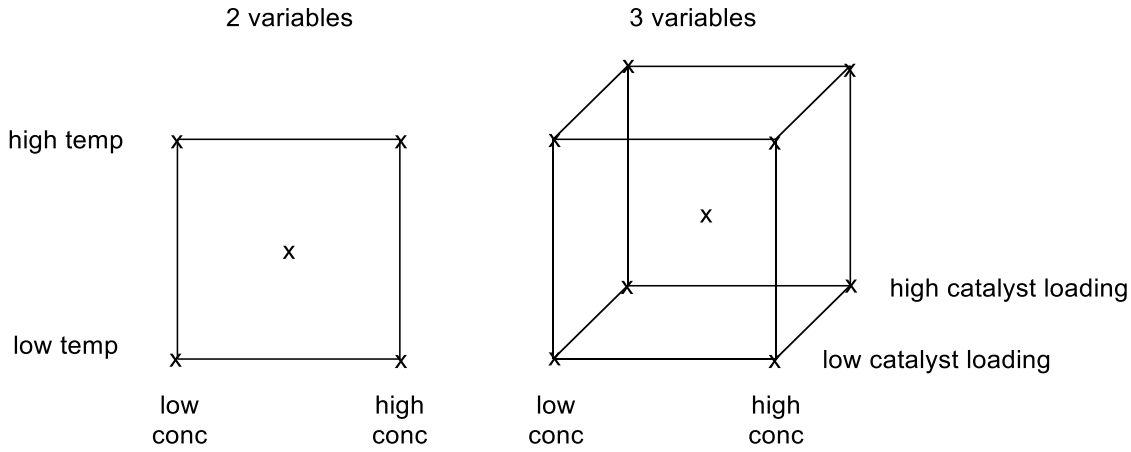

Figure 20 Demonstrating increased minimum number of experiments as variables are added

The effect on minimum reaction number upon further increased variables follows according Equation 1, where E is the minimum number of experiments required and n is the total variables. The addition of the constant 4 is to account for the centre point reaction and 3 repeat experiments, which are required to introduce confidence into the mathematical model.

$$E = 2^n + 4$$

Equation 1 Effect of increased variables on minimum reaction number

Although the effect of increased variables is easily predictable, when adding more and more components into a DoE, the exponential increase can lead to a large number of reactions being required, albeit with excellent coverage of the reaction space. For example, a reaction with variables (temperature, concentration, catalyst loading, volume, reagent 1 loading, reagent 2 loading) would require a minimum of 67 experiments. A solution to this problem of ever increasing experiments can be found in fractional factorial design, whereby multiple parameters are assigned to the same mathematical term (a concept known as aliasing). The main drawback of fractional factorial designs is that it may not be possible to definitively define the source that brings about a desired response (i.e. increased yield).

Historically, models for computing the reaction space were calculated by hand, in a prolonged process that often outweighed the time saved from performing the DoE. There are now a number of software models to greatly simplify the process. Examples include JMP, Minitab, Cornerstone, Design-Expert and MODDE. The following FED was performed using MODDE (Umetrics, Umea, Sweden) for the optimisation of sulfoxides with hydroxylamine. Initially 5 design factors were considered (Scheme 115).

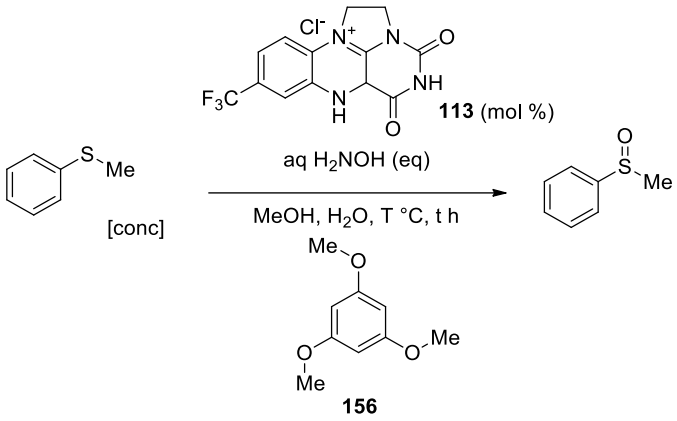

Scheme 115 Sulfoxide formation from sulfide with hydroxylamine

The factors investigated were; Thioanisole concentration (M), in order to understand the effect of overall concentration on the reaction. Hydroxylamine concentration (M), preliminary studies had suggested that the reaction might be catalytic with respect to hydroxylamine, and part of the reason for investigating this variable was to confirm that hypothesis. Flavin concentration (M), was investigated in order to determine whether the catalyst percentage could be dropped any further. Temperature (°C) was investigated as previous reactions had suggested that the reaction didn't serve to improve conversion, and water content % v/v which was investigated in order to maintain consistency when changing the concentration of aqueous hydroxylamine used (Table 24).

Table 24 Low, medium and high values

	[Sulfide] (M)	**[Hydroxylamine] (M)**	**[Flavin] (M)**	**Temperature (°C)**	**Water content (% v/v)**
Low	0.4	0.2	0.016	20	10
Med	0.6	0.9	0.028	30	12.5
High	0.8	1.6	0.040	40	15.0

The responses looked for are; Induction time, maximum observed rate, conversion after 12 hours, extrapolated final conversion and time to completion. All reactions were profiled by HPLC sampling over 12 hours and 1,3,5-trimethoxybenzene was added to ensure area % was representative of molar amounts and to calculate yield and rate conversion numbers. The fractional factorial design determined 15 reactions were necessary to define the experimental space (experimental section (Table 29).

The 15 reactions stem from 12 individual reactions (entries 1 – 12) and three repeats (13 – 15) to give a high level of mathematical certainty. The experiments were conducted in 2 batches (run 1 and run 2) of 7 and 8 parallel reactions on an Amigo Workstation (with the

capacity for up to 10 reactions in parallel). The experiment number and order were defined by the software (exp # and run order) in order to eliminate any systematic errors in the set up process. Aliquots were taken after 5 minutes, and then at 60, 120, 180, 240, 300, 360, 420, 480, 600, 720, 840, 1080 and 1440 minutes respectively, with the reaction halted upon aliquot extraction by 150-fold dilution.

As previously mentioned, 5 responses were examined, induction time, maximum rate, conversion after 12 h, eventual conversion, time to completion (reaction details in experimental section).

Models were not obtained for induction time and maximum observed rate as there were low levels of confidence in this data. Non-predictive models were obtained for conversion after 24 h, eventual conversion and time to completion, however as the models were not predictive, they only indicate general trends in factor effects for these responses (Figure 21).

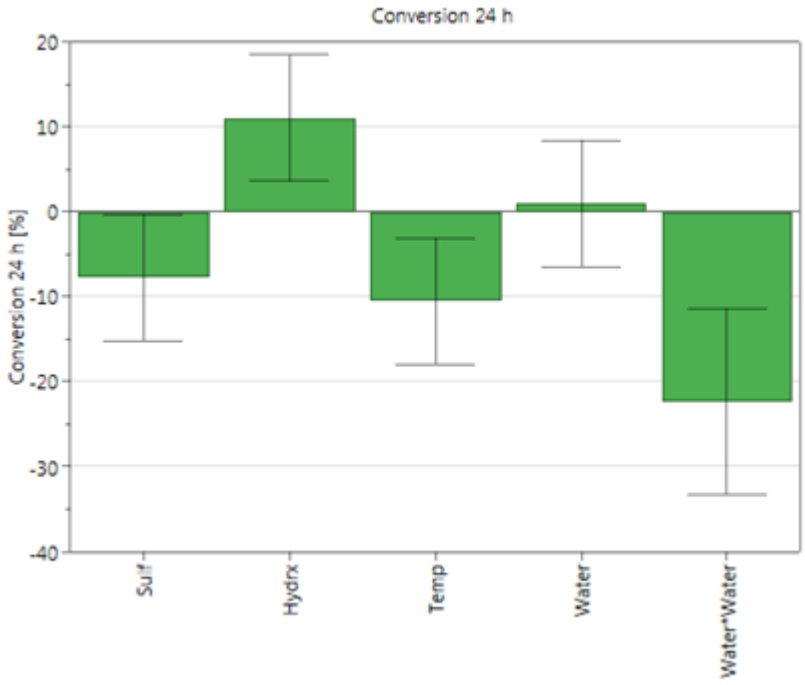

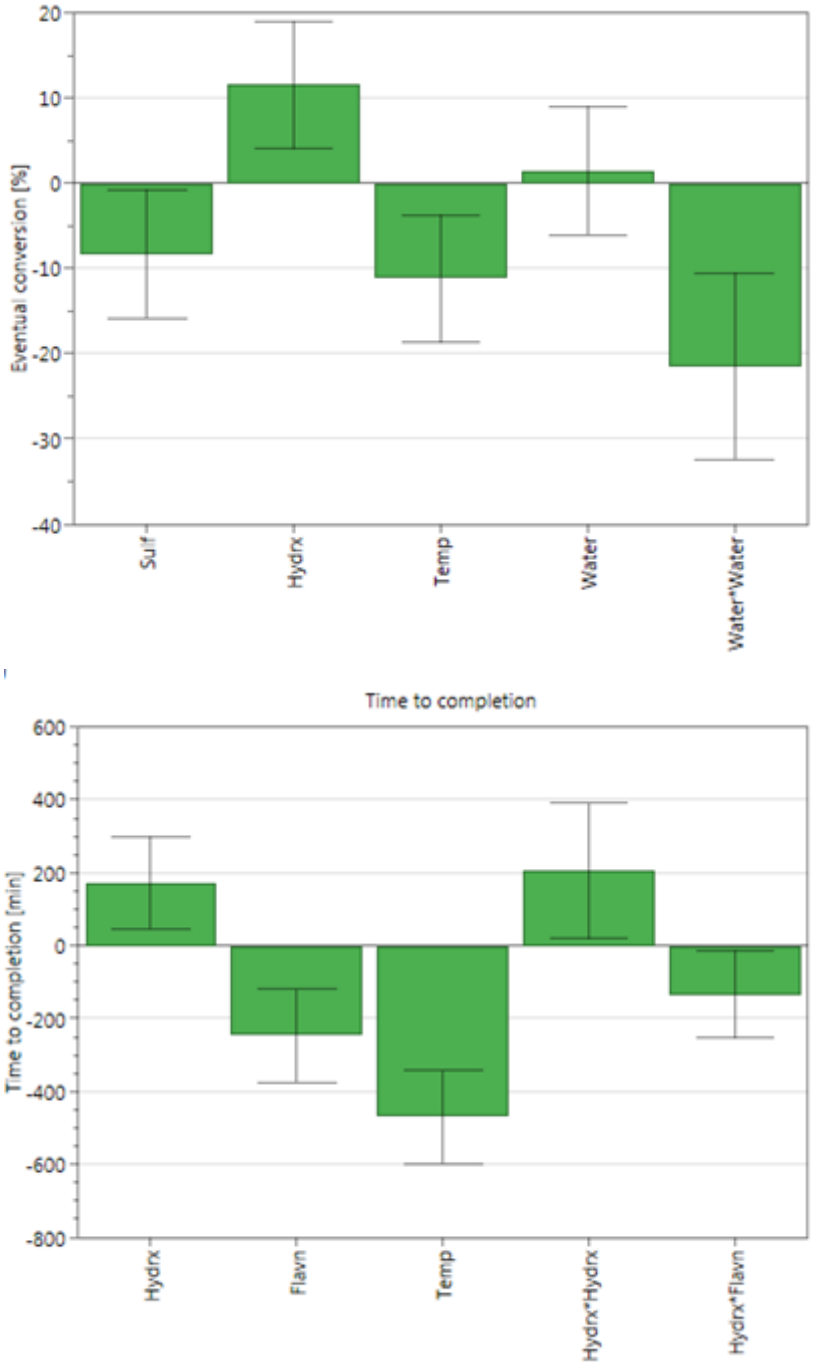

Figure 21 Coefficient plots for non-predictive models for conversion (24 h), eventual conversion and time to completion

Figure 21 demonstrates that the models are non-predictive as there are large error bars across the 3 responses modelled. The models show lower sulfide concentration leads to lower conversion after 24, and lower eventual conversion, suggesting that the reaction would benefit from higher concentrations, however, this is in contrast to previous investigations that suggested lower concentration is optimal. There is a significant dependence on hydroxylamine levels, which suggests that the reaction is not catalytic in terms of

hydroxylamine, which is a result that is in line with other flavin reaction partners (e.g. hydrogen peroxide). There is a negative correlation between temperature and conversion (both eventual and after 24 h), and it is suggested that high temperatures could lead to catalyst deactivation, although there are literature examples of the same flavin catalyst operating well at significantly higher temperatures (up to 85 °C).[176] It is suggested that the increased temperature leads to decreased dissolution of oxygen in the reaction solvent.[170] The effect of water was negligible, and did not serve to directly affect the conversion, however, the computed combined fractional effects of water appeared to have a significant effect on conversion. This could be explained through high levels of water affecting the phase solubility of the flavin catalyst. However, as the water levels were investigated, primarily to ensure consistency when adding an aqueous reagent, the negative impact was not a source of concern. Lower flavin levels impacted the time to completion, but did not appear to impact the conversion (eventual or after 24 h).

4. Investigation into flavin decomposition

4.1. Flavin and sodium azide interaction

In the continued search for suitable nitrogen sources to mediate the formation of sulfoximine from sulfoxides, we investigated the use of sodium azide. Thus far any co-reagents have been selected to take advantage of the sulfide nucleophilicity by utilizing flavin catalysis to create an electrophilic source of nitrogen **157**. This nitrogen centre would then be prone to nucleophilic attack from the sulphide substrate, creating the desired sulfilimine.

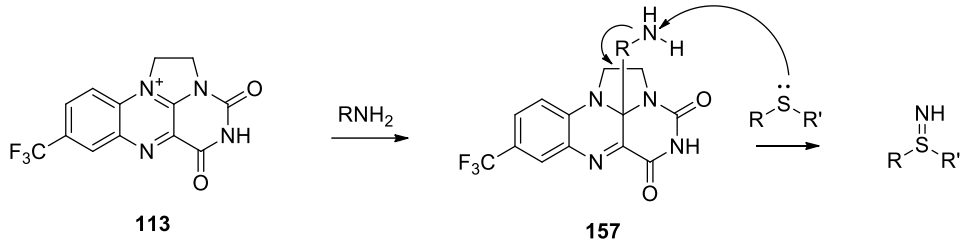

Scheme 116 Formation of an electrophilic source of N

It is for this reason of reactivity that the more nucleophilic sulphide has been selected, as opposed to the less nucleophilic sulfoxide. However, the majority of the reaction partners examined thus far have served to generate a reduced flavin reactant, which is then oxidised in the presence of atmospheric oxygen, resulting in an electrophilic hydroperoxyflavin species that is prone to nucleophilic attack from the sulfide. Furthermore, it is crucial for any flavin partner to interact with the flavinium catalyst to form any potentially active transition state. It is hypothesised that as azide is extremely nucleophilic and the electrophilic site of the flavin is well understood, reactionbetween the two will result in the formation of the reactive intermediate **158**.[177–179]

The use of sodium azide represents an alternate mode of action, whereby the highly nucleophilic azide can serve to a nitrenoid, leading to the imination of sulfoxides (Scheme 117).

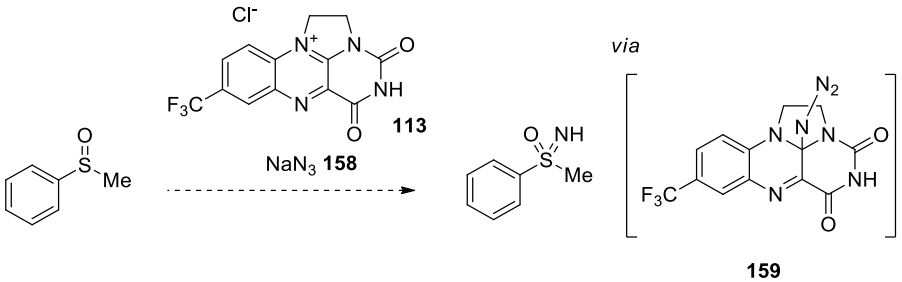

Scheme 117 Proposed route to sulfoximine formation

Despite the assertion that the use of explosive sodium azide has hampered the expansion of the sulfoximine core into pharmaceutical drug space, the potential synthetic value of this transformation was deemed significant enough to take the investigation forward.

A modified protocol published by Carbery *et al*. for the flavin catalysed synthesis of sulfoxides[146] was used as a starting point for the investigation into sodium azide, with methanol selected as the solvent due to its ability to solubilize the flavinium catalyst (Scheme 118).

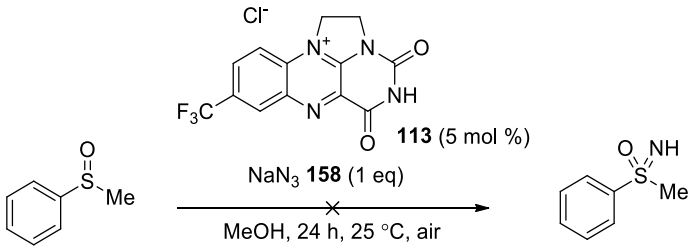

Scheme 118 Initial conditions for the imination of sulfoxides

Initial experiments were unsuccessful with regards to the formation of sulfoximines, with starting material being recovered in full, although significant colour change from yellow to red was observed immediately. Due to the propensity of the flavinium catalyst to be reduced and then use air as a terminal oxidant, the possibility that sodium azide was acting in this manner was investigated. This hypothesis was tested by substituting methyl phenyl sulfoxide with methyl phenyl sulfide in order to observe any sulfur oxidation (Scheme 119).

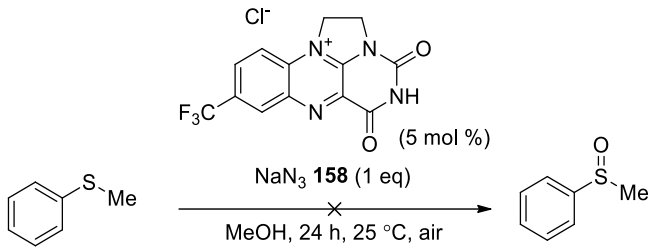

Scheme 119 Investigation of the action of sodium azide and flavinium salts towards sulfilimines

The reaction yet again led to recovery of the starting material. This was important to investigate as it is well documented that one of the strengths of the hydroperoxyflavin intermediate is to control the oxidation to sulfoxides without overoxidation the sulfone. The absence of any sulfoxide product, in this instance, suggests that sodium azide is not generating the hydroperoxyflavin. Despite this, it was clear that some reaction was taking place due to the colour change.

A yellow to red colour change was observed in this reaction with both the sulfide and sulfoxide starting materials. These colour changes were accompanied by the observation of

a new reaction components when thin layer chromatography (TLC) plates were visualised under UV light. Despite the recovery of sulfide, it was felt necessary to confirm that the sulfur components were not taking part in this reaction and a blank was run without either the sulfide or sulfoxide components (Scheme 120).

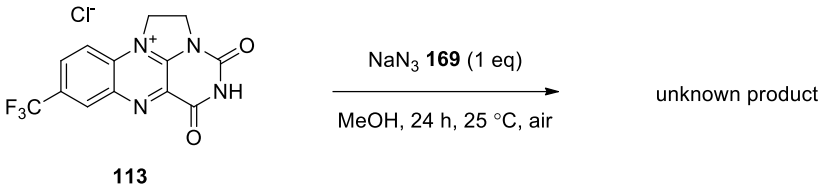

113

Scheme 120 Confirming sulfur components are a bystander in the reaction

Due to the strongly UV-active nature of the unknown product, it was assumed that it was some degredation of the photoactive flavin. This blank reaction resulted in the same colour change and an unknown product with the same Rf value as the previous reactions, leading to the conclusion that the sulfur containing compounds are not involved in the reaction. As the sodium azide is fulfilling a key objective of the flavin reaction partner by interacting with the flavin, it was decided to further investigate this reaction in order to understand that interaction, and if possible, modify it to achieve sulfur imination.

4.2. Investigation into sodium azide product structure

4.2.1. NMR investigation

The product was initially isolated and subjected to standard analysis techniques (^{1}H and ^{13}C NMR and mass spectrometry) which did little to assist in the structural assigning of the unknown molecule. The discrepancies between ^{1}H NMR spectra of the two compounds are shown below (Figure 22 and Figure 23).

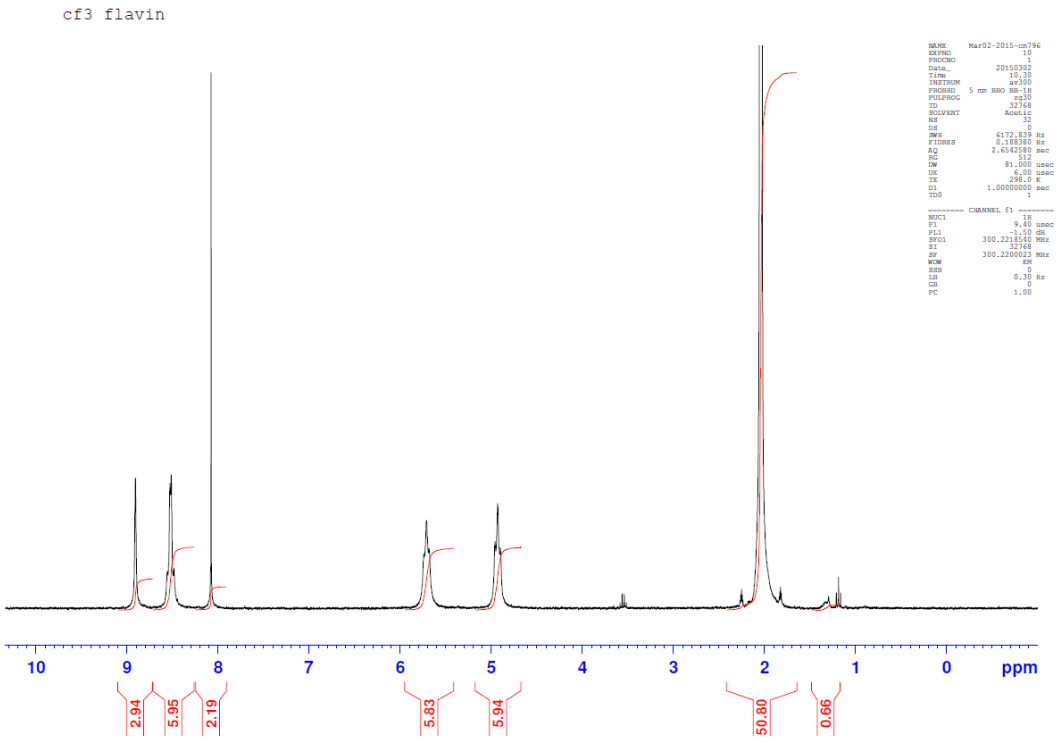

Figure 22 NMR of pure CF_3 flavin

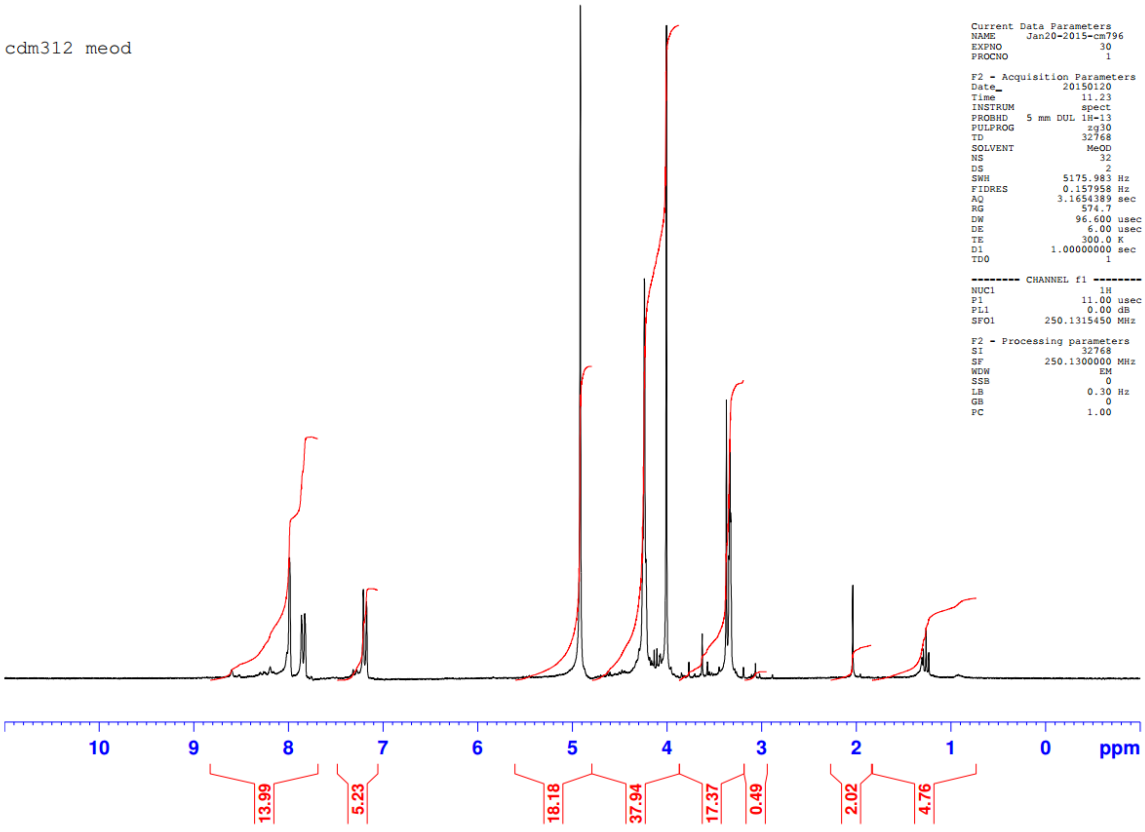

Figure 23 Unidentified sodium azide derived product

The ^{1}H NMR spectra of the degradation displays an upfield shift for the protons in the aromatic regions of the spectra. This is indicative of increased electron shielding and suggests that the electron density of the aromatic protons is higher in the unidentified product. There is also a new unidentified singlet in the aliphatic region of the spectrum.

The CF_3 group is strongly electron withdrawing and the loss of this group would result in the increased electron shielding for the aromatic and bridged protons that was observed. However, this method of removal would be most unusual and wouldn't account for the addition of the new singlet observed. Fluorine was investigated in the presence of the unknown with ^{19}F NMR, and it was found that a single fluorine environment was present, making it likely that CF_3 cleavage was not being observed.

4.3 UV-Vis investigation

As the reaction undergoes significant colour change, it was decided to qualify the colour change with the use of ultraviolet and visible (UV-Vis) spectroscopy. A series of spectra were taken to determine the change in absorption throughout the reaction. Initially spectra were obtained individually for the reaction starting materials **113** and **158** (Figure 24). The blanks were taken independently and the measurements for the reaction were taken as aliquots from the reaction mixture, which were then diluted to prevent saturation of the detector.

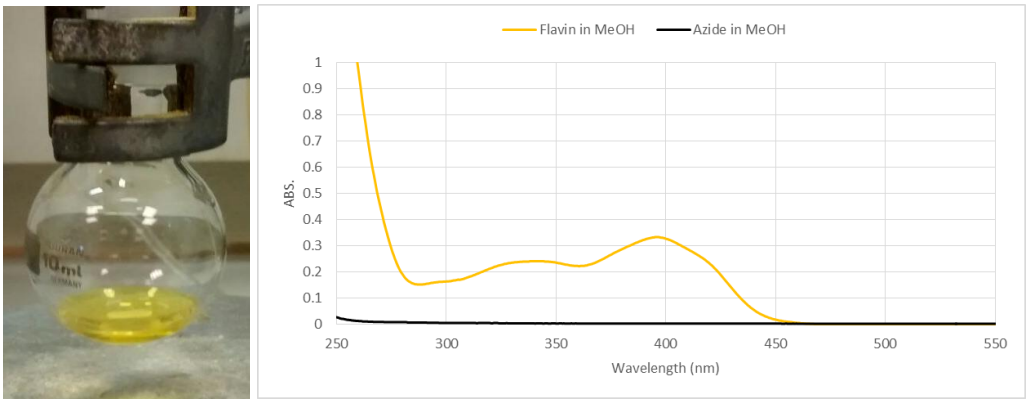

Figure 24 Individual blanks of sodium azide and CF_3 flavin in methanol

The UV spectrum of sodium azide in methanol shows no significant peaks, while the CF_3 flavin shows a significant peak at 400 nm with some shouldering at around 325 nm. There is an instant change in the UV-Vis trace of CF_3 flavin upon the addition of sodium azide (Figure 25).

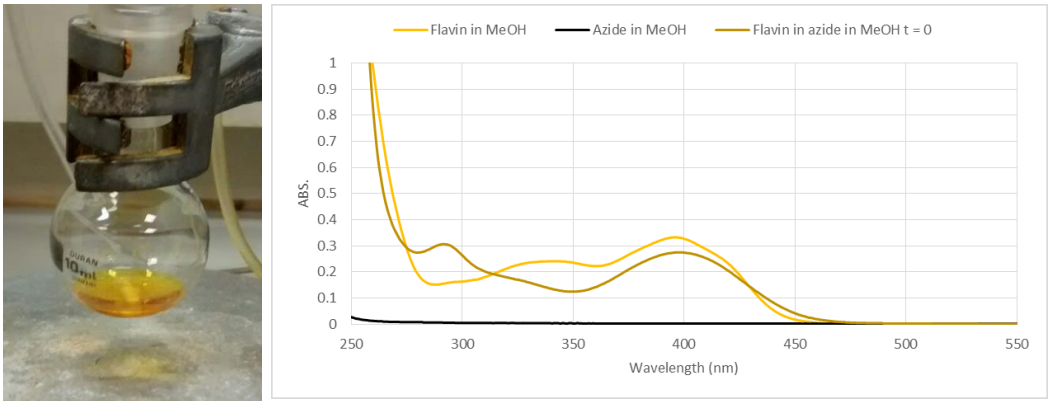

Figure 25 Addition of sodium azide to flavin

There is immediate lowering of the shoulder peak in the original flavin spectrum at around 340 nm, which decreases to become a minimum at 350 nm. There is also broadening of the original peak at 400 nm which is beginning to extend to longer wavelengths. Meanwhile the formation of a new peak at around 290 nm was observed. The qualitative effect of these changes was a colour change from the vibrant yellow of the flavin, to a deep orange shade. After 24 h, a final UV trace was taken from the reaction mixture (Figure 26).

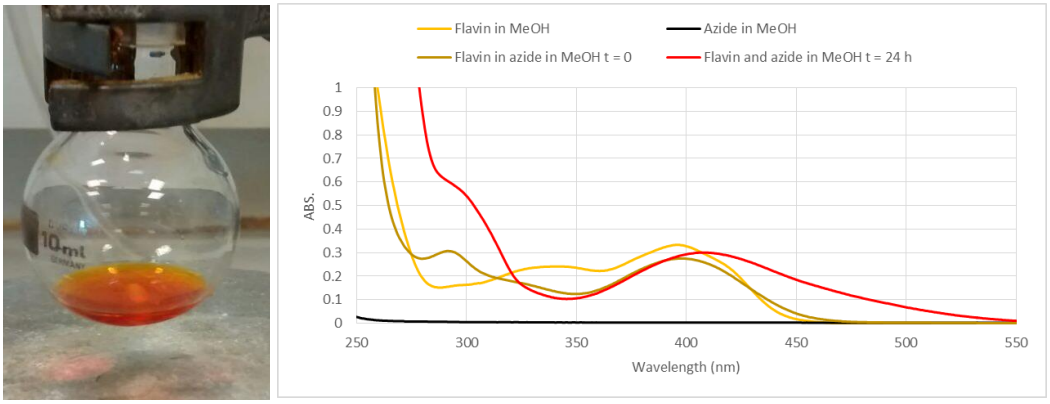

Figure 26 Sodium azide and flavin spectra after 24 h

From the final UV-Vis trace, you can see that that the initial shoulder at 340 nm has disappeared, while the shoulder that appeared at 290 nm upon addition of the sodium azide has continued to grow. Finally, the peak at 400 nm in the original CF_3 flavin spectra has shifted to 410 nm, as it did immediately upon the addition of sodium azide, extending towards wavelengths of over 500 nm.

The immediate change in the UV-Vis spectra indicates that there is a rapid reaction with the flavin upon addition of the sodium azide. As these peaks grow in strength over time, that could point to fast and slow steps for the formation of the observed product.

4.4 X-Ray Crystallography

A single crystal was obtained from a petroleum ether/ethyl acetate solvent system through the slow vapour diffusion of the petroleum ether antisolvent (Figure 27).

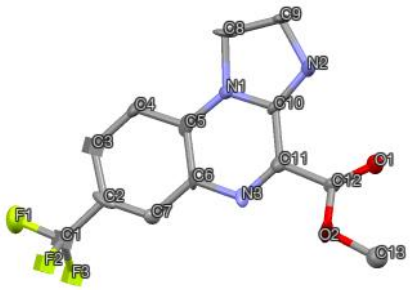

Figure 27 Crystal structure of unknown decomposition product

From the crystal structure, we can clearly see the loss of the imide portion of the isoaloxazine cycle, and the incorporation of a molecule of the reaction solvent, methanol, allowing us to identify the unknown compound (Scheme 121).

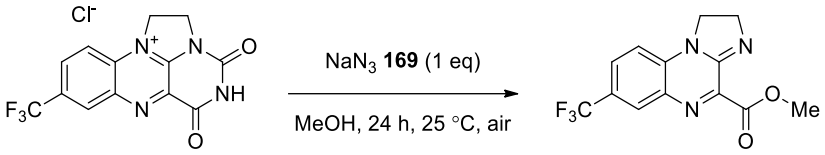

113 **171**

Scheme 121 Ring opening of CF_3 flavin by sodium azide in methanol

This is equivalent to a decomposition product previously observed by Cibulka *et al.* and Sayre *et al.* when flavinium reactions were performed in methanol under basic conditions.[147,180]

4.5 Electrospray ionization mass spectrometry

The mass spectra of both the purified product and the reaction mixture were observed in order to confirm this product as the significant reaction product. This was confirmed through observation of a peak at m/z= 298.080 (Figure 28).

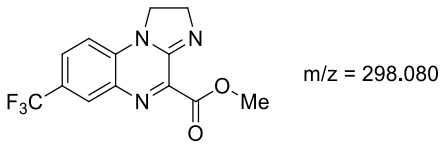

171

Figure 28 Decomposition product observed by ES/MS

Identification of the unknown structure allows for the hypothesis of a reaction mechanism in order to modify the flavin structure to make sulfur-nitrogen bond formation viable (Scheme 122).

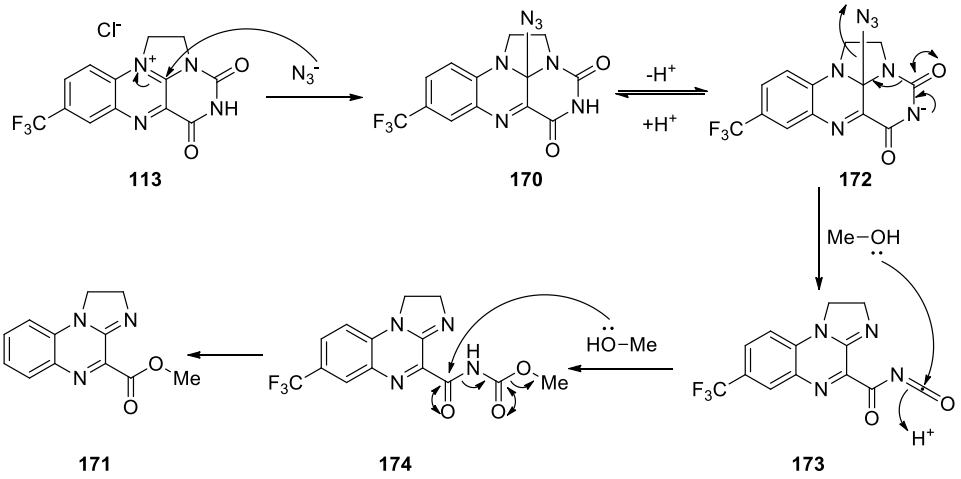

Scheme 122 Proposed mechanism for the formation of flavin decomposition with methanol

We propose that the initial step is attack by the nucleophilic azide, at the C3 of the flavin, forming the flavin-azide complex. Following the formation of this complex, the labile N_4 hydrogen is in equilibrium with the negatively charged nitrogen atom. Due to the neutral pH and the mild pK_a of the flavin-azide complex, the N_4 hydrogen will be predominantly bound. When the hydrogen is free, the carbonyl is prone to attack from the nitrogen lone pair, causing the release of the azide and the formation of a highly reactive isocyanate complex. This step is irreversible and short lived, as the isocyanate is then attacked by the abundant, and relatively nucleophilic hydroxyl of the solvent. Following the incorporation of the solvent into the ring opened flavin structure, a secondary solvent attack is observed at the base of the carbonyl C-1 position of the original ring system. This final step is reliant on the nucleophilicity of the reaction solvent. *In situ* IR would be a useful technique to probe this reaction mechanism.

4.6 Investigating the effect of solvent nucleophilicity

In order to confirm that nucleophilicity of the reaction solvent had an impact upon the product formed, we selected trifluoroethanol (TFE), specifically for its non-nucleophilic properties,[181,182] and the reaction was performed under standard conditions (Scheme 123).

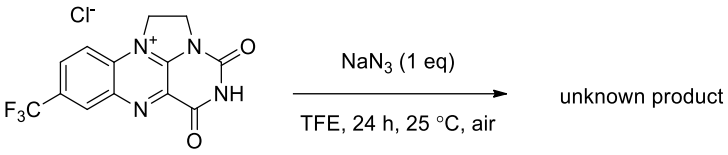

Scheme 123 CF_3 flavin and sodium azide in trifluoroethanol

The reaction proceeded as expected, with the formation of a new product with the same polarity and a qualitatively similar colour change observed. Following purification of the product, a single crystal was obtained from the same petroleum ether/ethyl acetate solvent system through slow vapour diffusion and X-ray crystallography was performed (Figure 29).

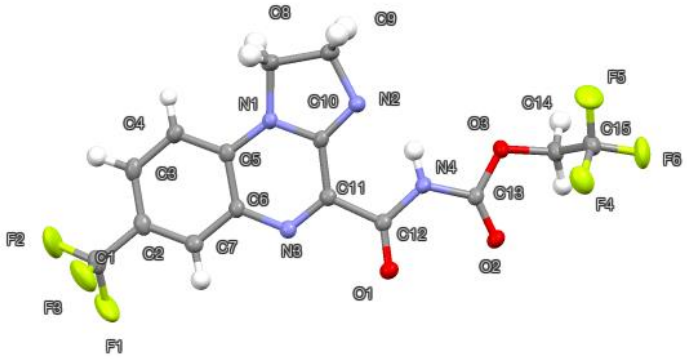

Figure 29 X-ray diffraction of flavin and sodium azide in TFE reaction.

It was clear from X-ray crystallography that this product was different than the methanol derived compound, and the new group was identified as the TFE ester (Scheme 124).

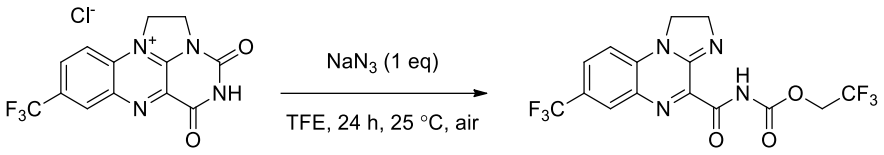

Scheme 124 Ring opening of CF_3 flavin by sodium azide in methanol

The flavin degradation in TFE gives **175,** which is not the compound expected, if the reaction were to follow the same mechanism that formed **171**. The trifluoroethanol fragment has formed a carbon-oxygen bond at C-2 of **113** whereas, the carbon-oxygen bond formation observed in **175** is at C-3 (Figure 30).

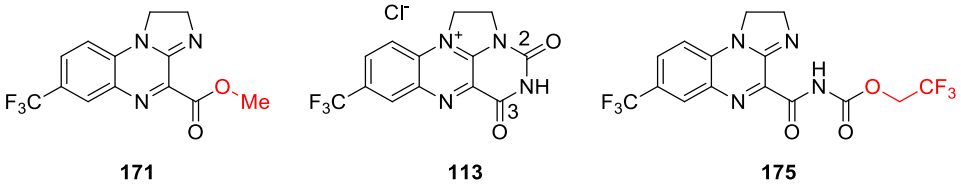

Figure 30 Methanol and trifluoroethanol decomposition compounds

Figure 30 shows that the reaction with the non-nucleophilic solvent, TFE supports the proposed hypothesis of a double attack of the methanol (
Scheme 122). This less nucleophilic solvent is unable to perform the secondary attack at the C-1 carbonyl position, and the imide cleaved product is not observed (Figure 31).

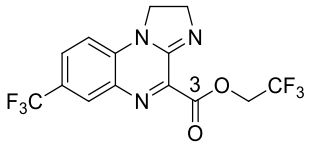

176

Figure 31 Hypothetical imide cleaved product of double solvent attack

With that in mind, we propose a mechanism for the degradation of CF_3 flavin and sodium azide with trifluoroethanol as a reaction solvent (Scheme 125).

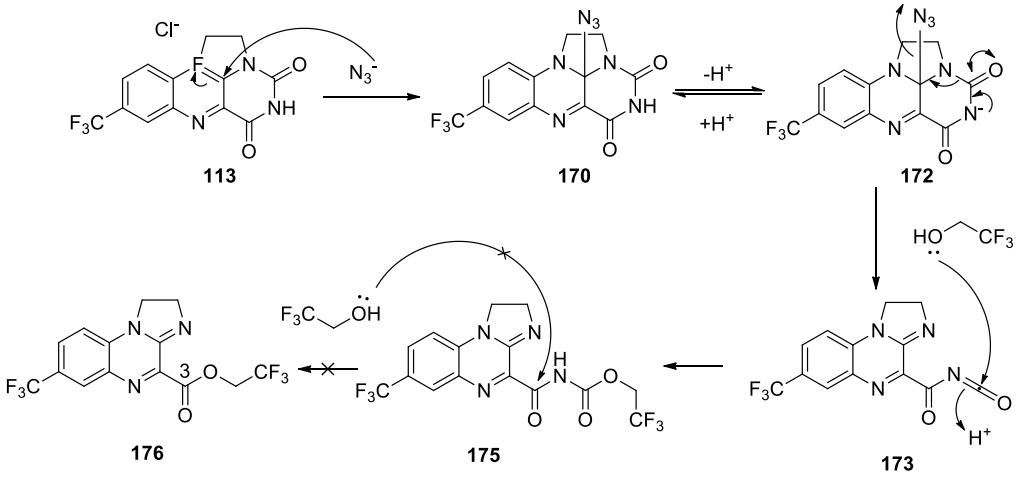

Scheme 125 Proposed mechanism for the formation of flavin decomposition with trifluoroethanol

As has been previously discussed in the case of the methanol mediated flavin decomposition (
Scheme 122), the initial reaction step is attack of the nucleophilic azide to the electrophilic riboflavin. This complex is in equilibrium between the secondary amine and the free N^- form, at which point the lone pair contributes to the formation of the isocyanate functional group, as the C-N bond of the isoalloxazine structure is broken and the azide is released. The lone pair of the alcohol attacks the highly reactive isocyanate, forming the product observed by X-ray diffraction.

4.7 Modification of CF_3 flavin

If the key step of this reaction was the formation of the isocyanate functional group, which leads to the ring opening of the flavin and loss of catalytic activity, it was necessary to modify the flavin in order to stop this side reaction. It was hypothesised that the modification of the

secondary amine of the CF_3 flavin the equilibrium occurring, preventing cleavage of the C-N bond. With that in mind, the methylation of the secondary amine was attempted.

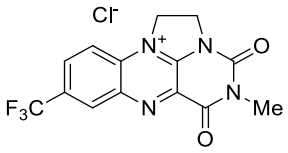

177

Figure 32 Methyl CF_3 flavin

There are two methods which could be envisaged to achieve the methylation of the original flavin: directly insert the methyl functional group onto the nitrogen of interest, or by modifying the synthetic route to directly incorporate the methyl group into the synthesis at an earlier point.

4.7.1 Chromium trioxide formation of methyl alloxan

The Cibulka group successfully synthesised a methyl flavinium by utilising 1-methylalloxan (instead of alloxan) in their synthesis (Scheme 126).[183,184]

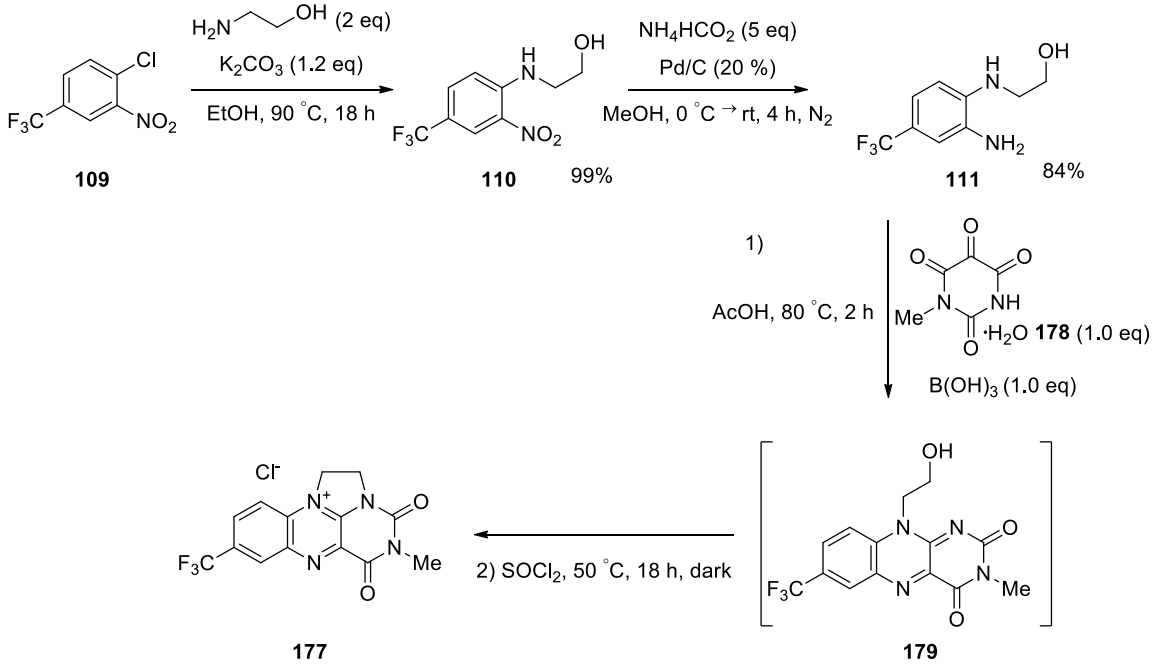

Scheme 126 Synthetic route to methyl substituted CF_3 flavin

The key reagent, 1-methylalloxan, is not commercially available, and a literature search yielded a preparative route for the formation of the heterocycle via *N*-methylbarbituric acid from a combination of publications (Scheme 127).

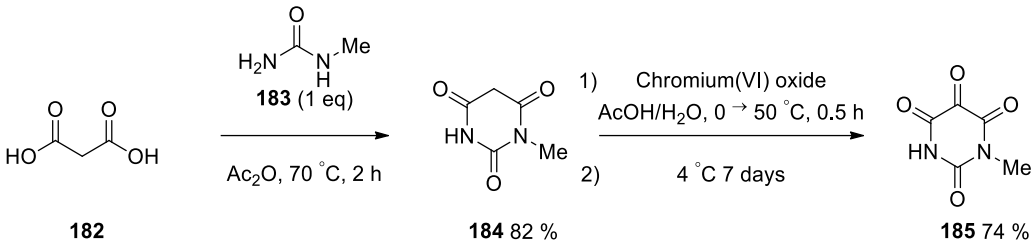

Scheme 127 1-methylalloxan synthesis[184,185]

The preparation of *N*-methylbarbituric acid from Mao *et al.* was taken forward as reported and their results were reproduced without further modification (Scheme 128).

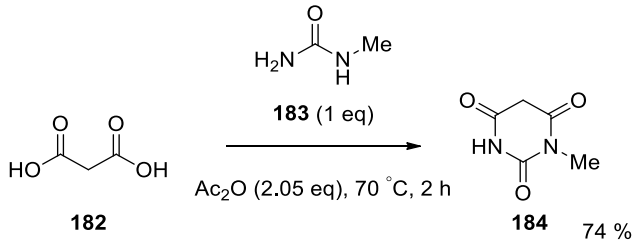

Scheme 128 Preparation of N-methylbarbituric acid

N-methylbarbituric acid was synthesised in 74 % yield after purification, which was comparable to the 82 % yield reported by Mao *et al*. The product was taken forward for subsequent oxidation with chromium trioxide according to the procedure reported by Cibulka *et al*. Their procedure was followed as reported (Scheme 129).

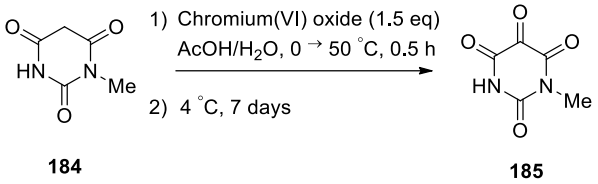

Scheme 129 Preparation of 1-methylalloxan

The results from Cibulka *et al.* were not reproducible and the reported white crystals could not be obtained. There was significant difficulty in washing the desired product from the sludgey reaction mixture, and there was no evidence of the desired product when the reaction mixture was investigated by mass spectrometry (Figure 33).

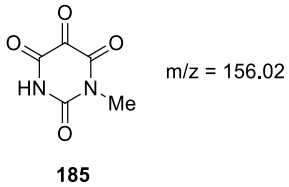

Figure 33 Unobserved 1-methylalloxan

Due to lack of successful formation of the desired product, in addition to the challenging reaction conditions and potent hazard and precautionary statements, it was decided that the

chromium trioxide-mediated oxidation of 1-methylbarbituric acid would not be investigated further, and alternative methods for the formation of 1-methylalloxan were investigated.

4.7.2 Tin (II) chloride formation of 1-methylalloxan

Following the unsuccessful formation of 1-methylalloxan with chromium trioxide, an alternative preparation was found with tin (II) chloride (Scheme 130).[186]

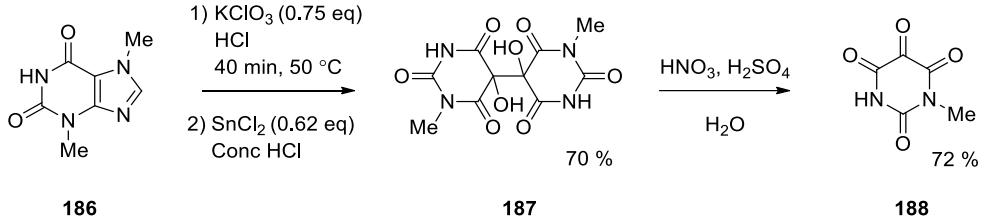

Scheme 130 Tin (II) chloride-mediated formation of 1-methylalloxan

The original synthesis was modified slightly and conditions were taken forward as reported by Sayre *et al*. (Scheme 131).[180]

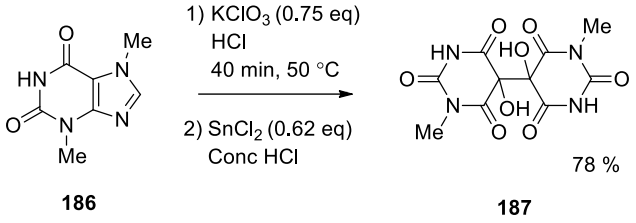

Scheme 131 Synthesis of N-methylalloxantin

The formation of *N*-methylalloxantin proceeded successfully with the formation of a clean white solid in 78 % yield. *N*-methylalloxantin was then stirred with nitric acid and left in a desiccator to crystallise over sulfuric acid (Scheme 132).

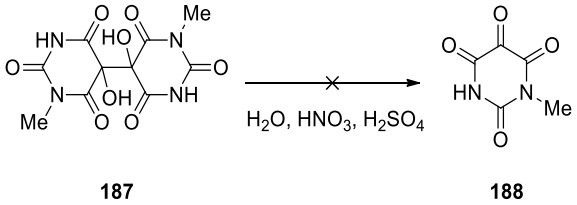

Scheme 132 Unsuccessful synthesis of 1-methylalloxan

After 2 weeks, 1-methylalloxan had not crystallised from the desiccator and upon neutralisation of the reaction mixture, *N*-methylalloxantin **187** was recovered. No formation of 1-methylalloxan was observed in the reaction mixture. This procedure was not investigated any further and alternate approaches were attempted for the formation of methyl CF_3 flavin.

4.7.3 Direct methylation

Following the failed syntheses of 1-methylalloxan, it was decided to directly methylate the secondary amine once it was already in position on the isoalloxazine ring structure. Previously, the isoalloxazine formation and subsequent cyclisation had been telescoped for synthetic ease. However, for the direct methylation of the flavin, it was necessary to isolate the uncyclized flavin (Scheme 133).

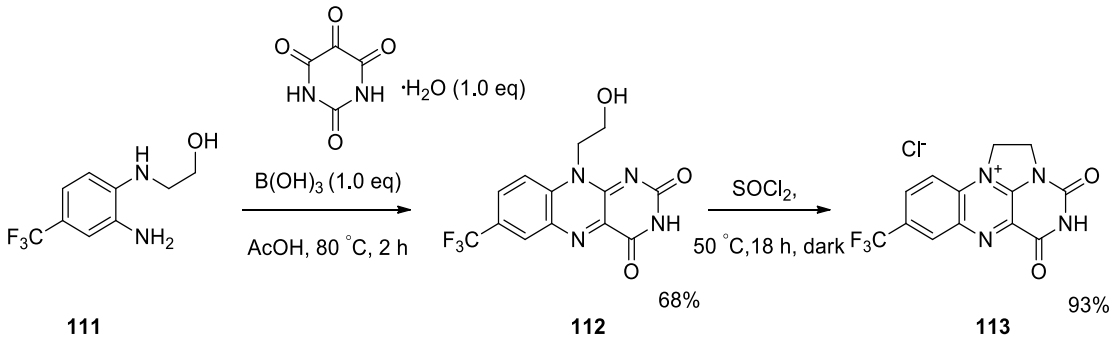

Scheme 133 Non-telescoped CF_3 flavinium synthesis

Following the isolation of the alcohol flavin, it was considered appropriate to react the product with base and a methylating agent. This approach had been previously reported on similar flavin systems (Scheme 134).[187,188]

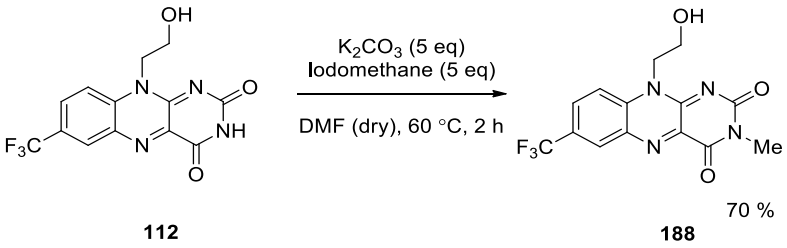

Scheme 134 Procedure for methylated flavin as reported by Cibulka *et al*.

The reaction conditions were initially taken forward without modification which led to the complete recovery of starting material. Repeated reactions did not lead to the reproduction of the reported results and modification of the base did not lead to the desired product.

Following the unsuccessful reaction through modification of the base, methyl trifluoromethanesulfonate, a stronger methylating agent was used (Scheme 135).

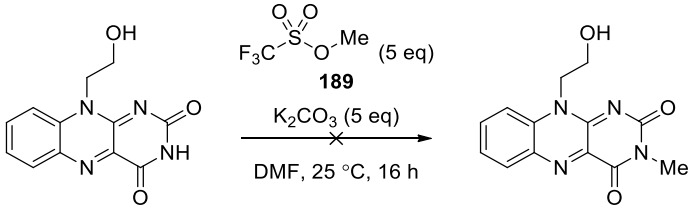

Scheme 135 Methyl trifluoromethanesulfonate as a methylating agent

Unfortunately, the use of this methylating agent was similarly unsuccessful for the formation of the desired product. Due to the difficulty in obtaining the methylated flavin required to continue probing the reaction mechanism, investigations into the decomposition were not taken forward.

5. Flavin mediated Sulfoximine Formation

Following the conclusion of the investigation into azide as a reaction partner for the formation of sulfoximines, the search for novel reagents for the synthesis was restarted. A recent publication from Bull *et al*. showed development of various electrophilic NH sources for the conversion of sulfoxides to sulfoximines in the presence of hypervalent iodine sources (Scheme 136).[109]

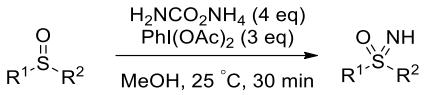

Scheme 136 Ammonium carbamate mediated sulfoximine formation

Hypervalent iodine species have been well documented in the formation of sulfoximines.[106,108,122,189–191] However, this is the first example of ammonium carbamate being used as an electrophilic nitrogen source. Its activity in flavin catalysed system was investigated (Scheme 137).

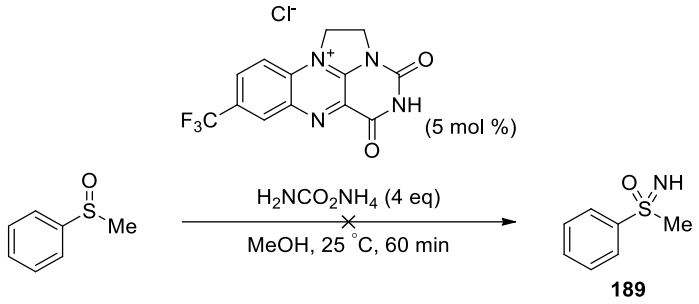

Scheme 137 Ammonium carbamate as a flavin reaction partner with sulfoxides

No sulfoximine formation was detected and the reaction led to the recovery of starting material. As previously discussed, the hypothesised mode of action is the formation of an elctrophillic form of nitrogen, which is then prone to attack from a nucleophilic sulfur. As sulfoxides have reduced nucleophilicity compared to the sulfide, the sensitivity of the system towards the sulfide was investigated (Scheme 138).

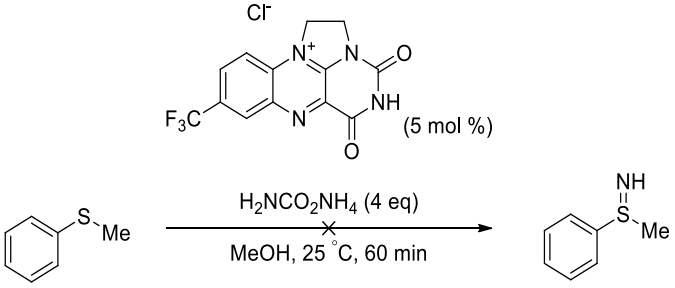

Scheme 138 Ammonium carbamate as a flavin reaction partner with sulfoxides

Disappointingly, there was no evidence of sulfilimine formation with the sulfide. Finally, taking into account the original ammonium carbamate and (diacetoxyiodo)benzene system, it was decided mimic the original conditions more closely, using the flavin stoichiometrically (Scheme 139).

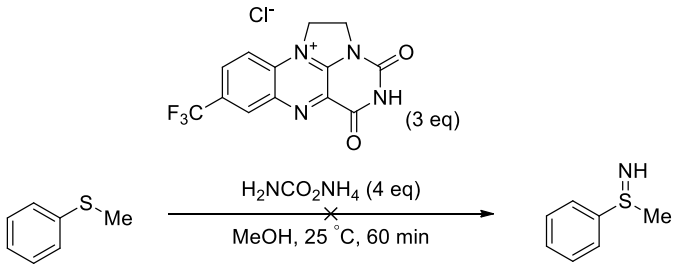

Scheme 139 Stoichiometric use of flavin for sulfilimine formation

When using the flavin stoichiometrically, there was an observable change over time when the reaction was monitored by TLC, with several new spots present. Additionally, there was a significant colour change from yellow to red. Disappointingly, the desired sulfilimine was not isolated, nor was the often-observed sulfoxide. However, mass loss of the starting sulfide was detected, confirming some reaction was taking place. Investigation of the reaction mixture by mass spectrometry revealed apparent formation of the corresponding sulfoximine (Figure 34).

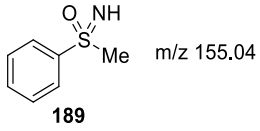

m/z 155.04

189

HRMS (ESI, +ve) m/z calcd. for C7H10NOS 156.0483; found 156.0467 (M+H)+

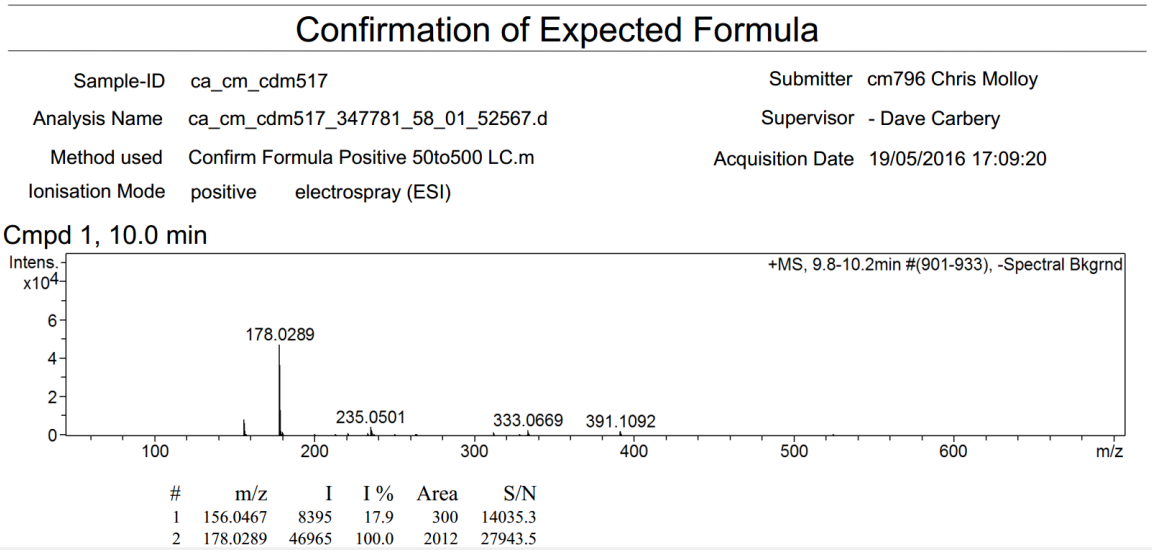

Figure 34 Methyl phenyl sulfoximine observed by ESI MS

Although the mass spectrometry result showed initial promise, the sulfoximine could not be isolated. This was attributed to a combination of very poor atom economy for the relatively heavy flavin, and the significant levels of flavin present in the reaction mixture. The colour change was similar to the colour change observed with the flavin decomposition with sodium azide, as was the Rf, although further investigation was not conducted at this stage.

At this early stage, there was no reason to persist with Bull's conditions, and the ammonium carbamate and flavin loadings were lowered to check their necessity, and a range of blank experiments conducted to confirm the importance of each reagent (Table 25).

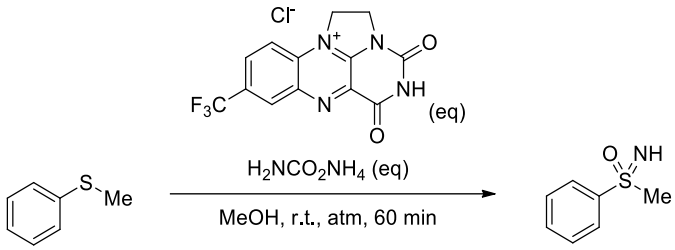

Table 25 Blank experiments for sulfoximine formation

Entry	113 eq	$H_2NCO_2NH_4$ eq	Atmosphere	Mass spec confirmation
1	0	1	Air	No
2	1	0	Air	No
3	3	4	Air	Yes
4	1	1	Air	Yes
5	0.05	1	Air	No
6	1	1	N_2	No
7	3	4	N_2	No

Entries 1 and 2 confirmed that both the flavin and ammonium carbamate are integral to the formation of sulfoximine, as without either there is no sulfoximine formation. It is observed that the sulfoximine is still present with lower loadings of **113** and of ammonium carbamate (entry 4), however, it was confirmed that the reaction is not catalytic in **113** as there was no conversion at 5 mol%. Finally, it was observed that there was no conversion under a N_2 atmosphere, and it was noted there also wasn't any colour change (entry 7).

As the previous flavin decomposition had been affected by the reaction solvent (chapter 4), a series of reactions were conducted to investigate whether the decomposition could be slowed by a variation in solvent. The effect of temperature upon the decomposition rate was also investigated (Table 26). Although conducting the reaction under an atmosphere of N_2

halted the decomposition, it did not lead to any detection of sulfoximine so was not looked into as a viable option at this stage.

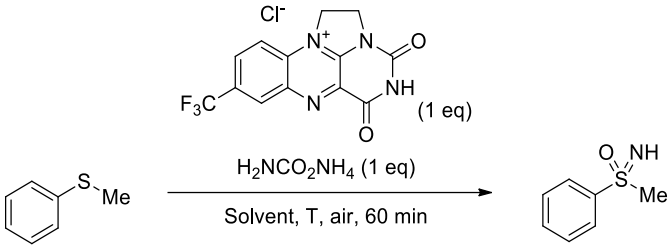

Table 26 Varying solvent and temperature in order to slow decomposition

Entry	Solvent	Breakdown time (min)	Temp (°C)
1	Methanol	60	r.t.
2	Trifluoroethanol	30	r.t.
3	Ethanol	60	r.t.
4	Acetonitrile	60	r.t.
5	Methanol	60	0
6	Methanol	60	-78

Unfortunately, the breakdown of flavin could not be shortened in any of the solvents selected. Trifluoroethanol led to an increased rate of decomposition (entry 2), while ethanol and acetonitrile did not affect the rate significantly (entries 3 and 4). Decreasing the temperature did not affect the rate of flavin breakdown (entries 5 and 6).

Although the reaction could not be optimised to prevent the breakdown of flavin, it was important to isolate the product and the reaction was scaled up in order to achieve that. When conducted on a 2 mmol scale, (S-methylsulfonimidoyl)benzene, was isolated in a 30% yield.

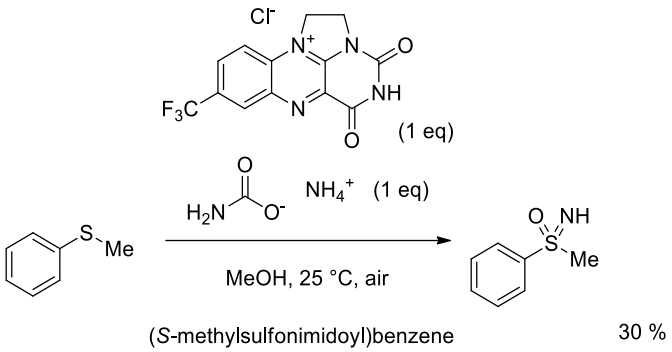

Scheme 140 Large scale sulfoximine formation from flavin and ammonium carbamate

When conducted on a 2 mmol scale, (S-methylsulfonimidoyl)benzene, was isolated in a 30% yield. Although this result was pleasing, the poor atom efficiency and the poor yield meant that it was decided not to take the reaction forward for further optimisation.

The scope of this reaction was investigated and a range of sulfides were exposed to the reaction conditions. Isolation of the desired sulfoximines was not possible, and formation was detected by mass spectrometry (Table 27).

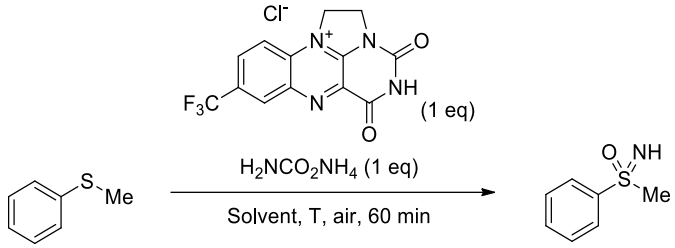

Table 27 Sulfoximines observed by mass spectrometry

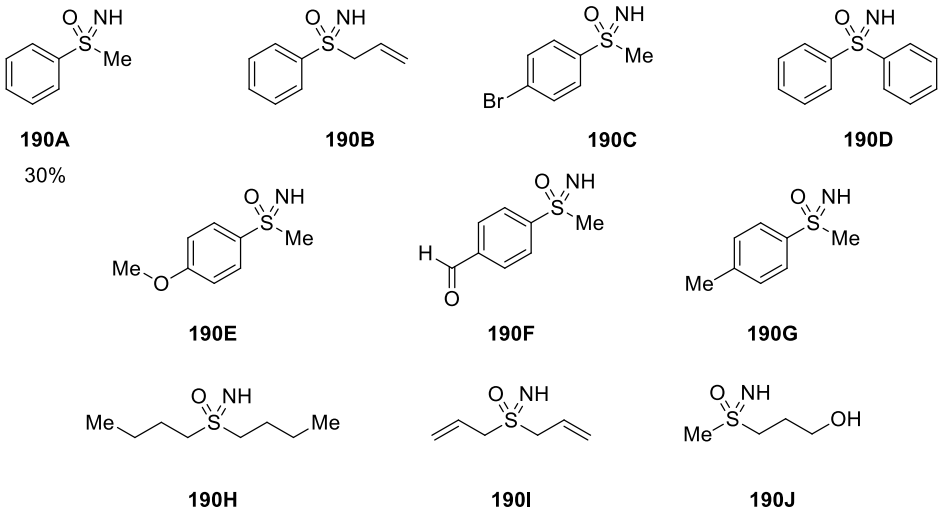

A range of sulfoximines were detected, however, being unable to isolate the desired products, is a significant barrier to the development of this reaction. Although methyl phenyl sulfoximine was isolated on large scale, this is not a practical approach due to the quantity of reagents required, and as such, the investigation was not taken further.

6. Computational Modelling of Materials

6.1 Aims and objectives

Computational modelling is used to gain insight into the nature of materials to allow experimental observations to be rationalised, and to predict adaptations which give desirable characteristics. The computational studies presented concern two main topics; electronic structure calculations are used to develop design rules for enhanced electrical conductivity in a subset of metal organic frameworks, and structural analogues of solar cell hole transport materials are investigated in order to achieve increased efficiency.

Metal-organic frameworks (MOFs) are a broad class of materials consisting of metal ions coordinated to organic ligands, resulting in multi-dimensional structures. The organic ligand will often feature multiple anionic sites (an important artefact in the formation of multi directional, ordered systems), and will be commercially available. MOFs have been hailed as the answer to a range of materials chemistry problems, primarily because their ordered, porous framework gives them a large surface area, which has been the focus of research across many branches of chemistry. Zeolitic imidazolate frameworks (ZIFs) are a subcategory of MOFs, structurally similar to zeolites, possessing exceptional thermal and chemical stability. ZIFs are composed of tetrahedrally-coordinated transition metal ions (often Zn^{2+} or Co^{2+}) with an imidazolate anion, in an M-Im-M motif. There have been limited reports of electronic device application with ZIFs and they are traditionally regarded as poor electrical conductors. However, the use of this class of MOFs has recently been reported for their use in photoelectrochemical core-shell heterostructures, as high-k dielectrics and super-capacitors.

It was hypothesised that design principles for achieving conductive ZIF materials could be developed using electronic structure calculations. In order to attain this, four ZIFs were selected, made up of two metal cations, $Co^{2+}(d^7)$ and $Zn^{2+}(d^{10})$ and two substituted imidazolate ligands, benzimidazolate (bIM) and methylimidazolate (mIM).

The ability to harness sunlight efficiently has long been a goal of scientific research. The first photovoltaic effect was observed by Aleandre Bacquerel in 1839, and since that first discovery, the significant scientific effort has been dedicated to the search for increasingly efficient methods of converting sunlight into energy. There are currently a wide variety of materials capable of performing the task; amorphous silicon solar cells, where amorphous

silicon is deposited in thin films onto a substrate such as glass; dye-sensitised solar cells (DSSCs), which are formed from a semiconductor placed between a photosensitive anode and an electrolyte; perovskite solar cells, most commonly hybrid perovskite solar cells, which have an absorber layer are made from repeating lattice crystal structures with the chemical formula ABX_3. Perovskite solar cells are made up of a number of layers, metal contact, electron interface layer, perovskite layer, hole interface and coated glass (usually coated with indium tin oxide, ITO). The hole interface layer is most commonly formed from $N^2,N^2,N^{2'},N^{2'},N^7,N^7,N^{7'},N^{7'}$-octakis(4-methoxyphenyl)-9,9′-spirobi[9H-fluorene]-2,2′,7,7′-tetramine (SPIRO-OMeTAD), a spirocyclic compound with assorted *p*-methyl ether motifs. Computational modelling is used to rationalise observed changes in ionisation potential, and corresponding efficiency, and then predict SPIRO-OMeTAD structural isomers that can be used for further increased efficiency.

6.2 Introduction to materials modelling

Materials modelling is a vital tool in modern materials science. The ability to characterise known systems, and assess hypothetical materials has led to the development of numerous simulation software packages.[192] The speed at which numerical simulations can be performed, and the increasing reliability of the prediction from quantum mechanical description of solids has led to the development of the field of computational materials design.[2]

The scope density functional theory (DFT) has historically been restricted to simple structures, with first-principle methodology only able to model a unit cell consisting of no more than tens of atoms. Modern computer hardware can be used for the direct simulation of thousands of atoms, leading to the modelling of chemical and physical properties of complex systems from reliable quantum mechanical simulations. This is crucial as materials chemistry is highly dependent upon physical properties and chemical structure.

The starting point, input, for any quantum mechanical calculation of crystalline solid is a crystal structure. This allows for the determination of the distribution of ground-state electrons for a specific arrangement of ions in an infinitely extending three-dimensional lattice. Crystallography can be challenging, with reported structures often containing; partially occupied lattice sites; solvent molecules; or missing hydrogen atoms. Hydrogen atoms are often misreported because of their low electron density which can lead to weak

diffraction signals, however, this omission can lead to falsely high-symmetry space groups being assigned, which are lowered when the hydrogen atoms are accounted for.

Additionally, Bragg's law is used to convert scattered X-rays to coherent angles of a crystal lattice. However, Bragg diffraction generates an average crystal structure, yet the local environment may differ significantly.[193] Vibrations and/or rotation of bonds or whole molecules is also a possibility in organic-inorganic systems.[194–197] Finally, structural disorder has been recognised as a potentially useful feature in complex systems, but is inherently problematic to model, and consequently has been neglected.

Once the input has been obtained, the physical properties, output, can be calculated. The experimental crystal structure (from experiment) is optimised for a specific description of interatomic interactions. Internal forces and external pressure are minimised for the three lattice vectors and all lattice sites across the system. A typical DFT exchange-correlation functional calculation (e.g., PBEsol[198]), usually agrees with experimental and measured parameters to within several percent.

A wealth of information can be gleaned from the calculation; strength of electron exchange interaction can be used to predict magnetic critical temperatures,[199] heats of formation can be used to screen hypothetical compositions,[200] and the composition of frontier orbitals can be used to explain catalytic activity.

6.3 Electronic structure design for nanoporus, electrically conductive zeolitic imidazolte frameworks

6.3.1 Introduction

Metal-organic frameworks (MOFs) are intrinsically ordered structures consisting of an infinite arrangement of metal clusters and organic ligands, forming one-, two-, or three-dimensional structures (Figure 35).

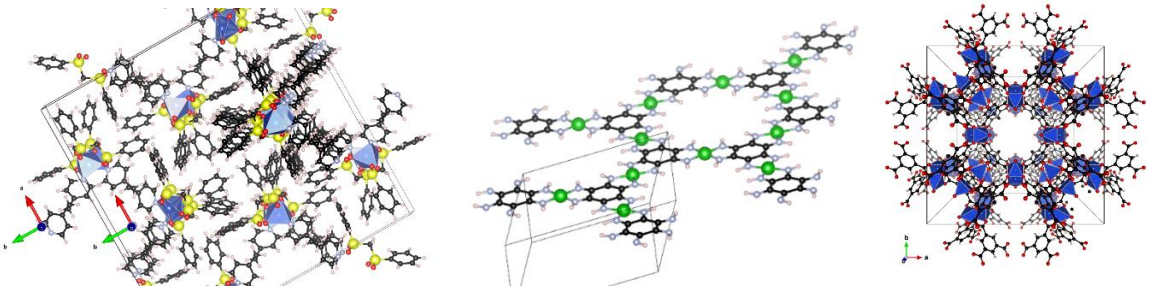

Figure 35 One-, two- and three-dimensional metal organic frameworks

This ordered network allows for topological control and chemical diversity, making MOFs attractive for a wide variety of variations. Their inherently porous nature gives them a large surface area, making them desirable for a range of applications, including gas storage, separation and chemical catalysis,[201,202] and as super-capacitors for energy storage.[203] Additionally, specific frameworks have been shown to be electrically conductive, and MOFs have been successfully used in thermoelectrics[204] and memory storage devices.[205–207] Electrically conductive MOFs could have implications on a range of currently undiscovered applications such as battery cathodes,[208,209] electrocatalysis,[210,211] transistors[212–214] and photovoltaics.[215,216] However, designing MOFs with molecular tunability has proved challenging as they are often thermally and mechanically unstable, which has hampered widespread application.

The emergence of conductive MOFs has resulted in the development of design principles for enhancement of molecular properties by modular tuning.[217,218] Conduction in MOFs has been classified into three areas: (i) through space transport, *via* π-stacking; (ii) through bond transport, relying on covalent bond networks and (iii) hopping transport, where charge carriers perform discrete jumps between structural units.[219] The π-stacking and bond transport conduction are the result of delocalised wavefunctions throughout the system and can be grouped as band transport mechanisms. These are typically associated with higher carrier mobilities than hopping transport.[220] Unfortunately, these modes of action can be challenging to achieve in MOFs due to poor hybridisation between the organic ligand and the metal ligand units. It is possible to implement design strategies for achieving conductive MOFs in order to create conductive pathways of continuous wavefunction overlap throughout the structure. This can be achieved through the addition of electro-activating molcules,[221] or with structures built from conductive $(MX)_\infty$ chains.[219]

6.3.2 Tunability of zeolitic imidazolate frameworks

Zeolitic imidazolate frameworks (ZIFs) allow for the chemical tunability of MOFs, yet they possess thermal and chemical stability of zeolite-like materials.[222–225] ZIFs are a sub-class of MOFs, constructed from an M-Im-M motif, where M is a divalent tetrahedral cation (often $Zn2^+$ or $Co2^+$) and Im is an imidazolate anion.[226,227] There is a perception that ZIFs are poor electrical conductors and there are few reports of their use in electronic device applications. However, their use as high-κ dielectrics,[228] as super-capacitors[229] and in

photoelectrochemical core-shell heterostructures is beginning to challenge[230] the view that ZIFs are electronically inert.

In an effort to aid the search for further electronically active ZIFs, a set of design principles have been proposed using electronic structure calculations to achieve conductive ZIF materials. Four ZIFs were studied by collaborators at the University of Manchester, comprised of two substituted imidazolate ligands, methylimidazolate (mIM) and benzimidazolate (bIM) and two metal cations, Zn^{2+} (d^{10}) and Co^{2+}. It has been demonstrated that the methylimidazolate ZIF-67, the Co^{2+} based ZIF is 1000 times more electrically conductive than the corresponding Zn^{2+} based ZIF-8 (Figure 36).[231]

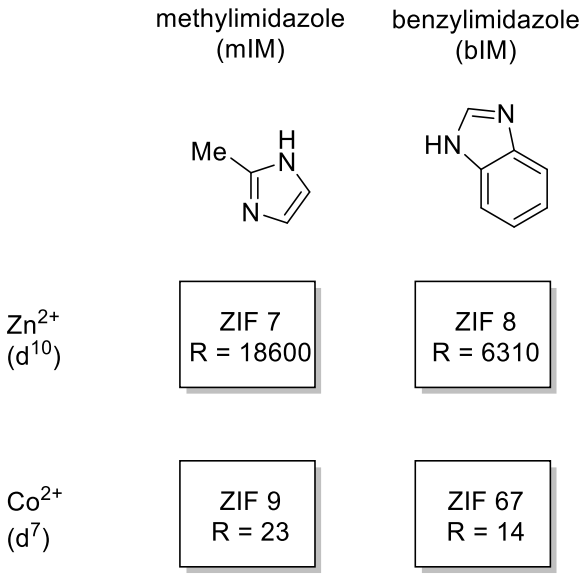

Figure 36 The modular construction of the four frameworks prepared by collaborators

Furthermore, the characterisation of benzimidazolate based ZIFs reveals increased conductivity for the Zn^{2+} based ZIF-7 over the Co^{2+} equivalent. From the permutations of these two metal centres and two ligands, four frameworks with similar geometric environments and tetrahedral metal ions, bridged by organic ligands and bonded through N lone pairs, the electronic structure influence on electrical conductivity can be predicted. The homogeneity of the geometry allows the role of orbital symmetry, electron configuration, ionisation potential and electron affinity to be highlighted.[232] The choice of metal ion (from its corresponding ionisation potential) and ligands designed for improved hybridisation can be used for the development of conductive ZIF materials.

The 4 ZIFs investigated by colleagues were analysed computationally in order to rationalise their findings. Co^{2+} based materials have a resistance of around 1000 times lower than those of their Zn^{2+} based counterparts. Additionally, bIM frameworks have significantly higher

resistance than the mIM frameworks for both metal centres. Bode phase plots demonstrate a difference in mode of action between Zn^{2+} and Co^{2+} ZIFs. The shape of the less conductive Zn^{2+} shows the phase starting near 0° at low frequency, before rising to a plateau around 70° for medium frequencies, before decreasing again to 0° at high frequencies. In contrast, the shape of the more conductive Co^{2+} ZIF plot is characteristic of pseudocapacitive behaviour,[233] with and initial plateau at low frequencies around 45°, before falling toward 0° as frequency increases.

Jamnik investigated the effect of mixed conductors with semi-blocking boundaries upon impedance spectroscopy,[234] whose work was expanded upon by Hong who separated the electronic and ionic contributions through analysis of the impedance response.[235] This technique allows for the conductivity of ZIFs -7, -8, -9 and -67 to be calculated from impedance spectroscopy (after normalisation for MOF electrode area and film thickness) (Table 28).

Table 28 Electrical properties of the four ZIFs studied. Charge transfer resistance(R_{CT}), conductivity (σ) from electrical impedance spectroscopy. Ionisation potential (IP) and electronic band gap (E_g) from hybrid DFT calculations

Material	R_{CT}(**Ω**)	σ($S.cm^{-1}$)	IP (eV)	E_g(eV)
ZIF-7	18600	4.5-9.0 x 10^{-10}	5.61	4.82
ZIF-8	6310	1.3-2.6 x 10^{-9}	5.73	5.29
ZIF-9	23	3.6-7.3 x 10^{-7}	5.21	3.01
ZIF-67	14	0.6-1.2 x 10_{-6}	5.62	4.25

The highest reported MOF conductivities are significantly higher than even the most conductive ZIF reported (ZIF-7),[218] however, R_{CT} defines the upper resistance limit, and includes contributions from interface contact resistance and other sources extrinsic to the ZIF. The consequence is that the reported conductivities are conservative estimates of framework conductivity that are within the order of magnitude of conductivities reported for other promising MOFs and organic conductors.[236]

6.3.3 Results

The orbital composition and spatial location of the valence and conduction bands determine most equilibrium properties of materials. Simple MOFs can be described in a similar fashion to classic molecular orbital diagrams, however, the inclusion of organic linkers or inorganic

nodes can complicate the description significantly. This is in part due to the fact that interesting interactions often take place at the organic-inorganic boundary. Electronic structure calculations can give insight into the energy, composition and distribution of the frontier extended orbitals (electronic band edges) of any compound. The band edges are highly dependent upon the chemistry between the organic ligand and the metal at their interface as both the valence and conduction bands are defined by the orbitals of the organic component. Therefore, organic functionalization can be used to modify the chemistry of the band edges[237,238] and the overall physical properties of the MOF.[239]

The character of the band edges was investigated to understand how the bonding interaction directly influences the valence and conduction band edges. The valence and conduction bands determine the electrical conductivity of a solid. The conduction band is the lowest range of vacant electronic states, while the valence band is the highest energy at which electrons are present. The difference between the conduction band and the valence band is the band gap. Holes (empty states) are transported in the valence band maximum, to the conduction band minimum, and a mostly filled valence band allows for good conductivity.

The DOS and electronic energy levels are calculated based on evacuated pore structures. The density of states is required in order to determine how many available states exist at each energy level. Density of state calculations are performed by decomposing the total electronic density of states into a partial density of states. This allows for the number of electrons at each level to be determined. ZIF-7 and ZIF-9 are structurally analogous (benzimidazole), and a marked increase in the metal character at the conduction band edge of the electronic DOS comparing Co^{2+} frameworks to Zn^{2+} frameworks. This increase in metal character is also observed for the methylimidazole ligand ZIFs, ZIF-8 and ZIF-67. There is almost 50% metal contribution to the conduction band edge, resulting from the d^7 electron configuration of Co^{2+} in contrast with the d^{10} configuration of Zn^{2+} .

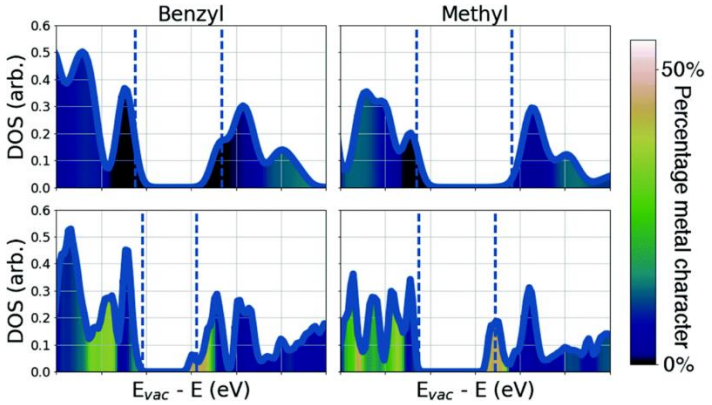

Figure 37 Electronic density of states plots of the four materials studied, showing the degree of metal contribution to the electronic states. The dashed blue line shows the valence and conduction band edges. Reproduced from ref[232] with permission from the Royal Society of Chemistry.

This resulting tetragonal environment leads to crystal field splitting on the Co^{2+} frameworks. The d^7 configuration allows empty Co d-states to hybridise with the ligand LUMO levels. Partial hybridization of the d_{xy}, d_{xz} and d_{yz} states allowing for interaction with the sp^2 hybridised orbital of the imidazole N. This leads to extended conduction states, bridging the imidazolate and the metal, explaining the significant increase in conduction observed with ZIF-9 and ZIF-67. This discovery highlights the importance of selecting metal ions that can participate in the formation of band edges in the framework, *i.e.*, metal ions with relatively shallow ionisation potential. A similar increase in conductivity is observed when replacing Mn^{2+} with Fe^{2+} where loosely bound Fe^{2+} electrons form the valence band edge.[236]

Additionally, switching from Zn^{2+} to Co^{2+} allows for improved hopping transport in the framework. This is achieved through the availability of alternate oxidation states of Cobalt (Co^{3+}),[240,241] which transfers charges between metal centres *via* the organic ligand. This mode of conduction is dependent on the overlap in energy of the linker and ligand frontier orbitals.

The effect of the ligands upon the conductivity of the framework could also be investigated. Both metals show increased conductivity for the methylimidazole containing frameworks, ZIF-8 and ZIF-67. The origin of this effect is related to the electronic structure of the ligand, the conduction pathway in ZIF frameworks depends on ligand N to metal interaction. A greater overlap between the ligand and the metal is the result of increased wavefunction overlap; in this case the key interaction is N ligand wavefunction with metal d_{xy}, d_{xz} and d_{yz} orbitals. Overlap strength is highly dependent upon the orientation of the ligand LUMO and the tetrahedral orientation of the ligands around the cation results in a stronger overlap for

the mIm framework. The spin resolved density of state shows that in ZIF-9 and ZIF-67 (Co^{2+} ZIFs), the conduction band minimum is formed from a single spin-down channel on the Co, hybridised with a spin-down channel on the N. This spin-dependent band edge structure suggests the possibility of utilising electron spin for improved electronic devices. Spin transport electronics (or spintronics), enables electron spin to be used as an additional degree of freedom. and has significant implications for data transfer and storage (Figure 38).

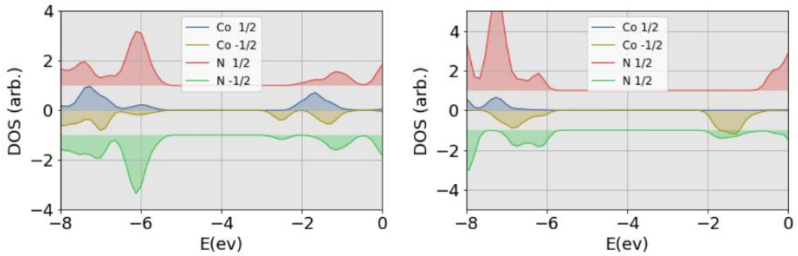

Figure 38 Spin resolved partial density of states plots for ZIF-9 (left) and ZIF-67 (right). Reproduced from ref[232] with permission from the Royal Society of Chemistry.

Quantum chemical calculations of the charged ligand molecules were performed to provide insight into the spatial resolution of the ligand wavefunctions. The extended π system of bIm acts as an electron withdrawing group, drawing electron density away from the key N sites, leading to an average of coefficients centred at the N site of 2.5 x 10^{-4} a.u. compared to 2.2 x 10^{-3} a.u. at the mIm N sites. The greater electron density of mIm is clear from contour plots of the wavefunction coefficients (Figure 39).

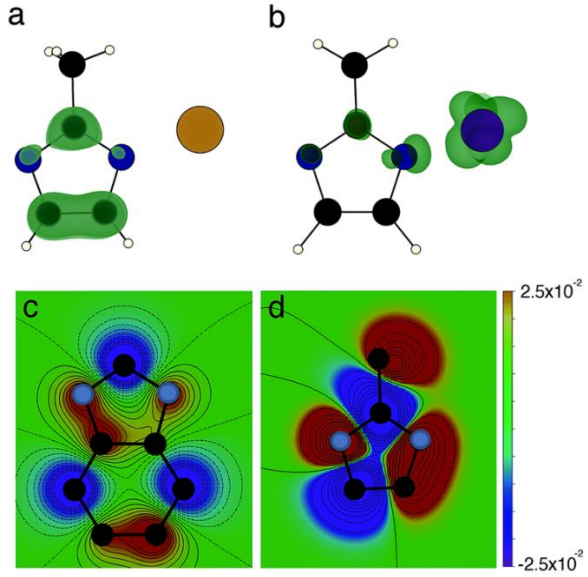

Figure 39 The effects of changing linker and ligand. Both isosurfaces are at 0.00025 e $Å^{-3}$ N atoms are in blue, C atoms are black, H atoms are white, Zn^{2+} is beige and Co^{2+} is indigo. Wavefunction coefficients are in atomic units.

Figure 39 shows the effect of changing the linker and ligand. (a) Shows the conduction band minimum isosurface of ZIF-8. It is observed that the conduction band does not extend outside the limit of the coordinated Co metal, giving insight into the poorer conductivity of cobalt ZIFs; (b) is conduction band minimum isosurface in ZIF-67. The CBM is significantly more extended in comparison to ZIF-8, which is expected from its increased conductivity. (c) Contour plot of the of the LUMO orbital coefficients of bIm, (d) contour plot of the of the LUMO orbital coefficients of mIm, C is black and N is grey (H atoms are suppressed). Wavefunction coefficients are in atomic units.

The contribution from π-stacking has not been discussed as it is unlikely to occur through extended covalent bonds, it is far more likely that conduction is mediated by a hopping mechanism. The availability of variable linker oxidation and ligand/linker wavefunctions are crucial for the effectiveness of hopping transport in frameworks.

This work leads to the proposal of design principles that should be considered when attempting to achieve conductive frameworks: (i) a metal cation with a shallow second ionisation potential and partially occupied/unoccupied d_{xy}, d_{xz} and d_{yz} orbitals and (ii) a ligand with high LUMO density at the N sites so hybridisation at the lingand/linker can be maximised, promoting the formation of an extended conduction band. The application of these principles indicate Fe^{2+} could act as a suitable replacement for Co^{2+}. Additionally, it is important the geometries of the new ligand do not obstruct the nitrogen sites sterically, or interfere with the packing of the extended lattice structure of the ZIF. For that reason, the size of any alternate ligand must be kept to a minimum.

6.3.4 Expansion to alternate organic ligands

Following the study of mIM and bIM, and their suitability as ligands for conductive ZIFs, the band gap of a series of imidazolates were investigated to search for new ligands that could give improved overlap at the N-M bond. In particular, the effect that the substitution of electron withdrawing/donating groups would have upon band gap. Initially the band gaps of the unsubstituted imidazole and 2-methylimidazole and 4-methylimidazole are calculated, with the unsubstituted imidazole (7.57 eV) having a higher bandgap than both the 2- 4-substituted methylimidazolates (6.96 eV and 6.90 eV).

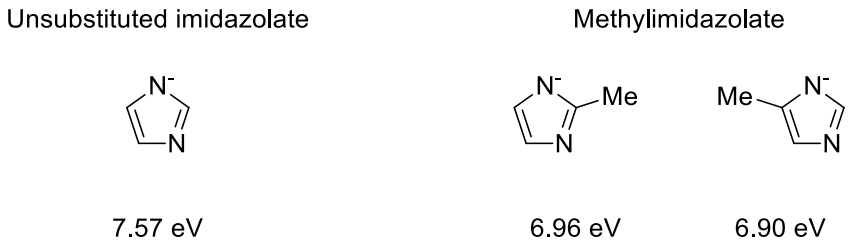

Figure 40 Unsubstituted and methyl substituted imidazolate band gap values

Subsequently, the effect of altering the position of a methoxy motif, an electron donating group, was investigated. This was followed by examining the effect of having multiple methoxy groups on a single ligand.

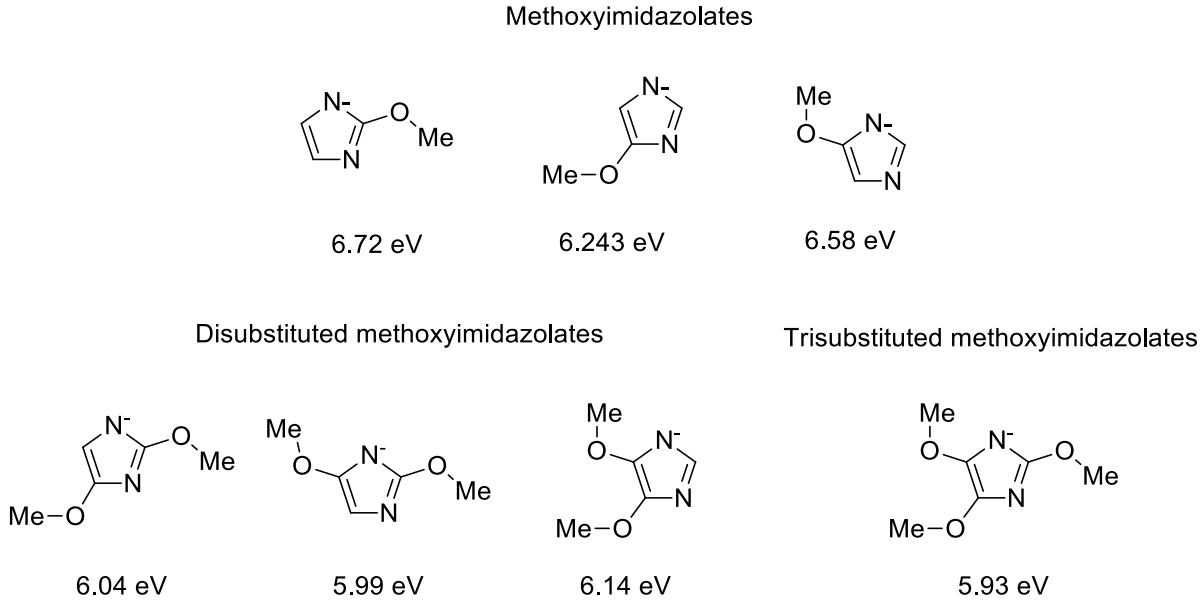

Figure 41 Methoxy-substituted imidazolate band gap values

It was found that the substitution of an electron donating methoxy group, in any position, resulted in a closer band gap when compared to the unsubstituted imidazolate. Notably, the highest band gap, was 2-methoxyimidazolate, with the position of the methoxy group affecting the band gap by almost 0.5 eV (2-methoxyimadazole to 4-methoxyimidazole). The addition of further methoxy groups led to an even greater decrease in the band gap.

This was followed by the investigation of the electron withdrawing trifluoro motifs on the imidazole ligand. Initially monosubstitution was investigated, which showed that the position of the CF_3 group played a significant role on the band gap. However, disubstution of the electron withdrawing group at the 4 and 5 positions had the most significant lowering of the band gap. Interestingly, the disubstituted electron donating groups had most impact at the 2,5 positions.

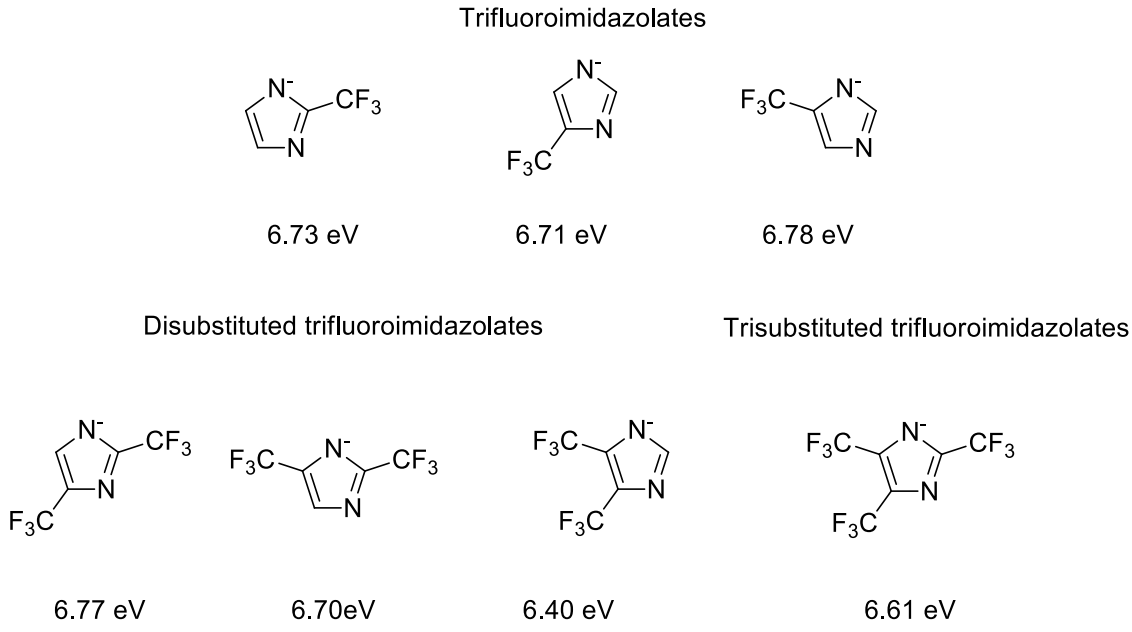

Figure 42 Trifluoro-substituted imidazolate band gap values

Finally, electron withdrawing and donating groups were combined in a single ligand investigate whether push/pull mechanisms could be used advantageously as organic ligands for frameworks.

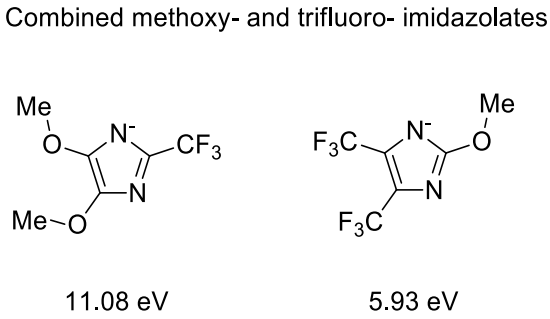

A very large difference in the band gap could be affected by the push/pull or pull/push structures when compared to the bare imidazole.

6.3.5 Methods

Density functional theory calculations were performed in order to understand the differences in the conductivity of each of the frameworks. Initially, the full framework is considered, using projector augmented waves[242] and periodic boundary conditions within the vasp code.[243] The PBEsol[198] functional was used to relax the frameworks, with a cut-off energy of 500 eV and Gamma point *k*-sampling. Resultant systems were then treated using a hybrid functional (HSE06[244]) to give a mixing percentage of the exact exchange (correcting for self-interaction errors in the PBEsol functional) to accurately represent the electronic structure.

The initial step of the calculation was the generation and primary optimisation of the ligand structure. The ligands were built by hand in Chem3D Pro 12.0 and a neutral or -1 charge state created (through the removal of the most acidic proton if necessary). The lowest energy state of organic structure was then determined using MM2 force field method. This method calculates the lowest potential energy of the system from the input structure, and allows a starting point to be reached though the generation of a .xyz file, i.e., a text file that contains the spatial information for each atom required to rebuild the organic structure in its mm2 optimised geometry. The numerical .xyz coordinates can then be used as the input for Gaussian09 calculations.

The first calculation run in Gaussian09 was a secondary geometry optimisation. The geometry is continually adjusted until a stationary point on the potential surface is found. To achieve this, a level of theory must be selected. For geometry optimisation the DFT hybrid functional B3LYP (Becke 88 exchange functional,[245] 3 parameter and Lee, Yang and Parr correlation functional[246]) and the split valence basis set 6-31G*. 6 is the number of primitive Gaussians comprising each core atomic orbital basis function. The valence orbitals are composed of two basis functions each. The initial basis function is a linear combination of 3 primitive Gaussian functions, which the 2nd basis function is a single primitive Gaussian function. The * represents the addition of six *d*-type Cartesian-Gaussian polarisation functions on the atoms with which we are concerned. Calculations on atoms with an atomic number of 21-30 (scandium – zinc) would be undertaken with a further ten *f*-type Cartesian-Gaussian polarisation functions. The 6-31G* basis set is not defined for atoms with an atomic number over 31 (Gallium). The Macrodensity package was used[247] to analyse wavefunctions of the LUMO levels of the mIm and bIm to generate the spherical average of the wavefunction coefficients at the N atoms, up to a radius of 2 Å. The spherical average is the mean of all the values of the wavefunction. 2 Å was selected as the radius as a compromise between computational complexity, and the decay of the wavefunction at greater distances, i.e., it becomes increasingly irrelevant at distances greater than 2 Å from the centre. The N LUMO hybridises with the metal, therefore higher wavefunction density at the N centre means greater overlap as the square of the wavefunction is the electron density when the orbital is occupied.

A Gaussian09 single point calculation is then performed with the geometry optimised coordinates using the same level of theory as the geometry optimisation. The required system band gap (E_g)information can then be extracted from the HOMO (highest Alpha occ.

eigenvalue) and LUMO (Alpha virt. eigenvalue) values generated by the calculation (HOMO – LUMO = E_g).

A powerful tool in Gaussian09 is the ability to output a range of file types, allowing the data to be interpreted with independent software packages. The cubegen utility proved to be very useful for the visualisation of molecular orbitals. The orbital of interest and desired output file type are defined at the beginning of the calculation by inputting a range of additional parameters for the output file.

The study of the electrical conductivity of four ZIF materials has resulted in the development of several design principles from the use of electronic structure calculations to explain observed trends. The four frameworks were comprised of two metal ions (Zn^{2+} and Co^{2+}) and two ligands (mIm and bImI). A significantly greater conductivity was observed when Co^{2+} was used as the linker, with up to four order of magnitude gain over Zn^{2+} linkers. This conductivity increase is explained through the availability of empty d-states contributing to the formation of the conduction band edge. Additionally, it was observed that mIm frameworks lead to increased conductivity of 1.5 to two orders of magnitude over the investigated bIm. This is attributed to differing wavefunction shapes of the LUMO level, which in the case of mIm, results in improved hybridisation with the metal linker, forming conduction pathways. The general principles of exploiting unoccupied d-states paired with the correct orbital symmetry to allow for good overlap with ligands, along with optimisation of ligand frontier orbitals, through the addition of electron withdrawing or donating groups on the ligand, offers a route to rational design of electrically conductive zeolitic imidazolate frameworks. These electrically conductive ZIFs pave the way for enhanced functionality of frameworks, in areas of CO_2 catalysis,[248] mixed matrix membranes,[249] energy storage,[250] drug delivery[251] and gas separation.[252]

6.4 Modular design of SPIRO-OMeTAD analogues as hole transport materials in solar cells

6.4.1 Introduction

The challenge of converting photons from sunlight into electrical energy has received significant scientific effort. Recently, solution-processed hybrid perovskite based solar cells have reached conversion efficiencies of 22.7%, values comparable with more mature silicon technologies.[253–263] A critical component of any solar cell is the transport between the ‘light harvesting’ active material and the external circuit without charge recombination. This

contact is responsible for selectively (and ideally efficiently) extracting electrons (or holes) from the active layer. In order to maximise the device potential and photocurrent, the energy levels of the contacts should be matched to the active layer of the solar cell.[264] The most widely employed absorber layer for hybrid perovskites is CH_3NH_3PbI,[265] however, alternative absorber layers are being developed,[266] and the ability to modulate energy levels of the selective contacts to match those of the absorber is essential to maximise power conversion efficiency.[267]

6.4.2 Increasing efficiency in hybrid perovskites

Most high-efficiency hybrid perovskite solar cells use the hole conductor N2,N2,N2′,N2′,N7,N7,N7′,N7′-octakis(4-methoxyphenyl)-9,9′-spirobi[9H-fluorene]-2,2′,7,7′-tetramine (SPIRO-OMeTAD).[268,269] SPIRO-OMeTAD is widely used in solution processed solar cells with an ionisation potential well matched to a number of active (light absorbing) layers. Smooth films can be formed as the material is an amorphous glass, as opposed to a partially crystalline phase.[269]

Electronic energy level alignment is important for solar cells but is commonly used in post-rationalisation of successful architectures, rather than as a design principle *a priori*. Seok and co-workers recently tuned the energy levels of SPIRO-OMeTAD by altering the connectivity of the of the methyl ethers on the amino phenyl motifs.[270] Seok *et al.* concluded that the placement of geminal *ortho*-methoxyphenyl, and *para*-methoxyphenyl motifs led to a cell with a 2% increase in conversion efficacy compared to the standard SPIRO-OMeTAD (germinal *para*-methoxyphenyl and *para*-methoxyphenyl) (Figure 43). Cyclic voltammetry showed the *ortho-*, *para-* placement led to an increase in oxidation potential, although repeated measurements with techniques such as differential pulse voltammetry would allow for more confidence in the increased oxidation potential, allowing its attribution to the increased efficiency observed. Cyclic voltammetry suffers from device-to-device performance variation, and syntheses from hybrid or organic electronic materials can lead to implicit doping. Additionally, the group observed the *meta*-methoxyphenyl, *para*-methoxyphenyl isomer led to reduced efficiency.

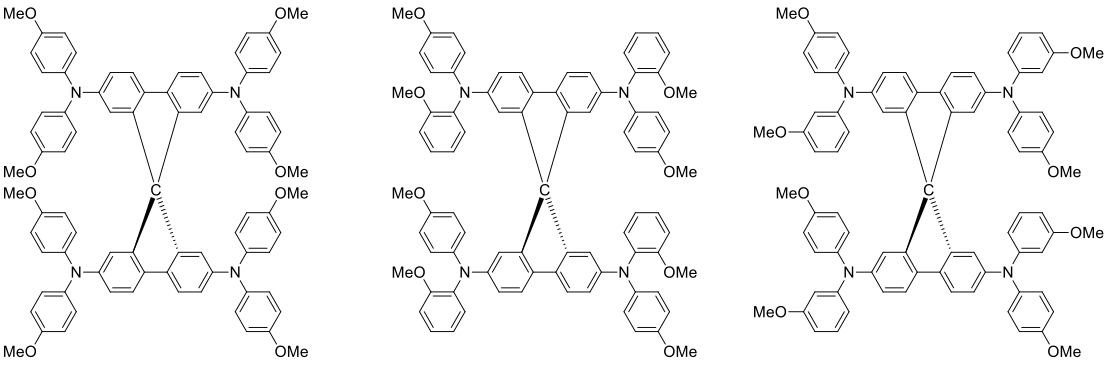

Figure 43 SPIRO-OMeTAD (left), *p*,*m*-methoxy (centre) and *p*,o-derivatives (right)

Lithium salts are often used to dope SPIRO-OMeTAD in order to obtain increased efficiency.[271] SPIRO-OMeTAD can function in neutral, one and two electron oxidised forms. Kohn-Sham plots can be used to show that the electron density is centred on the extended π network for the two systems (Figure 44).

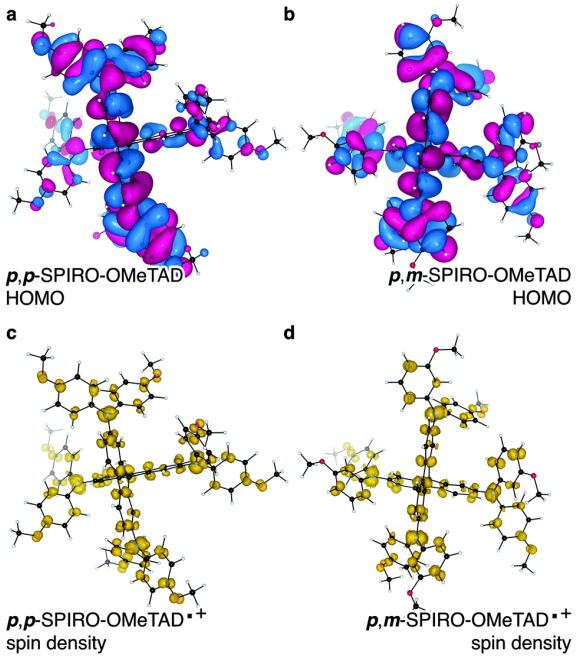

Figure 44 Kohn-Sham plots of *p*,*p*-SPIRO-OMeTAD and *p*,*m*-SPIRO-OMeTAD HOMO and SOMO. Reproduced from Ref.[272] with permission from the Royal Society of Chemistry.

In Figure 44 the HOMO of the more common *p*,*p*-SPIRO-OMeTAD is compared to the *p*,*m*-SPIRO-OMeTAD that was detrimental to efficiency. In addition to the HOMO, the singly-occupied molecular orbitals (SOMO) of the cationic radical state for two isomers can be compared. This qualitative interpretation can be used to for insight on the chemical bonding within the structure. a) shows the calculated *p*,*p*-SPIRO-OMeTAD highest-occupied molecular orbital (HOMO) while c) shows the associated one electron oxidised spin density.

b) shows the *p,m*-SPIRO-OMeTAD HOMO and d) is the associated one electron oxidised spin density. The oxidised doublet state (SOMO) is equivalent to the removal of a single electron from the extended π system; the associated spin density remains centred on the carbon system, but spin stabilisation comes from the surrounding heteroatoms. Furthermore, the contribution to the delocalised radical from the amino phenyl carbons appear unaffected by position of the methoxy ether motifs. The amino phenyl motifs are not part of the extended π system due to the violation of Hückel planarity.[273] The consequence of this absence of planarity is that chemical modifications would not be expected to affect the ionisation potential to the extent observed in a typical conjugated system.[274] Therefore, modification of the position of the methyl ether motifs should affect the energy level.

The energy level alignment of 12 isomers structurally related to *p,p*-SPIRO-OMeTAD were predicted to determine the suitability of modifying the side chains to improve efficiency. The calculations are performed using hybrid density functional theory (DFT), with atom-centred numerical basis functions. Kohn-Sham energy gaps are calculated using B3LYP, and reliable ionisation potentials were calculated with the data self-consistent field (ΔSCF) method. As relative ionisation potential was investigated, rather than an absolute value of the solid state, calculations were performed on a single molecule in the gas phase, as solid state calculations may be prone to molecular packing effects. These packing effects in a real system, could have a significant influence on device performance, rendering efforts to perform time consuming calculations on a solid state system obsolete. Neutral, closed shell SPIRO-OMeTAD analogues were constructed by hand, before geometries were relaxed to their potential energy minimum using B3LYP/6-31g* hybrid-DFT level of theory, in Gaussian09. The Kohn-Sham eigen values were extracted from the calculations.
The ΔSCF method of calculating ionisation potential was determined as the difference in total DFT energy between a resolved electronic structure configuration as the 1+ cation in a doublet spin configuration at neutral geometry and the neutral configuration.
Two amino aryl rings were used to define the *o*, *m*, and *p* positions of the compound, and the variation in the structural isomers led to modest electronic modulation, however, it is noteworthy in the context of hole extraction.

Two conclusions can be drawn from alternating the position of the methyl ether groups; (i) *meta*-methoxy substituents lead to an increase in ionisation potential. This is due to a reduction in structural symmetry (from decreased electron donating character of the oxygen)

resulting in a lower π system energy; (ii) *para*- and *ortho*- substituted result in decreased ionisation potential due to the increase in energy of the π system. Furthermore, multiple methoxy ether substitutions on the aromatic ring lead to a decrease in ionisation potential of the system from the repulsive interaction between neighbouring ring systems.

The Kohn-Sham energy gap (E_g) remains relatively constant in most cases, however, the HOMO eigen value deviates from the ΔSCF ionisation potential (Figure 45). The black dashed horizontal line refers to the IP of *p,p*-SPIRO-OMeTAD.

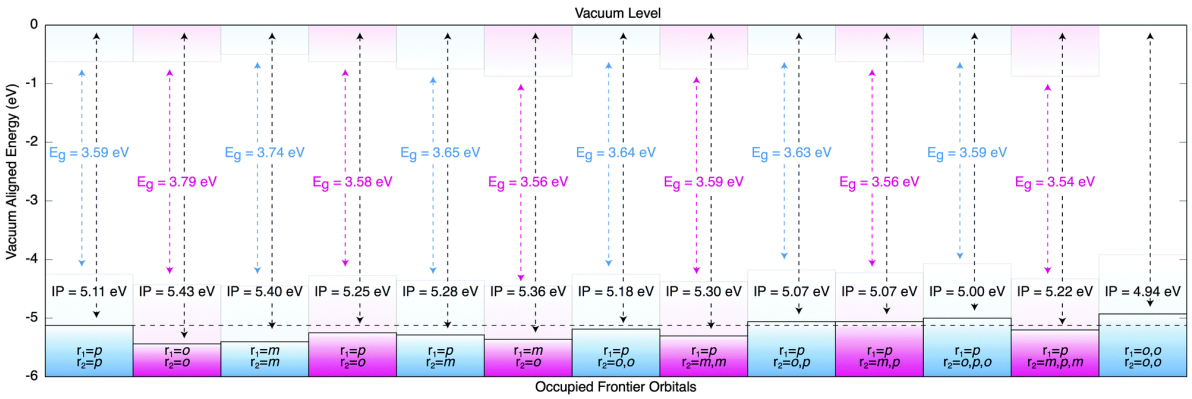

Figure 45 Kohn-Sham energy gaps (E_g) and ΔSCF ionisational potentials (IP) for a range of SPIRO-OMeTAD derivatives.

The suggests the Koopman approximation is insufficient for the prediction of qualitative trends. The ΔSCF values are in close agreement with experiment for the *p,p*- and *p,m*-analogues respectively,[270,275] though for the *p,o*-analogue the calculation contradicts experiment, predicting that an increase in efficiency should be observed, which is not observed in this case.[270] The *o,o*-SPIRO-OMeTAD analogue has a noticeably smaller ionisation potential than other analogues. The is expected to be due to the electron donating contribution from the *ortho*-positions and "through-space" conjugation of the amine motif.[276]

Modification of the energy levels of the contact material is only a partial fulfilment of the requirements for increased efficiency. Holes also need to be transported efficiently through avoidance of surface recombination. Prediction of charge carrier transport in a novel organic material is a highly complex calculation, as the full packing model and an understanding of the dielectric environment are required before microscopic charge transfer integrals can be calculated, which are needed to predict macroscopic mobility.[277] It is expected that the addition of bulky side chains would decrease the molecular packing density and coordination, reducing electronic overlap, and thus microscopic mobility.

In conclusion, alterations in the positioning of the methyl ether motifs on the hole conducting material SPIRO-OMeTAD have resulted in a change in HOMO energy, and the ionisation potentials of a variety of these structural isomers have been predicted. The computational method applied showed good correlation with experiment measures obtained from solution voltammetry. These synthetic variants offer flexibility in work function matching when designing (or optimising) hybrid perovskite solar cells, and are predicted to lead to increased efficiency.[272]

7. Conclusions

A range of new flavin-catalysed reactions have been developed and investigated with the aim of achieving sulfur oxidation. New preparations for the formation of sulfoxides from the corresponding sulfides and their mechanisms of action have been proposed. In the course of these investigations, flavin decomposition was discovered, isolated and probed. The understanding gained was then used to propose a solution to the decomposition, although this could not be actioned, despite exhaustive attempts. Ammonium carbamate was then used as a flavin reaction partner, which pleasingly resulted in the formation of sulfoximines in one step from the corresponding sulfide, although the reaction suffered from the same flavin decomposition that had been previously observed with sodium azide.

7.1 Flavin Catalysed Sulfur Oxidation

Hydrazine was initially investigated as a reaction partner for the oxidation of sulfides to sulfoxides, and the reaction proceeded cleanly, with excellent yields and low catalyst loading without any observation to the sulfoxide observed. The oxidation was effective for a range of aliphatic and aromatic sulfides. It was proposed that the reaction proceeded *via* a reduced flavin mechanism, and this was supported by the air free experiments that were conducted and the current literature regarding similar flavin/hydrazine systems. This investigation led to the discovery of a flavin precursor, alloxan, being active to the oxidation of sulfides for the formation of sulfoxides. This reaction was briefly probed, in order to rule out any transference of activity to flavin/hydrazine system. This was confirmed by the alloxan acting in a stochiometric manner with respect to the hydrazine, confirming that trace alloxan was not responsible for the activity observed in the flavin/hydrazine system. Nevertheless, this is the first example of sulfur oxidation from alloxan and hydrazine.

7.2 Flavin-Catalysed Sulfide Oxidation with Hydroxylamine

The modified hydroxylamine, *N*-hydroxybenzenesulfonamide was investigated as a co-reagent for flavin catalyst, but was found to undergo decomposition to nitroxyl. Unmodified hydroxylamine was then used to reduce our flavin catalyst, which then went on to form the hydroperoxyflavin, using air as a terminal oxidant, and a range of sulfoxides were formed from sulfides in good yields. This experiment was assisted in its optimisation by the use of

design of experiment methodologies. The reaction suffered from reproducibility issues, which were overcome by extracting the organics into an organic solvent, before removing the solvent *in vacuo*. Reaction kinetics were observed by continuous flow NMR spectroscopy and a reaction mechanism was postulated.

7.3 Investigation into flavin decomposition

An attempt to form a flavin stabilised, nucleophilic source of nitrogen that could be used for the formation of sulfoximines from sulfoxides, led to the observation of an unknown flavin product upon reaction with sodium azide. The product could not initially be characterised by standard techniques (NMR, mass spectrometry), and was ultimately positively identified by X-ray crystallography, after the investigation of a range of solvent systems to achieve formation of suitable crystals. A reaction mechanism was hypothesised for the interaction between sodium azide and flavin, which included the key isocyanate formation, which led irreversible flavin decomposition upon nucleophilic attack by the reaction solvent. This was probed with a range of solvents, and found that even non-nucleophilic trifluoroethanol incorporated into the flavin structure. It was hypothesised that the flavin transformation could be prevented by the insertion of a methyl group, and the formation of the methylflavin was attempted by a range of techniques, but got not be isolated.

7.4 Flavin mediated sulfoximine formation

The continued search for a flavin catalysed routes to sulfoximines from sulfides led to the investigation of ammonium carbamate as a co-reactant. Ammonium carbamate, was used as a source of electrophilic NH for the direct synthesis of sulfoximines. The reaction was not catalytic in flavin, and also suffered from decomposition of the flavin which led to deactivation. Techniques were explored to halt or slow the rate of deactivation, but these were unsuccessful. Methyl phenyl sulfoximine was isolated when the reaction was conducted on a suitably large scale, despite significant contamination from the decomposed flavin product. The presence of a range of sulfoximines was confirmed by mass spec. Although this reaction is the first example of a one step, flavin-mediated sulfoximine formation, it would require extensive further optimisation to make it synthetically useful, and as such, it was not deemed reasonable to continue the investigation.

7.5 Computational modelling

Computational modelling techniques were employed to investigate the physical properties of two different areas of materials science.

7.5.1 Conductivity of zeolitic imidazolate frameworks

Zeolitic imidazolate frameworks were prepared by collaborators, and through the use of density functional theory, explanations for their conductivity were proposed. Additionally, design principles were developed for the rational design of future ZIFs. Finally, the performance of new ligands containing electron withdrawing and donating groups were investigated, *via* band gap calculations, for their predicted performance as organic linger in conductive ZIFs.

7.5.2 Investigation of analogues for hybrid halide perovskite solar cells

Ionisation potentials of SPIRO-OMeTAD, a hole conducting material, and mothoxy and polymethoxy derivatives were predicted. This data was then used to predict and increase efficiency in hybrid halide perovskite solar cells. By changing the isomer, the HOMO level was changed, and the hole transport ability of the valence band maximum was affected.

8 Experimental

8.1 General Information

All reagents were purchased from commercial suppliers: Acros Organics, Alfa Aesar, Sigma Aldrich or Fluorochem and used without further purification. Flash chromatography was performed on chromatography grade, silica, 60 Å particle size 35-70 micron from Sigma Aldrich using the solvent system as stated. ^{1}H and ^{13}C NMR was performed on Brüker Avance 250 (^{1}H 250 MHz) Brüker Avance 300 (^{1}H 300 MHz and ^{13}C 75 MHz), Brüker Avance 400 (^{1}H 400 MHz and ^{13}C 100 MHz) and Brüker Avance 500 (^{1}H 500 MHz and ^{13}C 125 MHz) as stated. Chemical shifts are reported in parts per million (ppm) relative to tetramethylsilane (TMS) ($\delta = 0.00$). Coupling constants are reported in Hertz (Hz) and signal multiplicity is denoted as singlet (s), doublet (d), triplet (t), quartet (q), quintet (quin.), sextet (sex.), septet (sept.), multiplet (m), and broad (br). High resolution mass spectrometry electrospray (ESI) was performed on a Brüker μTOF using electrospray ionisation (ESI) in either positive or negative ionisation. HPLC data was recorded on an Agilent 1260 Infinity system using an Agilent Eclipse XDB-CN 5 μm, 4.6 x 150 mm cyano column.

Single-crystal X-ray experiments at the University of Bath were conducted using an Agilent Technologies Dual-Source Supernova diffractometer, equipped with an Eos Series 2 detector. Data were collected using Mo Kα radiation ($\lambda = 0.71073$ Å) to a resolution of 0.8 Å. The sample temperature was controlled using an Oxford Cryosystems Cryostream Plus, with experiments conducted at 100 K. The diffraction data were collected, indexed and integrated using the Agilent Technologies software CrysAlis Pro and the structures were solved using the program SHELXT. Crystal structure refinement was completed using the program SHELX and the results visualised using the CCDC software Mercury.[278]

UV/vis spectra were collected on either a Shimadzu UV-1800 or Agilent Cary 60 instrument, and stopped flow kinetics on a Hi-Tech Scientific Stopped Flow instrument.

8.2 Experimental Section

4-(Trifluoromethyl)-2-nitro-N-(2-hydroxyethyl)aniline 110

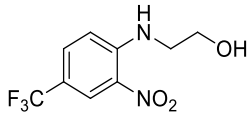

Ethanolamine (3.30 mL, 54.60 mmol) was added to a solution of 4-chloro-3-nitrobenzotrifluoride (2.67 mL, 18.20 mmol) in EtOH (50 mL). K_2CO_3 was added (2.77 g, 20.02 mmol), and the mixture was stirred at 90 ºC for 18 h. The reaction was cooled to R.T. and poured over 50 mL ice water. The organics were extracted, with EtOAc (3 x 50 mL), combined washed with brine. The organic layer was then dried with $MgSO_4$ and the solvent removed *in vacuo.* 4-(trifluoromethyl)-2-nitro-N-(2-hydroxyethyl)aniline (4.55 g, 99%) was obtained as a yellow solid.

^{1}H NMR (300 MHz, $CDCl_3$) 8.50 (s, 1H), 8.44 (s, 1H), 7.62 (d, 1H, *J* = 9.1 Hz), 6.99 (d, 1H, J = 9.0 Hz), 3.95 (m, 2H), 3.55 (m, 2H)

^{13}C NMR (125 MHz, $CDCl_3$) δ_C 147.1, 132.2 131.2, 125.5, 125.0, 122.1 (q, $J_{C,F}$ = 275 Hz), 114.6, 60.9, 45.0;

^{19}F NMR (470 MHz, $CDCl_3$) δ_F -62.8

IR ν_{max} (neat) 3370, 3301, 2953, 2637, 1574, 1270, 1245, 1132, 1056 cm^{-1}

MP 43-45 ˚C

HRMS (ESI, +ve) *m/z* calcd. for $C_9H_9N_2O_3F_3Na$ 273.0463, found: 273.0462 $(M+Na)^+$

Data in accordance with literature.[279]

2-((2-hydroxyethyl)amino)-5-(trifluoromethyl)aniline 111

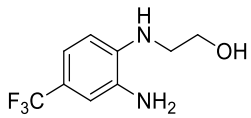

To a solution of 4-(trifluoromethyl)-2-nitro-N-(2-hydroxyethyl)aniline (1.25 g, 5 mmol) in MeOH (10 mL) at 0 ºC was added ammonium formate (1.58 g, 25 mmol) followed by 10 wt% palladium on carbon (0.25 g) under a positive pressure of N_2. The mixture was allowed to warm to r.t. and stirred until colourless (4 h). The black suspension was then filtered through celite and quickly washed before drying with CH_2Cl_2 (60 mL). The organic layer was collected and washed with saturated $NaHCO_3$ solution (30 mL) and brine (30 mL), before it was dried with $MgSO_4$ and solvent removed *in vacuo*. 2-((2-hydroxyethyl)amino)-5-(trifluoromethyl)aniline (0.93 g, 84%) was obtained as a fluffy pink solid.

^{1}H NMR (300 MHz, DMSO-d_6) δ_H 6.83 (m, 2H), 6.53 (m, 1H), 5.77 (q, J = 5.9 Hz, 2H), 5.06 (t, J = 5.9 Hz, 1H), 5.06 (br s, 2H), 4.77 (t, J = 5.7 Hz, 1H), 3.64 (q, J = 6.0 Hz, 2H),

^{13}C NMR (75 MHz, DMSO-d_6) δ_C 159.4, 135.5, 124.6 (q, $J_{C,F}$ = 270 Hz), 116.7 (q, $J_{C,F}$ = 31 Hz), 114.9, 109.9, 108.5, 59.7, 46.1.

^{19}F NMR (470 MHz, DMSO-d_6) -59.0 (s).

IR ν_{max} (neat) 3485, 3310, 3258, 2005, 1950, 1647, 1598, 1444, 1328 cm^{-1}

MP 95 ˚C.

HRMS (ESI, +ve) *m/z* calcd. for $C_9H_{10}F_3N_2O$, 219.0745. Found: 219.0743 $(M-H)^-$. Data in accordance with literature.[279]

7-(Trifluoromethyl)-1,10-ethylenealloxazinium chloride 113

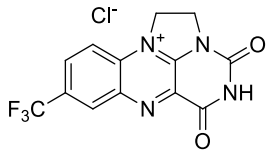

Under an atmosphere of N_2, 2-((2-hydroxyethyl)amino)-5-(trifluoromethyl)aniline (1.00 g, 4.54 mmol) was dissolved in 10 mL glacial acetic. To this was added alloxan monohydrate (0.72 g, 4.54 mmol) and boric acid (0.29 g, 4.54 mmol), and the mixture was stirred at 50 ºC under N_2 in the dark for 18 h. The suspension was then cooled in an ice bath and rapidly filtered, washed with CH_2Cl_2, and the filtrate dried under vacuum. The yellow solid collected was placed under N_2 in the dark and thionyl chloride (20 mL) was added slowly. The mixture was stirred at 50 ºC for 24 h, before the thionyl chloride was removed by filtration, and further washing with CH_2Cl_2. The yellow solid was recrystallised by initial hot filtration with 2,2,2-trifluoroethanol, before TFE was removed *in vacuo* and dissolution in formic acid followed by re-precipitation with Et_2O to give 7-(Trifluoromethyl)-1,10-ethyleneisoalloxazinium chloride (1.45 g, 93%) as a bright yellow solid.

^{1}H NMR (300 MHz, CD_3COOD-CF_3COOH 1:6) δ_H 9.02 (s, 1H), 8.66 (d, J = 7.4 Hz, 1H), 8.42 (d, J = 7.4 Hz, 1H), 8.02 (s, 1H), 5.70 (t, J = 7.5 Hz, 2H), 4.95 (t, J = 7.5 Hz, 2H);

^{13}C NMR (125 MHz, CD_3COOD-CF_3COOH 1:6) δ_C 165.0, 157.5, 145.7, 145.1, 139.8, 135.6, 135.3, 134.2, 131.6, 130.4, 120.6 (q, $J_{C,F}$ = 270), 118.7, 51.8, 46.3

^{19}F NMR (470 MHz, CD_3CO_2D) δ_F -63.4;

IR ν_{max} (neat) 3387, 3330, 2905, 2809, 1735, 1717, 1609, 1343, 1118 cm^{-1}

MP 192 – 193 ˚C

HRMS (ESI, +ve) *m/z* calcd. for $C_{13}H_8F_3N_4O_2$, 332.0497. Found: 332.0490 $(M+Na)^+$. Data in accordance with the literature.[279]

2-(5-chloro-2-nitrophenylamino)ethanol 122

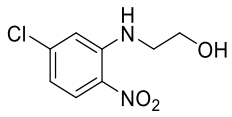

Potassium carbonate (4.00 g, 28.9 mmol) was dissolved in EtOH (100 mL), and 2,4-dichloro-1-nitrobenzene (5.00 g, 26.3 mmol) was added. To this was added ethanolamine (4.76 mL, 78.9 mmol), and the mixture was stirred at 90 °C for 18 h. The solution was then cooled to R.T and poured over ice water (50 mL). The organic components were extracted with EtOAc (3 x 50 mL), the organic layers were combined, and washed with brine (60 mL). The solvent was then removed *in vacuo.* The product was purified by column chromatography (CH_2Cl_2/EtOAc 9:1) to yield 2-(5-chloro-2-nitrophenylamino)ethanol (4.90 g, 95 %) as a vibrant orange solid.

^{1}H NMR (500 MHz, $CDCl_3$) δ_H 8.29 (br s, 1H), 8.13 (d, *J* = 9.1 Hz, 1H), 6.89 (d, *J* = 2.2 Hz, 1H), 6.63 (dd, *J* = 9.1, 2.2 Hz, 1H), 3.96 (t, *J* = 5.3 Hz, 2H), 3.48 (apparent q, *J* = 5.3 Hz, 2H), 1.69 (br s, 1H).

^{13}C NMR (125 MHz, $CDCl_3$) δ_C 146.0, 143.0, 128.8, 128.5, 116.3, 113.4, 60.9, 45.1.

IR ν_{max} (neat) 3470, 3324, 2964, 2884, 1615, 1562, 1188 cm^{-1}

MP 114 – 117 ˚C (lit = 116 ˚C[280])

HRMS (ESI, +ve) *m/z* calcd. for $C_8H_{10}N_2O_3Cl$ 217.0374, found: 217.0363 $(M+H)^+$. Data in accordance with literature.[279]

2-((2-hydroxyethyl)amino)-4-chloroaniline 123

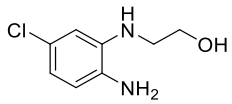

To a suspension of mossy tin (1.65 g, 13.9 mmol) in water (20 mL) was added 2-(5-chloro-2-nitrophenylamino)ethanol (1.00 g, 4.6 mmol). The reaction heated to 100 °C, hydrochloric acid d (conc., 8 mL) was added dropwise and stirred for 0.5 h. The reaction was cooled to 0 °C in an ice bath and made basic with 50% NaOH. The organic components were extracted with EtOAc (3 x 50 mL) before the organic layers were combined, dried over $MgSO_4$ and solvent removed *in vacuo*. 2-((2-hydroxyethyl)amino)-4-chloroaniline (0.57 g, 66 %) was obtained as an off white solid.

^{1}H NMR (500 MHz, $CDCl_3$) δ_H 7.25 (s, 1H), 6.73 – 6.54 (m, 2H), 3.97 – 3.80 (m, 2H), 3.34 – 3.18 (m, 2H), 2.93 (apparent br s, 3H)

^{13}C NMR (125 MHz, $CDCl_3$) δ_C 138.8, 132.9, 125.8, 118.4, 117.4, 112.1, 61.2, 46.2

IR ν_{max} (neat) 3348, 3324, 2818, 1599, 1418, 1054 cm^{-1}

MP MP 98 – 100 ˚C (lit = 104 ˚C[280])

HRMS (ESI, +ve) *m/z* calcd. for for $C_8H_{12}N_2OCl$, 187.0638. Found: 187.0611 $(M+H)^+$.

Data in accordance with literature.[279]

8-chloro-1,10-ethylenealloxazinium chloride 125

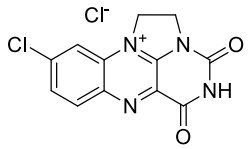

2-((2-hydroxyethyl)amino)-4-chloroaniline (0.50 g, 2.68 mmol) was dissolved in 10 mL glacial acetic acid and placed under a N_2 atmosphere. Alloxan monohydrate (0.43 g, 2.68 mmol) was added, followed by the addition of boric acid (0.17 g, 2.68 mmol) and the suspension heated to 50 °C for 18 h. The suspension was then cooled in an ice bath and rapidly filtered, washed with CH_2Cl_2, and the filtrate dried under vacuum. The yellow solid collected was placed under N_2 in the dark and thionyl chloride (20 mL) was added slowly. The mixture was stirred at 50 ºC for 24 h, before the thionyl chloride was removed by filtration, and further washing with CH_2Cl_2. The yellow solid was purified by dissolution in formic acid followed by re-precipitation with Et_2O to yield 8-chloro-1,10-ethylenealloxazinium chloride (0.37 g, 44 %).

^{1}H NMR (500 MHz, $CDCl_3$) δH 8.45 – 8.36 (m, 1H), 8.06 – 7.98 (m, 2H), 5.44 (t, *J* = 8.6 Hz, 2H), 4.87 (t, *J* = 8.6 Hz, 2H)

^{13}C NMR (125 MHz, $CDCl_3$) δC 149.8, 145.7, 143.7, 139.8, 134.2, 133.5, 130.5, 116.3, 115.7, 51.1, 45.1.

IR ν_{max} (neat) 3444, 3217, 1738, 1375 cm^{-1}

MP >350 ˚ C (lit > 350 ˚C)

HRMS (ESI, +ve) *m/z* calcd. for 275.0330, found: 241.0321 (M)+. Data in accordance with literature.[279]

2-nitro-*N*-(2-hydroxyethyl)aniline 115

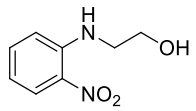

1-fluoro-2-nitrobenzene (2.00 mL, 19.0 mmol) was dissolved in EtOH (40 mL) and ethanolamine (3.52 mL, 57 mmol) was added. Potassium carbonate (2.81 g, 20.35 mmol) was then added and the reaction heated to 90 °C and stirred for 18 h. The reaction mixture was then cooled to R.T. and the solution poured over ice water (50 mL). The organic components were extracted with EtOAc (3 x 50 mL) and the organic layers combined and washed with brine (50 mL). The organic layer was dried with $MgSO_4$ and the solvent removed *in vacuo.* 2-nitro-N-(2-hydroxyethyl)aniline (3.04g, 88 %) was isolated as a deep orange solid.

^{1}H NMR (500 MHz, $CDCl_3$) $^1\delta_H$ 8.23 (br s, 1H), 8.17 (apparent dd, *J* = 8.6, 1.7 Hz, 1H), 7.48 – 7.40 (m, 1H), 6.89 (d, *J* = 8.6 Hz, 1H), 6.69 – 6.63 (m, 1H), 3.94 (t, *J* = 5.4 Hz, 2H), 3.51 (apparent q, *J* = 5.4 Hz, 2H), 1.94 (br s, 1H).

^{13}C NMR (125 MHz, $CDCl_3$) δ_C 145.6, 136.4, 132.4, 127.1, 115.7, 113.9, 61.1, 45.1.

IR ν_{max} (neat) 3463, 3336, 2964, 2877, 1622, 1567, 1508, 1418 cm^{-1}

MP MP 73 – 74 ˚C (lit: 74 – 75 ˚C[281])

HRMS (ESI, +ve) *m/z* calcd. for $C_8H_{11}N_2O_3$ 183.0770, found: 183.0734 $(M+H)^+$. Data in accordance with literature.[279]

2-((2-hydroxyethyl)amino)-aniline 116

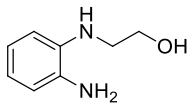

Ammonium formate (1.26 g, 20.0 mmol) was added to a solution of 2-nitro-N-(2-hydroxyethyl)aniline (0.73 g, 4.0 mmol) in MeOH (15 mL) at 0 °C. This was followed by the addition of 10 wt% palladium on carbon (104 mg). The reaction was left to warm to R.T. and stirred for 4 h, before the reaction mixture was filtered through celite and washed with CH_2Cl_2 (50 mL). The organic layer was washed successively with saturated $NaHCO_3$ (30 mL) and brine (30 mL). The organic layer was then isolated and dried with $MgSO_4$ and the solvent was removed *in vacuo* to yield 2-((2-hydroxyethyl)amino)-aniline (0.60 g, 98 %) as a dirty white solid.

^{1}H NMR (500 MHz, $CDCl_3$) δ_H 6.60 – 6.37 (m, 4H), 4.66 (t, J = 5.5 Hz, 2H), 4.41 (br s, 2H), 4.31 (br s, 1H), 3.60 (apparent q, J = 5.5 Hz, 2H), 3.10 – 3.04 (m, 1H)

^{13}C NMR (125 MHz, $CDCl_3$) δ_C 136.7, 135.8, 118.2, 117.4, 114.7, 110.3, 60.1, 46.5

IR ν_{max} (neat) 3403,3342, 3217, 2938, 1604, 1049 cm^{-1}

MP MP 104 - 105 ˚C (lit: 108 °C[280])

HRMS (ESI, +ve) *m/z* calcd. for $C_8H_{13}N_2O$ 153.1028, found: 153.1005 $(M+H)^+$. Data in accordance with literature.[279]

1,10-ethylenealloxazinium chloride 118

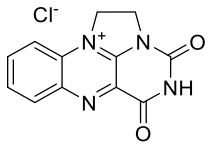

2-((2-hydroxyethyl)amino)-aniline (0.15, 0.8 mmol) was added to glacial acetic acid (5 mL) and stirred and an N_2 atmosphere. Alloxan monohydrate (0.16 g, 0.8 mmol) was added, followed by the addition of boric acid (0.06 g, 0.8 mmol) and the suspension heated to 50 °C for 18 h. The reaction mixture was cooled in an ice bath and filtered under vacuum. The bright orange solid was immediately placed under atmosphere of N_2, in the dark and thionyl chloride (5 mL) was added gradually. The reaction mixture was stirred at 50 °C for a further 18 h. It was then cooled to R.T. and the thionyl chloride was removed by vacuum filtration and the precipitate was washed with CH2Cl_2. The yellow solid was purified by dissolution in formic acid followed by re-precipitation with Et2O to yield 1,10-ethylenealloxazinium chloride (0.10 g, 41 %).

^{1}H NMR (500 MHz, $CDCl_3$) δ_H 8.49 (d, *J* = 8.4 Hz, 1H), 8.31 (t, *J* = 7.7 Hz, 1H), 8.08 (t, *J* = 7.7 Hz, 1H), 8.00 (d, *J* = 8.4 Hz, 1H), 5.49 (t, *J* = 7.6 Hz, 2H), 4.88 (t, *J* = 7.6 Hz, 2H).

^{13}C NMR (125 MHz, $CDCl_3$) δ_C 158.7, 146.0, 143.2, 141.3, 141.2, 133.2, 132.3, 131.0, 129.5, 116.5, 51.1, 45.1.

IR ν_{max} (neat) 3385, 3080, 2937, 2759, 1728, 1633, 1379 cm^{-1}

MP 218-220 ˚C (lit = 216 – 219 ˚C)

HRMS (ESI, +ve) *m/z* calcd. for $C_{13}H_9N_4O_2$ 241.0720, found: 241.0725 $(M)^+$. Data in accordance with literature.[279]

General procedure A for flavin catalysed sulfur oxidation by hydrazine

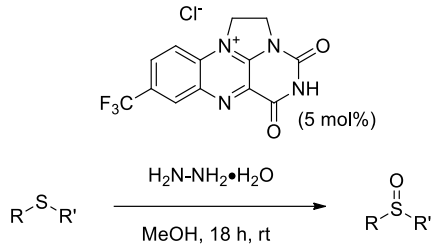

Hydrazine monohydrate solution (64-65%) (12 mg, 0.24 mmol) was added to a mixture of sulfide (0.2 mmol) and flavin catalyst (3.5 mg, 0.01 mmol, 5 mol %) in methanol (1 mL). The reaction mixture was stirred under air for 18 h and diluted with H2O (5 mL). Ethyl acetate (5 mL) was then added and the mixture was separated. The aqueous layer was then further extracted with EtOAc (3 x 5 mL) and the organic layers were combined, dried over magnesium sulfate and solvent removed in *vacuo*. The crude sulfoxide was purified by column chromatography (petroleum ether/EtOAc 0 – 100%).

Methyl phenyl sulfoxide 132A

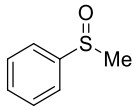

Following general procedure, A using methyl phenyl sulfide (25 mg) gave methyl phenyl sulfoxide. Product was purified by flash column chromatography [petroleum ether/ethyl acetate 50 to 100%] to give a white solid (21 mg, 71%).

^{1}H NMR (250 MHz, $CDCl_3$) δ_H 7.64 (d, 2H, *J* =7.4 Hz), 7.51 (m, 3H), 2.73 (s, 3H)

^{13}C NMR (125 MHz, $CDCl_3$) δ_C, 145.7, 131.1, 129.4, 123.5, 44.0;

IR ν_{max} (neat) 3062, 3000, 2903, 1477, 1092 cm^{-1}

MP 27 – 30 ˚C (lit 30 – 30.5 ˚C)[282]

HRMS (ESI, +ve) *m/z* calcd. For C_7H_9SO 141.0374, found: 141.0389 $(M+H)^+$. Data in accordance with literature.[283]

4-Methoxyphenyl methyl sulfoxide 132B

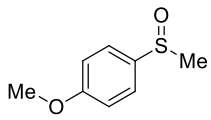

Following general procedure, A using methyl phenyl sulfide (31 mg) with 64-65% $N_2H_4.H_2O$ gave methyl phenyl sulfoxide. Product was purified by flash column chromatography [petroleum ether 40-60 °C/ethyl acetate 50 to 100%] to give an a white solid (31 mg, 75%).

^{1}H NMR (400 MHz, $CDCl_3$): δ_H 7.56 (d, *J* = 8.9 Hz, 2H), 7.01 (d *J* = = 8.9 Hz, 2H), 3.84 (s, 3H), 2,68 (s, 3H);

^{13}C NMR (100 MHz, $CDCl_3$) δ_C 151.7, 136.7, 125.2, 114.8, 55.4, 44.0;

IR ν_{max} (neat) 2997, 2866, 1651, 1451, 1027 cm^{-1}

MP 42 ˚C (lit 42.1 – 43.0 ˚C)[284]

HRMS (ESI, +ve) *m/z* calcd. for $C_8H_{11}O_2S$ 171.0435; found 171.0427 $(M+H)^+$ Data in accordance with literature.[283]

Diphenyl Sulfoxide 132C

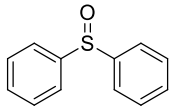

Following general procedure, A using diphenyl sulfide (84 μL, 0.5 mmol) gave diphenyl sulfoxide (41 mg, 75 %) as a pale beige solid.

^{1}H NMR (300 MHz, $CDCl_3$) δ_H 7.62 (m, 6H), 7.41 (m, 4H);

^{13}C NMR (125 MHz, $CDCl_3$) δ_C 145.6, 131.2, 129.4, 124.5;

IR ν_{max} (neat) 2954, 2920, 1496, 1468, 1372;

MP 67 – 69 ˚C (lit 69 – 60 ˚C)[285]

HRMS (ESI, +ve) *m/z* calcd. for $C_{12}H_{11}OSNa$ 225.0350; found 225.0350 $(M+Na)^+$ Data in accordance with literature.[286]

1-Bromo-4-methylsulfinylbenzene 132D

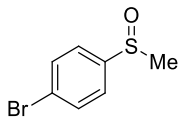

Following general procedure, A using 4-(methylthio)bromobenzene (203 μL, 0.5 mmol) gave 1-Bromo-4-methylsulfinylbenzene (44 mg, 62 %) as a dirty white solid. **^{1}H NMR** (400 MHz, $CDCl_3$): δ_H 7.67 – 7.69 (d, 2H, *J* = 5 Hz), 7.51 – 7.55 (d, 2H, *J* = 10), 2.73 (s, 3H);

^{13}C NMR (100 MHz, $CDCl_3$): δ_C 107.3, 95.0, 87.8, 87.5, 42.0;

IR ν_{max} (neat) 3093, 2997, 2914, 1433, 1489, 1308;
MP 76 ˚C (74 – 77 ˚C)[287]

HRMS (ESI, +ve) *m/z* calcd. for $C_7H_7BrOSNa$ 240.9299; found 240.0300 $(M+Na)^+$. Data in accordance with literature.[288]

1-Methyl-4-(methylsulfinyl)benzene 132E

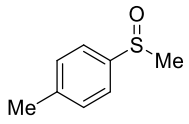

Following general procedure, A using 4-(methylthio)toluene (135 μL, 1 mmol) gave methyl phenyl sulfoxide (31 mg, 64 %) as an off white solid.

^{1}H NMR (400 MHz, MeOH-*d4*) 7.57 (d, *J* = 8.2 Hz, 2H), 7.39 (d, *J* = 7.9 Hz, 2 Hz), 2.77 (s 3H), 2.42 (s, 3H);

^{13}C NMR (100 MHz, MeOH- *d4*) δ_C 142.9, 141.9, 130.4, 123.9, 43.3, 21.8;

IR ν_{max} (neat) 3432, 2919, 1453, 1057, 1045, 959;

MP 39 - 41 ˚C (41.9 – 42.9 ˚C)[289]

HRMS (ESI, +ve) *m/z* calcd. for $C_8H_{11}OS$ 155.0531; found 155.0528 $(M+H)^+$. Data in accordance with literature.[290]

3-(Allylsulfinyl)prop-1-ene 132F

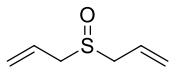

Following general procedure, A using 3-prop-2-enylsulfanylprop-1-ene (64 μL, 0.5 mmol) gave 3-(allylsulfinyl)prop-1-ene (26.04 mg 75%) as a brown oil.

^{1}H NMR (500 MHz, $CDCl_3$): δ_H 5.85 – 5.94 (m, 2H), 5.38 – 5.47 (m, 4H), 3.38 – 3.55 (m, 4H);

^{13}C NMR (125 MHz, $CDCl_3$): δ_C 125.7, 123.6, 54.2.

IR ν_{max} (neat) 1620, 1058;

HRMS (ESI, +ve) *m/z* calcd. for $C_6H_{10}SONa$ 153.0350; found 153.0354 Data in accordance with literature.[291]

1-(Butylsulfinyl)butane 132G

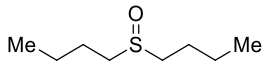

Following general procedure, A using methyl phenyl sulfide (174 μL, 1 mmol) gave 1-(butylsulfinyl)butane (32 mg, 95 %) as a clear, pale yellow powder.

^{1}H NMR (250 MHz, CDCl3): δH 2.60 – 2.72 (t, 4H, *J* = 6.6), 1.71 – 1.80 (m, 4H), 1.45 – 1.55 (m, 4H), 0.97 (t, 6H, *J* = 7.2);

^{13}C NMR (75 MHz, CDCl3): δC 52.1, 24.7, 22.1, 13.8.

IR ν_{max} (neat) 1017 cm^{-1};

MP 35 – 36 ˚C (lit 34 – 35 ˚C)[291]

HRMS (ESI, +ve) *m/z* calcd. for $C_8H_{19}OS$ 163.1156; found 163.1168. Data in accordance with literature.[291]

3-(Methylsulfinyl)-1-propanol 132H

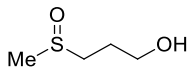

Following general procedure, A using 3-(Methylthio)-1-propanol (103 μL, 1 mmol) gave 3-(methylsulfinyl)-1-propanol (25 mg, 91 %) as a clear, colourless oil.

^{1}H NMR (250 MHz, $CDCl_3$): δ_H 1.85 (m, 2H), 2.55 (s, 3H), 2.71 (t, 2H, 7.1), 3.55 (t, 2H, *J* = 6.6);

^{13}C NMR (75 MHz, $CDCl_3$): δ_C 56.1, 48.6, 38.0, 32.4;

FTIR ν_{max} (neat) 3321, 2974, 2880, 1457, 1273 cm^{-1},

HRMS (ESI, -ve) *m/z* calcd. for $C_8H_{19}OS$ 163.1157, found: 196.1126 $(M-H)^-$ Data in accordance with literature.[292]

Sulfur oxidation with alloxan and hydrazine 134

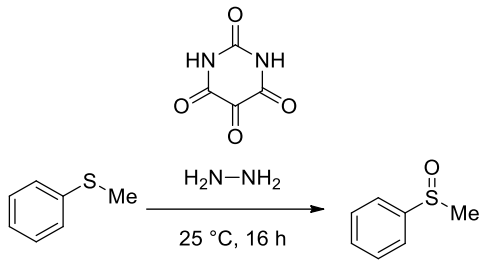

Methyl phenyl sulfide (25 mg, 0.2 mmol) was added to a suspension of alloxan monohydrate (32 mg, 0.2 mmol) and hydrazine monohydrate solution (64-65%) (10 mg, 0.2 mmol) in methanol (1 mL). The reaction was stirred under air for 16 h. After this time it was diluted with H_2O (5 mL), ethyl acetate (5 mL) was then added and the mixture separated. The aqueous layer was then further extracted with EtOAc (3 x 5 mL) and the organic layers were combined, dried over magnesium sulfate and solvent removed *in vacuo*. Product was purified by flash column chromatography [petroleum:ethyl acetate 0 - 100%] to give methyl phenyl sulfoxide (25 mg, 90%) as a pale-yellow oil.

^{1}H NMR (250 MHz, $CDCl_3$) δ_H 7.64 (d, 2H, *J* =7.4 Hz), 7.51 (m, 3H), 2.73 (s, 3H)

^{13}C NMR (125 MHz, $CDCl_3$) δ_C, 145.7, 131.1, 129.4, 123.5, 44.0;

IR ν_{max} (neat) 3062, 3000, 2903, 1477, 1092 cm^{-1}

MP 27 – 30 ˚C (lit 30 – 30.5 ˚C)[282]

HRMS (ESI, +ve) *m/z* calcd. For C_7H_9SO 141.0374, found: 141.0389 $(M+H)^+$. Data in accordance with literature.[283]

4-Amino-4-methylmorpholin-4-ium iodide 138

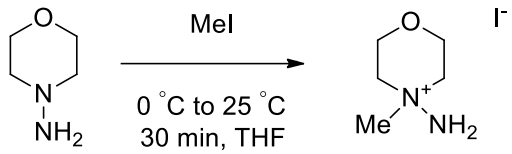

A solution of 4-aminomorpholine (102.0 mg, 1.0 mmol) in THF (1 mL) was cooled to 0°C and methyliodide (145 mg, 1.0 mmol, 1.05 eq.) was added dropwise. The reaction mixture was stirred for 30 minutes under air. The white precipitate was then filtered and rinsed with diethyl ether and left to dry. The solid was dissolved was in a hot mixture of ethanol and methanol (3:1) and was left to cool to recrystallize the product. It was filtered from solution and washed with cold ethanol to give white crystals (188.0 mg, 77%).

^{1}H NMR (250MHz, DMSO-d_6): δ_H 5.97 (s, 2H), 3.99 (ddd, *J*=13.1, 9.3, 3.0 Hz, 2H), 3.89 (dt, *J*=13.0, 3.3 Hz, 2H), 3.58 (ddd, *J*=12.6, 9.0, 3.5 Hz, 2H), 3.42 (d, *J*=13.1 Hz, 3H), 3.35 (s, 3H);

^{13}C NMR (75 MHz, DMSO-d_6): δ_C 62.9, 60.7, 56.9.

IR ν_{max} (neat): 3270, 1456, 1092, 894 cm^{-1};

MP 168 – 171 ˚C

HRMS (ESI, +ve) *m/z* calcd. For $C_5H_{13}N_2O$ 117.1028, found: 117.1028 $(M+H)^+$. Data in accordance with literature.[160]

4-Amino-4-methylmorpholin-4-ium nitrate 139

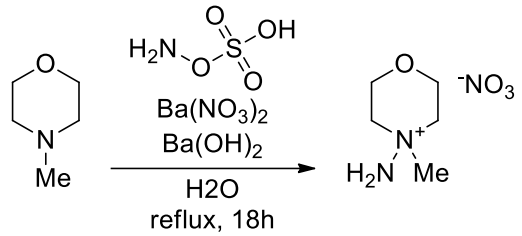

Barium nitrate (2.6 g, 10 mmol) was added to a suspension of barium hydroxide (3.15 g, 10 mmol) and *N*-methyl morpholine (1 g, 40 mmol) in H_2O (10 mL). This was added in dropwise to a solution of hydroxylamine-*O*-sulfonic acid (1.13 g, 12.5 mmol) in H_2O (20 mL) to give a white precipitate. The mixture was then heated at reflux for 18 h. The white precipitate removed by filtration and the solvent *removed in vacuo* to give a white crystalline solid. This was then recrystallised (H_2O) to give the hydrazinium nitrate salt (0.15 g, 30%) as a white solid.

^{1}H NMR (400 MHz, DMSO): δ = 5.96 (2 H, br), 3.99-3.93 (2 H, m), 3.87-3.82 (2 H, m), 3.59-3.53 (2 H, m), 3.44-3.52 (2 H, m), 3.33 (3 H, s).

^{13}C NMR (100 MHz, DMSO): δ = 62.2, 60.4, 56.6. Data in accordance with literature.

IR ν_{max} (neat) 3270, 1456, 1092, 894 cm^{-1}

MP ˚C (lit ˚C)[282]

HRMS (ESI, +ve) *m/z* calcd. For $C_5H_{13}N_2O$ 117.1028, found: 117.1028 $(M+H)^+$. Data in accordance with literature.[160]

General procedure for flavin catalysed sulfur oxidation by hydroxylamine hydrochloride (general procedure B)

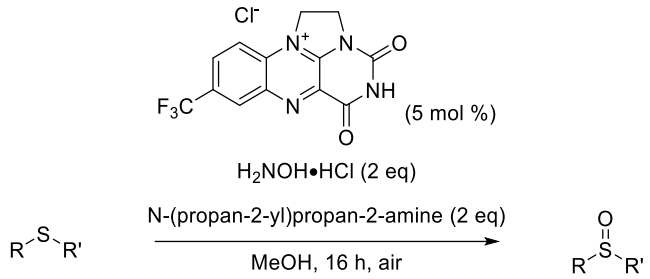

Hydroxylamine hydrochloride (69.5 mg, 1.0 mmol) was added to a mixture of sulfide (0.5 mmol) in methanol (5 mL). *N*-(propan-2-yl)propan-2-amine (280 μL, 2 mmol) was added followed by flavin catalyst (8.6 mg, 25 μmol, 5 mol %). The reaction mixture was stirred under air for 16 h and then diluted with H2O (5 mL). The organic components were extracted with ethyl acetate (3 x 15 mL) and the organic layers combined. Ethyl acetate was dried over magnesium sulfate and solvent removed *in vacuo* and the crude sulfoxide was purified by column chromatography (petroleum ether/EtOAc 0 – 100%).

General procedure for flavin catalysed sulfur oxidation by aqueous hydroxylamine (general procedure C)

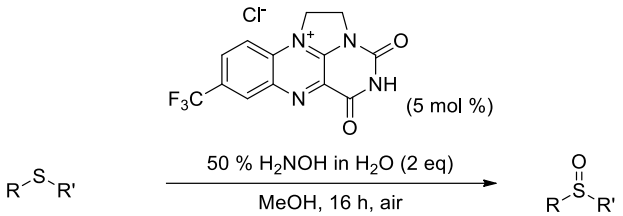

50 % hydroxylamine in water (122.6 μL, 2.0 mmol) was added to a mixture of sulfide (1 mmol) in methanol (10 mL). Lastly, the flavin catalyst (17.2 mg, 50 μmol, 5 mol %) was added. The reaction mixture was stirred under air for 16 h and then diluted with H_2O (5 mL). The organic components were extracted with ethyl acetate (3 x 15 mL) and the organic layers combined. Ethyl acetate was dried over magnesium sulfate and solvent removed *in vacuo* and the crude sulfoxide was purified by column chromatography (petroleum ether/EtOAc 0 – 100%).

(2-Propen-1-ylsulfinyl)-benzene 156C

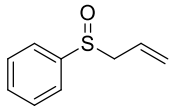

Following general procedure C using (2-propen-1-ylthio)benzene (147 μL, 1 mmol) gave (2-propen-1-ylsulfinyl)-benzene (78 mg, 48 %) as a clear, pale yellow oil.

^{1}H NMR (500 MHz, $CDCl_3$) δ_H 3.44 – 3.47 (d, 2H, *J* = 7.5), 5.08 – 5.16 (m, 1H), 5.23 – 5.28 (m 1H) 5.47 – 5.68 (m, 1H), 7.42 – 7.54 (m, 5H)

^{13}C NMR (125 MHz, $CDCl_3$) δ_C 60.7, 123.9, 124.3, 125.2, 129.0, 131.1, 142.8.

IR ν_{max} (neat) 3078, 2960, 1621, 1503, 1372, 1058 cm^{-1}

HRMS (ESI, +ve) *m/z* calcd. for C9H11OS 167.0531; found 167.0530 $(M+H)^+$. Data in accordance with literature.[293]

4-(Methylsulfinyl)benzaldehyde oxime 156F

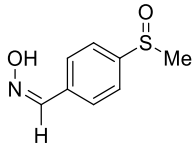

Following general procedure C using 4-(methylthio)benzaldehyde oxime (167 mg, 1 mmol) gave 4-(methylsulfinyl)benzaldehyde oxime (82 mg, 45 %) as a white powder.

^{1}H NMR (250 MHz, $CDCl_3$): δ_H 2.78 (s, 3H), 7.66 – 7.68 (d, 2H, *J* = 4.3), 7.72 – 7.74 (d, 2H, *J* = 5.2), 8.16 (s, 1H,);

^{13}C NMR (75 MHz, $CDCl_3$): δ_C 148.6, 146.6, 135.4, 127.8, 124.1, 43.7; Data in accordance with literature.

IR ν_{max} (neat) 3556, 1477, 1032 cm^{-1}

MP 115 ˚C (lit 115 – 117 ˚C)

HRMS (ESI, -ve) *m/z* calcd. $C_8H_8NO_2S$ 182.0275; found 182.0284 $(M-H)^-$. for Data in accordance with literature.[294]

Dimethyl sulfoxide 156H

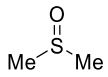

Following general procedure C using (methylsulfanyl)methane (73 μL, 1 mmol) gave dimethyl sulfoxide (41 mg, 52 %) as a clear, colourless oil.

^{1}H NMR (250 MHz, $CDCl_3$): δ_H 2.62 (s, 6H);

^{13}C NMR (75 MHz, $CDCl_3$): δ_C 40.6; Data in accordance with literature.

IR ν_{max} (neat): 2995, 2907, 1429, 1401, 1301, 1056 cm^{-1}. Data in accordance with literature.[295]

1-(methylsulfinyl)-dodecane 156I

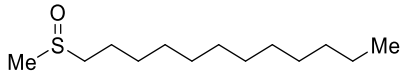

Following general procedure C using 1-(methylthio)dodecane (257 μL, 1 mmol) gave 1-(methylsulfinyl)-dodecane (121 mg, 51 %) as a white solid.

^{1}H NMR (250 MHz, *d*^{6}-DMSO): δ_H 0.88 (t, 3H, *J* = 7.0), 1.19 – 1.52 (m, 18 H), 1.71 -1.82 (m, 2H), 2.56 (s, 3H) 2.78 – 2.61 (m, 2H);

^{13}C NMR (75 MHz, *d*^{6}-DMSO): δ_C 52.0, 38.5, 32.0, 30.0, 29.6, 29.2, 23.1, 16.8, 14.0;

FTIR ν_{max} (neat) 2925, 2854, 1462, 1377, 1299, 721 cm^{-1},

MP 65 °C (Lit 65 °C)[296]

HRMS (ESI, +ve) *m/z* calcd. for $C_{13}H_{29}OS$ 233.1939. found 233.1932 $(M+H)^+$ Data in accordance with literature.[297]

Methyl 3-methylsulfinylpropanoate 156K

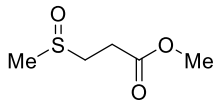

Following general procedure C using methyl 3-(methylthio)propionate (125 μL, 1 mmol) gave methyl 3-methylsulfinylpropanoate (52 mg, 35 %) as a clear, yellow oil.

^{1}H NMR (250 MHz, $CDCl_3$): δ_H 2.60 (s, 3H), 2.87 (m, 2H), 3.05 (m, 2H), 3.72 (s, 3H);

^{13}C NMR (75 MHz, $CDCl_3$): δ_C 171.86, 52.35, 49.05, 38.96, 26.86;

FTIR ν_{max} (neat) 3005, 2955, 2920, 1734, 1620, 1376, 1253, 1028;

HRMS (ESI, +ve) *m/z* calcd. for $C_5H_{11}O_3S$ 151.0429; found 151.0429 $(M+H)^+$. Data in accordance with literature.[298]

Methyl 7-(trifluoromethyl)-1,2-dihydroimidazo[1,2-a]quinoxaline-4-carboxylate 175

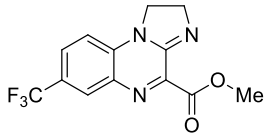

Sodium azide was added to a solution of flavin **113** in MeOH and stirred for 2 hrs. The reaction solvent was then removed in *vacuo* and the crude compound purified was purified by column chromatography (petroleum ether/EtOAc 0 – 100%) to give methyl 7-(trifluoromethyl)-1,2-dihydroimidazo[1,2-a]quinoxaline-4-carboxylate in a 28%

^{1}H NMR (500 MHz, $CDCl_3$) δ_H 8.68 (s, 1H), 8.41 (d, 1H, J = 8.5 Hz), 8.01 (d, 1H, J = 8.5 Hz), 5.26 (t, 2H, J = 10.0 Hz), 4.48 (t, 2H, J = 10.0), 4.12 (s, 3H);

^{13}C NMR (125 MHz, $CDCl_3$) δ_C 163.1, 149.9, 137.9, 135.7, 133.9, 133.3, 130.2,130.1 (q, J_{CF} = 33.0 Hz) 124.7 (q, J_{CF} = 271.6 Hz), 118.3, 54.6, 46.1

^{19}F NMR (470 MHz, $CDCl_3$) δ_F -63.4;

IR ν_{max} (neat) 3327, 2971, 1748, 1715, 1672, 1343, 1118 cm^{-1}

MP 167– 170 ˚C

HRMS (ESI, +ve) *m/z* calcd. for $C_{13}H_{11}F_3N_3O_2$, 298.0803. Found: 298.0821 $(M+H)^+$.

3387, 3330, 2905, 2809, 1735, 1717, 1609, 1343, 1235

General procedure for flavin mediated sulfoximine formation from sulfides with ammonium carbamate (general procedure D)

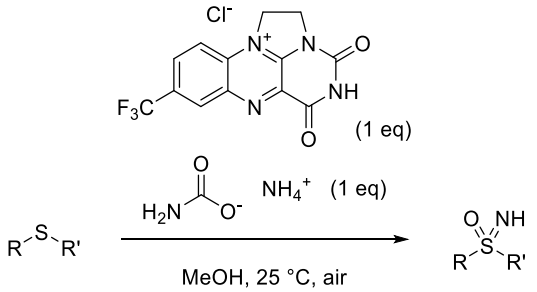

Sulfide (0.5 mmol) was dissolved in MeOH (10 mL), which was followed by the addition of ammonium carbamate (39 mg, 0.5 mmol) and finally the addition of CF_3 flavin (172 mg, 0.5 mmol). The reaction was stirred under air for 1 hour at which point the reaction mixture was filtered through a plug of silica, washed with ethyl acetate (30 mL) and the solvent mixture was then removed *in vacuo.*

S-Methyl-S-phenylsulfoximine 190A

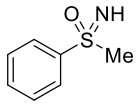

Methyl phenyl sulfide (232 µL, 2 mmol) was dissolved in MeOH (40 mL), which was followed by the addition of ammonium carbamate (156 mg, 2 mmol) and finally the addition of CF_3 flavin (688 mg, 0.5 mmol). The reaction was stirred under air for 1 hour at which point the reaction mixture was diluted in H_2O (20 mL) and the organics extracted with EtOAC (3 x 60). The organic layers were then combined, and washed with brine (75 mL), dried with $MgSO_4$ and the solvent removed *in* vacuo. The reaction mixture was additionally purified using column chromatography, petroleum ether/EtOAc 0 – 100%. S-Methyl-S-phenylsulfoximine was isolated as a pale-yellow oil (94 mg, 30%).

^{1}H NMR (400 MHz, $CDCl_3$) δ_H 8.06 (d, J = 8 Hz, 2H), 7.60 (m, 3H), 3.10 (s, 3H), 2.70 (br s, 1H),

^{13}C NMR (100 MHz, $CDCl_3$) δ_C 143.7, 133.5, 129.7, 128.0, 46.5

IR ν_{max} (neat) 3269, 1645, 1445, 1221, 1099 cm^{-1}

HRMS (ESI, +ve) *m/z* calcd. for $C_7H_{10}NOS$ 156.0483; found 156.0467 $(M+H)^+$. Data in accordance with literature.[299]

S-phenyl-S-2-propenyl-sulfoximine 190B

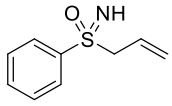

Following general procedure D using (2-propen-1-ylthio)benzene (73 μL, 0.5 mmol), sulfoximine was detected by mass spectrometry from the crude reaction mixture. The pure sulfoximine could not be isolated.

HRMS (ESI, +ve) *m/z* calcd. for $C_9H_{12}NOS$ 182.0640; found 182.0641 Data in accordance with literature.[107]

S-(4-Bromophenyl)-S-methylsulfoximine 190C

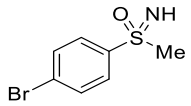

Following general procedure D using 4-(methylthio)bromobenzene (102 μL, 0.5 mmol), sulfoximine was detected by mass spectrometry from the crude reaction mixture. The pure sulfoximine could not be isolated.

HRMS (ESI, +ve) *m/z* calcd. for C_7H_9BrNOS 233.9588; found 233.9569 $(M+H)^+$. Data in accordance with literature.[300]

S,S-Diphenylsulfoximine 190D

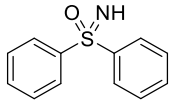

Following general procedure DE using diphenyl sulfid (84 μL, 0.5 mmol), sulfoximine was detected by mass spectrometry from the crude reaction mixture. The pure sulfoximine could not be isolated.

HRMS (ESI, +ve) *m/z* calcd. for $C_{12}H_{12}NOS$ 218.0640; found 218.0647 $(M+H)^+$. Data in accordance with literature.[80]

S-(4-Methoxyphenyl)-S-methylsulfoximine 190E

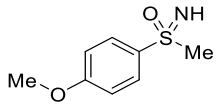

Following general procedure D using methyoxy phenyl sulfide (69 μL, 0.5 mmol), sulfoximine was detected by mass spectrometry from the crude reaction mixture. The pure sulfoximine could not be isolated.

HRMS (ESI, +ve) *m/z* calcd. for $C_8H_{12}NO_2S$ 186.0589; found 186.0594 $(M+H)^+$. Data in accordance with literature.[80]

4-(methyl sulfoximine)benzaldehyde 190F

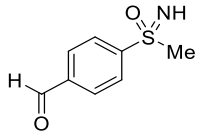

Following general procedure D using 4-(methylthio)-benzaldehyde (67 μL, 0.5 mmol), sulfoximine was detected by mass spectrometry from the crude reaction mixture. The pure sulfoximine could not be isolated.

HRMS (ESI, +ve) *m/z* calcd. for $C_8H_{10}NO2S$ 184.0432; found 184.0432 $(M+H)^+$. Data in accordance with literature.[107]

S-Methyl-S-(4-methylphenyl)-sulfoximine 190G

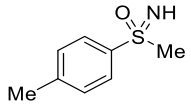

Following general procedure D using 4-(methylthio)toluene (68 μL, 0.5 mmol), sulfoximine was detected by mass spectrometry from the crude reaction mixture. The pure sulfoximine could not be isolated.

HRMS (ESI, +ve) *m/z* calcd. for $C_8H_{12}NOS$ 170.0639; found 170.0630 $(M+H)^+$. Data in accordance with literature.[107]

S,S-Dibutylsulfoxime 190H

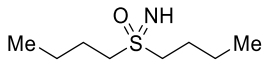

Following general procedure D using butyl sulfide (87 μL, 0.5 mmol), sulfoximine was detected by mass spectrometry from the crude reaction mixture. The pure sulfoximine could not be isolated.

HRMS (ESI, +ve) *m/z* calcd. for $C_8H_{20}NOS$ 178.1266; found 178.1269 $(M+H)^+$.

Allyl sulfoximine 190I

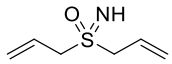

Following general procedure E using 3-prop-2-enylsulfanylprop-1-ene (64 μL, 0.5 mmol), sulfoximine was detected by mass spectrometry from the crude reaction mixture. The pure sulfoximine could not be isolated.

HRMS (ESI, +ve) *m/z* calcd. for C6H12NOS 146.0640; found 146.0637 $(M+H)^+$.

3-(Methylsulfinyl)-1-propanol 190J

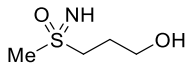

Following general procedure D using 3-(methylthio)-1-propanol (52 μL, 0.5 mmol), sulfoximine was detected by mass spectrometry from the crude reaction mixture. The pure sulfoximine could not be isolated.

HRMS (ESI, +ve) *m/z* calcd. for $C_4H_{12}NO_2S$ 138.0588; found 138.0589 $(M+H)^+$.

8.3 Factorial Experiment Design Conditions

Table 29 Conditions required by MODDE to construct a mathematical model

Run #	Exp #	Run Order	[Sulfide] (M)	[Hydroxylamine] (M)	[Flavin] (M)	Temperature (°C)	Water content (% v/v)
1	1	5	0.6	1.6	0.04	40	15
2	2	11	0.8	0.9	0.04	40	10
1	3	3	0.8	1.6	0.028	20	10
2	4	14	0.8	1.6	0.016	30	15
2	5	13	0.8	0.2	0.016	40	12.5
1	6	6	0.8	0.2	0.04	20	15
2	7	10	0.6	0.2	0.016	20	10
1	8	1	0.4	0.9	0.016	20	15
2	9	9	0.4	0.2	0.028	40	15
1	10	4	0.4	0.2	0.04	30	10
2	11	8	0.4	1.6	0.04	20	12.5
1	12	7	0.4	1.6	0.016	40	10
1	13	2	0.6	0.9	0.028	30	12.5
2	14	15	0.6	0.9	0.028	30	12.5
2	15	12	0.6	0.9	0.028	30	12.5

Table 30 Responses from design of experiment

Exp No	Induction time (min)	Max rate (mM/min)	Conversion 24 h (%)	Eventual conversion (%)	Time to completion (min)
1	60	0.04	4.5	4.5	300
2	800	0.13	10	10	24
3	200	0.24	35	35	1680
4	100	0.45	43	47	1680
5	0	0.3	9	9	420
6	100	0.11	13	14	1680
7	200	0.06	10	12	1680
8	100	0.11	36	42	1680
9	0	0.26	19	19	420
10	0	0.28	24	24	540
11	100	0.34	98	100	1560
12	200	0.13	25	28	1560
13	100	0.61	56	56	720
14	0	0.2	50	50	1000
15	0	0.38	53	53	900

8.4 Computational methods

Until the turn the 20th century, when Max Plank developed a radical proposal that would form the foundation of quantum mechanics, all models were based on classical physics; that is to say, they could not differentiate between the macroscopic and microscopic. Max Plank proposed, as a solution to the black body problem, that light should be treated as discrete packages of information, and not as analogues.

The black body problem describes a discrepancy between experiment and classical theory on the microscopic scale. A hypothetical piece of material that absorbs energy from its surroundings, and perfectly radiates the equivalent energy (as light) according to its temperature. This material lacks the ability to reflect any energy from its surroundings. A black body is a hypothetical perfect absorber and radiator of energy, which at the time of classical physics, were defined by Rayleigh-Jean's law and Wien's approximation. The creation of a blackbody equivalent led to the discovery that Rayleigh-Jean's law was able to describe experimental results at large wavelengths, however, there was a significant

discrepancy between the experimental and predicted results at short wavelengths. Conversely, Wein's approximation was able to describe thermal emission accurately at short wavelengths but could not match experimental at long wavelengths.

Max Planks proposal was that black body radiation was limited to certain specific values, and not all values as previously thought, i.e., it was quantized. This quantisation was responsible in reconciling the differences between observation and prediction at the microscopic level, which could not be explained by classical method. It became clear that quantisation was not just a characteristic of light, but also of fundamental particles of matter. In atoms, this results in discrete energy levels of electrons; observable in the form of UV and visible light line spectra.

This discovery regarding the quantisation of particles led to Louis de Broglie's theory of matter waves, stating that particles can exhibit wave characteristics and waves can exhibit particle characteristics. This was further expanded on by Erwin Schrödinger with his invention of wave mechanics, which introduced the Schrödinger equation.

The Schrödinger equation

According to quantum mechanics, all sub-atomic particles display wave-like properties. The behaviour of these particles can be described by a corresponding de Broglie wave. This wave is known as the wavefunction ψ defines all physical properties of a system. Any quantum system can be described by the Schrödinger equation (Equation 2).

$$H\,\psi = E\,\psi$$

Equation 2

Where H is the Hamiltonian operator, ψ is the wavefunction (the eigenfunction for a given Hamiltonian) and E is the system energy. The wavefunction ψ contains all the information it is possible to know about the particle, takes as variables the positions of electrons, neutrons and protons. Expansion of the wavefunction leads to the following Schrödinger equation (Equation 3).

$$H\,\psi_i(\vec{x_1}, \dots, \vec{x_N}, \vec{R_1}, \dots, \vec{R_1}, \dots, \vec{R_M}) = E\,\psi_i(\vec{x_1}, \dots, \vec{x_N}, \vec{R_1}, \dots, \vec{R_1}, \dots, \vec{R_M})$$

Equation 3

Where $\vec{x_N}$ describes the positions of the Nth electron, and $\vec{R_M}$ describes the position of the Mth nucleus (protons and neutrons). In order to solve the Schrödinger equation, it is necessary to define the Hamiltonian operator.

The Hamiltonian Operator

The Hamiltonian operator encompasses two components, kinetic energy and potential energy of a system (e.g. a molecule). The kinetic and potential components can be further separated into the kinetic energies of the nuclei and the kinetic energies of the electrons.

$$H = T_e + T_n + V_{ne} + V_{ee} + V_{nn}$$

Equation 4

Where T_e and T_n are kinetic energy components for the electrons and nuclei respectively; V_{ne} is the attractive potential between electrons and nuclei, and V_{ee} and V_{nn} represent the inter-electronic and inter-nuclear repulsion potentials. Developing the notation of each term generates the following form of the Hamiltonian operator.

$$H = -\sum_i \frac{\hbar^2}{2m_e}\nabla_i^2 - \sum_k \frac{\hbar^2}{2m_k}\nabla_k^2 - \sum_i \sum_k \frac{e^2 Z_k}{r_{ik}} + \sum_{i<j} \frac{e^2}{r_{ij}} + \sum_{k<l} \frac{e^2 Z_k Z_l}{r_{kl}}$$

Equation 5

Where i and j are indices identifying individual electrons, running up to the total number of electrons, k and l are indices identifying individual nuclei, running up to the total number of nuclei. $\hbar$ is Planck's constant divided by 2π, m_e is the mass of the electron, m_k is the mass of the nucleus k, $\nabla^2$is the laplacian operator, e is the charge on the electron, Z is atomic number, and r_{ab} is the distance between particles a and b.

It is now easier to observe how the Hamilton operator is split into kinetic and potential energy terms. The first two terms of the Hamiltonian operator contribute the kinetic energy terms (Equation 6);

$$H = -\sum_i \frac{\hbar^2}{2m_e}\nabla_i^2 - \sum_k \frac{\hbar^2}{2m_k}\nabla_k^2 + potential\ energy\ terms$$

Equation 6

And the last 3 terms contribute to the potential energy (Equation 7). These potential energy terms are expressed exactly as they would be in quantum mechanics;

$$H = kinetic\ energy\ terms - \sum_i \sum_k \frac{e^2 Z_k}{r_{ik}} + \sum_{i<k} \frac{e^2}{r_{ij}} + \sum_{k<l} \frac{e^2 Z_k Z_l}{r_{kl}}$$

Equation 7

With knowledge of the component parts of the Schrödinger equation, the changes in the physical properties of a system over time can be described. By replacing the wavefunction

with electron density, the energy of a system can by described. This assumption forms the basis of density functional theory.

Density Functional Theory (DFT)

DFT is based on electron density ρ, and this information is readily available from X-ray diffraction experiments. For the energy of the system to be appropriately described, the electron density must be calculated with the correct Hamiltonian operator.

The Hohenberg Kohn Theorem

The foundations for modern DFT were laid out by Enrico Fermi and H. L. Thomas in 1927.[301] Subsequently, in the 1964 publication by Hohenberg and Kohn demonstrated that DFT can be exact in principle.[302] Their research proved that the interaction of ground state electron gas with an external potential can be defined as a unique functional of the electron density as long as a specific external potential is defined for a particular electron density and vice versa. Consequently, the external potential fixes H, which makes it a unique functional of electron density. This can be displayed mathematically.

$$\rho \Rightarrow \{N, Z, R\} \Rightarrow V_{ext} \Rightarrow H \Rightarrow \psi_0 \Rightarrow E_0$$

Equation 8

Where ρ is electron density, $\{N, Z, R\}$ are vectors, V_{ext} is the external potential applied to the system due to the presence of the nuclei. H is the appropriate Hamiltonian operator and ψ_0 and E_0 are the wavefunction and energy of the system in its ground state respectively. Subsequently, the Kohn Sham approach developed a model for how DFT can be performed in practice.

The Kohn Sham approach

The Hohenberg Kohn approach does not adequately deal with the orbital-free model, resulting in a poor representation of kinetic energy. This weakness was addressed by Kohn and Sham in 1965, who stated that observed problems are connected to the manner in which the kinetic energy is described. In order to resolve this problem, they introduced a theoretical system built from sets of orbitals (one electron functions) where the electrons contained are non-interacting. In this case, each electron is subjected to an average repulsion field,

generated by all other electrons in the system. The total energy was divided into component parts, electron nucleus interactions and electron electron interactions:

$$E[\rho] = T_s[\rho] + \int [\hat{V}_{ext}(r)\rho(r)dr + \int \hat{J}(r)\rho(r)dr$$

Equation 9

Where $T_s[\rho]$ is the electron kinetic energy of the hypothetical system, and ρ is equivalent to the non-interacting electrons in the real system. $\hat{J}(r)$ is the classical Coulomb interaction between electrons. $\hat{V}_{ext}$ has previously been defined as the external potential applied to the system due to the presence of the nuclei. $\hat{J}(r)$ and $\hat{V}_{ext}$ can be defined mathematically:

$$\hat{J}(r) = \int \frac{\rho(r')}{r' - r}\, dr'$$

Equation 10

$$\hat{V}_{ext} = \sum_A \frac{Z_A}{|\, R_A - r\,|}$$

Equation 11

r' and r represent the coordinate in space of the electron density that the electron is interacting with and the coordinate of the electron in the orbital respectively. This allows the effect of the electron cloud upon the individual electron to be calculated. The kinetic energy can be expressed in terms of orbitals as:

$$T_S[\rho] = -\frac{1}{2}\sum_{i=1}^{N} < \varphi_i \,|\, \nabla^2 \,|\varphi_i >$$

Equation 12

Finally, φ_i are the 1 electron orbitals and E_{XC} is a term that accounts all the other contributions to the energy which are not already accounted for. These include electron exchange, correlation energy and correction for the self-interaction included in the Coulomb term. It also includes the portion of the kinetic energy which corresponds to the differences between the non-interacting and the real system. As this term is unknown, an approximation must be made in order to calculate the energy of the system. There are a number of approximations that can be used to model the $E_{XC}[\rho]$ functional.

Exchange and correlation functionals

Non-classical contributions to the potential energy are contained in the $E_{XC}[\rho]$ functional. The contributions are due to electron-electron interaction and the differences in the kinetic

energy of the real and theoretical systems. Several functionals can be used to approximate this exchange-correlation; Local density approximation, generalised gradient approximation and hybrid functionals are functionals that have been demonstrated to accurately account for the non-classical potential energy contributions.

Local Density Approximation (LDA)

The LDA takes the electronic density of a uniform electron gas and is the most basic exchange correlation functional. The uniform electron gas gives a constant value for electronic density which is not reflective of the rapid variation of electron densities in a normal system.

$$\rho = \frac{N}{V}$$

Equation 13

Where ρ is electron density, N is the total number of electrons in a system and V is the gas volume. Although LDA provides only a rough approximation, the form of the exchange and correlation energy functionals are known to a very high degree of accuracy. The use of LDA reliable gives accurate results for the prediction of molecular properties such as structure, vibrational frequency and charge moment. However, flaws in the technique are observed regarding bond energies and energy barriers in a chemical reaction, consequently, LDA should be avoided for energetic calculations. For open-shell systems, the electronic density ρ can be replaced with spin electron densities ρ_α and ρ_β where:

$$\rho = \rho_\alpha + \rho_\beta$$

Equation 14

This alteration is known as local spin-density approximation: LSDA. Nusair *et* al. developed a LDSA functional based on high-level quantum Monte Carlo calculations for uniform electron gases.[303] They were able to produce a correlation energy for spin-polarized homogenous electron gas, allowing them to reliable determine the magnitude of non-local corrections to the local spin density approximation.

Generalised Gradient Approximation (GGA)

As LDA gives a constant value of electron density, which we know to be not the case, a new type of functional was needed that was more representative: The generalised gradient approximation. The GGA functional accounts for the gradient of electron density $\nabla\rho$. The use of an electron density gradient allows for a truer representation of the non-homogenous

nature of electron density in a system. The GGA can be divided into exchange and correlation terms, allowing them to be solved individually:

$$E_{XC}^{GGA} = E_{X}^{GGA} + E_{C}^{GGA}$$

Equation 15

There are numerous examples of commonly used GGA functionals used in computational chemistry:

B[245]

Beck *et* al. developed an exchange functional that provides a gradient correction to the LSDA exchange energy. It includes a parameter fitted on known data from rare gas atoms.

P86[198]

Perdew *et* al. developed a correlation functional that provides a gradient correction to LSDA which includes an empirical parameter fitted for an atom of neon.

PW91[304,305]

PW91 is a modification of P86 which was developed by Burke *et* al. and is an exchange-correlation functional.

B95[306]

Beck *et al*. also developed a correlation factor that does not contain any empirical parameters. B95 treats the self-interaction error inherent in the real and theoretical electron interactions better.

PBE[307]

PBE is an exchange-correlation functional devolped by Perdew, Burke and Ernzerhof

LYP[246]

Lee, Yang and Parr developed a correlation functional that is extensively used with the GGA. The LYP functional contains 4 empirical parameters fitted to the helium atom.

GGA Hybrid Functionals

The functionals covered thus far are somewhat inadequate as they all poorly represent the exchange problem of electronic self-interaction (although this is somewhat dealt with by B95). There exists a method of computation whereby the exchange part is defined exactly: The Hartree-Fock (HF) method. However, combination of HF and DFT results in poorer results than GGA in DFT. To avoid this apparent compounding of errors from the combination of two approaches, the correlation and exchange parts of each computational method were combined so a functional that presents an improvement on GGA could be

obtained. Through a combination of HF, GGA and LSDA functionals, the exact exchange and correlation parts of the hybrid functional can be described. The main elements of this hybrid functional are often generated from the generalised gradient approximation, leading to GGA hybrid functionals.

There are several GGA hybrid functional that have been developed and are commonly used computationally;

B3[306]

B3 was developed by Becke and contains a combination of LSDA and GGA functional. It contains exact exchange information.

PBE0[308]

Barone and Adamo developed PBE0 (alternatively known as PBE1PBE) and is a combination of the PBE GGA exchange functional and the HF exchange functional. However, the contributions from GGA and HF are not equivalent, resulting in an improvement over GGA.

The exchange-correlation term is described by a combination of exchange and correlation functionals, in order to obtain hybrid functionals such as: B1B95, B1LYP or B3P86.

DFT is a method to calculate the energy of 1 e orbitals in a system, however, these orbitals must first be chosen. This is achieved through selection of the appropriate basis set.

Basis Sets

Atomic orbitals (or molecular orbitals) are created by basis functionals. Basis functionals are composed of a linear combination of functions, each of which contain a number of coefficients that are to be determined. There are two main types of basis set; Localised and plane wave basis sets. The most commonly used basis sets are Slater-type orbitals, and Gaussian-type orbitals.

Slater-type orbitals

Slater-type orbitals (STOs) have the exponential dependence: $e^{-\zeta r}$, where ζ is the constant relating to the effective charge of the nucleus and r is the distance of the electron from the atomic nucleus.

$$\eta^{STO} = N\, r^{n-1}\, e^{-\zeta r}\, Y_{lm}\,(\theta, \phi)$$

Equation 16

Where ζ and r are unchanged, N is a normalisation factor, Θ and ϕ are spherical coordinates, Y_{lm} is the angular momentum (describing the effective shape), and n, l and m are principal, angular momentum and magnetic classical quantum numbers respectively.

STOs accurately describe the behaviour of hydrogen atomic orbitals as it features a cusp at $r = 0$ and good exponential decay for increased values of r. However, the product of two STOs centred on two different atoms is a four centre-two electron integral, which are very time consuming to calculate and are thus difficult to deal with. Consequently, it is often favourable to use Gaussian-type orbitals instead.

Gaussian-type orbitals

Gaussian-type orbitals (GTOs) have the exponential dependence $e^{-\alpha r^2}$, making the mathematical expression of real AOs;

$$\eta^{GTO} = N\, x^l\, y^m z^n\, e^{-\alpha r^2}$$

Equation 17

Where N remains a normalisation factor and x, y and z are Cartesian coordinates.

GTOs, in contrast to STOs, do not show a cusp at $r = 0$ and decrease rapidly for large values of r making them less favourable for describing the behaviour of hydrogen atomic orbitals. However, GTOs are often a better basis set as the product of two GTOs on two different atoms is a third atom, located between the two original atoms, avoiding the computationally complex, four-centre-two electron integrals. GTOs are so favourable, that several GTOs can be combined to approximate an STO, which is more efficient than using an STO itself.

The degree of precision (and computational complexity) of a basis set is definded by the number of contracted functions (CGF) used to represent each atomic orbital.For example, the STO-3G basis set is formed by a linear combination of three CGF functions, with the G indicating a combination of contracted Gaussian functions, combining to resemble an STO. Increased precision can be obtained through the use of two or more functions to describe each type of orbital. Double and trible-zeta basis sets are often chosen as a compromise between good precision and computational complexity.

The most important electrons are the ones that are affected by a chemical reaction, i.e. the valence electrons, and consequently, it is important to have a flexible description of these electrons. Certain basis sets treat the core and valence orbitals differently, and these are

called split valence basis sets. The most common example of a split valence basis set is the 6-31G basis set, which uses the nomenclature:

X-YZG

Where X represents the number of primitive GTOs used to describe a single contracted Gaussian function of the core, and Y and Z represent the number of primitive GTOs describing valence orbitals. Further primitive GTOs can be added for increased precision. In the case of 6-31G, it is composed of two functions, containing three and one primitive GTOs respectively.

Bonding between atoms induces polarisation, a deformation of the electronic cloud around each atom. Additions can be made to the basis sets to allow for polarisation and/or diffuse functions. In order to allow for polarisation/diffusion, functions with higher angular momentum are added to the basis set. That is to say the addition of a p function to H allows for polarisation. This is the same process as the addition of a d-function to a basis set containing p-valence orbitals, or the addition of f-functions to d-valence orbitals. For more precise results, both polarisation and diffusion functions can be included, transforming our original 6-31G basis set to 6-31G(pd). The diffuse functions describe the part of the orbital that is most distant from the nuclei, and these can have a significant role when describing the behaviour of anions or diffuse electronic clouds of second or third row transition metals. They can also be represented by alternative nomenclature: 6-31+G. Where + represents the inclusion of a diffuse function.

The alternative type of basis set to localised (STO and GTO) is plane wave, which has advantages of decreased computational complexity.

Plane Waves

Plane waves form the basis set used for the majority of calculations on periodic systems. This is due in part to the representation being equivalent to a Fourier series. That is to say that plane waves can represent a function as the sum of simple sine waves. Each orbital wavefunction is expressed as a combination of plane waves, differing by reciprocal lattice vectors.

$$\psi_i^k(r) = \sum_G a_{i,k+G} \exp(i(k+G)\cdot r)$$

Equation 18

This approximation can be inserted into the Kohn-Sham equation for DFT, which leads to the expansion of that equation;

$$\sum_{G'}\{\frac{\hbar^2}{2m}|k+G|\delta_{GG'}+V_{ion}(G-G')+V_{elec}(G-G')+V_{XC}(G-G')\}a_{i,K+G'}=\varepsilon_i a_{i,k+G'}$$

Equation 19

Where $\delta_{GG'}$ is 1, except when $G-G'\neq 0$, when $\delta_{GG'}$ is 1. V_{ion}, V_{elec} and V_{XC} represent the electron-nuclei, electron-electron and exchange correlation functionals. In practice this approach results in two problems in a macroscopic lattice;

- The sum of G' is in principle a Fourier series over an infinite number of reciprocal lattice vectors
- In a macroscopic there are an infinite number of k points within the first Brillouin zone.

There are practical solutions to both of these however. As the valence electrons are largely responsible for the physical bonding and chemical properties, it is common to consider only the valence electrons and bundle an approximation for the core electrons with the nuclear core. The core electrons remain unaffected by the atomic environment. When representing valence electrons as a plane wave basis set, we must take into account for the fact that as we near the atomic nuclei, the wavefunctions in question show increasingly rapid oscillations. This is due to the fact that the wavefunction must be orthogonal to those of the core electrons. The rapid oscillations result in a large kinetic energy, and a significant number of plane waves would be required to properly model this behaviour. In real terms this would mean accounting for a large number of terms in the plane wave expansion of the orbital [ref - $\psi_i^k(r)=\sum_G a_{i,k+G}\exp(i(k+G)\cdot r)$]. Further-more, solid systems often contain heavy elements which have a higher number of core electrons, compounding these oscillations. Fortunately, in the inner region, the high kinetic energy is cancelled out by the high electrostatic potential energy of interaction with the nucleus.

One method of dealing with this problem is to approximate the true potential with a pseudopotential. This can account for the interaction of the valence electrons with the combined core electrons and nucleus. The pseudopotential is a potential function with wavefunctions of the same size and shape of the true wavefunction outside the core region, but with fewer nodes inside the core. This allows for the number of terms to be reduced, which drastically reduces the computational complexity of the problem.

Pseudopotentials can be generated from all-electron atomic calculations, which are relatively simple. The valence pseudopotential is then required to reproduce the properties and behaviour of the valence electrons in the full calculation. The pseudopotential is dependant on orbital angular momentum of the wavefunction of the s, p, d, orbitals, and the total valence electron density within the core radius should be equal to that in the all electron environment. These pseudopotentials are termed 'non-local norm-conserving'. Additionally, relativistic effects can be included in pseudopotentials which are often present when modelling heavy metals.

Pseudopotentials exist in a number of functional forms. Once the functional form has been selected, the parameters can be varied as desired. Each functional form requires a differing number of plane waves for their representation, which decides the degree to which they can be applied to varying atomic environments. 'Soft' pseudopotentials require fewer plane waves, which are computationally desirable, however, this can lead to transferability issues. The desire for computational simplicity led to the development of 'ultrasoft' or 'supersoft' pseudopotentials, which require fewer plane waves still.

Calculation of infinite plane waves is avoided in practice through the implementation of a kinetic energy cutoff, whereby any plane waves with a kinetic energy that falls below this level are discounted. The cutoff level can used depends on the system being investigated. Elements in the first-row approach closer to the nucleus than elements further down a period. Therefore, an element with 2p valence electrons, such carbon, would have a higher cutoff than it's equivalent 3p element, sulfur in this case. Consequently, it can be said that sulfur can use a softer pseudopotential. In practice this means more plane waves are needed in the case of carbon (i.e. more reciprocal lattice vectors). The basis function is not associated with specific atoms in the plane wave expansion but are defined over the whole cell. The coefficients $a_{i,K+G}$ are obtained by making an initial estimate of the electron density variation $\rho(r)$, and Kohn-Sham and overlap matrices are constructed. Diagonalisation can then generate eigenfunctions and eigen vectors from which the Kohn-Sham orbitals can be constructed, allowing the density for the next iteration to be obtained.

The second principle that must be considered when calculating the band structure of a material is that the calculation must be performed for all k vectors in the Brillouin zone. This leads to the assumption that for a macroscopic solid, an infinite number of vectors, k, would be required to generate the band structure. However, it is possible to sample the Brillouin

zone at discrete points. This practice is made possible because the wavefunctions are almost identical when they are close together in k space, and consequently can be represented by a single sampling point. A weighting factor is then applied to each single discrete value, relating to the volume of space it represents. A denser the set of k vectors, leads to smaller error, but increased computational complexity.

There are various methods for selecting suitable sets of k vectors, which can result in accurate approximations for properties such as charge density. Monkhorst and Pack developed a popular method in 1976. The size and shape of the system can also influence the selection of k vectors. If a unit cell is large, then it may be possible to sample a single vector. However, it is typical to sample between 10 and 100 vectors for any given system, in order to understand the structural and electronic properties of a solid. Certain properties require a greater vector density, for example, the calculation of optical properties of a metal could require up to a 1000 fold increase in k vectors. Ideally, the calculation should converge in terms of the number of wave vectors, k, considered, and in terms of the reciprocal lattice vectors, G.

Finally, the symmetry of the Brillouin zone may sometimes need to be considered. In some instances, the symmetry of the Brillouin zone can result in a sample being taken from a small section of the zone, rather than over the whole zone. This is a consequence of point symmetry of the Brillouin zone, rather than a consequence of the overall transitional symmetry of the lattice matrix. The sampling of the smallest possible section can be referred to as the irreducible part of the Brillouin zone.

Crystal data for sodium azide induced flavin decomposition in TFE

Table 1. Crystal data and structure refinement for new.

Identification code	e15drc1new	
Empirical formula	C15 H10 F6 N4 O3	
Formula weight	408.27	
Temperature	100(2) K	
Wavelength	0.71073 Å	
Crystal system	orthorhombic	
Space group	P b c a	
Unit cell dimensions	a = 10.2098(3) Å	□= 90.0°.
	b = 13.5134(4) Å	□= 90.0°.
	c = 22.8684(7) Å	□ = 90.0°.
Volume	3155.13(16) $Å^3$	
Z	8	
Density (calculated)	1.719 Mg/m^3	
Absorption coefficient	0.168 mm^{-1}	
F(000)	1648	
Crystal size	0.3 x 0.2 x 0.2 mm^3	
Theta range for data collection	3.502 to 26.632°.	
Index ranges	-12<=h<=11, -16<=k<=15, -19<=l<=28	
Reflections collected	2846	
Independent reflections	2359 [R(int) = 0.026]	
Absorption correction	Semi-empirical from equivalents	
Refinement method	Full-matrix least-squares on F^2	
Data / restraints / parameters	2846/293/0	
Goodness-of-fit on F^2	1.02	
Final R indices [I>2sigma(I)]	R1 = 0.0344, wR2 = 0.0858	
R indices (all data)	R1 = 0.0451	

Bibliography

(1) Johansson, L. B. A.; Davidsson, A.; Lindblom, G.; Naqvi, K. R. Electronic Transitions in the Isoalloxazine Ring and Orientation of Flavins in Model Membranes Studied by Polarized Light Spectroscopy. *Biochemistry (Mosc.)* **1979**, *18* (19), 4249–4253.

(2) Mattevi, A. To Be or Not to Be an Oxidase: Challenging the Oxygen Reactivity of Flavoenzymes. *Trends Biochem. Sci.* **2006**, *31* (5), 276–283.

(3) Blyth, A. W. LVI.—The Composition of Cows' Milk in Health and Disease. *J. Chem. Soc., Trans.* **1879**, *35* (0), 530–539.

(4) Karrer, P.; Schöpp, K.; Benz, F. Synthesen von Flavinen IV. *Helv. Chim. Acta* **1935**, *18* (1), 426–429.

(5) Warburg, O. The Chemical Constitution of Respiration Ferment. *Science* **1928**, *68* (1767), 437–443.

(6) Theorell, H. Purification of the Active Group of the Yellow Enzyme. *Biochem Z* **1935**, No. 344, 275.

(7) Krebs, H. A. Metabolism of Amino-Acids. *Biochem. J.* **1935**, *29* (7), 1620–1644.

(8) Christian, W.; Warburg, O. Isolation of the Prosthetic Group of the D-Amino Acid Oxidase. *Biochem. Z.* **1938**, *298*, 150–168.

(9) Alfieri, A.; Malito, E.; Orru, R.; Fraaije, M. W.; Mattevi, A. Revealing the Moonlighting Role of NADP in the Structure of a Flavin-Containing Monooxygenase. *Proc. Natl. Acad. Sci.* **2008**, *105* (18), 6572–6577.

(10) Gutierrez, A.; Lian, L.-Y.; Wolf, C. R.; Scrutton, N. S.; Roberts, G. C. K. Stopped-Flow Kinetic Studies of Flavin Reduction in Human Cytochrome P450 Reductase and Its Component Domains. *Biochemistry (Mosc.)* **2001**, *40* (7), 1964–1975.

(11) Rutter, J.; Winge, D. R.; Schiffman, J. D. Succinate Dehydrogenase—Assembly, Regulation and Role in Human Disease. *Mitochondrion* **2010**, *10* (4), 393–401.

(12) Harrison, R. Structure and Function of Xanthine Oxidoreductase: Where Are We Now? *Free Radic. Biol. Med.* **2002**, *33* (6), 774–797.

(13) Murty, C. V.; Adiga, P. R. Pregnancy Suppression by Active Immunization against Gestation-Specific Riboflavin Carrier Protein. *Science* **1982**, *216* (4542), 191–193.

(14) Riboflavin-Binding Proteins. *Annu. Rev. Nutr.* **1988**, *8* (1), 279–299.

(15) Susin, S. A.; Lorenzo, H. K.; Zamzami, N.; Marzo, I.; Snow, B. E.; Brothers, G. M.; Mangion, J.; Jacotot, E.; Costantini, P.; Loeffler, M.; et al. Molecular Characterization of Mitochondrial Apoptosis-Inducing Factor. *Nature* **1999**, *397* (6718), 441–446.

(16) Lessons From Biodegradation. *Annu. Rev. Microbiol.* **1987**, *41* (1), 1–24.

(17) De la Rosa, M. A.; Roncel, M.; Navarro, J. A. Flavin-Mediated Photoregulation of Nitrate Reductase: A Key Point of Control in Inorganic Nitrogen Photosynthetic Metabolism. *Bioelectrochem. Bioenerg.* **1989**, *22* (3), 355–364.

(18) Jorns, M. S.; Wang, B.; Jordan, S. DNA Repair Catalyzed by Escherichia Coli DNA Photolyase Containing Only Reduced Flavin: Elimination of the Enzyme's Second Chromophore by Reduction with Sodium Borohydride. *Biochemistry (Mosc.)* **1987**, *26* (21), 6810–6816.

(19) Fischer, M.; Bacher, A. Biosynthesis of Riboflavin. *EcoSal Plus* **2010**, *4* (1).

(20) Müller, F. Spectroscopy and Photochemistry of Flavins and Flavoproteins. *Photochem. Photobiol.* **1981**, *34* (6), 753–759.

(21) Poudel, P. P.; Arimitsu, K.; Yamamoto, K. Self-Assembled Ion-Pair Organocatalysis – Asymmetric Baeyer–Villiger Oxidation Mediated by Flavinium–cinchona Alkaloid Dimer. *Chem. Commun.* **2016**, *52* (22), 4163–4166.
(22) Valton, J.; Fontecave, M.; Douki, T.; Kendrew, S. G.; Nivière, V. An Aromatic Hydroxylation Reaction Catalyzed by a Two-Component FMN-Dependent Monooxygenase THE ActVA-ActVB SYSTEM FROM STREPTOMYCES COELICOLOR. *J. Biol. Chem.* **2006**, *281* (1), 27–35.
(23) Binda, C.; Newton-Vinson, P.; Hubálek, F.; Edmondson, D. E.; Mattevi, A. Structure of Human Monoamine Oxidase B, a Drug Target for the Treatment of Neurological Disorders. *Nat. Struct. Mol. Biol.* **2002**, *9* (1), 22–26.
(24) Hajjar, N. P.; Hodgson, E. Flavin Adenine Dinucleotide--Dependent Monooxygenase: Its Role in the Sulfoxidation of Pesticides in Mammals. *Science* **1980**, *209* (4461), 1134–1136.
(25) Nelson, D. L.; Cox, M. M. *Lehninger Principles of Biochemistry*, Fifth.; W.H. Freeman and Company, 2008.
(26) Smith, J. R. L.; Jerina, D. M.; Kaufman, S.; Milstein, S. Aromatic Hydroxylation Mediated by Flavin Autoxidation: Lack of the NIH Shift. *J. Chem. Soc., Chem. Commun.* **1975**, No. 21, 881–882.
(27) Fagan, R. L.; Palfey, B. A. 7.03 - Flavin-Dependent Enzymes. In *Comprehensive Natural Products II*; Elsevier: Oxford, 2010; pp 37–113.
(28) *Lehninger's Principles Of Biochemistry 5e*.
(29) Kemal, C.; Chan, T. W.; Bruice, T. C. Reaction of 3O2 with Dihydroflavins. 1. N3,5-Dimethyl-1,5-Dihydrolumiflavin and 1,5-Dihydroisoalloxazines. *J. Am. Chem. Soc.* **1977**, *99* (22), 7272–7286.
(30) Thomson, C. W. (Charles W. *The Voyage of the "Challenger" : The Atlantic : A Preliminary Account of the General Results of the Exploring Voyage of H.M.S. "Challenger" during the Year 1873 and the Early Part of the Year 1876*; New York : Harper, 1878.
(31) Macheroux, P.; Ghisla, S.; Hastings, J. W. Spectral Detection of an Intermediate Preceding the Excited State in the Bacterial Luciferase Reaction. *Biochemistry (Mosc.)* **1993**, *32* (51), 14183–14186.
(32) Baldwin, T. O.; Christopher, J. A.; Raushel, F. M.; Sinclair, J. F.; Ziegler, M. M.; Fisher, A. J.; Rayment, I. Structure of Bacterial Luciferase. *Curr. Opin. Struct. Biol.* **1995**, *5* (6), 798–809.
(33) Sheng, D.; Ballou, D. P.; Massey, V. Mechanistic Studies of Cyclohexanone Monooxygenase: Chemical Properties of Intermediates Involved in Catalysis. *Biochemistry (Mosc.)* **2001**, *40* (37), 11156–11167.
(34) Entsch, B.; Ballou, D. P.; Massey, V. Flavin-Oxygen Derivatives Involved in Hydroxylation by P-Hydroxybenzoate Hydroxylase. *J. Biol. Chem.* **1976**, *251* (9), 2550–2563.
(35) Entsch, B.; Berkel, W. J. van. Structure and Mechanism of Para-Hydroxybenzoate Hydroxylase. *FASEB J.* **1995**, *9* (7), 476–483.
(36) Hastings, J. W.; Balny, C.; Peuch, C. L.; Douzou, P. Spectral Properties of an Oxygenated Luciferase—Flavin Intermediate Isolated by Low-Temperature Chromatography. *Proc. Natl. Acad. Sci.* **1973**, *70* (12), 3468–3472.
(37) Thorpe, C.; Kim, J. J. Structure and Mechanism of Action of the Acyl-CoA Dehydrogenases. *FASEB J.* **1995**, *9* (9), 718–725.
(38) Kemal, C.; Bruice, T. C. Simple Synthesis of a 4a-Hydroperoxy Adduct of a 1,5-Dihydroflavine: Preliminary Studies of a Model for Bacterial Luciferase. *Proc. Natl. Acad. Sci.* **1976**, *73* (4), 995–999.

(39) Bruice, T. C.; Noar, J. B.; Ball, S. S.; Venkataram, U. V. Monooxygen Donation Potential of 4a-Hydroperoxyflavins as Compared with Those of a Percarboxylic Acid and Other Hydroperoxides. Monooxygen Donation to Olefin, Tertiary Amine, Alkyl Sulfide, and Iodide Ion. *J. Am. Chem. Soc.* **1983**, *105* (8), 2452–2463.
(40) Oae, S.; Ogawa Asada, K.; Yoshimura, T.; Fujimori, K. Oxidation of Amines with 4a-FIEt-OOH: An Enzyme Model of FAD-Containing Monooxygenase. *Heterocycles* **1992**, *33* (1), 189.
(41) Murahashi, S.; Oda, T.; Masui, Y. Flavin-Catalyzed Oxidation of Amines and Sulfur Compounds with Hydrogen Peroxide. *J. Am. Chem. Soc.* **1989**, *111* (13), 5002–5003.
(42) Imada, Y.; Iida, H.; Ono, S.; Murahashi, S.-I. Flavin Catalyzed Oxidations of Sulfides and Amines with Molecular Oxygen. *J. Am. Chem. Soc.* **2003**, *125* (10), 2868–2869.
(43) Sánchez, M. A.; Mainar, A. M.; Pardo, J. I.; López, M. C.; Urieta, J. S. Solubility of Nonpolar Gases in 2,2,2-Trifluoroethanol and 1,1,1,3,3,3-Hexafluoropropan-2-Ol at Several Temperatures and 101.33 kPa Partial Pressure of Gas. *Can. J. Chem.* **2001**, *79* (10), 1460–1465.
(44) Marsh, B. J.; Carbery, D. R. Chemoselective Sulfide Oxidation Mediated by Bridged Flavinium Organocatalysts. *Tetrahedron Lett.* **2010**, *51* (17), 2362–2365.
(45) Žurek, J.; Cibulka, R.; Dvořáková, H.; Svoboda, J. N1,N10-Ethylene-Bridged Flavinium Salts Derived from L-Valinol: Synthesis and Catalytic Activity in H2O2 Oxidations. *Tetrahedron Lett.* **2010**, *51* (7), 1083–1086.
(46) Imada, Y.; Kitagawa, T.; Wang, H.-K.; Komiya, N.; Naota, T. Flavin-Catalyzed Aerobic Oxidation of Sulfides in Aqueous Media. *Tetrahedron Lett.* **2013**, *54* (7), 621–624.
(47) Laird, T. Safety Special Section Editorial. *Org. Process Res. Dev.* **2010**, *14* (6), 1479–1479.
(48) Murahashi, S.-I.; Zhang, D.; Iida, H.; Miyawaki, T.; Uenaka, M.; Murano, K.; Meguro, K. Flavin-Catalyzed Aerobic Oxidation of Sulfides and Thiols with Formic Acid/Triethylamine. *Chem. Commun.* **2014**, *50* (71), 10295–10298.
(49) Kotoučová, H.; Strnadová, I.; Kovandová, M.; Chudoba, J.; Dvořáková, H.; Cibulka, R. Biomimetic Aerobic Oxidative Hydroxylation of Arylboronic Acids to Phenols Catalysed by a Flavin Derivative. *Org. Biomol. Chem.* **2014**, *12* (13), 2137–2142.
(50) Imada, Y.; Iida, H.; Ono, S.; Masui, Y.; Murahashi, S.-I. Flavin-Catalyzed Oxidation of Amines and Sulfides with Molecular Oxygen: Biomimetic Green Oxidation. *Chem. – Asian J.* **2006**, *1* (1–2), 136–147.
(51) Kamerbeek, N. M.; Janssen, D. B.; van Berkel, W. J. H.; Fraaije, M. W. Baeyer–Villiger Monooxygenases, an Emerging Family of Flavin-Dependent Biocatalysts. *Adv. Synth. Catal.* **2003**, *345* (6–7), 667–678.
(52) Mazzini, C.; Lebreton, J.; Furstoss, R. Flavin-Catalyzed Baeyer−Villiger Reaction of Ketones: Oxidation of Cyclobutanones to γ Lactones Using Hydrogen Peroxide. *J. Org. Chem.* **1996**, *61* (1), 8–9.
(53) Nanni, E. J.; Sawyer, D. T.; Ball, S. S.; Bruice, T. C. Redox Chemistry of N5-Ethyl-3-Methyllumiflavinium Cation and N5-Ethyl-4a-Hydroperoxy-3-Methyllumiflavin in Dimethylformamide. Evidence for the Formation of the N5-Ethyl-4a-Hydroperoxy-3-Methyllumiflavin Anion via Radical-Radical Coupling with Superoxide Ion. *J. Am. Chem. Soc.* **1981**, *103* (10), 2797–2802.

(54) Chen, S.; Foss, F. W. Aerobic Organocatalytic Oxidation of Aryl Aldehydes: Flavin Catalyst Turnover by Hantzsch's Ester. *Org. Lett.* **2012**, *14* (19), 5150–5153.
(55) Penzer, G. R.; Radda, G. K. The Chemistry and Biological Function of Isoalloxazines (Flavines). *Q. Rev. Chem. Soc.* **1967**, *21* (1), 43–65.
(56) Moore, W. M.; Spence, J. T.; Raymond, F. A.; Colson, S. D. Photochemistry of Riboflavin. I. The Hydrogen Transfer Process in the Anaerobic Photobleaching of Flavins. *J. Am. Chem. Soc.* **1963**, *85* (21), 3367–3372.
(57) Heelis, P. F. The Photophysical and Photochemical Properties of Flavins (Isoalloxazines). *Chem. Soc. Rev.* **1982**, *11* (1), 15–39.
(58) Lechner, R.; König, B. Oxidation and Deprotection of Primary Benzylamines by Visible Light Flavin Photocatalysis. *Synthesis* **2010**, *2010* (10), 1712–1718.
(59) Svoboda, J.; Schmaderer, H.; König, B. Thiourea-Enhanced Flavin Photooxidation of Benzyl Alcohol. *Chem. – Eur. J.* **2008**, *14* (6), 1854–1865.
(60) Schmaderer, H.; Hilgers, P.; Lechner, R.; König, B. Photooxidation of Benzyl Alcohols with Immobilized Flavins. *Adv. Synth. Catal.* **2009**, *351* (1–2), 163–174.
(61) Shinkai, S.; Yamaguchi, T.; Manabe, O.; Toda, F. Enantioselective Oxidation of Sulphides with Chiral 4a-Hydroperoxyflavin. *J. Chem. Soc. Chem. Commun.* **1988**, No. 21, 1399–1401.
(62) Murahashi, S.-I. Synthetic Aspects of Metal-Catalyzed Oxidations of Amines and Related Reactions. *Angew. Chem. Int. Ed. Engl.* **1995**, *34* (22), 2443–2465.
(63) Jurok, R.; Cibulka, R.; Dvořáková, H.; Hampl, F.; Hodačová, J. Planar Chiral Flavinium Salts – Prospective Catalysts for Enantioselective Sulfoxidation Reactions. *Eur. J. Org. Chem.* **2010**, *2010* (27), 5217–5224.
(64) Murahashi, S.-I.; Ono, S.; Imada, Y. Asymmetric Baeyer–Villiger Reaction with Hydrogen Peroxide Catalyzed by a Novel Planar-Chiral Bisflavin. *Angew. Chem. Int. Ed.* **2002**, *41* (13), 2366–2368.
(65) Trost, B. M.; Matsuoka, R. T. N-Nitrosulfoximines as Chemical Chameleons for Asymmetric Synthesis. *Synlett* **1992**, *1992* (01), 27–30.
(66) Reggelin, M.; Zur, C. Sulfoximines: Structures, Properties and Synthetic Applications. *Synthesis* **2000**, *2000* (01), 1–64.
(67) Bordwell, F. G.; Branca, J. C.; Johnson, C. R.; Vanier, N. R. Acidities of Sulfoximines and Related Oxosulfonium Cations. Cyclopropyl Effects and Structures of .alpha.-Sulfonyl-Type Carbanions. *J. Org. Chem.* **1980**, *45* (19), 3884–3889.
(68) Mellanby, E. On Production of Canine Hysteria with Agenized Flour. *Br. Med. J.* **1947**, *2* (4520), 288–289.
(69) Reliene, R.; Schiestl, R. H. Glutathione Depletion by Buthionine Sulfoximine Induces DNA Deletions in Mice. *Carcinogenesis* **2006**, *27* (2), 240–244.
(70) Lücking, U. Sulfoximines: A Neglected Opportunity in Medicinal Chemistry. *Angew. Chem. Int. Ed Engl.* **2013**, *52* (36), 9399–9408.
(71) Walker, D. P.; Zawistoski, M. P.; McGlynn, M. A.; Li, J.-C.; Kung, D. W.; Bonnette, P. C.; Baumann, A.; Buckbinder, L.; Houser, J. A.; Boer, J.; et al. Sulfoximine-Substituted Trifluoromethylpyrimidine Analogs as Inhibitors of Proline-Rich Tyrosine Kinase 2 (PYK2) Show Reduced hERG Activity. *Bioorg. Med. Chem. Lett.* **2009**, *19* (12), 3253–3258.
(72) Siemeister, G.; Lücking, U.; Wengner, A. M.; Lienau, P.; Steinke, W.; Schatz, C.; Mumberg, D.; Ziegelbauer, K. BAY 1000394, a Novel Cyclin-Dependent Kinase Inhibitor, with Potent Antitumor Activity in Mono- and in Combination Treatment upon Oral Application. *Mol. Cancer Ther.* **2012**, *11* (10), 2265–2273.

(73) Lindsay, J. G.; Owen, C. S.; Wilson, D. F. Azide Binding to Cytochrome c Oxidase: Effects on the Oxidation-Reduction and Spectral Properties of Cytochromes a and a3. *Bioelectrochem. Bioenerg.* **1987**, *17* (3), 369–381.
(74) Toru, T.; Bolm, C. *Organosulfur Chemistry in Asymmetric Synthesis*; John Wiley & Sons, 2008.
(75) Johnson, C. R.; Haake, M.; Schroeck, C. W. Chemistry of Sulfoxides and Related Compounds. XXVI. Preparation and Synthetic Applications of (Dimethylamino)phenyloxosulfonium Methylide. *J. Am. Chem. Soc.* **1970**, *92* (22), 6594–6598.
(76) Rayner, D. R.; Von Schriltz, D. M.; Day, J.; Cram, D. J. Stereospecific Interconversions of Optically Active Sulfoxides, Sulfilimines, and Sulfoximines. *J. Am. Chem. Soc.* **1968**, *90* (10), 2721–2723.
(77) Müller, J. F. K.; Vogt, P. Cu(I)-Catalyzed Sulfoximination. *Tetrahedron Lett.* **1998**, *39* (27), 4805–4806.
(78) Johnson, C. R.; Lavergne, O. Preparation of Free Sulfoximines by Treatment of N-Tosylsulfoximines with Sodium Anthracenide. *J. Org. Chem.* **1989**, *54* (4), 986–988.
(79) Bolm, C.; Muñiz, K.; Aguilar, N.; Kesselgruber, M.; Raabe, G. The Search for Benchrotrenes and Ferrocenes Containing a Chiral Sulfoximido Group: Preparation and Structural Properties. *Synthesis* **1999**, *1999* (07), 1251–1260.
(80) García Mancheño, O.; Bistri, O.; Bolm, C. Iodinane- and Metal-Free Synthesis of N-Cyano Sulfilimines: Novel and Easy Access of NH-Sulfoximines. *Org. Lett.* **2007**, *9* (19), 3809–3811.
(81) Pandey, A.; Bolm, C. Metal-Free Synthesis of N-Cyano-Substituted Sulfilimines and Sulfoximines. *Synthesis* **2010**, *2010* (17), 2922–2925.
(82) Tamura, Y.; Sumoto, K.; Minamikawa, J.; Ikeda, M. A Novel Method for Sulfilimines and Sulfoximines. *Tetrahedron Lett.* **1972**, *13* (40), 4137–4140.
(83) Carpino, L. A. O-Acylhydroxylamines. II. O-Mesitylenesulfonyl-, O-P-Toluenesulfonyl- and O-Mesitoylhydroxylamine1. *J. Am. Chem. Soc.* **1960**, *82* (12), 3133–3135.
(84) TAMURA, Y.; MINAMIKAWA, J.; IKEDA, M. O-Mesitylenesulfonylhydroxylamine and Related Compounds - Powerful Aminating Reagents. *Synthesis* **1977**, *1977* (01), 1–17.
(85) Yamagishi, F. G.; Rayner, D. R.; Zwicker, E. T.; Cram, D. J. Stereochemistry of Sulfur Compounds. V. Stereochemical Reaction Cycles That Involve Cyclic Sulfoxides, Sulfimides, and Sulfoximides. *J. Am. Chem. Soc.* **1973**, *95* (6), 1916–1925.
(86) Moriyama, M.; Kuriyama, K.; Iwata, T.; Furukawa, N.; Numata, T.; Oae, S. ABSOLUTE CONFIGURATION AND CIRCULAR DICHROISM OF S-O-METHOXYPHENYL-S-PHENYLSULFIMIDES AND SULFOXIMIDES. *Chem. Lett.* **1976**, *5* (4), 363–366.
(87) Huang, S.-L.; Swern, D. Oxidation of N-Acyl-, N-Sulfonyl-, and N-Arylsulfilimines to Sulfoximines by M-Chloroperoxybenzoate Anion. *J. Org. Chem.* **1979**, *44* (14), 2510–2513.
(88) Kirihara, M.; Itou, A.; Noguchi, T.; Yamamoto, J. Tantalum Carbide or Niobium Carbide Catalyzed Oxidation of Sulfides with Hydrogen Peroxide: Highly Efficient and Chemoselective Syntheses of Sulfoxides and Sulfones. *Synlett* **2010**, *2010* (10), 1557–1561.

(89) Sabol, M. A.; Davenport, R. W.; Andersen, K. K. Some Stereochemical Relationships among Sulfoxides, Sulfilimines, and Sulfoximines. *Tetrahedron Lett.* **1968**, *9* (18), 2159–2160.
(90) Christensen, B. W. Nucleophilic Substitution at Sulphur with Retention of Configuration. *J. Chem. Soc. Chem. Commun.* **1971**, No. 11, 597b–598.
(91) Cram, D. J.; Day, J.; Rayner, D. R.; Von Schriltz, D. M.; Duchamp, D. J.; Garwood, D. C. Stereochemistry of Sulfur Compounds. I. Stereochemical Reaction Cycles Involving an Open Chain Sulfoxide, Sulfimide, and Sulfoximide. *J. Am. Chem. Soc.* **1970**, *92* (25), 7369–7384.
(92) Bolm, C.; Bienewald, F. Asymmetric Sulfide Oxidation with Vanadium Catalysts and H2O2. *Angew. Chem. Int. Ed. Engl.* **1996**, *34* (23–24), 2640–2642.
(93) Akhatou, A.; Rahimi, M.; Cheboub, K.; Ghosez, L.; Hanquet, G. Acid Promoted Enantioselective Oxygen-Atom Transfer from N-Alkyl Binaphthyl-Derived Oxaziridines onto Sulfides. *Tetrahedron* **2007**, *63* (27), 6232–6240.
(94) Kunieda, N.; Motoki, H.; Kinoshita, M. AN ENANTIOMER DIFFERENTIATING REACTION OF P-TOLYLSULFINYLCARBANION WITH (−)-MENTHYL CARBOXYLATES. *Chem. Lett.* **1978**, *7* (7), 713–716.
(95) Harmata, M.; Zheng, P.; Huang, C.; Gomes, M. G.; Ying, W.; Ranyanil, K.-O.; Balan, G.; Calkins, N. L. Expedient Synthesis of Sulfinamides from Sulfonyl Chlorides. *J. Org. Chem.* **2007**, *72* (2), 683–685.
(96) Johnson, C. R.; Kirchhoff, R. A. Oxidation of N-(P-Tolylsulfonyl)sulfilimines to N-(P-Tolylsulfonyl)sulfoximines with Alkaline Hydrogen Peroxide. *J. Org. Chem.* **1979**, *44* (13), 2280–2280.
(97) Johnson, C. R.; Bis, K. G.; Cantillo, J. H.; Meanwell, N. A.; Reinhard, M. F. D.; Zeller, J. R.; Vonk, G. P. Preparation and Reactions of Sulfonimidoyl Fluorides. *J. Org. Chem.* **1983**, *48* (1), 1–3.
(98) Harmata, M. A New Sulfoximine Synthesis. *Tetrahedron Lett.* **1989**, *30* (4), 437–440.
(99) Johnson, C. R.; Schroeck, C. W. Chemistry of Sulfoxides and Related Compounds. XLV. Asymmetric Syntheses Using Optically Active Oxosulfonium Alkylides. *J. Am. Chem. Soc.* **1973**, *95* (22), 7418–7423.
(100) Brandt, J.; Gais, H.-J. An Efficient Resolution of (±)-S-Methyl-S-Phenylsulfoximine with (+)-10-Camphorsulfonic Acid by the Method of Half-Quantities. *Tetrahedron Asymmetry* **1997**, *8* (6), 909–912.
(101) Dong, S.; Frings, M.; Cheng, H.; Wen, J.; Zhang, D.; Raabe, G.; Bolm, C. Organocatalytic Kinetic Resolution of Sulfoximines. *J. Am. Chem. Soc.* **2016**, *138* (7), 2166–2169.
(102) Bach, T.; Körber, C. The Preparation of N-Tert-Butyloxycarbonyl-(Boc-)Protected Sulfoximines and Sulfimines by an Iron(II)-Mediated Nitrene Transfer from BocN3 to Sulfoxides and Sulfides. *Eur. J. Org. Chem.* **1999**, *1999* (5), 1033–1039.
(103) Mancheño, O. G.; Bolm, C. Iron-Catalyzed Imination of Sulfoxides and Sulfides. *Org. Lett.* **2006**, *8* (11), 2349–2352.
(104) Mancheño, O. G.; Dallimore, J.; Plant, A.; Bolm, C. Iron(II) Triflate as an Efficient Catalyst for the Imination of Sulfoxides. *Org. Lett.* **2009**, *11* (11), 2429–2432.
(105) Cren, S.; Kinahan, T. C.; Skinner, C. L.; Tye, H. A Study of the Functional Group Compatibility of Sulfoximination Methods. *Tetrahedron Lett.* **2002**, *43* (15), 2749–2751.
(106) Okamura, H.; Bolm, C. Rhodium-Catalyzed Imination of Sulfoxides and Sulfides: Efficient Preparation of N-Unsubstituted Sulfoximines and Sulfilimines. *Org. Lett.* **2004**, *6* (8), 1305–1307.

(107) Miao, J.; Richards, N. G. J.; Ge, H. Rhodium-Catalyzed Direct Synthesis of Unprotected NH-Sulfoximines from Sulfoxides. *Chem. Commun.* **2014**, *50* (68), 9687–9689.
(108) Cho, G. Y.; Bolm, C. Silver-Catalyzed Imination of Sulfoxides and Sulfides. *Org. Lett.* **2005**, *7* (22), 4983–4985.
(109) Zenzola, M.; Doran, R.; Degennaro, L.; Luisi, R.; Bull, J. A. Transfer of Electrophilic NH Using Convenient Sources of Ammonia: Direct Synthesis of NH Sulfoximines from Sulfoxides. *Angew. Chem. Int. Ed.* **2016**, *55* (25), 7203–7207.
(110) Lohier, J.-F.; Glachet, T.; Marzag, H.; Gaumont, A.-C.; Reboul, V. Mechanistic Investigation of the NH-Sulfoximination of Sulfide. Evidence for λ6-Sulfanenitrile Intermediates. *Chem. Commun.* **2017**, *53* (12), 2064–2067.
(111) Yoshimura, T.; Tsukurimichi, E.; Kita, H.; Fujii, H.; Shimasaki, C. Kinetic Study on the Alkaline Hydrolysis of S,S-Diaryl-N-Halosulfilimines. *Bull. Chem. Soc. Jpn.* **1990**, *63* (6), 1764–1769.
(112) Candy, M.; Guyon, C.; Mersmann, S.; Chen, J.-R.; Bolm, C. Synthesis of Sulfondiimines by N-Chlorosuccinimide-Mediated Oxidative Imination of Sulfiliminium Salts. *Angew. Chem. Int. Ed. 51* (18), 4440–4443.
(113) Ritter, J. J.; Minieri, P. P. A New Reaction of Nitriles. I. Amides from Alkenes and Mononitriles1. *J. Am. Chem. Soc.* **1948**, *70* (12), 4045–4048.
(114) Roy, K.-M. Sulfones and Sulfoxides. In *Ullmann's Encyclopedia of Industrial Chemistry*; Wiley-VCH Verlag GmbH & Co. KGaA, 2000.
(115) Varma, R. S.; Saini, R. K.; Meshram, H. M. Selective Oxidation of Sulfides to Sulfoxides and Sulfones by Microwave Thermolysis on Wet Silica-Supported Sodium Periodate. *Tetrahedron Lett.* **1997**, *38* (37), 6525–6528.
(116) Leonard, N. J.; Johnson, C. R. Periodate Oxidation of Sulfides to Sulfoxides. Scope of the Reaction. *J. Org. Chem.* **1962**, *27* (1), 282–284.
(117) McKillop, A.; A. Tarbin, J. Sodium Perborate - a Cheap and Effective Reagent for the Oxidation of Anilines and Sulphides. *Tetrahedron Lett.* **1983**, *24* (14), 1505–1508.
(118) KENNEDY, R. J.; STOCK, A. M. The Oxidation of Organic Substances by Potassium Peroxymonosulfate. *J. Org. Chem.* **1960**, *25* (11), 1901–1906.
(119) Trost, B. M.; Curran, D. P. Chemoselective Oxidation of Sulfides to Sulfones with Potassium Hydrogen Persulfate. *Tetrahedron Lett.* **1981**, *22* (14), 1287–1290.
(120) Yu, B.; Liu, A.-H.; He, L.-N.; Li, B.; Diao, Z.-F.; Li, Y.-N. Catalyst-Free Approach for Solvent-Dependent Selective Oxidation of Organic Sulfides with Oxone. *Green Chem.* **2012**, *14* (4), 957–962.
(121) Goheen, D.; Bennett, C. Notes- Oxidation of Dialkyl Sulfides with Nitric Acid. *J. Org. Chem.* **1961**, *26* (4), 1331–1333.
(122) Li, B.; Liu, A.-H.; He, L.-N.; Yang, Z.-Z.; Gao, J.; Chen, K.-H. Iron-Catalyzed Selective Oxidation of Sulfides to Sulfoxides with the Polyethylene Glycol/O2 System. *Green Chem.* **2012**, *14* (1), 130–135.
(123) Feng, J.-B.; Gong, J.-L.; Wu, X.-F. The First Zinc-Catalyzed Oxidation of Sulfides to Sulfones Using H2O2 as Green Oxidant. *RSC Adv.* **2014**, *4* (55), 29273–29275.
(124) Gogoi, S. R.; Boruah, J. J.; Sengupta, G.; Saikia, G.; Ahmed, K.; Bania, K. K.; Islam, N. S. Peroxoniobium(V)-Catalyzed Selective Oxidation of Sulfides with Hydrogen Peroxide in Water: A Sustainable Approach. *Catal. Sci. Technol.* **2014**, *5* (1), 595–610.
(125) Hardy, F. E.; Speakman, P. R. H.; Robson, P. The Vanadium Pentoxide-Catalysed Oxidation of Thio-Compounds with Hydrogen Peroxide. *J. Chem. Soc. C Org.* **1969**, No. 18, 2334–2336.

(126) Kwan, S. K.; Hye, J. H.; Chan, S. C.; Chi, S. H. Tellurium Dioxide Catalyzed Selective Oxidation of Sulfides to Sulfoxides with Hydrogen Peroxide. *Tetrahedron Lett.* **1990**, *31* (20), 2893–2894.
(127) Barton, D. H. R.; Li, W.; Smith, J. A. Binuclear Manganese Complexes as Catalysts in the Selective and Efficient Oxidation of Sulfides to Sulfones. *Tetrahedron Lett.* **1998**, *39* (39), 7055–7058.
(128) Matteucci, M.; Bhalay, G.; Bradley, M. Mild and Highly Chemoselective Oxidation of Thioethers Mediated by Sc(OTf)3. *Org. Lett.* **2003**, *5* (3), 235–237.
(129) Choudary, B. M.; Reddy, C. R. V.; Prakash, B. V.; Kantam, M. L.; Sreedhar, B. The First Example of Direct Oxidation of Sulfides to Sulfones by an Osmate Molecular Oxygen System. *Chem. Commun.* **2003**, No. 6, 754–755.
(130) Capozzi, M. A. M.; Centrone, C.; Fracchiolla, G.; Naso, F.; Cardellicchio, C. A Study of Factors Affecting Enantioselectivity in the Oxidation of Aryl Benzyl Sulfides in the Presence of Chiral Titanium Catalysts. *Eur. J. Org. Chem.* **2011**, *2011* (23), 4327–4334.
(131) Arterburn, J. B.; Nelson, S. L. Rhenium-Catalyzed Oxidation of Sulfides with Phenyl Sulfoxide. *J. Org. Chem.* **1996**, *61* (7), 2260–2261.
(132) Zhou, X.-T.; Ji, H.-B.; Cheng, Z.; Xu, J.-C.; Pei, L.-X.; Wang, L.-F. Selective Oxidation of Sulfides to Sulfoxides Catalyzed by Ruthenium (III) Meso-Tetraphenylporphyrin Chloride in the Presence of Molecular Oxygen. *Bioorg. Med. Chem. Lett.* **2007**, *17* (16), 4650–4653.
(133) Xu, L.; Cheng, J.; Trudell, M. L. Chromium(VI) Oxide Catalyzed Oxidation of Sulfides to Sulfones with Periodic Acid. *J. Org. Chem.* **2003**, *68* (13), 5388–5391.
(134) Bordoloi, A.; Vinu, A.; Halligudi, S. B. One-Step Synthesis of SBA-15 Containing Tungsten Oxide Nanoclusters: A Chemoselective Catalyst for Oxidation of Sulfides to Sulfoxides under Ambient Conditions. *Chem. Commun.* **2007**, No. 45, 4806–4808.
(135) Pitchen, P.; Kagan, H. B. An Efficient Asymmetric Oxidation of Sulfides to Sulfoxides. *Tetrahedron Lett.* **1984**, *25* (10), 1049–1052.
(136) Katsuki, T.; Sharpless, K. B. The First Practical Method for Asymmetric Epoxidation. *J. Am. Chem. Soc.* **1980**, *102* (18), 5974–5976.
(137) Pitchen, P.; Dunach, E.; Deshmukh, M. N.; Kagan, H. B. An Efficient Asymmetric Oxidation of Sulfides to Sulfoxides. *J. Am. Chem. Soc.* **1984**, *106* (26), 8188–8193.
(138) Furia, F. D.; Modena, G.; Seraglia, R. Synthesis of Chiral Sulfoxides by Metal-Catalyzed Oxidation with T-Butyl Hydroperoxide. *Synthesis* **1984**, *1984* (04), 325–326.
(139) Brunel, J. M.; Kagan, H. B. Catalytic Asymmetric Oxidation of Sulfides With High Enantioselectivities. *Synlett* **1996**, *1996* (04), 404–406.
(140) Adam, W.; Korb, M. N.; Roschmann, K. J.; Saha-Möller, C. R. Titanium-Catalyzed, Asymmetric Sulfoxidation of Alkyl Aryl Sulfides with Optically Active Hydroperoxides. *J. Org. Chem.* **1998**, *63* (10), 3423–3428.
(141) Palucki, M.; Hanson, P.; Jacobsen, E. N. Asymmetric Oxidation of Sulfides with H2O2 Catalyzed by (salen)Mn(III) Complexes. *Tetrahedron Lett.* **1992**, *33* (47), 7111–7114.
(142) Noda, K.; Hosoya, N.; Irie, R.; Yamashita, Y.; Katsuki, T. Catalytic Asymmetric Oxidation of Sulfides Using (salen)manganese(III) Complex as a Catalyst. *Tetrahedron* **1994**, *50* (32), 9609–9618.
(143) Nakajima, K.; Kojima, M.; Fujita, J. Asymmetric Oxidation of Sulfides to Sulfoxides by Organic Hydroperoxides with Optically Active Schiff Base-Oxovanadium(IV) Catalysts. *Chem. Lett.* **1986**, *15* (9), 1483–1486.

(144) Bolm, C.; Bienewald, F. Asymmetric Sulfide Oxidation with Vanadium Catalysts and H2O2. *Angew. Chem. Int. Ed. Engl.* **1996**, *34* (23–24), 2640–2642.
(145) Cotton, H.; Elebring, T.; Larsson, M.; Li, L.; Sörensen, H.; von Unge, S. Asymmetric Synthesis of Esomeprazole. *Tetrahedron Asymmetry* **2000**, *11* (18), 3819–3825.
(146) Marsh, B. J.; Carbery, D. R. Chemoselective Sulfide Oxidation Mediated by Bridged Flavinium Organocatalysts. *Tetrahedron Lett.* **2010**, *51* (17), 2362–2365.
(147) Li, W.-S.; Zhang, N.; Sayre, L. M. N1,N10-Ethylene-Bridged High-Potential Flavins: Synthesis, Characterization, and Reactivity. *Tetrahedron* **2001**, *57* (21), 4507–4522.
(148) Bergstad, K.; Bäckvall, J.-E. Mild and Efficient Flavin-Catalyzed H2O2 Oxidation of Tertiary Amines to Amine N-Oxides. *J. Org. Chem.* **1998**, *63* (19), 6650–6655.
(149) Murahashi, S.; Oda, T.; Masui, Y. Flavin-Catalyzed Oxidation of Amines and Sulfur Compounds with Hydrogen Peroxide. *J. Am. Chem. Soc.* **1989**, *111* (13), 5002–5003.
(150) Imada, Y.; Iida, H.; Naota, T. Flavin-Catalyzed Generation of Diimide: An Environmentally Friendly Method for the Aerobic Hydrogenation of Olefins. *J. Am. Chem. Soc.* **2005**, *127* (42), 14544–14545.
(151) Massey, V. Activation of Molecular Oxygen by Flavins and Flavoproteins. *J. Biol. Chem.* **1994**, *269* (36), 22459–22462.
(152) Chu, J.-W.; Trout, B. L. On the Mechanisms of Oxidation of Organic Sulfides by H2O2 in Aqueous Solutions. *J. Am. Chem. Soc.* **2004**, *126* (3), 900–908.
(153) Kice, J. L.; Chiou, S.; Weclas, L. Mechanism of the Oxidation of O-Nitro- and O-Benzoylbenzeneselenenic Acids by Peracids, Hydroperoxides, and Hydrogen Peroxide. *J. Org. Chem.* **1985**, *50* (14), 2508–2516.
(154) Imada, Y.; Naota, T. Flavins as Organocatalysts for Environmentally Benign Molecular Transformations. *Chem. Rec.* **2007**, *7* (6), 354–361.
(155) Murray, A. T.; King, R.; Donnelly, J. V. G.; Dowley, M. J. H.; Tuna, F.; Sells, D.; John, M. P.; Carbery, D. R. Symbiotic Transition-Metal and Organocatalysis for Catalytic Ambient Amine Oxidation and Alkene Reduction Reactions. *ChemCatChem* **2016**, *8* (3), 510–514.
(156) Rerup, C.; Tarding, F. Streptozotocin- and Alloxan-Diabetes in Mice. *Eur. J. Pharmacol.* **1969**, *7* (1), 89–96.
(157) Lenzen, S. The Mechanisms of Alloxan- and Streptozotocin-Induced Diabetes. *Diabetologia* **2008**, *51* (2), 216–226.
(158) Saifer, A.; Oreskes, I. Color Reaction oK Amino Acids with Alloxan, Isatin, and Ninhydrin in Circular Paper Chromatography. *Anal. Chem.* **1956**, *28* (4), 501–504.
(159) Srogl, J.; Voltrova, S. Copper/Ascorbic Acid Dyad as a Catalytic System for Selective Aerobic Oxidation of Amines. *Org. Lett.* **2009**, *11* (4), 843–845.
(160) Armstrong, A.; Carbery, D. R.; Lamont, S. G.; Pape, A. R.; Wincewicz, R. N-Amino-N-Methylmorpholinium Salts: Highly Active Aziridination Reagents for Chalcones. *Synlett* **2006**, *2006* (15), 2504–2506.
(161) Jørgensen, B. B.; Revsbech, N. P. Colorless Sulfur Bacteria, Beggiatoa Spp. and Thiovulum Spp., in O2 and H2S Microgradients. *Appl. Environ. Microbiol.* **1983**, *45* (4), 1261–1270.
(162) Drago, C.; Caggiano, L.; Jackson, R. F. W. Vanadium-Catalyzed Sulfur Oxidation/Kinetic Resolution in the Synthesis of Enantiomerically Pure Alkyl Aryl Sulfoxides. *Angew. Chem. Int. Ed.* **2005**, *44* (44), 7221–7223.
(163) Wu, X.-F. A General and Selective Zinc-Catalyzed Oxidation of Sulfides to Sulfoxides. *Tetrahedron Lett.* **2012**, *53* (33), 4328–4331.

(164) Das, R.; Chakraborty, D. Cu(II)-Catalyzed Oxidation of Sulfides. *Tetrahedron Lett.* **2010**, *51* (48), 6255–6258.
(165) Secci, F.; Frongia, A.; Piras, P. P. Ammonium Salt Catalyzed Oxidation of Organosulfides to Organosulfoxydes. *Tetrahedron Lett.* **2014**, *55* (3), 603–605.
(166) Chen, S.; Hossain, M. S.; Foss, F. W. Organocatalytic Dakin Oxidation by Nucleophilic Flavin Catalysts. *Org. Lett.* **2012**, *14* (11), 2806–2809.
(167) Dakin H. D. The Oxidation of Hydroxy Derivatives of Benzaldehyde, Acetophenone and Related Substances. *Am. Chem. J. 42* (6), 477–498.
(168) Lee, M. J. C.; Shoeman, D. W.; Goon, D. J. W.; Nagasawa, H. T. N-Hydroxybenzenecarboximidic Acid Derivatives: A New Class of Nitroxyl-Generating Prodrugs. *Nitric Oxide* **2001**, *5* (3), 278–287.
(169) Reeves, A. M.; Love, S. Laboratory Preparation and Decontamination of Mustard. *Science* **1948**, *107* (2773), 204–204.
(170) Tham, M. J.; Walker, R. D.; Gubbins, K. E. Diffusion of Oxygen and Hydrogen in Aqueous Potassium Hydroxide Solutions. *J. Phys. Chem.* **1970**, *74* (8), 1747–1751.
(171) Imada, Y.; Kitagawa, T.; Iwata, S.; Komiya, N.; Naota, T. Oxidation of Sulfides with Hydrogen Peroxide Catalyzed by Synthetic Flavin Adducts with Dendritic Bis(acylamino)pyridines. *Tetrahedron* **2014**, *70* (2), 495–501.
(172) Li, J.-S.; Qiu, Z.; Li, C.-J. Palladium-Catalyzed Synthesis of N-Cyclohexyl Anilines from Phenols with Hydrazine or Hydroxylamine via N-N/O Cleavage. *Adv. Synth. Catal.* n/a-n/a.
(173) Vajrala, N.; Martens-Habbena, W.; Sayavedra-Soto, L. A.; Schauer, A.; Bottomley, P. J.; Stahl, D. A.; Arp, D. J. Hydroxylamine as an Intermediate in Ammonia Oxidation by Globally Abundant Marine Archaea. *Proc. Natl. Acad. Sci.* **2013**, *110* (3), 1006–1011.
(174) Rundlöf, T.; Mathiasson, M.; Bekiroglu, S.; Hakkarainen, B.; Bowden, T.; Arvidsson, T. Survey and Qualification of Internal Standards for Quantification by 1H NMR Spectroscopy. *J. Pharm. Biomed. Anal.* **2010**, *52* (5), 645–651.
(175) Vij, D. R. *Handbook of Applied Solid State Spectroscopy*; Springer Science & Business Media, 2007.
(176) Murray, A. T.; Matton, P.; Fairhurst, N. W. G.; John, M. P.; Carbery, D. R. Biomimetic Flavin-Catalyzed Aldehyde Oxidation. *Org. Lett.* **2012**, *14* (14), 3656–3659.
(177) Swain, C. G.; Scott, C. B. Quantitative Correlation of Relative Rates. Comparison of Hydroxide Ion with Other Nucleophilic Reagents toward Alkyl Halides, Esters, Epoxides and Acyl Halides1. *J. Am. Chem. Soc.* **1953**, *75* (1), 141–147.
(178) Mayr, H.; Patz, M. Scales of Nucleophilicity and Electrophilicity: A System for Ordering Polar Organic and Organometallic Reactions. *Angew. Chem. Int. Ed. Engl.* **1994**, *33* (9), 938–957.
(179) Phan, T. B.; Breugst, M.; Mayr, H. Towards a General Scale of Nucleophilicity? *Angew. Chem. Int. Ed.* **2006**, *45* (23), 3869–3874.
(180) Li, W.-S.; Sayre, L. M. Reaction of Amines with N1,N10-Ethylene-Bridged Flavinium Salts: The First NMR Spectroscopic Evidence of C10a Tetrahedral Amine Adducts. *Tetrahedron* **2001**, *57* (21), 4523–4536.
(181) Minegishi, S.; Kobayashi, S.; Mayr, H. Solvent Nucleophilicity. *J. Am. Chem. Soc.* **2004**, *126* (16), 5174–5181.
(182) Kevill, D. N.; Kamil, W. A. Solvent Nucleophilicity of 2,2,2-Trifluoroethanol-Ethanol Mixtures. *J. Org. Chem.* **1982**, *47* (19), 3785–3787.
(183) Špačková, J.; Svobodová, E.; Hartman, T.; Stibor, I.; Kopecká, J.; Cibulková, J.; Chudoba, J.; Cibulka, R. Visible Light [2+2] Photocycloaddition Mediated by

Flavin Derivative Immobilized on Mesoporous Silica. *ChemCatChem* **2017**, *9* (7), 1177–1181.
(184) Cibulka, R.; Baxová, L.; Dvořáková, H.; Hampl, F.; Ménová, P.; Mojr, V.; Plancq, B.; Sayin, S. Catalytic Effect of Alloxazinium and Isoalloxazinium Salts on Oxidation of Sulfides with Hydrogen Peroxide in Micellar Media. *Collect. Czechoslov. Chem. Commun.* **2009**, *74* (6), 973–993.
(185) Mao, Y.; Tian, W.; Huang, Z.; An, J. Convenient Synthesis of Toxoflavin That Targets β-Catenin/Tcf4 Signaling Activities. *J. Heterocycl. Chem.* **2014**, *51* (3), 594–597.
(186) Biltz, H. Alloxan-Anhydrid Und Seine Methylderivate. *Berichte Dtsch. Chem. Ges.* **1912**, *45* (3), 3659–3675.
(187) Geetanjali; Singh, R.; Chauhan, S. M. S. A New and Improved N -3 Alkylation of 10-Substituted Isoalloxazines Using 1,8-Diazabicyclo[5.4.0]undec-7-Ene in Benzene. *Synth. Commun.* **2003**, *33* (4), 613–620.
(188) Zelenka, J.; Hartman, T.; Klímová, K.; Hampl, F.; Cibulka, R. Phase-Transfer Catalysis in Oxidations Based on the Covalent Bonding of Hydrogen Peroxide to Amphiphilic Flavinium Salts. *ChemCatChem* **2014**, *6* (10), 2843–2846.
(189) Schäfer, S.; Wirth, T. A Versatile and Highly Reactive Polyfluorinated Hypervalent Iodine(III) Compound. *Angew. Chem. Int. Ed.* **2010**, *49* (15), 2786–2789.
(190) García Mancheño, O.; Bolm, C. Comparative Study of Metal-Catalyzed Iminations of Sulfoxides and Sulfides. *Chem. – Eur. J.* **2007**, *13* (23), 6674–6681.
(191) Wang, H.; Cheng, Y.; Becker, P.; Raabe, G.; Bolm, C. Synthesis of Sulfoximidoyl-Containing Hypervalent Iodine(III) Reagents and Their Use in Transition-Metal-Free Sulfoximidations of Alkynes. *Angew. Chem. Int. Ed.* **2016**, *55* (41), 12655–12658.
(192) Lejaeghere, K.; Bihlmayer, G.; Björkman, T.; Blaha, P.; Blügel, S.; Blum, V.; Caliste, D.; Castelli, I. E.; Clark, S. J.; Corso, A. D.; et al. Reproducibility in Density Functional Theory Calculations of Solids. *Science* **2016**, *351* (6280), aad3000.
(193) Dove, M. T. Theory of Displacive Phase Transitions in Minerals. *Am. Mineral.* **1997**, *82* (3–4), 213–244.
(194) Kieslich, G.; Forse, A. C.; Sun, S.; Butler, K. T.; Kumagai, S.; Wu, Y.; Warren, M. R.; Walsh, A.; Grey, C. P.; Cheetham, A. K. Role of Amine–Cavity Interactions in Determining the Structure and Mechanical Properties of the Ferroelectric Hybrid Perovskite [NH3NH2]Zn(HCOO)3. *Chem. Mater.* **2016**, *28* (1), 312–317.
(195) Kieslich, G.; Kumagai, S.; Butler, K. T.; Okamura, T.; Hendon, C. H.; Sun, S.; Yamashita, M.; Walsh, A.; Cheetham, A. K. Role of Entropic Effects in Controlling the Polymorphism in Formate ABX3 Metal–organic Frameworks. *Chem. Commun.* **2015**, *51* (85), 15538–15541.
(196) Leguy, A. M. A.; Frost, J. M.; McMahon, A. P.; Sakai, V. G.; Kochelmann, W.; Law, C.; Li, X.; Foglia, F.; Walsh, A.; O'Regan, B. C.; et al. The Dynamics of Methylammonium Ions in Hybrid Organic-Inorganic Perovskite Solar Cells. *Nat. Commun.* **2015**, *6*, 7124.
(197) Brivio, F.; Frost, J. M.; Skelton, J. M.; Jackson, A. J.; Weber, O. J.; Weller, M. T.; Goñi, A. R.; Leguy, A. M. A.; Barnes, P. R. F.; Walsh, A. Lattice Dynamics and Vibrational Spectra of the Orthorhombic, Tetragonal, and Cubic Phases of Methylammonium Lead Iodide. *Phys. Rev. B* **2015**, *92* (14), 144308.

(198) Perdew, J. P.; Ruzsinszky, A.; Csonka, G. I.; Vydrov, O. A.; Scuseria, G. E.; Constantin, L. A.; Zhou, X.; Burke, K. Restoring the Density-Gradient Expansion for Exchange in Solids and Surfaces. *Phys. Rev. Lett.* **2008**, *100* (13), 136406.
(199) Svane, K. L.; Saines, P. J.; Walsh, A. Magnetoelastic Coupling in the Cobalt Adipate Metal–organic Framework from Quasi-Harmonic Lattice Dynamics. *J. Mater. Chem. C* **2015**, *3* (42), 11076–11080.
(200) Hendon, C. H.; Tiana, D.; Vaid, T. P.; Walsh, A. Thermodynamic and Electronic Properties of Tunable II–VI and IV–VI Semiconductor Based Metal–organic Frameworks from Computational Chemistry. *J. Mater. Chem. C* **2012**, *1* (1), 95–100.
(201) Gascon, J.; Corma, A.; Kapteijn, F.; Llabrés i Xamena, F. X. Metal Organic Framework Catalysis: Quo Vadis? *ACS Catal.* **2014**, *4* (2), 361–378.
(202) Sumida, K.; Rogow, D. L.; Mason, J. A.; McDonald, T. M.; Bloch, E. D.; Herm, Z. R.; Bae, T.-H.; Long, J. R. Carbon Dioxide Capture in Metal–Organic Frameworks. *Chem. Rev.* **2012**, *112* (2), 724–781.
(203) Sheberla, D.; Bachman, J. C.; Elias, J. S.; Sun, C.-J.; Shao-Horn, Y.; Dincă, M. Conductive MOF Electrodes for Stable Supercapacitors with High Areal Capacitance. *Nat. Mater.* **2017**, *16* (2), 220–224.
(204) Erickson, K. J.; Léonard, F.; Stavila, V.; Foster, M. E.; Spataru, C. D.; Jones, R. E.; Foley, B. M.; Hopkins, P. E.; Allendorf, M. D.; Talin, A. A. Thin Film Thermoelectric Metal–Organic Framework with High Seebeck Coefficient and Low Thermal Conductivity. *Adv. Mater.* **2015**, *27* (22), 3453–3459.
(205) Worrall, S. D.; Bissett, M. A.; Hirunpinyopas, W.; Attfield, M. P.; Dryfe, R. A. W. Facile Fabrication of Metal–organic Framework HKUST-1-Based Rewritable Data Storage Devices. *J. Mater. Chem. C* **2016**, *4* (37), 8687–8695.
(206) Yoon, S. M.; Warren, S. C.; Grzybowski, B. A. Storage of Electrical Information in Metal–Organic-Framework Memristors. *Angew. Chem. Int. Ed.* **2014**, *53* (17), 4437–4441.
(207) Pan, L.; Ji, Z.; Yi, X.; Zhu, X.; Chen, X.; Shang, J.; Liu, G.; Li, R.-W. Metal-Organic Framework Nanofilm for Mechanically Flexible Information Storage Applications. *Adv. Funct. Mater.* **2015**, *25* (18), 2677–2685.
(208) Férey, G.; Millange, F.; Morcrette, M.; Serre, C.; Doublet, M.-L.; Grenèche, J.-M.; Tarascon, J.-M. Mixed-Valence Li/Fe-Based Metal–Organic Frameworks with Both Reversible Redox and Sorption Properties. *Angew. Chem. Int. Ed.* **2007**, *46* (18), 3259–3263.
(209) Zhang, Z.; Yoshikawa, H.; Awaga, K. Monitoring the Solid-State Electrochemistry of Cu(2,7-AQDC) (AQDC = Anthraquinone Dicarboxylate) in a Lithium Battery: Coexistence of Metal and Ligand Redox Activities in a Metal–Organic Framework. *J. Am. Chem. Soc.* **2014**, *136* (46), 16112–16115.
(210) Ahrenholtz, S. R.; Epley, C. C.; Morris, A. J. Solvothermal Preparation of an Electrocatalytic Metalloporphyrin MOF Thin Film and Its Redox Hopping Charge-Transfer Mechanism. *J. Am. Chem. Soc.* **2014**, *136* (6), 2464–2472.
(211) Nohra, B.; El Moll, H.; Rodriguez Albelo, L. M.; Mialane, P.; Marrot, J.; Mellot-Draznieks, C.; O'Keeffe, M.; Ngo Biboum, R.; Lemaire, J.; Keita, B.; et al. Polyoxometalate-Based Metal Organic Frameworks (POMOFs): Structural Trends, Energetics, and High Electrocatalytic Efficiency for Hydrogen Evolution Reaction. *J. Am. Chem. Soc.* **2011**, *133* (34), 13363–13374.
(212) Campbell, M. G.; Sheberla, D.; Liu, S. F.; Swager, T. M.; Dincă, M. Cu3(hexaiminotriphenylene)2: An Electrically Conductive 2D Metal–Organic

Framework for Chemiresistive Sensing. *Angew. Chem. Int. Ed.* **2015**, *54* (14), 4349–4352.
(213) Usman, M.; Mendiratta, S.; Lu, K.-L. Semiconductor Metal–Organic Frameworks: Future Low-Bandgap Materials. *Adv. Mater.* **2017**, *29* (6), n/a-n/a.
(214) Kreno, L. E.; Leong, K.; Farha, O. K.; Allendorf, M.; Van Duyne, R. P.; Hupp, J. T. Metal–Organic Framework Materials as Chemical Sensors. *Chem. Rev.* **2012**, *112* (2), 1105–1125.
(215) Butler, K. T.; Hendon, C. H.; Walsh, A. Electronic Chemical Potentials of Porous Metal–Organic Frameworks. *J. Am. Chem. Soc.* **2014**, *136* (7), 2703–2706.
(216) Stavila, V.; Talin, A. A.; Allendorf, M. D. MOF-Based Electronic and Opto-Electronic Devices. *Chem. Soc. Rev.* **2014**, *43* (16), 5994–6010.
(217) Grau-Crespo, R.; Aziz, A.; Collins, A. W.; Crespo-Otero, R.; Hernández, N. C.; Rodriguez-Albelo, L. M.; Ruiz-Salvador, A. R.; Calero, S.; Hamad, S. Modelling a Linker Mix-and-Match Approach for Controlling the Optical Excitation Gaps and Band Alignment of Zeolitic Imidazolate Frameworks. *Angew. Chem. Int. Ed.* **2016**, *55* (52), 16012–16016.
(218) Sun, L.; Campbell, M. G.; Dincă, M. Electrically Conductive Porous Metal–Organic Frameworks. *Angew. Chem. Int. Ed.* **2016**, *55* (11), 3566–3579.
(219) Park, S. S.; Hontz, E. R.; Sun, L.; Hendon, C. H.; Walsh, A.; Van Voorhis, T.; Dincă, M. Cation-Dependent Intrinsic Electrical Conductivity in Isostructural Tetrathiafulvalene-Based Microporous Metal–Organic Frameworks. *J. Am. Chem. Soc.* **2015**, *137* (5), 1774–1777.
(220) Brédas, J.-L.; Beljonne, D.; Coropceanu, V.; Cornil, J. Charge-Transfer and Energy-Transfer Processes in π-Conjugated Oligomers and Polymers: A Molecular Picture. *Chem. Rev.* **2004**, *104* (11), 4971–5004.
(221) Talin, A. A.; Centrone, A.; Ford, A. C.; Foster, M. E.; Stavila, V.; Haney, P.; Kinney, R. A.; Szalai, V.; Gabaly, F. E.; Yoon, H. P.; et al. Tunable Electrical Conductivity in Metal-Organic Framework Thin-Film Devices. *Science* **2014**, *343* (6166), 66–69.
(222) Moggach, S. A.; Bennett, T. D.; Cheetham, A. K. The Effect of Pressure on ZIF-8: Increasing Pore Size with Pressure and the Formation of a High-Pressure Phase at 1.47 GPa. *Angew. Chem. 121* (38), 7221–7223.
(223) Fairen-Jimenez, D.; Moggach, S. A.; Wharmby, M. T.; Wright, P. A.; Parsons, S.; Düren, T. Opening the Gate: Framework Flexibility in ZIF-8 Explored by Experiments and Simulations. *J. Am. Chem. Soc.* **2011**, *133* (23), 8900–8902.
(224) Bouëssel du Bourg, L.; Ortiz, A. U.; Boutin, A.; Coudert, F.-X. Thermal and Mechanical Stability of Zeolitic Imidazolate Frameworks Polymorphs. *APL Mater.* **2014**, *2* (12), 124110.
(225) Krause, S.; Bon, V.; Senkovska, I.; Stoeck, U.; Wallacher, D.; Többens, D. M.; Zander, S.; Pillai, R. S.; Maurin, G.; Coudert, F.-X.; et al. A Pressure-Amplifying Framework Material with Negative Gas Adsorption Transitions. *Nature* **2016**, *532* (7599), 348–352.
(226) Phan, A.; Doonan, C. J.; Uribe-Romo, F. J.; Knobler, C. B.; O'Keeffe, M.; Yaghi, O. M. Synthesis, Structure, and Carbon Dioxide Capture Properties of Zeolitic Imidazolate Frameworks. *Acc. Chem. Res.* **2010**, *43* (1), 58–67.
(227) Lewis, D. W.; Ruiz-Salvador, A. R.; Gómez, A.; Rodriguez-Albelo, L. M.; Coudert, F.-X.; Slater, B.; Cheetham, A. K.; Mellot-Draznieks, C. Zeolitic Imidazole Frameworks: Structural and Energetics Trends Compared with Their Zeolite Analogues. *CrystEngComm* **2009**, *11* (11), 2272–2276.

(228) Eslava, S.; Zhang, L.; Esconjauregui, S.; Yang, J.; Vanstreels, K.; Baklanov, M. R.; Saiz, E. Metal-Organic Framework ZIF-8 Films As Low-κ Dielectrics in Microelectronics. *Chem. Mater.* **2013**, *25* (1), 27–33.
(229) Worrall, S. D.; Mann, H.; Rogers, A.; Bissett, M. A.; Attfield, M. P.; Dryfe, R. A. W. Electrochemical Deposition of Zeolitic Imidazolate Framework Electrode Coatings for Supercapacitor Electrodes. *Electrochimica Acta* **2016**, *197*, 228–240.
(230) Zhan, W.; Kuang, Q.; Zhou, J.; Kong, X.; Xie, Z.; Zheng, L. Semiconductor@Metal–Organic Framework Core–Shell Heterostructures: A Case of ZnO@ZIF-8 Nanorods with Selective Photoelectrochemical Response. *J. Am. Chem. Soc.* **2013**, *135* (5), 1926–1933.
(231) Worrall, S. D.; Mann, H.; Rogers, A.; Bissett, M. A.; Attfield, M. P.; Dryfe, R. A. W. Electrochemical Deposition of Zeolitic Imidazolate Framework Electrode Coatings for Supercapacitor Electrodes. *Electrochimica Acta* **2016**, *197*, 228–240.
(232) Butler, K. T.; Worrall, S. D.; Molloy, C. D.; Hendon, C. H.; Attfield, M. P.; Dryfe, R. A. W.; Walsh, A. Electronic Structure Design for Nanoporous, Electrically Conductive Zeolitic Imidazolate Frameworks. *J. Mater. Chem. C* **2017**.
(233) Taberna, P. L.; Simon, P.; Fauvarque, J. F. Electrochemical Characteristics and Impedance Spectroscopy Studies of Carbon-Carbon Supercapacitors. *J. Electrochem. Soc.* **2003**, *150* (3), A292–A300.
(234) Jamnik, J. Impedance Spectroscopy of Mixed Conductors with Semi-Blocking Boundaries. *Solid State Ion.* **2003**, *157* (1), 19–28.
(235) Wang, C.; Hong, J. Ionic/Electronic Conducting Characteristics of LiFePO4 Cathode Materials The Determining Factors for High Rate Performance. *Electrochem. Solid-State Lett.* **2007**, *10* (3), A65–A69.
(236) Sun, L.; Hendon, C. H.; Minier, M. A.; Walsh, A.; Dincă, M. Million-Fold Electrical Conductivity Enhancement in Fe2(DEBDC) versus Mn2(DEBDC) (E = S, O). *J. Am. Chem. Soc.* **2015**, *137* (19), 6164–6167.
(237) Shen, L.; Liang, R.; Luo, M.; Jing, F.; Wu, L. Electronic Effects of Ligand Substitution on Metal–organic Framework Photocatalysts: The Case Study of UiO-66. *Phys. Chem. Chem. Phys.* **2014**, *17* (1), 117–121.
(238) Nasalevich, M. A.; Hendon, C. H.; Santaclara, J. G.; Svane, K.; Linden, B. van der; Veber, S. L.; Fedin, M. V.; Houtepen, A. J.; Veen, M. A. van der; Kapteijn, F.; et al. Electronic Origins of Photocatalytic Activity in d^0 Metal Organic Frameworks. *Sci. Rep.* **2016**, *6*, 23676.
(239) Allen, C. A.; Cohen, S. M. Exploration of Chemically Cross-Linked Metal–Organic Frameworks. *Inorg. Chem.* **2014**, *53* (13), 7014–7019.
(240) Dincă, M.; Léonard, F. Metal–organic Frameworks for Electronics and Photonics. *MRS Bull.* **2016**, *41* (11), 854–857.
(241) Walsh, A.; Butler, K. T.; Hendon, C. H. Chemical Principles for Electroactive Metal–organic Frameworks. *MRS Bull.* **2016**, *41* (11), 870–876.
(242) Blöchl, P. E. Projector Augmented-Wave Method. *Phys. Rev. B* **1994**, *50* (24), 17953–17979.
(243) Kresse, G.; Joubert, D. From Ultrasoft Pseudopotentials to the Projector Augmented-Wave Method. *Phys. Rev. B* **1999**, *59* (3), 1758–1775.
(244) Heyd, J.; Scuseria, G. E.; Ernzerhof, M. Erratum: "Hybrid Functionals Based on a Screened Coulomb Potential" [J. Chem. Phys. 118, 8207 (2003)]. *J. Chem. Phys.* **2006**, *124* (21), 219906.
(245) Becke, A. D. Density-functional Thermochemistry. III. The Role of Exact Exchange. *J. Chem. Phys.* **1993**, *98* (7), 5648–5652.

(246) Lee, C.; Yang, W.; Parr, R. G. Development of the Colle-Salvetti Correlation-Energy Formula into a Functional of the Electron Density. *Phys. Rev. B* **1988**, *37* (2), 785–789.
(247) Butler, K. T.; Buckeridge, J.; Catlow, C. R. A.; Walsh, A. Crystal Electron Binding Energy and Surface Work Function Control of Tin Dioxide. *Phys. Rev. B* **2014**, *89* (11), 115320.
(248) Wang, S.; Yao, W.; Lin, J.; Ding, Z.; Wang, X. Cobalt Imidazolate Metal–Organic Frameworks Photosplit CO2 under Mild Reaction Conditions. *Angew. Chem. Int. Ed.* **2014**, *53* (4), 1034–1038.
(249) Hao, L.; Li, P.; Yang, T.; Chung, T.-S. Room Temperature Ionic Liquid/ZIF-8 Mixed-Matrix Membranes for Natural Gas Sweetening and Post-Combustion CO2 Capture. *J. Membr. Sci.* **2013**, *436*, 221–231.
(250) Yu, D.; Wu, B.; Ge, L.; Wu, L.; Wang, H.; Xu, T. Decorating Nanoporous ZIF-67-Derived NiCo2O4 Shells on a Co3O4 Nanowire Array Core for Battery-Type Electrodes with Enhanced Energy Storage Performance. *J. Mater. Chem. A* **2016**, *4* (28), 10878–10884.
(251) Sun, C.-Y.; Qin, C.; Wang, X.-L.; Yang, G.-S.; Shao, K.-Z.; Lan, Y.-Q.; Su, Z.-M.; Huang, P.; Wang, C.-G.; Wang, E.-B. Zeolitic Imidazolate Framework-8 as Efficient pH-Sensitive Drug Delivery Vehicle. *Dalton Trans.* **2012**, *41* (23), 6906–6909.
(252) Gücüyener, C.; van den Bergh, J.; Gascon, J.; Kapteijn, F. Ethane/Ethene Separation Turned on Its Head: Selective Ethane Adsorption on the Metal−Organic Framework ZIF-7 through a Gate-Opening Mechanism. *J. Am. Chem. Soc.* **2010**, *132* (50), 17704–17706.
(253) Carnie, M. J.; Charbonneau, C.; Davies, M. L.; Troughton, J.; Watson, T. M.; Wojciechowski, K.; Snaith, H.; Worsley, D. A. A One-Step Low Temperature Processing Route for Organolead Halide Perovskite Solar Cells. *Chem. Commun.* **2013**, *49* (72), 7893–7895.
(254) Hendon, C. H.; Yang, R. X.; Burton, L. A.; Walsh, A. Assessment of Polyanion (BF4− and PF6−) Substitutions in Hybrid Halide Perovskites. *J. Mater. Chem. A* **2015**, *3* (17), 9067–9070.
(255) Frost, J. M.; Butler, K. T.; Brivio, F.; Hendon, C. H.; van Schilfgaarde, M.; Walsh, A. Atomistic Origins of High-Performance in Hybrid Halide Perovskite Solar Cells. *Nano Lett.* **2014**, *14* (5), 2584–2590.
(256) Jeon, N. J.; Lee, J.; Noh, J. H.; Nazeeruddin, M. K.; Grätzel, M.; Seok, S. I. Efficient Inorganic–Organic Hybrid Perovskite Solar Cells Based on Pyrene Arylamine Derivatives as Hole-Transporting Materials. *J. Am. Chem. Soc.* **2013**, *135* (51), 19087–19090.
(257) Park, B.; Philippe, B.; Gustafsson, T.; Sveinbjörnsson, K.; Hagfeldt, A.; Johansson, E. M. J.; Boschloo, G. Enhanced Crystallinity in Organic–Inorganic Lead Halide Perovskites on Mesoporous TiO2 via Disorder–Order Phase Transition. *Chem. Mater.* **2014**, *26* (15), 4466–4471.
(258) Butler, K. T.; Frost, J. M.; Walsh, A. Ferroelectric Materials for Solar Energy Conversion: Photoferroics Revisited. *Energy Environ. Sci.* **2015**, *8* (3), 838–848.
(259) Kojima, A.; Teshima, K.; Shirai, Y.; Miyasaka, T. Organometal Halide Perovskites as Visible-Light Sensitizers for Photovoltaic Cells. *J. Am. Chem. Soc.* **2009**, *131* (17), 6050–6051.
(260) Malinkiewicz, O.; Yella, A.; Lee, Y. H.; Espallargas, G. M.; Graetzel, M.; Nazeeruddin, M. K.; Bolink, H. J. Perovskite Solar Cells Employing Organic Charge-Transport Layers. *Nat. Photonics* **2014**, *8* (2), 128–132.

(261) Ono, L. K.; Qi, Y. Research Progress on Organic–inorganic Halide Perovskite Materials and Solar Cells. *J. Phys. Appl. Phys.* **2018**, *51* (9), 093001.
(262) Bhachu, D. S.; Scanlon, D. O.; Saban, E. J.; Bronstein, H.; Parkin, I. P.; Carmalt, C. J.; Palgrave, R. G. Scalable Route to CH3NH3PbI3 Perovskite Thin Films by Aerosol Assisted Chemical Vapour Deposition. *J. Mater. Chem. A* **2015**, *3* (17), 9071–9073.
(263) Burschka, J.; Pellet, N.; Moon, S.-J.; Humphry-Baker, R.; Gao, P.; Nazeeruddin, M. K.; Grätzel, M. Sequential Deposition as a Route to High-Performance Perovskite-Sensitized Solar Cells. *Nature* **2013**, *499* (7458), 316–319.
(264) Butler, K. T.; Vullum, P. E.; Muggerud, A. M.; Cabrera, E.; Harding, J. H. Structural and Electronic Properties of Silver/Silicon Interfaces and Implications for Solar Cell Performance. *Phys. Rev. B* **2011**, *83* (23), 235307.
(265) Momblona, C.; Malinkiewicz, O.; Roldán-Carmona, C.; Soriano, A.; Gil-Escrig, L.; Bandiello, E.; Scheepers, M.; Edri, E.; Bolink, H. J. Efficient Methylammonium Lead Iodide Perovskite Solar Cells with Active Layers from 300 to 900 Nm. *APL Mater.* **2014**, *2* (8), 081504.
(266) Boix, P. P.; Agarwala, S.; Koh, T. M.; Mathews, N.; Mhaisalkar, S. G. Perovskite Solar Cells: Beyond Methylammonium Lead Iodide. *J. Phys. Chem. Lett.* **2015**, *6* (5), 898–907.
(267) Butler, K. T.; Harding, J. H. Atomistic Simulation of Doping Effects on Growth and Charge Transport in Si/Ag Interfaces in High-Performance Solar Cells. *Phys. Rev. B* **2012**, *86* (24), 245319.
(268) Bach, U.; Lupo, D.; Comte, P.; Moser, J. E.; Weissörtel, F.; Salbeck, J.; Spreitzer, H.; Grätzel, M. Solid-State Dye-Sensitized Mesoporous TiO_2 Solar Cells with High Photon-to-Electron Conversion Efficiencies. *Nature* **1998**, *395* (6702), 583–585.
(269) Fabregat-Santiago, F.; Bisquert, J.; Cevey, L.; Chen, P.; Wang, M.; Zakeeruddin, S. M.; Grätzel, M. Electron Transport and Recombination in Solid-State Dye Solar Cell with Spiro-OMeTAD as Hole Conductor. *J. Am. Chem. Soc.* **2009**, *131* (2), 558–562.
(270) Jeon, N. J.; Lee, H. G.; Kim, Y. C.; Seo, J.; Noh, J. H.; Lee, J.; Seok, S. I. O-Methoxy Substituents in Spiro-OMeTAD for Efficient Inorganic–Organic Hybrid Perovskite Solar Cells. *J. Am. Chem. Soc.* **2014**, *136* (22), 7837–7840.
(271) Nguyen, W. H.; Bailie, C. D.; Unger, E. L.; McGehee, M. D. Enhancing the Hole-Conductivity of Spiro-OMeTAD without Oxygen or Lithium Salts by Using Spiro(TFSI)2 in Perovskite and Dye-Sensitized Solar Cells. *J. Am. Chem. Soc.* **2014**, *136* (31), 10996–11001.
(272) T. Murray, A.; M. Frost, J.; H. Hendon, C.; D. Molloy, C.; R. Carbery, D.; Walsh, A. Modular Design of SPIRO-OMeTAD Analogues as Hole Transport Materials in Solar Cells. *Chem. Commun.* **2015**, *51* (43), 8935–8938.
(273) Hückel, E. Quantentheoretische Beiträge zum Benzolproblem. *Z. Für Phys.* **1931**, *70* (3–4), 204–286.
(274) Hendon, C. H.; Tiana, D.; Fontecave, M.; Sanchez, C.; D'arras, L.; Sassoye, C.; Rozes, L.; Mellot-Draznieks, C.; Walsh, A. Engineering the Optical Response of the Titanium-MIL-125 Metal–Organic Framework through Ligand Functionalization. *J. Am. Chem. Soc.* **2013**, *135* (30), 10942–10945.
(275) Kim, H.-S.; Lee, C.-R.; Im, J.-H.; Lee, K.-B.; Moehl, T.; Marchioro, A.; Moon, S.-J.; Humphry-Baker, R.; Yum, J.-H.; Moser, J. E.; et al. Lead Iodide Perovskite Sensitized All-Solid-State Submicron Thin Film Mesoscopic Solar Cell with Efficiency Exceeding 9%. *Sci. Rep.* **2012**, *2*.

(276) Martinez, C. R.; Iverson, B. L. Rethinking the Term “pi-Stacking.” *Chem. Sci.* **2012**, *3* (7), 2191–2201.
(277) Nelson, J.; Kwiatkowski, J. J.; Kirkpatrick, J.; Frost, J. M. Modeling Charge Transport in Organic Photovoltaic Materials. *Acc. Chem. Res.* **2009**, *42* (11), 1768–1778.
(278) Macrae, C. F.; Bruno, I. J.; Chisholm, J. A.; Edgington, P. R.; McCabe, P.; Pidcock, E.; Rodriguez-Monge, L.; Taylor, R.; Streek, J. van de; Wood, P. A. Mercury CSD 2.0 – New Features for the Visualization and Investigation of Crystal Structures. *J. Appl. Crystallogr.* **2008**, *41* (2), 466–470.
(279) Li, W.-S.; Zhang, N.; Sayre, L. M. N1,N10-Ethylene-Bridged High-Potential Flavins: Synthesis, Characterization, and Reactivity. *Tetrahedron* **2001**, *57* (21), 4507–4522.
(280) Kremer, C. B. Alkanolamines. VI. Physiologically Active Compounds. I. The Preparation of Substituted Anilino Alcohols. *J. Am. Chem. Soc.* **1939**, *61* (6), 1321–1324.
(281) Kommi, D. N.; Jadhavar, P. S.; Kumar, D.; Chakraborti, A. K. “All-Water” One-Pot Diverse Synthesis of 1,2-Disubstituted Benzimidazoles: Hydrogen Bond Driven “synergistic Electrophile–nucleophile Dual Activation” by Water. *Green Chem.* **2013**, *15* (3), 798–810.
(282) Sato, K.; Hyodo, M.; Aoki, M.; Zheng, X.-Q.; Noyori, R. Oxidation of Sulfides to Sulfoxides and Sulfones with 30% Hydrogen Peroxide under Organic Solvent- and Halogen-Free Conditions. *Tetrahedron* **2001**, *57* (13), 2469–2476.
(283) Yuan, Y.; Shi, X.; Liu, W. Transition-Metal-Free, Chemoselective Aerobic Oxidations of Sulfides and Alcohols with Potassium Nitrate and Pyridinium Tribromide or Bromine. *Synlett* **2011**, *2011* (04), 559–564.
(284) Xie, N.; Binstead, R. A.; Block, E.; Chandler, W. D.; Lee, D. G.; Meyer, T. J.; Thiruvazhi, M. Reduction of Permanganate by Thioanisole: Lewis Acid Catalysis. *J. Org. Chem.* **2000**, *65* (4), 1008–1015.
(285) Bahrami, K.; Khodaei, M. M.; Sheikh Arabi, M. TAPC-Promoted Oxidation of Sulfides and Deoxygenation of Sulfoxides. *J. Org. Chem.* **2010**, *75* (18), 6208–6213.
(286) Lindén, A. A.; Johansson, M.; Hermanns, N.; Bäckvall, J.-E. Efficient and Selective Sulfoxidation by Hydrogen Peroxide, Using a Recyclable Flavin−[BMIm]PF6 Catalytic System. *J. Org. Chem.* **2006**, *71* (10), 3849–3853.
(287) Shaabani, A.; Rahmati, A.; Farhangi, E. Selective and Efficient Oxidation of Sulfides and Thiols with a 1,1,3,3-Tetramethylguanidine/Br2 Complex. *J. Sulfur Chem.* **2006**, *27* (4), 287–291.
(288) Ali, M. H.; Hedell, J.; Wencewicz, T. Oxidation of Sulfides to Sulfoxides with 1, 3-Dibromo-5, 5-Dimethylhydantoin in the Presence of Hydrated Silica Gel. *J. Sulfur Chem.* **2009**, *30* (2), 160–166.
(289) Hanson, P.; J. Hendrickx, R. A. A.; Lindsay Smith, J. R. An Investigation by Means of Correlation Analysis into the Mechanisms of Oxidation of Aryl Methyl Sulfides and Sulfoxides by Dimethyldioxirane in Various Solvents. *Org. Biomol. Chem.* **2008**, *6* (4), 745–761.
(290) Caupène, C.; Boudou, C.; Perrio, S.; Metzner, P. Remarkably Mild and Simple Preparation of Sulfenate Anions from β-Sulfinylesters: A New Route to Enantioenriched Sulfoxides. *J. Org. Chem.* **2005**, *70* (7), 2812–2815.
(291) Rafiee, E.; Baltork, I. M.; Tangestaninejad, S.; Azad, A.; Moinee, S. Tin(II) Polyoxometalate as an Efficient Catalyst for the Selective Oxidation of Sulfides to Sulfoxides. *Z. Für Naturforschung B* **2014**, *61* (5), 601–606.

(292) Harpp, D. N.; Vines, S. M.; Montillier, J. P.; Chan, T. H. Organic Sulfur Chemistry. Part XXII. The Reaction of Sulfinate Esters with Grignard and Organocopper Lithium Reagents. A Useful Route to Chiral Sulfoxides. *J. Org. Chem.* **1976**, *41* (25), 3987–3992.
(293) Lakouraj, M. M.; Tajbakhsh, M.; Shirini, F.; Tamami, M. V. A. HIO3 in the Presence of Wet SiO2: A Mild and Efficient Reagent for Selective Oxidation of Sulfides to Sulfoxides under Solvent-Free Conditions. *Synth. Commun.* **2005**, *35* (6), 775–784.
(294) Jeyakumar, K.; Chand, D. K. Selective Oxidation of Sulfides to Sulfoxides and Sulfones at Room Temperature Using H2O2 and a Mo(VI) Salt as Catalyst. *Tetrahedron Lett.* **2006**, *47* (27), 4573–4576.
(295) Ning Chen and Jiaxi Xu. HCOOH, an Inexpensive, Convenient, and Practical 13C NMR Solvent for Strong Polar Amino Acids and Their Derivatives. *Lett. Org. Chem.* **2009**, *6* (4), 349–353.
(296) Jerchel, D.; Dippelhofer, L.; Renner, D. Über Langkettige Sulfoxyde, Sulfone Und Sulfoximine. *Chem. Ber.* **1954**, *87* (7), 947–955.
(297) Egami, H.; Katsuki, T. Fe(salan)-Catalyzed Asymmetric Oxidation of Sulfides with Hydrogen Peroxide in Water. *J. Am. Chem. Soc.* **2007**, *129* (29), 8940–8941.
(298) Yang, C.; Jin, Q.; Zhang, H.; Liao, J.; Zhu, J.; Yu, B.; Deng, J. Tetra-(Tetraalkylammonium)octamolybdate Catalysts for Selective Oxidation of Sulfides to Sulfoxides with Hydrogen Peroxide. *Green Chem.* **2009**, *11* (9), 1401–1405.
(299) Gaillard, S.; Papamicaël, C.; Dupas, G.; Marsais, F.; Levacher, V. Ortho-Lithiation of S-Tert-Butyl-S-Phenylsulfoximines. New Route to Enantiopure Sulfinamides via a de-Tert-Butylation Reaction. *Tetrahedron* **2005**, *61* (34), 8138–8147.
(300) Cho, G. Y.; Okamura, H.; Bolm, C. Synthesis and Palladium-Catalyzed Coupling Reactions of Enantiopure P-Bromophenyl Methyl Sulfoximine. *J. Org. Chem.* **2005**, *70* (6), 2346–2349.
(301) Thomas, L. H. The Calculation of Atomic Fields. *Math. Proc. Camb. Philos. Soc.* **1927**, *23* (5), 542–548.
(302) Hohenberg, P.; Kohn, W. Inhomogeneous Electron Gas. *Phys. Rev.* **1964**, *136* (3B), B864–B871.
(303) Vosko, S. H.; Wilk, L.; Nusair, M. Accurate Spin-Dependent Electron Liquid Correlation Energies for Local Spin Density Calculations: A Critical Analysis. *Can. J. Phys.* **1980**, *58* (8), 1200–1211.
(304) Perdew, J. P.; Wang, Y. Accurate and Simple Analytic Representation of the Electron-Gas Correlation Energy. *Phys. Rev. B* **1992**, *45* (23), 13244–13249.
(305) Perdew, J. P.; Chevary, J. A.; Vosko, S. H.; Jackson, K. A.; Pederson, M. R.; Singh, D. J.; Fiolhais, C. Atoms, Molecules, Solids, and Surfaces: Applications of the Generalized Gradient Approximation for Exchange and Correlation. *Phys. Rev. B* **1992**, *46* (11), 6671–6687.
(306) Becke, A. D. Density-functional Thermochemistry. IV. A New Dynamical Correlation Functional and Implications for Exact-exchange Mixing. *J. Chem. Phys.* **1996**, *104* (3), 1040–1046.
(307) Perdew, J. P.; Burke, K.; Ernzerhof, M. Generalized Gradient Approximation Made Simple. *Phys. Rev. Lett.* **1996**, *77* (18), 3865–3868.
(308) Adamo, C.; Barone, V. Toward Reliable Density Functional Methods without Adjustable Parameters: The PBE0 Model. *J. Chem. Phys.* **1999**, *110* (13), 6158–6170.

9 Appendix

This is the Author Accepted Manuscript of an article published in final form as Butler, KT, Worrall, SD, Molloy, CD, Hendon, CH, Attfield, MP, Dryfe, RAW & Walsh, A 2017, 'Electronic structure design for nanoporous, electrically conductive zeolitic imidazolate frameworks', Journal of Materials Chemistry C, vol. 5, no. 31, pp. 7726-7731. and available online via https://doi.org/10.1039/c7tc03150e

9.1 Electronic structure design for nanoporous, electrically conductive seolitic imidazolate frameworks

Journal Name

ARTICLE TYPE

Cite this: DOI: 10.1039/xxxxxxxxxx

Electronic structure design for nanoporous, electrically conductive zeolitic imidazolate frameworks

Keith T. Butler,*[a] Stephen D. Worrall,[b], Christopher D. Molloy [a], Christopher H. Hendon [c], Martin P Attfield [b], Robert AW Dryfe [d] and Aron Walsh[e,f]

Received Date
Accepted Date

DOI: 10.1039/xxxxxxxxxx

www.rsc.org/journalname

Electronic structure calculations are used to develop design rules for enhanced electrical conductivity in zeolitic imidazolate frameworks. The electrical resistivity of Co^{2+} based zeolitic imidazolate frameworks has previously been found to be ~ 1000 times lower than that of Zn^{2+} based materials. The electrical conductivity of the frameworks can also be tuned by ligand molecule selection. Using density functional theory calculations, this controllable electrical conductivity is explained in terms of tuneable conduction band edge character, with calculations revealing the improved hybridisation and extended band character of the Co^{2+} frameworks. The improvements in the methylimidazolate frameworks are understood in terms of improved frontier orbital matching between metal and ligand. The modular tuneability and previously demonstrated facile synthesis provides a route to rational design of stable framework materials for electronic applications. By outlining these design principles we provide a route to the future development of stable, electrically conductive zeolitic imidazolate frameworks.

Metal-organic frameworks (MOFs) are nanoporous materials with intrinsically ordered framework structures based on modular metal cluster and organic ligand compositions. The combination of topological control and chemical diversity make MOFs attractive candidates for a variety of applications. To date, much of the research in the area of MOFs has concentrated on exploiting their large surface area and great success has been achieved in fields such as gas-storage, separation and chemical catalysis [1–3] and as super-capacitors for energy storage. [4] Recent reports of electrical conductivity in MOF structures could open the door to many new applications, such as battery cathodes [5,6], electrocatalysts [7,8], transistors [9–12] and photovoltaics. [13,14] MOFs have already made an impact as components in thermoelectrics [15] and memory storage. [16–18] Despite the promise held by MOFs for the design of modular electronic components with molecular tunability, they are often mechanically and thermally unstable, hampering widespread application.

The exciting advances in conductive MOFs have resulted in the emergence of design principles for enhancing electrical properties by modular tuning. [19,20] The conduction mechanisms of MOFs have been divided into three broad classes: (i) Through space transport, via π–stacking; (ii) through bond transport, relying on covalent bond networks and (iii) hopping transport, where charge carriers make discrete jumps between structural units. [21] The first two mechanisms (band transport) rely on delocalised wavefunctions across the system and are associated with higher carrier mobilities than hopping transport. [22] Typically in MOFs, however, band transport is difficult to achieve, due to poor hybridisation between metal linker and organic ligand units. Possible design strategies for achieving conductive MOFs include the addition of electro-activating molecules, [23] or designing structures with conductive $(MX)_\infty$ chains [21] – in both cases tunable conductivity is achieved by establishing conductive pathways of continuous wavefunction overlap throughout the structure.

Zeolitic imidazolate frameworks (ZIFs) maintain the chemical tunability of MOFs with the virtue of possessing the thermal and chemical stability of zeolite-like materials. [24–28] ZIFs are a subclass of MOFs, built around the M-Im-M motif, where M is a divalent tetrahedral cation (typically, but not exclusively, Zn^{2+} or Co^{2+}) and Im is an imidazolate anion [29,30]. There have been few reports of electronic device applications for ZIFs; they are typically viewed as poor electrical conductors. Nonetheless, their use as high-κ dielectrics [31], in photoelectrochemical core-shell het-

[a] Department of Chemistry, University of Bath, BA2 7AY, UK; E-mail: k.t.butler@bath.ac.uk
[b] Centre for Nanoporous Materials, School of Chemistry, University of Manchester, Oxford Road, Manchester M13 9PL, United Kingdom
[c] Department of Chemistry, Massachusetts Institute of Technology, Cambridge, Massachusetts 02139, USA.
[d] School of Chemistry, University of Manchester, Oxford Road, Manchester M13 9PL, United Kingdom
[e] Department of Materials, Imperial College London, Exhibition Road, London, SW7 2AZ, UK.
[f] Department of Materials Science and Engineering, Yonsei University, Seoul, South Korea.

This journal is © The Royal Society of Chemistry [year]

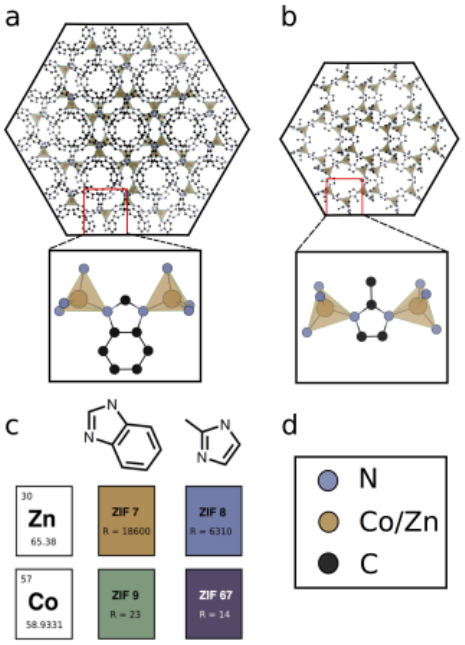

Fig. 1 (a) The structure of ZIF-7(9), with a close up of the Zn(Co)-ligand-Zn(Co) conductive bridge. (b) The structure of ZIF-8(67), with a close up of the Zn(Co)-ligand-Zn(Co) conductive bridge. (c) The modular make-up of ligand and metal for construction of the four frameworks studies, each framework is reported along with its room temperature electrical resistance in Ω. (d) Colour key for (a) and (b) carbon: black; nitrogen: petrol blue; M(II): gold.

erostructures[32] and super-capacitors[33] has been recently been reported, which challenges the perception of ZIFs as electronically inert materials.

Here, we set out to elucidate molecular design principles for achieving conductive ZIF materials using electronic structure calculations. We concentrate on four ZIFs, comprised of two metal cations, Zn^{2+} (d^{10}) and Co^{2+} (d^7) and two substituted imidazolate ligands, methylimidazolate (mIM) and benzimidazolate (bIM). Some of us have previously demonstrated how the Co^{2+}-based ZIF-67 has more than 1000 times greater electrical conductivity than Zn^{2+}-based ZIF-8 or ZIF-7. In this work we additionally characterise ZIF-9, which is Co^{2+}-based, but has the same ligand as ZIF-7, see Figure 1. The comparison of four materials based on permutations of two metals and two ligands ensures frameworks with similar geometric structures, consisting of metal ions in a tetrahedral environment, bridged by organic linkers, which bond to the metals through N lone pairs, see Figure 1. The homogeniety of the geometries allows us to isolate the electronic structure influence on electrical conductivity, highlighting the role of orbital symmetry, electron configuration, ionisation potential and electron affinity. We demonstrate how choice of metal (based on ionisation potential) and design of ligands (for improved hybridisation) can be used to lead to the development of conductive, stable ZIF materials.

ZIF coated electrodes were prepared by a process of electrochemical deposition, which has been previously applied to the growth of ZIF thin films[34,35]. This approach to thin film growth has the great advantage of not requiring the high temperatures or long synthesis times of many other MOF thin film preparation routes and has been extensively reported for porous material synthesis[36,37]. The use of mild conditions and lack of requirement of any specialised equipment also makes electrochemically deposited ZIFs promising from a scale-up and applications perspective. Frameworks can easily be coated onto electrodes where epitaxial relations between the substrate and framework exist.[38] ZIF coated electrodes were synthesised by holding two metal foil electrodes in a heated, de-aerated electrolyte solution containing linker under a fixed potential difference of 2.5 V for a set time. The synthesis and characterisation of ZIF-7, ZIF-8 and ZIF-67 have been reported previously by some of us [33], the details for ZIF-9 are presented in the supporting information.

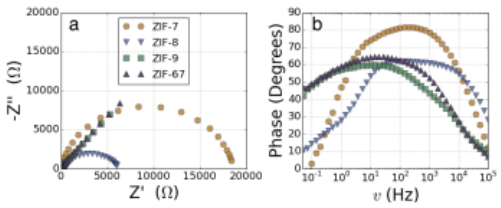

Fig. 2 (a) Nyquist plots of ZIF-7, ZIF-8, ZIF-9 and ZIF-67. (b) Bode phase plots of ZIF-7, ZIF-8, ZIF-9 and ZIF-67.

We have previously reported the electrochemical impedance spectroscopy (EIS) results for ZIF-7, ZIF-8 and ZIF-67[33], here we have repeated the experiments, including ZIF-9 in the set for consistency. EIS in a symmetrical two electrode configuration, of ZIF-7, ZIF-8, ZIF-9 and ZIF-67, was performed to obtain electrical resistance characteristics, full details are available in the supporting information (SI). Nyquist plots of the two Zn^{2+} ZIFs (ZIF-7 and ZIF-8; Figure 2 a) display a clear semi-circular shape, those of the Co^{2+} ZIFs (ZIF-9 and ZIF-67) are instead composed almost entirely of a ~ 45°, linear, diffusion dominated region with almost no discernible semi-circular character. The data were fitted with a Randles circuit to obtain values for the solution resistance (R_s, determined by the electrolyte) and the charge-transfer resistance (R_{CT}, determined by the framework).

The resistance of the Co^{2+} based materials is around 1000 times smaller than that of the Zn^{2+} based materials, as previously reported[33], Table 1. A new finding is that the resistance of the mIM frameworks is significantly smaller for both metals than the

This journal is © The Royal Society of Chemistry [year]

Table 1 Electrical properties of the materials studied. Charge transfer resistance (R_{CT}) and conductivity σ from electrical impedance spectroscopy. Ionisation potential (IP) and electronic band gap (E_g) from hybrid DFT calculations.

Material	R_{CT} (Ω)	σ (S cm^{-1})	IP (eV)	E_g (eV)
ZIF-7	18600	$4.5 - 9.0\times10^{-10}$	5.61	4.82
ZIF-8	6310	$1.3 - 2.6\times10^{-9}$	5.73	5.29
ZIF-9	23	$3.6 - 7.3\times10^{-7}$	5.21	3.01
ZIF-67	14	$0.6 - 1.2\times10^{-6}$	5.62	4.25

resistance in the bIM frameworks. The Bode phase plots (Figure 2 b) similarly show a significant difference in the behaviour between the Zn^{2+} and Co^{2+} ZIFs. The shape of the Co^{2+} ZIF plots are characteristic of pseudocapacitive behaviour,[39] with the initial plateau in the phase at $\sim 45°$ followed by a steady decrease in phase towards 0° with increasing frequency. The shape of the Zn^{2+} ZIF plots show a different behaviour with the phase starting close to 0° at low frequency, before rising to plateau between 60° and 80° at medium frequencies and then finally decreasing again at higher frequencies.

Following the analysis of Jamnik[40] and developed by Wang and Hong,[41] the electronic and ionic contributions to mixed conductivity can be separated by analysis of the impedance frequency response. The conductivities, reported in Table 1, of the samples are obtained by normalising for the MOF electrode area (1.2 cm^2) and film thickness (10 - 20 μm). We note that even the highest conductivity is significantly lower than some of the champion MOF conductors reported to date;[19] however, R_{CT} represents an upper limit to the resistance of the ZIF and includes contributions from interface contact resistance and other sources extrinsic to the ZIF. Therefore, the conductivities reported here are a conservative estimate of the framework conductivity and are nonetheless of the order of conductivities found in other promising MOFs and organic conductors.[42]

To understand the differences in conductivity of the frameworks, we have performed density functional theory (DFT) calculations. We first consider the full framweork, employing periodic boundary conditions and projector augmented waves[43] within the VASP[44] code, we use a hybrid functional (HSE06[45]) to accurately represent the electronic structure, full details are available in the SI. The electronic density of states (DOS) of the four materials are presented in Figure 3, the DOS and electronic energy levels are calculated based on evacuated pore structures, available as .cif files (see data access statement). We begin by examining the effect of metal substitution, ZIF-7 and ZIF-9 are structurally analogous, as are ZIF-8 and ZIF-67. In both cases there is a marked increase in the metal character at the conduction band edge of the electronic DOS comparing the Co^{2+} frameworks to the Zn^{2+} frameworks. In both Co^{2+} based materials there is close to 50% metal contribution to the conduction band edge, this results from the d^7 electron configuration of Co^{2+}, compared to the d^{10} configuration of Zn^{2+}. In the Co^{2+} frameworks the empty d-states of the metal are available to hybridise with the ligand LUMO levels. The tetragonal environment results in a crystal field splitting on the Co^{2+} with partially occupied d_{xy}, d_{xz} and d_{yz} states, which can interact with the sp^2 hybridised N. This hybridisation results in extended conduction states, bridging the imidazolate and the metal (Figure 4 b) and results in the greatly improved conductivity in the Co^{2+} frameworks. This finding highlights the importance of choosing metal ions with relatively shallow ionisation potentials, which allow them to participate in the formation of band edges in the framework, we note that a similar improvement in conductivity was reported when replacing Mn^{2+} by Fe^{2+}, when the loosely bound Fe^{2+} electrons form the valence band edge.[42]

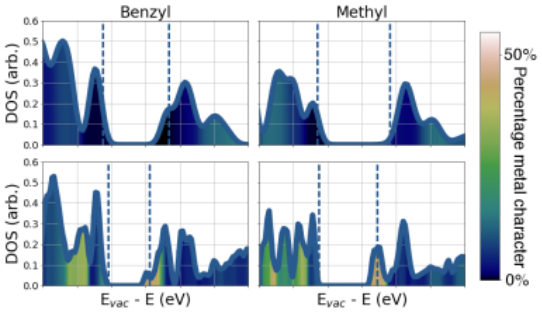

Fig. 3 Electronic density of states plots of the four materials studied, showing the degree of metal contribution to the electronic states. The valence and conduction bad edges are highlighted by dashed blue lines. Upper row, Zn^{2+} ZIFs; Lower Co^{2+} ZIFs.

Another important difference between Co^{2+} and Zn^{2+} is the availability of alternative oxidation states for Co, i.e. Co^{3+}. The availability of multiple oxidation states promotes hopping transport in a framework,[46,47] with charges being transferred between metal centres via the organic ligand. This type of conduction is dependent on the overlap in energy of the ligand and linker frontier orbitals.[46] In ZIFs we know the configuration of the metal atomic orbitals, in order to assess the possibility of hopping of oxidation states we require knowledge of the ligand frontier orbitals.

We now turn our attention to the role of the ligand in determining the framework conductivity. In the case of both metals the framework with the mIm shows superior conductivity. This cannot be ascribed to a separation effect, as the M ⋯ M distance in the presence of both ligands is very similar; we therefore suggest that the origin of this effect is related to the electronic structure of the ligand. The conduction pathway in the ZIF frameworks depends on the ligand N to metal interaction. The strength of the overlap between the ligand and the metal depends on the extent to which their wavefunctions overlap; in this case ligand N wavefunction with metal d_{xy},d_{xz} or d_{yz} orbitals. Given the orientation of the ligands tetrahedrally about the cation, the overlap of the orbitals with the d-orbitals of the metal is highly dependent on the spatial extent of the ligand LUMO. The spin resolved density of states (supporting information, Figure S4) shows that in each of the Co materials the conduction band minimum is formed from a single spin-down channel on the Co, hybridised with a spin-down

channel on the N. This spin-dependent band edge structure can have important consequences for the carrier transport and suggests the intriguing possibility of Co-based ZIF spin filters.

We have performed quantum chemical calculations of the charged ligand molecules to provide an understanding of the spatial resolution of the ligand wavefunctions. These calculations of the molecules in isolation are performed using GAUSSIAN09 [48], with the B3LYP functional [49,50] and 6-31G* basis sets. [51] Using the MACRODENSITY package, [52] we analyse wavefunctions of the LUMO levels of the mIm and bIm studied here, calculating the spherical average of the wavefunction coefficients about the N atoms, with a radius of 2Å. The extended π system of the bIm withdraws density away from the N sites, resulting in an average of coefficients centred at the N site of 2.5×10^{-4} a.u., compared to 2.2×10^{-3} a.u. at the mIm N sites. The contours of the wavefunction coefficients are plotted in Figure 3 (c) and (d); the greater density in the mIm is clear from this plot.

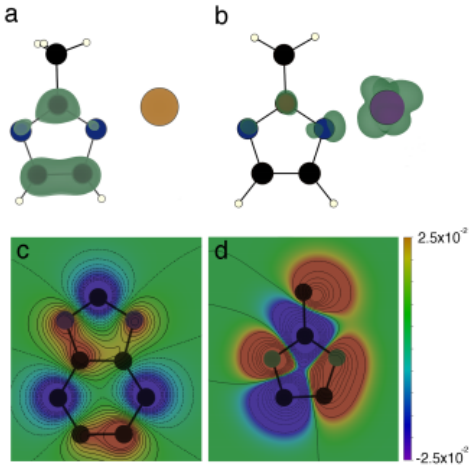

Fig. 4 The effects of changing linker and ligand. (a) Conduction band minimum isosurface in ZIF-8; (b) conduction band minimum isosurface in ZIF-67. Both isosurfaces are at 0.00025 eÅ^{-3} and concentrate on the structural unit displayed in Figure 1, N atoms are in blue, C atoms are black, H atoms are white, Zn^{2+} is beige and Co^{2+} is indigo. (c) Contour plot of the of the LUMO orbital coefficients of bIm, C is black and N is grey (H atoms are suppressed) (d) contour plot of the of the LUMO orbital coefficients of mIm, C is black and N is grey (H atoms are suppressed). Wavefunction coefficients are in atomic units.

Of the three conduction mechanisms outlined earlier the conduction in ZIFs cannot be via $\pi-$stacking and is unlikely to occur through extended covalent bonds; therefore, it is likely to be mediated by a hopping mechanism. As outlined in a recent review of these mechanisms the overlap of ligand/linker wavefunctions and the availability of variable linker oxidation states are crucial for the efficacy of hopping transport in frameworks. We propose that conductive ZIFs can be rationally designed by choosing: (i) a metal cation with a shallow second ionisation potential and partially occupied/unoccupied d_{xy},d_{xz},d_{yz} orbitals and (ii) a ligand with high LUMO density at the N sites the degree of hybridisation can be maximised, promoting the formation of an extended conduction band. A systematic search of metal species screening for (II) oxidation states in tetrahedral environments, with a suitable second ionisation potential was performed using our recently published SMACT code, [53] suggesting Fe^{2+} as a promising cation replacement for Co^{2+}. Screening of candidate ligands can be achieved through relatively low-cost calculations of molecular imidazolate species.

We have studied the electrical conductivity of four ZIF materials, using electronic structure calculations to explain observed trends. The four frameworks are made from a combination of two metals (Zn^{2+} and Co^{2+}) and two ligands (bIm and mIm). The Co^{2+} frameworks display a significantly greater electrical conductivity than the Zn^{2+} based frameworks, by 3 to 4 orders of magnitude, as reported previously [33]. Here, we explain how this increased conductivity in Co^{2+} based frameworks is linked to the availability of empty d-states for forming the conduction band edge. We find that mIm frameworks are more conductive than the bIm frameworks by 1.5 to 2 times; this is explained by the wavefunction shape of LUMO level of mIm, which offers improved hybridisation with the metal linkers to form conduction pathways. This general principle of ensuring unoccupied d-states with the correct orbital symmetry to overlap with ligands, along with ligand frontier orbital levels optimised through the addition of electron donating or withdrawing groups, offers a route to rational design of electrically conductive zeolitic imidazolate frameworks. Such electrically conductive ZIFs would open the way for enhanced functionality of frameworks, where they are used in fields such as gas separation [54], CO_2 catalysis [55], energy storage [56], mixed matrix membranes [57] and drug delivery [58].

We acknowledge membership of the UK's HPC Materials Chemistry Consortium (EPSRC EP/L000202) and access to computational resources through PRACE. A.W. acknowledges support from the Royal Society for a University Research Fellowship and K.T.B. is funded by EPSRC (EP/M009580/1 and EP/J017361/1). SDW acknowledges the NoWNANO DTC for funding. RAWD would like to thank the EPSRC (UK, grant references EP/K039547/1 and EP/K016954/1) for support.

Data access statement: analysis scripts used examine the density of states, and the optimised crystal structures are available on-line, free of charge, from https://github.com/keeeto/conductive-zifs-data.

References

1 K. Sumida, D. L. Rogow, J. A. Mason, T. M. McDonald, E. D. Bloch, Z. R. Herm, T.-H. Bae and J. R. Long, *Chem. Rev.*, 2012, **112**, 724–781.

2 J. Gascon, A. Corma, F. Kapteijn and F. X. L. i Xamena, *ACS Catal.*, 2014, **4**, 361–378.

3 J. Liu, L. Chen, H. Cui, J. Zhang, L. Zhang and C.-Y. Su, *Chem. Soc. Rev.*, 2014, **43**, 6011–6061.

This journal is © The Royal Society of Chemistry [year]

4 D. Sheberla, J. C. Bachman, J. S. Elias, C.-J. Sun, Y. Shao-Horn and M. Dincă, *Nat. Mater.*, 2016.

5 Z. Zhang, H. Yoshikawa and K. Awaga, *J. Am. Chem. Soc.*, 2014, **136**, 16112–16115.

6 G. Férey, F. Millange, M. Morcrette, C. Serre, M.-L. Doublet, J.-M. Grenèche and J.-M. Tarascon, *Angew. Chem. Int. Ed.*, 2007, **46**, 3259–3263.

7 B. Nohra, H. E. Moll, L. M. R. Albelo, P. Mialane, J. Marrot, C. Mellot-Draznieks, M. O'Keeffe, R. N. Biboum, J. Lemaire, B. Keita, L. Nadjo and A. Dolbecq, *J. Am. Chem. Soc.*, 2011, **133**, 13363–13374.

8 S. R. Ahrenholtz, C. C. Epley and A. J. Morris, *J. Am. Chem. Soc.*, 2014, **136**, 2464–2472.

9 M. Usman, S. Mendiratta and K.-L. Lu, *Adv. Mater.*, 2017, **29**, 1605071–n/a.

10 K. T. Butler, C. H. Hendon and A. Walsh, *ACS Appl. Mater. Inter.*, 2014, **6**, 22044–22050.

11 M. G. Campbell, D. Sheberla, S. F. Liu, T. M. Swager and M. Dincă, *Angew. Chem. Int. Ed*, 2015, **54**, 4349–4352.

12 L. E. Kreno, K. Leong, O. K. Farha, M. Allendorf, R. P. Van Duyne and J. T. Hupp, *Chem. Rev.*, 2012, **112**, 1105–25.

13 V. Stavila, a. a. Talin and M. D. Allendorf, *Chem. Soc. Rev.*, 2014.

14 K. T. Butler, C. H. Hendon and A. Walsh, *J. Am. Chem. Soc.*, 2014, **136**, 2703–6.

15 K. J. Erickson, F. Léonard, V. Stavila, M. E. Foster, C. D. Spataru, R. E. Jones, B. M. Foley, P. E. Hopkins, M. D. Allendorf and A. A. Talin, *Adv. Mater.*, 2015, **27**, 3453–3459.

16 L. Pan, Z. Ji, X. Yi, X. Zhu, X. Chen, J. Shang, G. Liu and R.-W. Li, *Adv. Funct. Mater.*, 2015, **25**, 2677–2685.

17 S. M. Yoon, S. C. Warren and B. A. Grzybowski, *Angew. Chem. Int. Ed*, 2014, **53**, 4437–4441.

18 S. D. Worrall, M. A. Bissett, W. Hirunpinyopas, M. P. Attfield and R. A. W. Dryfe, *J. Mater. Chem. C*, 2016, **4**, 8687–8695.

19 L. Sun, M. G. Campbell and M. Dincă, *Angew. Chem. Int. Ed*, 2016, **55**, 3566–3579.

20 R. Grau-Crespo, A. Aziz, A. W. Collins, R. Crespo-Otero, N. C. HernÃąndez, L. M. Rodriguez-Albelo, A. R. Ruiz-Salvador, S. Calero and S. Hamad, *Angewandte Chemie International Edition*, 2016, **55**, 16012–16016.

21 S. S. Park, E. R. Hontz, L. Sun, C. H. Hendon, A. Walsh, T. Van Voorhis and M. Dincă, *J. Am. Chem. Soc.*, 2015, **137**, 1774–1777.

22 J.-L. Brédas, D. Beljonne, V. Coropceanu, and J. Cornil, *Chem. Rev.*, 2004, **104**, 4971–5004.

23 A. A. Talin, A. Centrone, A. C. Ford, M. E. Foster, V. Stavila, P. Haney, R. A. Kinney, V. Szalai, F. El Gabaly, H. P. Yoon, F. Léonard and M. D. Allendorf, *Science*, 2014, **343**, 66–9.

24 S. Krause, V. Bon, I. Senkovska, U. Stoeck, D. Wallacher, D. M. Többens, S. Zander, R. S. Pillai, G. Maurin, F.-X. Coudert and S. Kaskel, *Nature*, 2016, **532**, 348–352.

25 B. Chen, Z. Yang, Y. Zhu and Y. Xia, *J. Mater. Chem. A*, 2014, **2**, 16811–16831.

26 L. B. du Bourg, A. U. Ortiz, A. Boutin and F.-X. Coudert, *APL Materials*, 2014, **2**, 124110.

27 D. Fairen-Jimenez, S. A. Moggach, M. T. Wharmby, P. A. Wright, S. Parsons and T. Düren, *J. Am. Chem. Soc*, 2011, **133**, 8900–8902.

28 S. Moggach, T. Bennett and A. Cheetham, *Angew. Chem.*, 2009, **121**, 7221–7223.

29 A. Phan, C. J. Doonan, F. J. Uribe-Romo, C. B. Knobler, M. O'Keeffe and O. M. Yaghi, *Acc. Chem. Res.*, 2010, **43**, 58–67.

30 D. W. Lewis, A. R. Ruiz-Salvador, A. Gomez, L. M. Rodriguez-Albelo, F.-X. Coudert, B. Slater, A. K. Cheetham and C. Mellot-Draznieks, *CrystEngComm*, 2009, **11**, 2272–2276.

31 S. Eslava, L. Zhang, S. Esconjauregui, J. Yang, K. Vanstreels, M. R. Baklanov and E. Saiz, *Chem. Mater.*, 2013, **25**, 27–33.

32 W. wen Zhan, Q. Kuang, J. zhang Zhou, X. jian Kong, Z. xiong Xie and L. sun Zheng, *J. Am. Chem. Soc*, 2013, **135**, 1926–1933.

33 S. D. Worrall, H. Mann, A. Rogers, M. A. Bissett, M. P. Attfield and R. A. Dryfe, *Electrochim. Acta*, 2016, **197**, 228 – 240.

34 W.-w. Zhan, Q. Kuang, J.-z. Zhou, X.-j. Kong, Z.-x. Xie and L.-s. Zheng, *Journal of the American Chemical Society*, 2013, **135**, 1926–1933.

35 H. Al-Kutubi, A. Dikhtiarenko, H. R. Zafarani, E. J. R. Sudholter, J. Gascon and L. Rassaei, *CrystEngComm*, 2015, **17**, 5360–5364.

36 M. Li and M. Dincă, *J. Am. Chem. Soc*, 2011, **133**, 12926–12929.

37 M. Li and M. Dincă, *Chem. Mater.*, 2015, **27**, 3203–3206.

38 K. T. Butler, Y. Kumagai, F. Oba and A. Walsh, *J. Mater. Chem. C*, 2016, **4**, 1149–1158.

39 P. L. Taberna, P. Simon and J. F. Fauvarque, *J. Electrochem. Soc.*, 2003, **150**, A292.

40 J. Jamnik, *Sol. State Ion.*, 2003, **157**, 19 – 28.

41 C. Wang and J. Hong, *Electrochem. Solid-State Lett.*, 2007, **10**, A65–A69.

42 L. Sun, C. H. Hendon, M. a. Minier, A. Walsh and M. Dincă, *J. Am. Chem. Soc.*, 2015, **137**, 6164–7.

43 P. E. Blöchl, *Phys. Rev. B*, 1994, **50**, 17953–17979.

44 G. Kresse, *Phys. Rev. B*, 1999, **59**, 1758–1775.

45 J. Heyd, G. E. Scuseria and M. Ernzerhof, *J. Chem. Phys.*, 2006, **124**, 219906.

46 M. Dincă and F. Léonard, *MRS Bull.*, 2016, **41**, 854–857.

47 A. Walsh, K. T. Butler and C. H. Hendon, *MRS Bull.*, 2016, **41**, 870–876.

48 M. J. Frisch, G. W. Trucks, H. B. Schlegel, G. E. Scuseria, M. A. Robb, J. R. Cheeseman, G. Scalmani, V. Barone, G. A. Petersson, H. Nakatsuji, X. Li, M. Caricato, A. Marenich, J. Bloino, B. G. Janesko, R. Gomperts, B. Mennucci, H. P. Hratchian, J. V. Ortiz, A. F. Izmaylov, J. L. Sonnenberg, D. Williams-Young, F. Ding, F. Lipparini, F. Egidi, J. Goings, B. Peng, A. Petrone, T. Henderson, D. Ranasinghe, V. G. Zakrzewski, J. Gao, N. Rega, G. Zheng, W. Liang, M. Hada, M. Ehara, K. Toyota, R. Fukuda, J. Hasegawa, M. Ishida, T. Nakajima, Y. Honda, O. Kitao, H. Nakai, T. Vreven, K. Throssell, J. A.

Montgomery, Jr., J. E. Peralta, F. Ogliaro, M. Bearpark, J. J. Heyd, E. Brothers, K. N. Kudin, V. N. Staroverov, T. Keith, R. Kobayashi, J. Normand, K. Raghavachari, A. Rendell, J. C. Burant, S. S. Iyengar, J. Tomasi, M. Cossi, J. M. Millam, M. Klene, C. Adamo, R. Cammi, J. W. Ochterski, R. L. Martin, K. Morokuma, O. Farkas, J. B. Foresman, and D. J. Fox, *Gaussian 09 Revision A.02*, Gaussian Inc. Wallingford CT 2016.

49 A. D. Becke, *J. Chem. Phys.*, 1993, **98**, 5648–5652.

50 C. Lee, W. Yang and R. G. Parr, *Phys. Rev. B*, 1988, **37**, 785–789.

51 R. Ditchfield, W. J. Hehre and J. A. Pople, *J. Chem. Phys.*, 1971, **54**, 724–728.

52 K. T. Butler, J. Buckeridge, C. R. A. Catlow and A. Walsh, *Phys. Rev. B*, 2014, **115320**, 1–6.

53 D. W. Davies, K. T. Butler, A. J. Jackson, A. Morris, J. M. Frost, J. M. Skelton and A. Walsh, *Chem*, 2016, **1**, 617 – 627.

54 C. G"ucüyener, J. van den Bergh, J. Gascon and F. Kapteijn, *Journal of the American Chemical Society*, 2010, **132**, 17704–17706.

55 S. Wang, W. Yao, J. Lin, Z. Ding and X. Wang, *Angewandte Chemie International Edition*, 2014, **53**, 1034–1038.

56 D. Yu, B. Wu, L. Ge, L. Wu, H. Wang and T. Xu, *J. Mater. Chem. A*, 2016, **4**, 10878–10884.

57 L. Hao, P. Li, T. Yang and T.-S. Chung, *Journal of Membrane Science*, 2013, **436**, 221 – 231.

58 C.-Y. Sun, C. Qin, X.-L. Wang, G.-S. Yang, K.-Z. Shao, Y.-Q. Lan, Z.-M. Su, P. Huang, C.-G. Wang and E.-B. Wang, *Dalton Trans.*, 2012, **41**, 6906–6909.

This journal is © The Royal Society of Chemistry [year]

Modular design and control of nanoporous, electrically conductive zeolitic imidazolate frameworks

Keith T. Butler, Stephen Worrall, Christopher D. Molloy, Christopher H. Hendon, Martin P Attfield, Robert AW Dryfe, and Aron Walsh

Supporting Information

1. Experimental

1.1. Materials

Co foil (99.9%) and Zn foil (99.9%) were obtained from Advent Research Materials. 2-methylimidazole (mIM) (99%) was obtained from Aldrich. Benzimidazole (bIM) (99%), N,N-dimethylformamide (DMF) (99.7%) and tetraethylammonium tetrafluoroborate (TEATFB) (99%) were obtained from Alfa Aesar. Acetonitrile (HPLC grade) was obtained from Fisher Scientific. Ultra-pure water (18.2 MΩ cm resistivity) was obtained from a Milli-Q Millipore Direct 8 purification unit. Methanol (≥99.8%), tributylmethylammonium methyl sulphate (TBMAMS) (≥95%) and Whatman Grade 1 Qualitative Filter Paper were obtained from Sigma Aldrich. All materials were used as received.

1.2. Synthesis of ZIF coated electrodes

ZIF coated electrodes were synthesised by holding two metal foil electrodes (geometric area ~16 cm^2 in the case of Zn and 2 cm^2 in the case of Co) ~ 2 cm apart in a heated, de-aerated electrolyte solution containing linker. A PGSTAT302N potentiostat (Metrohm Autolab B.V., The Netherlands) was used to apply a fixed potential difference of 2.5 V between the two metal foil electrodes for a set time. Table 1 contains the specific conditions used for the synthesis of ZIF-7, 8, 9 and 67 respectively. The coated anodes were rinsed three times with methanol post synthesis to remove unreacted linker and supporting electrolyte.

Table 1 Synthetic conditions used for the anodic growth of ZIF-7, 8, 9 and 67 coatings.

	Electrodes	Linker c/mol dm^{-3}	vol% DMF / vol% H_2O	MTBAMS c/ mol dm^{-3}	T/°C	t/min
ZIF-7	Zn	bIM 0.52	100 / 0	0.06	55	120
ZIF-8	Zn	mIM 3.00	0 / 100	0.06	55	60
ZIF-9	Co	bIM 0.24	75 / 25	0.06	100	210
ZIF-67	Co	mIM 0.24	75 / 25	0.06	100	300

1.3. Characterisation of ZIF coated electrodes

The identity of the ZIF on a given anode surface was confirmed using a PANalytical X'Pert X-ray diffractometer. Powder X-ray diffraction (PXRD) patterns of the coatings were obtained using Cu-Kα radiation at 40 kV and 30 mA, in the range 5 – 30 2θ° (with a step size of 0.017 2θ° and scan step time of 66 s) whilst spinning at 16 revolutions s^{-1}.

The ZIF coatings were further characterised on the anode surface using a FEI Quanta 200 (Environmental) Scanning Electron Microscope (E)SEM. All images were obtained at 20kV, under low vacuum with a water vapour pressure of 0.83 Torr utilising a backscattered electron detector.

1.4. Electrochemical impedance spectroscopy

Electrochemical impedance spectroscopy (EIS) measurements were performed in a symmetrical two electrode configuration. ZIF-7 or ZIF-8 coated, 2 cm^2 Zn foil electrodes and ZIF-9 or ZIF-67 coated, 2 cm^2 Co foil electrodes were separated by Whatman Grade 1 Qualitative Filter Paper in 1M TEATFB in acetonitrile. EIS was performed using a PGSTAT302N potentiostat (Metrohm Autolab B.V., The Netherlands) over the frequency range 1 MHz – 200 mHz with a 10 mV RMS perturbation voltage. The experimental Nyquist plots were fitted with the Randles circuit, with the Warburg element removed, giving the simplified Randles circuit for the fitting of the plots for ZIF-7 and ZIF-8 due to the absence of a linear component at low frequency.

2. Results and Discussion

2.1. Characterisation of ZIF coated electrodes

PXRD confirms that the coatings obtained on the Zn and Co electrode surfaces are ZIF-7 and ZIF-8, and ZIF-9 and ZIF-67, respectively (Figure 1). The synthesis of a ZIF-9 coating via the anodic dissolution technique is reported here for the first time, whilst the other three ZIFs have been obtained as coatings via this method previously.[1] SEM images of the ZIF coatings (Figure 2) show that there is no obvious difference in size the irregular particles that compose the different coatings.

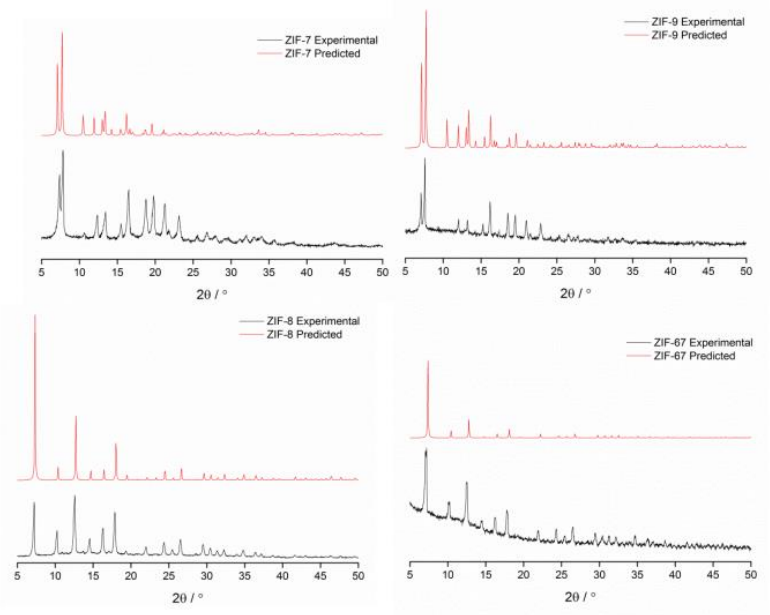

Figure S1 PXRD patterns of the coatings of the bIM ZIFs, ZIF-7 and ZIF-9 (A) and the mIM ZIFs, ZIF-8 and ZIF-67 (B) compared to predicted patterns.

2.2. Electrochemical impedance spectroscopy

The Nyquist plots (Figure 3A) for ZIF-7, ZIF-8, ZIF-9 and ZIF-67 show that the solution resistance values R_s for all four ZIF coated electrodes, defined by the real axis value at the high frequency intercept of the plot, are indistinguishable from one another on this scale. As R_s is primarily a function of the electrolyte solution this similarity is to be expected. It is also clear that the charge transfer resistance values R_{CT} of the two Zn ZIFs (ZIF-7 and ZIF-8), defined by the real axis value at the low frequency intercept of the semi-circular kinetically dominated region of the plot, are significantly greater than the R_{CT} of the Co ZIFs (ZIF-9 and ZIF-67). Whilst the Nyquist plots of ZIF-7 and ZIF-8 are

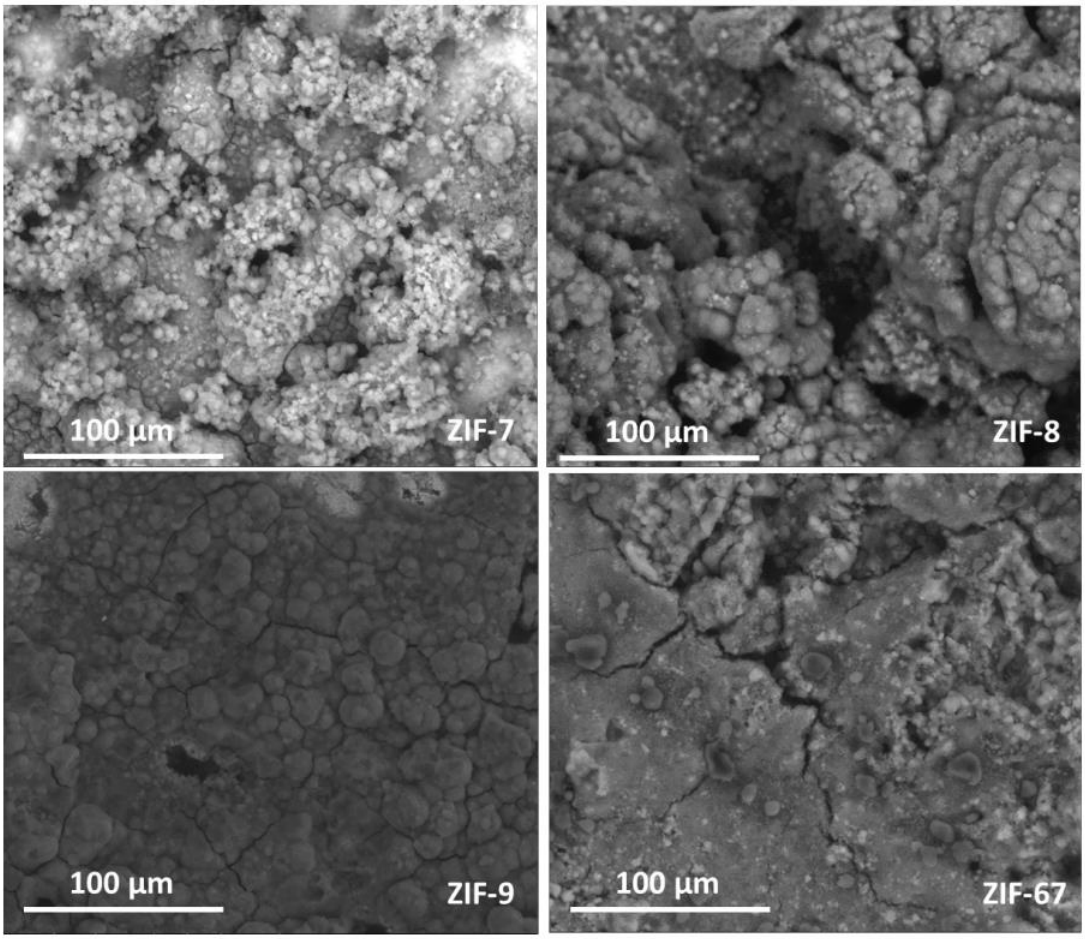

Figure S2 Backscattered electron SEM images of the ZIF-7, ZIF-8, ZIF-9 and ZIF-67 coatings on the electrode surface.

entirely composed of a semi-circular, kinetically dominated region the Nyquist plots for ZIF-9 and ZIF-67 are instead composed almost entirely of a ~ 45°, linear, diffusion dominated region with almost no discernible semi-circular region even when analysing the high frequency intercept in great detail (Figure 3B). It should also be noted that is a significant ~ 3 fold difference between the R_{CT} values of the two Zn ZIFs. As we have reported previously the semi-circular shape of the plots for the Zn ZIFs show that over the frequency range used these materials acted as resistors, with the width of the semicircle proportional to the charge transfer resistance.[1] In contrast the linear shape, and ~ 45°

angle of the plots for the Co ZIFs make clear that over the frequency range used they acted as pseudocapacitors.[1]

In order to obtain values for R_S and R_{CT} (Table 2) the Nyquist plots for the Co ZIFs were fitted with the Randles circuit (Figure 4A) whilst those for the Zn ZIFs were fitted with the simplified Randles circuit (Figure 4B). The R_s values are all within 2 Ω of each other as expected whilst the Zn ZIF R_{CT} values are two orders of magnitude larger than those for the Co ZIFs. Interestingly the bIM ZIFs have higher R_{CT} values than the corresponding mIM ZIFs.

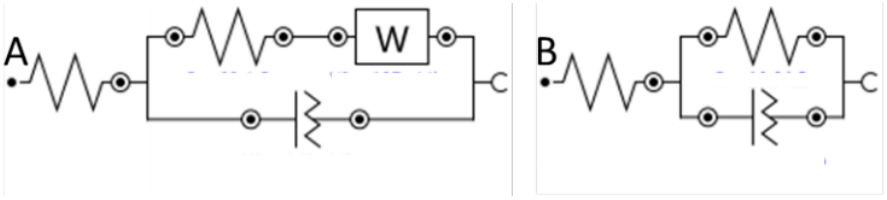

Figure S3 Randles (A) and simplified Randles (B) circuits used for fitting Nyquist plots .

The Bode phase plots (Figure 5) similarly show a significant difference in the behaviour between the Zn and Co ZIFs which we have observed in previous work.[1] In summary the shape of the Co ZIF plots are characteristic of pseudocapacitive behaviour, with the initial plateau in the phase at ~ 45° followed by a steady decrease in phase towards 0° with increasing frequency. The shape of the Zn ZIF plots show a different behaviour with the phase starting close to 0° at low frequency, before rising to plateau between 60° and 80° at medium frequencies and then finally decreasing again at higher frequencies. This behaviour indicates corrosion of the underlying metal electrode.

2 Computational

Calculations on the framework structures were carried out under periodic boundary conditions, using the projector-augmented wave (PAW)[2], pseudopotential approach in the VASP[3] code. The structures were initially relaxed using the PBEsol[4] functional, with a cutoff energy of 500 eV and Gamma point *k*-space sampling. In order to obtain a quantitative electronic structure the resultant systems were then treated using the HSE06[5] functional, mixing a percentage of exact exchange, to correct for self-interaction errors in the PBEsol functional. Gas phase electronic structures of the ligand molecules were obtained from Gaussian 09, using the B3LYP functional and the 6-31G* basis set.

To get a better idea of how the overlap of ligand and linker depends on the spin states of the species in the Co based ZIFs (9 and 67) we have plotted the spin density of states for the Co d-orbitals and N p-orbitals in Figure S4. These plots reveal that the conduction band minimum in both cases consists of a hybridisation of N p- and Co d- spin -1/2 orbitals. This highlights the importance of matching the spin states of the ligand and linker and moreover suggests that the framework would serve as a filter for spin – only allowing for the conduction of a single polarity of spin quantum number throughout the material.

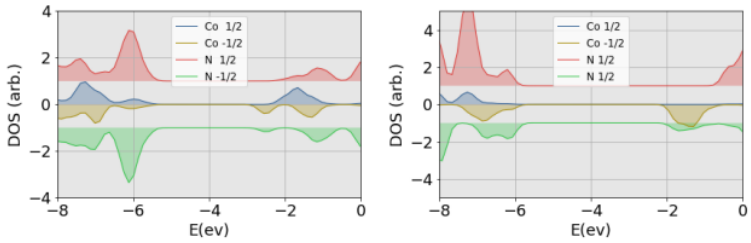

Figure S4 Spin resolved partial density of states plots for ZIF-9 (left) and ZIF-67 (right). Energy scales are referenced against the vacuum level. For Co, the d-orbital and for N the p-orbital DOS are plotted. The N DOS have been offset by +/- 1 arbitrary unit for clarity.

References

[1] S. D. Worrall, H. Mann, A. Rogers, M. A. Bissett, M. P. Attfield and R. A. W. Dryfe, *Electrochim. Acta*, 2016, **197**, 228-240.

. [2] P. E. Blöchl, "Projector augmented-wave method," *Phys. Rev. B*, vol. 50, no. 24, pp. 17953– 17979, Dec. 1994.

. [3] G. Kresse, "From ultrasoft pseudopotentials to the projector augmented-wave method," *Phys. Rev. B*, vol. 59, no. 3, pp. 1758–1775, Jan. 1999.

. [4] J. P. Perdew, A. Ruzsinszky, G. I. Csonka, O. A. Vydrov, G. E. Scuseria, L. A. Constantin, X. Zhou, and K. Burke, "Restoring the density-gradient expansion for exchange in solids and surfaces.," *Phys. Rev. Lett.*, vol. 100, no. 13, p. 136406, Apr. 2008.

. [5] J. Heyd, G. E. Scuseria, and M. Ernzerhof, "Erratum: 'Hybrid functionals based on a screened Coulomb potential' [J. Chem. Phys. 118, 8207 (2003)]," *J. Chem. Phys.*, vol. 124, no. 21, p. 219906, Jun. 2006.

9.2 Modular design of SPIRO-OMeTAD analogues as hole transport materials in solar cells

This is the author accepted manuscript of an article published in final form in Murray, AT, Frost, JM, Hendon, CH, Molloy, CD, Carbery, DR & Walsh, A 2015, 'Modular design of SPIROOMeTAD analogues as hole transport materials in solar cells', Chemical Communications, vol. 51, no. 43, pp. 8935-8938 and available online via: https://doi.org/10.1039/C5CC02129D

Modular design of SPIRO-OMeTAD analogues as hole transport materials in solar cells

Alexander T. Murray†, Jarvist M. Frost†, Christopher H. Hendon†, Christopher D. Molloy, David R. Carbery, Aron Walsh[a]

Received Xth XXXXXXXXXX 20XX, Accepted Xth XXXXXXXXX 20XX
First published on the web Xth XXXXXXXXXX 200X
DOI: 10.1039/b000000x

We predict the ionisation potentials of the hole-conducting material SPIRO-OMeTAD and twelve methoxy isomers and polymethoxy derivatives. Based on electronic and economic factors, we identify the optimal compounds for application as *p*-type hole-selective contacts in hybrid halide perovskite solar cells.

Considerable scientific effort has been focused on the challenge of converting sunlight to electricity. Recently, solution-processed hybrid perovskite based solar cells have reached power conversion efficiencies of 20.1%, values competitive with the mature silicon technologies.[1–10] A critical component of any solar cell (or optoelectronic device) is the electrical contact, which needs to efficiently and selectively extract electrons or holes from the active layer. In order to maximise the photovoltage and photocurrent, the energy levels of the contacts should be well-matched to the active layer of the device.[11] As new hybrid perovskites and alternative absorber layers are being developed for solar cells, beyond the widely employed $CH_3NH_3PbI_3$, the ability to modulate the energy levels of the selective contacts to match those of the absorber[12] will be essential in order to maximise power conversion efficiency.

Most high-efficiency hybrid perovskite solar cells use the hole conductor N^2,N^2,N^2',N^2',N^7,N^7,N^7',N^7'-octakis(4-methoxyphenyl)-9,9'-spirobi[9H-fluorene]-2,2',7,7'-tetramine (SPIRO-OMeTAD, Figure 1a).[14,15] SPIRO-OMeTAD is widely used in solution processed solar cells with an ionisation potential well matched to a number of active (light absorbing) layers. The material forms an amorphous glass, rather than a partially crystalline phase, enabling smooth films to be formed.[16]

Electronic energy level alignment is important for solar cells, but is commonly used in post-rationalisation of successful architectures rather than as a design principle *a priori*. One compelling example was recently presented by Il Seok and co-workers, where the energy levels of SPIRO-OMeTAD were tuned by altering the connectivity of the methoxy ethers on the amino phenyl motifs.[17] Similarly, other groups are interested in the computational design of contacts for more mature photovoltaic technologies.

From the study of Il Seok, it was concluded that the geminal *ortho*-methoxyphenyl, *para*-methoxyphenyl arrangement pro-

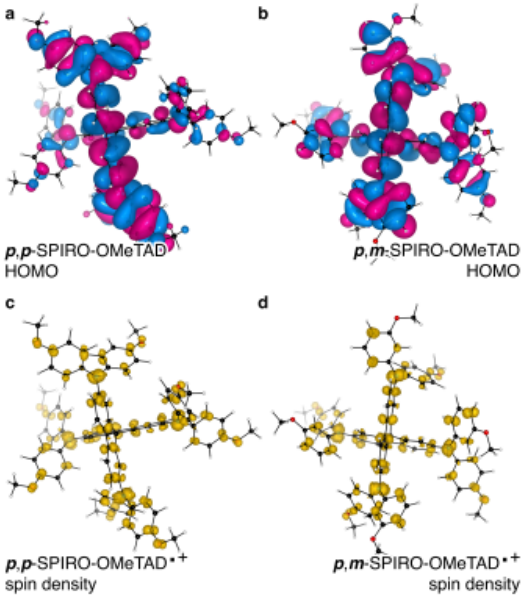

Fig. 1 Calculated *p,p*-SPIRO-OMeTAD highest-occupied molecular orbital (HOMO) (**a**) and the associated one electron oxidised spin density (**c**) and *p,m*-SPIRO-OMeTAD HOMO (**b**) and the associated one electron oxidised spin density (**d**). The plots were made with a HOMO isovalue = 0.03 e/Å^3 and spin-density isovalue = 0.01 e/Å^3 in the code VESTA.[13]

† These authors contributed equally to this work and hence share first authorship. Electronic supplementary information (ESI) available: Full cost analysis and computational methods. See DOI: XX.XXXX/XXXXXXXX

[a] *Department of Chemistry, University of Bath, Claverton Down, Bath, BA2 7AY, United Kingdom. Tel: 01225 384 913; Twitter: @lonepair; E-mail: A.Walsh@bath.ac.uk*

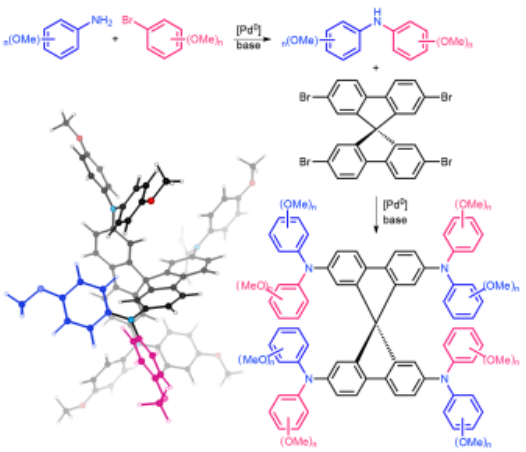

Fig. 2 Sequential synthesis of SPIRO-OMeTAD derivatives and B3LYP optimised geometry of *p,p*-SPIRO-OMeTAD with r_1 and r_2 highlighted in blue and pink.

duced a cell with +2 % boost in conversion efficiency relative the typical SPIRO-OMeTAD (geminal *para*-methoxyphenyl, *para*-methoxyphenyl). They also found that the geminal *meta*-methoxyphenyl, *para*-methoxyphenyl isomer was detrimental to hole conduction. This increase in efficiency was correlated with an increase in oxidation potential as estimated from cyclic voltammetry, which has limited accuracy. Careful measurements using techniques such as differential pulse voltammetry (which allows for low concentration voltammetry measurements, avoiding aggregation) would allow more accurate and informative measurements with the broadly the same experimental setup.[18] Variation in device-to-device performance, and issues such as implicit doping[19] from various syntheses of hybrid or organic electronic materials, means that it requires extremely large study to provide the definitive answer of which material is optimal.

In solar cells, SPIRO-OMeTAD can be used in the neutral, one and two electron oxidised forms. Chemical doping with lithium salts is typically performed to increase conductivity.[20] Figure 1 shows the Kohn-Sham highest occupied molecular orbital (HOMO) of the neutral, and the singly-occupied molecular orbital (SOMO) of the cationic radical state of the most common SPIRO-OMeTAD isomer (*p,p*-SPIRO-OMeTAD), as well as the *p*, *m* isomer previously found to be detrimental. These frontier orbitals provide a qualitative interpretation of the chemical bonding. Both the HOMO and SOMO show similar electronic structure: the electron density is centred on the extended π network, primarily on the carbons.

The oxidised doublet state can be viewed as the removal of an electron from this π system; the associated spin density is centred again on the carbon system, but there is significant spin stabilisation from the heteroatoms (*i.e.* N). Additionally, the amino phenyl carbons, as defined by the position of the methoxy ether motifs, do not appear to affect the contribution to the delocalised radical. This effect is notable as the amino phenyl motifs are not part of the extended π system due to the violation of Hückel planarity.[21]

Due to the lack of π planarity, we would not expect organic modifications to affect the ionisation potential to the extent we observe for typical planar conjugated systems.[22] This suggests that isomer modifications should allow for energy level modulation, within a narrow range, through repositioning of the methoxy ether motifs.[23,24]

To investigate the possible synthetic scope in modifying the side chains, we have predicted the energy level alignment of *p,p*-SPIRO-OMeTAD and 12 structurally related isomers (Figure 3). These calculations are by hybrid density functional theory (DFT) with atom-centered numerical basis functions (see SI for full details). We report both the Kohn-Sham energy gap (from B3LYP), and more reliable ionisation potentials were calculated with the delta self-consistent field (ΔSCF) method. All calculations were of a single molecule in the gas phase, as we were looking for relative variations in the ionisation potential, rather than an absolute value for the solid state, which may be influenced by molecular packing. We do not consider these values to be definitive. More accurate model chemistries might achieve more precise gas phase values, but the variation caused by solid state packing in the real system would have more of an effect on device performance and the overall accuracy of such predictions.

As detailed in Figure 2, we defined the two aminoaryl rings as r_1 and r_2, and used *o*, *m*, and *p* to refer to regiochemistry relative to the amine (or bromide). These correspond to the 2-, 3- and 4- positions, respectively. The predicted electronic modulation is modest, but important in the context of efficient hole extraction. Two important conclusions can be made: (i) *meta*-methoxy substitutions result in generally increased ionisation potentials, as the contribution of the oxygen donation is reduced with reduced structural symmetry (lowering the energy of the π system); (ii) *para*- and *ortho*- substituted derivatives result in decreased ionisation potentials due to the increased energy of the π system. In the cases of poly-OMe substitutions, the decreased ionisation potential is also realised by the repulsive interaction between neighbouring rings.

The Kohn-Sham energy gap (E_g, written in colour in Figure 3) is relatively constant for all isomers. Here, the HOMO eigenvalue deviates from our ΔSCF ionisation potential, suggesting that Koopman's approximation is insufficient for predicting even qualitative trends. However, our ΔSCF calculations are in close agreement with the experimentally determined ionisation potential for the *p,p*- analogue,[25] and with

This journal is © The Royal Society of Chemistry [year]

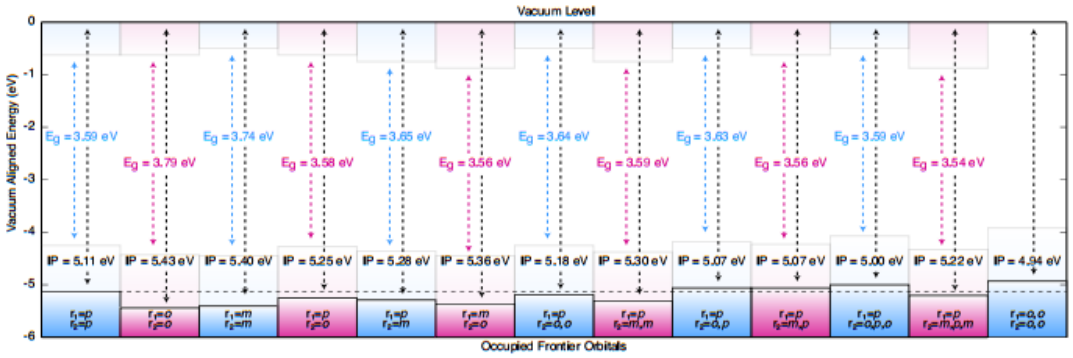

Fig. 3 The calculated single-particle Kohn-Sham energy gaps (E_g) and ΔSCF ionisational potentials (IP) for a range of SPIRO-OMeTAD derivatives (as defined in Figure 2). The black dashed horizontal line refers to the IP of *p,p*-SPIRO-OMeTAD.

the *p,m*- analogue,[17] though we contradict experiment and predict that the *p,o*- analogue[17] should see an enhancement.

An especially interesting molecule is the case in which $r_1 = r_2 = o,o$. This derivative has a notably smaller ionisation potential than other analogues, which is likely due to both the electron donating contribution of the *ortho*- positions and 'through-space' conjugation to the amine motif.[26]

Tuning the energy levels in a contact material is only a partial fulfilment of the requirements – we also need to transport the holes efficiently, and so avoid surface recombination. Calculating charge carrier mobility for a novel organic material is extremely difficult, as a full model of packing and an understanding of the dielectric environment is required before microscopic charge transfer integrals can be calculated and a macroscopic mobility predicted.[27]

One expects that adding bulky side chains would decrease the molecular packing density and coordination number, and so reduce the electronic overlap and thus microscopic mobility.

A barrier to the large-scale production of novel solar cells is the cost of SPIRO-OMeTAD. This can be partially attributed to the recent fluctuations in supply and demand, but is also due to the cost of the starting materials. A typical synthesis of SPIRO-OMeTAD begins with the Pd-catalysed coupling of anisidine (*para*-methoxyaniline) and *para*-methoxybromobenzene to form a secondary aniline. Four equivalents of the aniline are then resubjected to similar coupling conditions with the brominated spiro core; 2,2',7,7'-Tetrabromo-9,9'-spirobi[9H-fluorene], Figure 2, forming *p,p*-SPIRO-OMeTAD.[17] In principle, any commercially available aniline and aryl bromide could be used to construct a diverse library of electronically dissimilar SPIRO-OMeTAD derivatives. Assuming isomer transferable reaction conditions (*i.e.* the use of the same catalysts, purification methods and yeilds) we have included a rudimentary cost break down associated with the reagents required for our library (see Supporting Information for a full cost analysis).

Beyond the cases considered here, greater electronic variability should be achievable through substitution about the fluorene core (direct conjugation modulation). However, given the current lack of commercial availability of alternate core materials, this could be a more synthetically challenging endeavour. Recent advances in aryl C-H activation chemistry could find a useful application in the functionalisation of these molecules.[28–31]

In conclusion, we have calculated the ionisation potentials of a variety of analogues of the hole conducting material SPIRO-OMeTAD, varying the HOMO energy through alterations to the positioning of methoxy groups on the pendant aryl rings of the molecule. Our method is computationally efficient, has been shown to offer good agreement with experimental measures from solution voltammetry. We predict that these synthetic variants offer flexibility in work function matching for solar cell design and optimisation, and that the majority of analogues could be candidates for large-scale development and application.

Acknowledgements

We thank K. Tobias Butler for lyrical insights. We acknowledge membership of the U.K.'s HPC Materials Chemistry Consortium, which is funded by EPSRC Grant EP/L000202. Additional support has been received from EPSRC Grants EP/ K016288/1 and EP/J017361/1, the Royal Society, and the ERC (Grant no. 277757).

References

1 J. Burschka, N. Pellet, S.-J. Moon, R. Humphry-Baker, P. Gao, M. K. Nazeeruddin and M. Grätzel, *Nature*, 2013, **499**, 316.

2 O. Malinkiewicz, A. Yella, Y. H. Lee, G. M. Espallargas, M. Grätzel, M. K. Nazeeruddin and H. J. Bolink, *Nat. Photon.*, 2014, **8**, 128.
3 A. Kojima, K. Teshima, Y. Shirai and T. Miyasaka, *J. Am. Chem. Soc.*, 2009, **131**, 6050.
4 N. J. Jeon, J. Lee, J. H. Noh, M. K. Nazeeruddin, M. Grätzel and S. I. Seok, *J. Am. Chem. Soc.*, 2013, **135**, 19087–19090.
5 J. M. Frost, K. T. Butler, F. Brivio, C. H. Hendon, M. van Schilfgaarde and A. Walsh, *Nano Lett.*, 2014, **14**, 2584.
6 C. H. Hendon, R. X. Yang, L. A. Burton and A. Walsh, *J. Mater. Chem. A*, 2015, DOI: 10.1039/C4TA05284F.
7 M. J. Carnie, C. Charbonneau, M. L. Davies, J. Troughton, T. M. Watson, K. Wojciechowski, H. Snaith and D. A. Worsley, *Chem. Commun.*, 2013, **49**, 7893.
8 D. S. Bhachu, D. O. Scanlon, E. J. Saban, H. Bronstein, I. P. Parkin, C. J. Carmalt and R. Palgrave, *J. Mater. Chem. A*, 2015, Advance.
9 B.-W. Park, E. M. J. Johansson, B. Philippe, T. Gustafsson, K. Sveinbjörnsson, A. Hagfeldt and G. Boschloo, *Chem. Mater.*, 2014, **26**, 4466–4471.
10 K. T. Butler, J. M. Frost and A. Walsh, *Energy Environ. Sci.*, 2015, **8**, 838–848.
11 K. T. Butler, P. E. Vullum, A. M. Muggerud, E. Cabrera and J. H. Harding, *Phys. Rev. B*, 2011, **83**, 235307.
12 K. T. Butler, J. M. Frost and A. Walsh, *Mater. Horiz.*, 2015, **2**, 228–231.
13 K. Momma and F. Izumi, *J. App. Cryst.*, 2008, **41**, 653–658.
14 U. Bach, P. Comte, J. E. Moser, F. Weissörtel, J. Salbeck, H. Spreitzer and M. Grätzel, *Nature*, 1998, **395**, 583.
15 M. M. Lee, J. Teuscher, T. Miyasaka, T. N. Murakami and H. J. Snaith, *Science*, 2012, **338**, 643.
16 F. Fabregat-Santiago, J. Bisquert, L. Cevey, P. Chen, M. Wang, S. M. Zakeeruddin and M. Grätzel, *J. Am. Chem. Soc.*, 2009, **131**, 558.
17 N. J. Jeon, H. G. Lee, Y. C. Kim, J. Seo, J. H. Noh, J. Lee and S. I. Seok, *J. Am. Chem. Soc.*, 2014, **136**, 7837.
18 J. M. Frost, M. A. Faist and J. Nelson, *Advanced Materials*, 2010, **22**, 4881–4884.
19 T. Kirchartz and J. Nelson, *Phys. Rev. B*, 2012, **86**, 165201.
20 W. H. Nguyen, C. D. Bailie, E. L. Unger and M. D. McGehee, *J. Am. Chem. Soc.*, 2014, **136**, 10996.
21 E. Hckel, *Z. Phys.*, 1931, **70**, 204.
22 C. H. Hendon, D. Tiana, M. Fontecave, C. Sanchez, L. D'arras, C. Sassoye, L. Rozes, C. Mellot-Draznieks and A. Walsh, *J. Am. Chem. Soc.*, 2013, **135**, 10942.
23 A. T. Murray, P. Matton, N. W. G. Fairhurst, M. P. John and D. R. Carbery, *Org. Lett.*, 2012, **14**, 3656.
24 C. H. Hendon, D. R. Carbery and A. Walsh, *Chem. Sci.*, 2014, **5**, 1390–1395.
25 H.-S. Kim, C.-R. Lee, J.-H. Im, K.-B. Lee, T. Moehl, A. Marchioro, S.-J. Moon, R. Humphry-Baker, J.-H. Yum, J. E. Moser, M. Grätzel and N.-G. Park, *Sci. Rep.*, 2012, **2**, 1.
26 C. R. Martinez and B. L. Iverson, *Chem. Sci.*, 2012, **3**, 2191.
27 J. Nelson, J. J. Kwiatkowski, J. Kirkpatrick and J. M. Frost, *Acc. Chem. Res.*, 2009, **42**, 1768–1778.
28 F. W. Patureau, C. Nimphius and F. Glorius, *Org. Lett.*, 2011, **13**, 6346.
29 J. Wencel-Delord, C. Nimphius, F. W. Patureau and F. Glorius, *Chem. Asian J.*, 2012, **7**, 1208.
30 H. Wang, C. Grohmann, C. Nimphius and F. Glorius, *J. Am. Chem. Soc.*, 2012, **134**, 19592.
31 C. Arroniz, J. G. Denis, A. Ironmonger, G. Rassias and I. Larrosa, *Chem. Sci.*, 2014, **5**, 3509.

This journal is © The Royal Society of Chemistry [year]

Supplementary Information: Modular design of SPIRO-OMeTAD analogues as hole transport materials in solar cells

*Alexander T. Murray, Jarvist M. Frost, Christopher H. Hendon, Christopher D. Molloy, David R. Carbery and Aron Walsh**

Department of Chemistry, University of Bath, Bath, BA2 7AY, UK

Cost Analysis

At present, the cost of *p*,*p*-SPIRO-OMeTAD is approximately £227 ($344 USD)/g (Sigma-Aldrich UK). Given the per gram cost of both *p*-methoxyaniline and *p*-methoxylbromobenzene are inexpensive (<£0.10/g, Sigma- Aldrich UK) the bulk synthetic cost is attributed to the spiro-fluorene precursor 2,2',7,7'-Tetrabromo-9,9'- spirobi[9H-fluorene], £77 ($116 USD)/g (Sigma Alrich UK), and the Pd catalysts, both of which are constant. It is unsurprising that the crowded all-carbon quaternary spiro-centre is expensive to produce. However, the peripheral aryl fragments used to form the secondary aniline may also become costly with increased substitution complexity, and this could negatively impact the balance of systems cost of a module, despite an increase in device efficiency.

The costs of primary anilines and bromides (Tables S1 and S2, respectively) used in the typical synthetic pathway are presented in Table S3. There are only three derivatives that have notably high associated costs: the r1 =*p*, r2 =*o*,*o*, the r1 =*p*, r2 =*o*,*p*,*o* and the desir- able r1=*o*, *o*, r2=*o*, *o*. The r1=*p*, r2=*o* derivative, as synthesised by Il Seok and co-workers, should be no more costly than the r1=*p*, r_W=*p*-derivative (typical SPIRO-OMeTAD). In particular, the marginal cost of the di-substituted aniline that would be used for the r1=*o*, *o*, r2=*o*, *o* compound is £63 ($93 USD)/g as opposed to the *p*,*p*-aniline at £0.19/g.[32,33] Four equivalents of this secondary aniline impacts the overall cost significantly. Nevertheless, for fundamental research *o*,*o*- *o*,*o*-SPIRO-OMeTAD should be an interesting and promising molecule, particularly with the potential economies of scale for the anilines.

Computational Details

The SPIRO-OMeTAD analogues were constructed by hand, starting with the SPIRO-OMeTAD archetype. Geometries were then relaxed to their potential energy minimum at the B3LYP/6-31g* hybrid-DFT level of theory in vacuum, as a closed-shell neutral configuration. The Kohn-Sham eigenvalues (HOMO and LUMO frontier orbital energies) were extracted from these calculations.

The delta-SCF method was used to more accurately estimate the ionization potential of each system. Here, the ionization potential was evaluated as being the difference in total DFT energy between the neutral configuration, and a resolved electronic structure configuration (at the neutral geometry) as the 1+ cation in a doublet spin configuration.

All calculations were with performed with Gaussian09.

Table S1. Costing of methoxyanilines from commercial suppliers

ANILINES	£/g	SUPPLIER
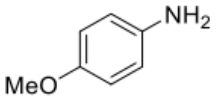	0.08	Sigma-Aldrich
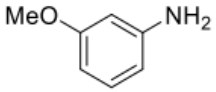	0.28	Sigma-Aldrich
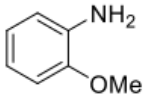	0.08	Sigma-Aldrich
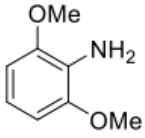	27.8	Alfa-Aesar
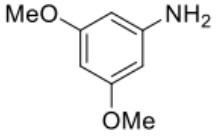	2.16	Alfa-Aesar
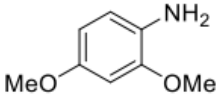	0.43	Sigma-Aldrich
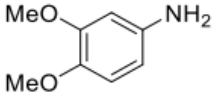	2.48	Sigma-Aldrich
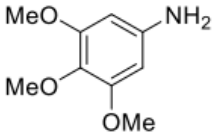	2.69	Alfa-Aesar

Table S2. Costing of methoxyaryl bromides from commercial suppliers

BROMIDES	£/g	SUPPLIER
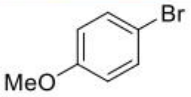	0.11	Sigma-Aldrich
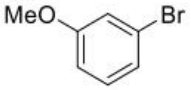	0.62	Sigma-Aldrich
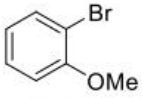	0.61	Sigma-Aldrich
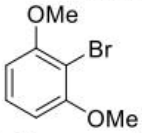	35.5	Sigma-Aldrich
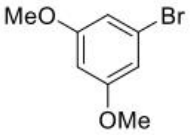	2.17	Alfa-Aesar
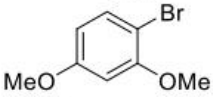	1.08	Alfa-Aesar
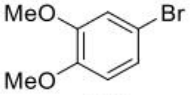	1.49	Sigma-Aldrich
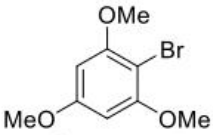	158	Sigma-Aldrich
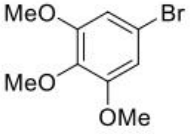	1.87	Sigma-Aldrich

Table S3. Relative costing from building blocks

r_1	r_2	r_1 = aniline, r_2 = bromide / £	r_1 = bromide, r_2 = aniline / £
p	*p*	0.19	N/A
m	*m*	0.9	N/A
o	*o*	0.69	N/A
p	*m*	0.7	0.39
p	*o*	0.69	0.19
p	*o,o*	35.58	27.91
p	*m,m*	2.25	2.27
p	*o,p*	1.16	0.54
p	*m,p*	1.57	2.59
p	*o,p,o*	158.08	N/A
p	*m,p,m*	1.95	2.8
o,o	*o,o*	63.3	N/A